Structural Performance of Partially Confined Concrete-Filled Steel Tubular Columns under Combined Axial and Lateral Cyclic Loadings

A thesis submitted for the degree of

Doctor of Philosophy

By

Prasanta Kar

Department of Civil Engineering

Indian Institute of Technology Guwahati

Guwahati – 781039, India

This page is intentionally left blank

to Sri Sri Thakur Anukul Chandra

to my dearest parents

Nripendra and Prabhasini

This page is intentionally left blank

Declaration

I hereby declare that this thesis entitled '**Structural Performance of Partially Confined Concrete-Filled Steel Tubular Columns under Combined Axial and Lateral Cyclic Loadings**' has been generated by me and purely represents my PhD work. Any material from unpublished or published work from others is referenced appropriately.

Prasanta Kar

Prasanta Kar

Reg. No: 166104031

Date: 05/06/2023

Place: IIT Guwahati

This page is intentionally left blank

Certificate

This is to certify that the thesis entitled '**Structural Performance of Partially Confined Concrete-Filled Steel Tubular Columns under Combined Axial and Lateral Cyclic Loadings**' being submitted by **Mr. Prasanta Kar** to the Indian Institute of Technology Guwahati, India for the award of degree of **Doctor of Philosophy** is a record of genuine research work carried out by him under our supervision.

The thesis work, in our opinion is worthy of considering for the award of degree of **Doctor of Philosophy** in accordance with the regulation of the institute.

(Dr. Arun Chandra Borsaikia)
Senior Technical Officer
Department of Civil Engineering
Indian Institute of Technology Guwahati, India

(Dr. Konjengbam Darunkumar Singh)
Professor
Department of Civil Engineering
Indian Institute of Technology Guwahati, India

Date: 05/06/2023
Place: IIT Guwahati

Date: 05/06/2023
Place: IIT Guwahati

This page is intentionally left blank

Acknowledgements

Foremost I would like to express my sincere gratitude and appreciation to my supervisors, **Prof. Konjengbam Darunkumar Singh** and **Dr. Arun Chandra Borsaikia** for their constant encouragement, unconditional support, continued inspiration and guidance throughout my research work. I am so grateful to have them as my supervisors, who have moulded me to a new individual. To me, they are not only my supervisors but also life-long mentors, from whom I have acquired a lot of priceless proficiency apart from academics.

I am thankful to the members of my doctoral committee: Prof. Arbind Kumar Singh (Chairman), Prof. Hrishikesh Sharma and Prof. Karuna Kalita, who have generously offered their time and support to review my research work from time to time. Their suggestions, remarks and encouragements have been absolutely invaluable.

I would like to acknowledge the financial support, technical assistance, testing facilities etc., provided by Department of Civil Engineering, Indian Institute of Technology Guwahati to carry out this research work.

The instrumental facilities, in particular, Wire cut EDM, CO2 laser cutting machine etc., provided by the Department of Mechanical Engineering, Indian Institute of technology Guwahati is gratefully acknowledged. Also the testing facility provided by Central Instrument Facility at Indian Institute of Technology Guwahati is gratefully acknowledged.

I would like to extend my thanks to all the PhD scholars of our research team at Indian Institute of Technology Guwahati, in particular Dr. Sonu, Dr. Sachidananda, Dr, Narendra, Dr. Haloi and Dr. Mushahary for their participation in discussion regarding experimental investigations.

I would like to specially thank my friend Mr. Saroj Sahu, who always supported me through thick and thin making my life easy.

Finally, but not the least, I would like to specially thank my family members – Nripendra Kar (Father), Prabhasini Kar (Mother), Dipa Kar (Sister), Gopa Kar (Sister), Sushanta Kar (Brother) and Indrani Dutta (Wife) for their love, constant support and encouragement through the course of my research work. With all my love, I would like to dedicate this thesis to them.

Prasanta Kar

Abstract

In this research work, an innovative strengthening technique has been proposed for square CFST columns. An experimental investigation on partially confined concrete-filled steel tubular (PCCFST) square columns (i.e., short inner concrete core confinement near the support), using circular hollow section (CHS) configuration as partial inner confinement, under combined axial and cyclic lateral loadings has been performed. Hysteretic behavior of load, ultimate lateral strength, energy dissipation capacity, and ductility of the PCCFST columns were studied as a function of (a) the ratio of the height of the inner tube to the diameter of the outer tube (0-2.5) and (b) diameter/width ratio of inner tube to outer tube (0.44, and 0.53). Based on the investigation, it has been seen that the height and diameter of the inner CHS have an evident influence on the cyclic performance of the columns. Ultimate lateral strength, energy dissipation capacity, and ductility were enhanced by ~ 15.3%, 11.4%, and 9.6%, respectively, up to a height of 1.5D of inner CHS. Enhancement of the cyclic performance of PCCFST column with the height of inner CHS beyond 1.5D is not very significant. Based on the limited experimental results herein and code provisions (Eurocode 4 1994), a design rule has been proposed to predict the ultimate lateral strength of the square PCCFST columns.

A Similar study has also been extended for circular CFST columns. Based on the study, it has been seen that the maximum lateral strength, ductility, and energy dissipation ability were enhanced by a maximum of ~ 16%, 24%, and 14%, respectively, in comparison to the unstrengthen circular CFST. Based on the Eurocode (Eurocode 4 1994) and limited experimental data obtained from the present study, a new design guideline has also been proposed.

An innovative retrofitting technique has been proposed to externally retrofit the damaged square and circular CFST and partially confined CFST columns. The external retrofitting was carried out using either square or circular CFST sections. The effect of the sectional shape of the retrofitting CFST on the structural performance has been assessed under combined axial and lateral cyclic loading. Studies have been carried out to investigate the hysteretic behavior, ultimate lateral strength, and energy dissipation capacity of the retrofitted specimens. The experimental study showed that the square retrofitted columns could regain the ultimate lateral strength and energy dissipation capacity by ~ 121%-134% and ~110%-115%, respectively, for the retrofitting CFST element considered. The regain in the ultimate lateral strength, and energy dissipation capacity of the circular retrofitted columns was found to be ~ 113%-139% and ~116% to 135%, respectively.

Contents

List of tables

List of figures

Notations

A_c	Cross-sectional area of the core concrete
A_a	Cross-sectional area of the steel tube
CCFT	Confined concrete-filled steel tube
CFRP	Carbon fiber reinforced polymer
CFST	Concrete-filled steel tube
CHS	Circular hollow section
D	Width of the outer square hollow section steel tube
D_i	Diameter of inner circular hollow section steel tube
D_0	Width/Diameter of outer retrofitting steel element
f_{cu}	Concrete cube strength
f_{ck}	Cylinder compressive strength of the concrete
f_y	Yield strength of steel
f_u	Ultimate strength of steel
GFRP	Glass-fiber-reinforced polymers
H	Clear height (length between the top of the stiff reinforced concrete) footing and the location of lateral load application
H_i	Height of inner circular hollow section steel tube
H_0	Height of the retrofitting steel element
K	Average secant stiffness
MSA	Maximum size aggregate
M_{Euro}	Maximum moment capacity of the CFST column as per EC4
M_p	Plastic moment capacity of the CFST column
M_{max}	Maximum bending capacity of the CFST column

n	Axial load level
N	Measured axial load
N_0	Applied axial compressive load
N_u	Axial compressive capacity
PCCFST	Partially confined concrete-filled steel tube
P	Measured lateral load
P_u	Average ultimate lateral strength obtained from the tested PCCFST specimen
P_{ue}	Predicted ultimate lateral strength of the PCCFST specimen
RC	Reinforced concrete
SHS	Square hollow section
t	Thickness of the outer square hollow section steel tube
t_i	Thickness of inner circular hollow section steel tube
t_0	Thickness of the retrofitting steel element
UTM	Universal testing machine
θ	Drift angle
δ	Axial displacement
Δ	Lateral displacement at the column head
λ	Average strength degradation coefficient
μ	Displacement ductility coefficient
Δ_y	Yield displacement
Δ_u	Displacement when the lateral load falls to 85 % of the ultimate lateral strength

Chapter 1

Introduction

1.1 BACKGROUND

The use of concrete-filled steel tubes (CFST) as structural members has become prevalent and widespread in the past few decades because of its various advantages, such as high bearing capacity, ductility, easy construction, time, and cost-saving (e.g. Han *et al.* 2014). The use of CFST can result in reduced cross-sections, improvement of structural aesthetics, high-temperature and blast resistances (e.g. Wang *et al.* 2017a, 2019). It was also observed that the shrinkage strain for the concrete in CFST columns was minimal because of the sealed environment provided by the outer steel tube (e.g. Ichinose *et al.* 2001). The continuous lateral confinement provided by the outer steel tube resists both crushing and spalling of the core concrete, thereby enhancing the strength and inelastic deformation of the confined concrete. At the same time, the core concrete restrains the inward local buckling of the outer steel tube, increasing the load carrying capacity of the outer steel tube. All these advantages have made CFST members widely recognized and have led to extensive use in the construction industry. Therefore, the use of CFST is mostly increasing in large span bridges and tall buildings. Figure 1.1 shows Ganhaizi Bridge, Sichuan China where CFST built-up columns were used in piers. The advantages of using

CFST structures in bridges is that, the tedious process of framework are absent. Figure 1.2 shows the Shenzhen Plaza, which is one of the tallest building in the world (72^{nd} rank). The total height of the building is 356 meter. The columns of the building are made up of CFST. Figure 1.3 shows the Canton Tower in Guangzhou, China, where the total height of the tower is 600 meter. A total of 24 inclined circular concrete-filled steel tubular members were used in the construction. Figure 1.4 shows a long-span transmission tower built in China. It is the largest electricity pylons in the world with a height of 370 meter. The tower stands on four concrete-filled steel tubular columns. The diameter of each column is 2000 mm and the concrete is filled up to 210-meter height.

CFST members are generally considered to possess favorable characteristics for use in high seismic regions (e.g. Schneider and Alostaz 1998). Due to the enhanced confinement and ductility of the CFST members, several researches have been initiated to understand their cyclic behavior (e.g. Elchalakani and Zhao 2008; Fam *et al.* 2004; Gajalakshmi and Helena 2012; Liang *et al.* 2007b; Liu *et al.* 2008; Patel *et al.* 2014; Qin *et al.* 2015; Serras *et al.* 2016; Usami and Ge 1998; Varma *et al.* 2004 etc.). Hsu and Yu 2003 reported that CFST members subjected to cyclic loading exhibited local buckling failure at the plastic hinge zone near the support region (0.45D-0.95D height, where D is the width of the outer steel section), while the remaining part of the member was seen to be undamaged. The post-buckling behavior of CFST members has been seen to be governed by the deterioration rate of the tube plates/walls in the plastic hinge region. Wu *et al.* 2012 observed that the local buckling of the outer steel tubes in square CFST columns occurred in the support region for a length of about 0.2B-0.83B (where B is the width of the outer steel section). It was reported that the total energy dissipated by the cyclic specimen was dominated by the flexural energy dissipated in the failure region (i.e. within 0.8D from the base of the column)(Varma *et al.* 2002). Thus, the strength and stiffness of the CFST members are seen to be governed by the deterioration rate of the member at the plastic hinge (damaged / failure) region, while the remaining portion of the test length experienced elastic unloading.

It may be worthwhile to mention that the current earthquake-resistant design requires strong column and weak beam behavior (e.g. Irfani and Vimala 2019). Hence, strengthening the plastic hinge region of the column, for improved flexural strength and energy-dissipating capacity became a focus point for many of the researchers.

In the literature (shown in **Chapter 2**), investigations have been reported to enhance the strength and ductility of the plastic hinge region, under lateral cyclic loading; by providing external and internal stiffeners confining the plastic region with either steel plates or carbon fiber reinforced polymer (CFRP) wrapping or reinforced concrete (RC). Hsu and Juang 2000 found that the strength and energy dissipation capacities of the hollow steel tube could be enhanced economically by strengthening the plastic hinge zone with cross ties, by approximately 17% and 42%, respectively. This work was extended by Hsu and Yu 2003, and the same method was applied to CFST columns. Based on the study, energy dissipation and strength was reported to enhance by ~ 30% and ~5%, respectively. It was also observed that the cyclic behavior of the CFST column could be improved significantly by providing additional confinement of carbon fiber reinforced polymer (CFRP) wrap externally at the plastic hinge region, for a distance of ~0.8D (Xiao *et al.* 2005). Mao and Xiao 2006 fabricated confined concrete-filled steel tube (CCFT) columns by welding thick steel plates, steel strips, and steel angles externally in the plastic hinge region and reported an increase in ductility of ~ 67% with respect to the conventional CFST columns, with no significant strength enhancement. Zhang *et al.* 2015 observed that the cyclic performance of hybrid FRP-concrete-steel double-skin tubular column could be enhanced by filling the inner void in the plastic hinge region. Similar experiments were performed by Yu *et al.* 2016, where both CFRP and GFRP were externally used to confine the expected plastic hinge region. An experimental investigation was carried out by Xu *et al.* 2016 on the CFST column partially encased by an outer reinforced concrete (RC) component and studied the effect of height of the outer RC component on the strength, stiffness, and ductility on square columns. On increasing the height of the outer RC component from 2B to 3B, with respect to the base of the column, an enhancement in strength of ~ 5% was seen. Liu *et al.* 2021 developed two internal strength enhancement schemes: a) diagonal rib stiffeners, and b) circular stiffeners. The stiffener region was confined upto a height equivalent to the width of the outer section. It was observed that the stiffened columns exhibited excellent seismic performance with higher lateral resistance, better ductility, and greater energy dissipation capacity compared to the unstiffened counterpart columns.

It is evident from the above discussion that research on the cyclic behavior of confined CFST, is very limited and mostly confined externally (thereby affecting the aesthetics and outer column dimensions). Further, to the best of author's knowledge, no work has been reported in public domain on retrofitting of the damaged CFST columns.

As a research in this direction, a novel inner confinement technique has been introduced, named partially confined concrete-filled steel tubular (PCCFST) column (using short inner concrete core confinement near the support). In this work, an attempt has been made to investigate experimentally the effects of partial confinement using concentric inner steel circular hollow section (CHS). The present work mainly focuses on the effects of the height and diameter of the inner CHS steel tube at the base/support on the cyclic performance (ultimate lateral strength, energy dissipation capacity, and ductility) of CFST columns under combined constant axial and cyclically varying lateral loadings. The results of the experimental program have been presented in the form of variation of ultimate lateral strength, energy dissipation capacity, and ductility as a function of the height, and diameter of the inner steel tube.

Further a novel retrofitting technique using CFST to retrofit CFST or plastic hinge strengthened-CFST has also been proposed in the current study. In this work, the effectiveness of using CFST and the effects of the shape of the retrofitting CFST to retrofit CFST and plastic hinge strengthened-CFST was studied. Therefore, in the present work, two CFST sections (square and circular) have been used to retrofit damaged CFST and plastic hinge strengthened-CFST and assess the cyclic performance (energy dissipation capacity and ultimate lateral strength) of the retrofitted columns under constant axial and cyclic lateral loading.

1.2 OBJECTIVES

Based on the research gaps presented above, an experimental investigation to study the structural behavior of CFST under combined axial and cyclic lateral loadings has been carried out for various configurations of strengthened and retrofitted CFSTs listed below:

1) Partially confined square CFST columns,
2) Partially confined circular CFST columns,
3) Retrofitted partially confined square CFST columns,
4) Retrofitted partially confined circular CFST columns.

1.3 THESIS OUTLINE

The thesis comprised of seven chapters. Brief outlines of the experimental study carried out in this research work have been provided below:

An introduction to concrete-filled steel tubular member has been presented in **Chapter 1**. Further, the importance and need of strengthening the concrete-filled steel tubular member are briefly presented. The application and popularity of these structural members in the construction industry has been reported. Then the need of retrofitting these structural members are briefly explained. Finally, key objectives of the present investigation have been presented.

In **Chapter 2,** focused literature reviews on CFSTs, double skin CFSTs, double tube CFSTs and strengthened-CFSTs under combined axial and lateral cyclic loadings have been reported, followed by research gap areas.

In **Chapter 3,** the cyclic performance of the square partially confined CFST columns have been investigated through experimental programme. The effect of diameter and height of the inner circular steel tube on the overall performance of the partially confined CFST columns have been assessed under constant axial and lateral cyclic loadings. Key results have been presented in the form of ultimate lateral strength, energy dissipation capacity, strength degradation, stiffness degradation, ductility coefficient etc. A simplified design guidelines based on the experimental data and eurocode has been proposed to estimate the ultimate lateral strength of square partially confined CFST columns.

Similar studies have been made for circular partially confined CFST columns under constant axial and lateral cyclic loadings in **Chapter 4.**

In **Chapter 5,** an investigation was carried out on retrofitting the damaged square partially confined CFST columns presented in **Chapter 4**, under combined constant axial compressive loading and cyclic lateral loading. The effectiveness of using the novel retrofitting technique proposed in the current chapter has been assessed in terms of ultimate lateral strength and energy dissipation capacity.

In **Chapter 6,** a similar retrofitting technique as presented in **Chapter 5**, has been applied on the damaged circular partially confined CFST columns presented in **Chapter 4** and its cyclic performance have been assessed in terms of ultimate lateral strength and energy dissipation capacity.

The final chapter, **Chapter 7,** summarises the key findings from the current research work. Also the scope of future works is highlighted in the current chapter.

Appendices are also provided showing sample design calculations to estimate the ultimate lateral strength for partially confined CFST columns under combined axial and lateral cyclic loading, concrete mix design calculations, chemical compositions of the steel tubes used etc.

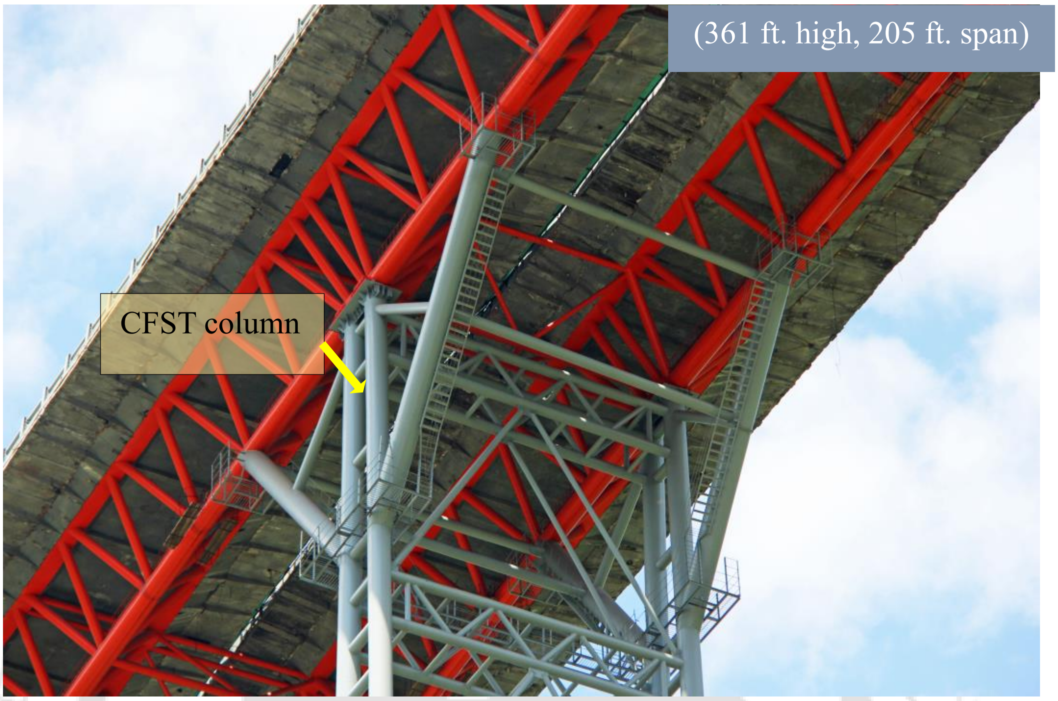

Figure 1.1: Ganhaizi Bridge, China (Source: highestbridges.com)

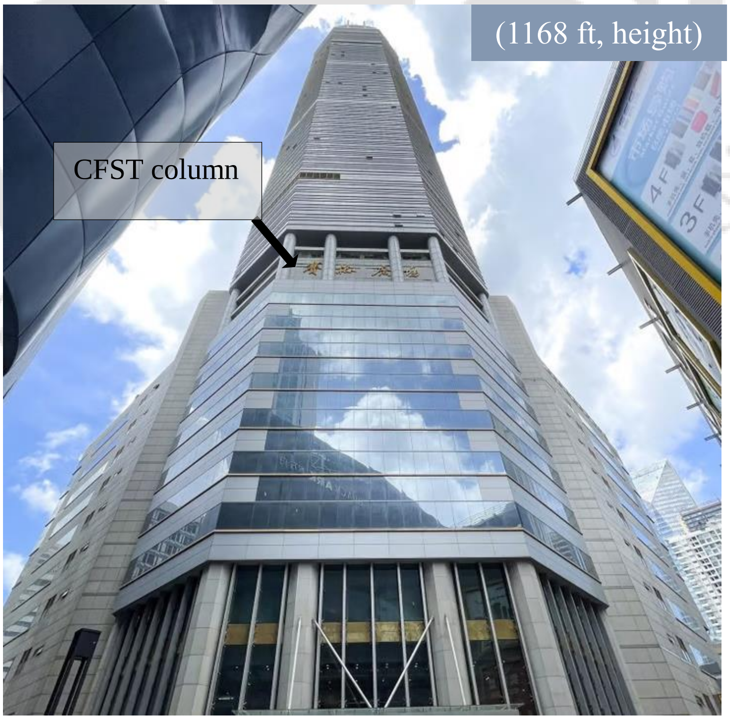

Figure 1.2: Shenzhen Plaza, China (Source: scmp.com/)

Figure 1.3: Canton Tower, China (Source: en.wikipedia.org)

Figure 1.4: Zhoushan electricity pylon, China

Chapter 2

Literature Review

2.1 INTRODUCTION

This chapter presents a review of the research activities that have been reported and are relevant to the present study. Firstly, a review of the previous research works (experimental, analytical and numerical studies) on CFST columns under combined axial compression and cyclic lateral loading have been presented. Studies on different constructional configuration of CFST columns named concrete-filled double skin steel tube (CFDST) and concrete-filled double tube (CFDT) columns under same loading condition as mentioned above were also reviewed. One of the major concern in designing the CFST column is the premature local buckling of the steel tube. To counter the same, stiffened/confined/strengthened CFST has been introduced. A brief review of the research work performed in strengthening the plastic hinge region to enhance the cyclic performance has been presented then. These CFST columns could be strengthened either internally or externally.

Due to the enhanced confinement and ductility of the CFST members, several researches have been initiated to understand their cyclic behavior (e.g. Elchalakani and Zhao 2008; Fam *et al.* 2004; Gajalakshmi and Helena 2012; Liang *et al.* 2007a; Liu *et al.* 2008; Patel *et al.* 2014; Qin *et al.* 2015; Serras *et al.* 2016; Usami and Ge

1998; Varma *et al.* 2004). Many researchers reported that CFST members subjected to cyclic loading exhibited local buckling failure at the plastic hinge zone near the support region (Hsu and Yu 2003; Varma *et al.* 2002) while the remaining part of the member was seen to remain undamaged (i.e. the post-buckling behavior of CFST members has been seen to be governed by the deterioration rate of the tube plates/walls in the plastic hinge region). Thus, the strength and stiffness of the CFST members are seen to be governed by the deterioration rate of the member at the plastic hinge (damaged / failure) region, while the remaining portion of the test length experienced elastic unloading. Hence, strengthening the plastic hinge region of the column, for improved flexural strength and energy-dissipating capacity became a focus point for many of the researchers.

A very limited literatures have been reported to enhance the strength and ductility of the columns under lateral cyclic loading; by providing external and internal stiffeners confining the plastic hinge region with either steel plates or fiber reinforced polymer (FRP) wrapping or reinforced concrete (RC) (Hsu and Yu 2003; Liu *et al.* 2021; Mao and Xiao 2006; Xiao *et al.* 2005; Xu *et al.* 2016; Yu *et al.* 2016). Zhang *et al.* 2015 observed that the cyclic performance of hybrid FRP-concrete-steel double-skin tubular column could be enhanced by filling the inner void in the plastic hinge region.

2.2 CFST UNDER COMBINED CONSTANT AXIAL AND CYCLIC LATERAL LOADING

Ge and Usami, 1996 investigated experimentally the influence of the filled-in concrete on the strength, ductility and energy absorption capacity of the partial concrete-filled steel box column under constant axial force and cyclic lateral loading. It was observed that concrete-filled steel box column exhibit prominent earthquake resistance characteristics in undergoing the inelastic action. It was also concluded that the ductility of the thin walled steel box column can be increased by filling the steel section with concrete.

Varma *et al.* 2002 experimentally investigated the seismic behavior of columns made from high strength materials. The effect of width to thickness ratio, yield stress of the steel tube and the axial load level on the stiffness strength and ductility of high strength columns were studied. It was reported that the total energy dissipated by the cyclic specimen was dominated by the flexural energy dissipated in the failure region (i.e. within 0.8D from the base of the column). A fiber based model was developed for the CFST column specimens and was found to have good agreement with the test result.

Elremaily and Azizinamini 2002 studied the behavior and failure mode/pattern of concrete-filled tube columns under constant axial load in addition to cyclic lateral load. An analytical model was developed to predict the capacity of the column accounting for the interaction between steel and concrete. It was observed that concrete strength (40-140 MPa) and axial load ratio (0.2-0.42) have very minimal effect on the energy dissipation capacity.

Han *et al.* 2003 performed an experimental investigation on Square hollow section (SHS) and rectangular hollow section (RHS) under constant axial load and cyclically increasing flexural loading. A mechanical model was developed for SHS and RHS. A parametric study was carried out on lateral load versus lateral displacement relationship. A formula for calculating the ductility coefficient of the composite member was also developed.

Varma *et al.* 2004 performed tests on high strength square beam column specimen subjected to constant axial load and cyclically varying flexural load. It was reported that the total energy dissipated by the cyclic specimen is dominated by the flexural energy dissipated in the failure region (plastic hinge region). The cyclic curvature ductility ($\mu_{\phi\text{-}c}$) decreases significantly with an increase in the axial load level. At higher axial load level, the steel tube b/t ratio and yield stress (σ_y) have a small influence on $\mu_{\phi\text{-}c}$. At lower axial load level, increasing the steel tube b/t ratio or σ_y reduces $\mu_{\phi\text{-}c}$. The failure segment for each specimen was about 20% of the length from the base, while the remaining portion of the test length unloaded elastically.

Fam *et al.* 2004 investigated experimentally the strength and ductility of CFST columns under different bond (Concrete-steel) and end loading conditions. It was reported that bond and end loading condition didn't affect the flexural strength of columns significantly. CFST Columns failed by fracture of the steel tube in the local buckling zone as a result of successive buckling and straightening. Maximum plastic hinge length observed was 13.4% of the length of the specimen.

Elchalakani and Zhao 2008 performed experimental investigation on concrete-filled cold formed steel tubes under variable amplitude cyclic pure bending. It was found that the CFT column shows a stable behavior up to local buckling and then shows considerable degradation in strength and ductility. New sectional slenderness limits for design and construction of seismic resisting structural systems were determined.

Liu *et al.* 2008 observed that the behavior (strength and ductility) of concrete-filled steel tube columns under combination of both axial loading and cyclic bi axial loading (cyclic diagonal loading). It was found that under such loading energy dissipation ability decreases with increase in axial load ratio. The moment capacity decreases as the width to thickness ratio increases.

Zubydan and Elsabbagh 2011 developed a mathematical model to evaluate the cyclic behavior of concrete-filled steel tube beam-column with rectangular cross section considering the local buckling effect of steel. The result obtained from the mathematical model was compared with the experimental data of the existing literature and was found to be in good agreement.

Gajalakshmi and Helena 2012 performed experimental investigation to quantify the cumulative damage of concrete in-filled steel tube (CFT) and steel fiber reinforced concrete in-filled steel tube (SCFT) columns subjected to lateral cyclic loading. Parameters considered are diameter to thickness ratio of the steel tube and the type of infill namely plain cement concrete and steel fiber reinforced concrete. An equation has been proposed to predict the damage index of in-filled column. Optimum volume fraction of fiber was suggested to be 1% for the steel fiber reinforced concrete. It was concluded that SCFT columns exhibit about 1.5-2 times more absorption capacity, enhance ductility and reduce damage index compares to CFT columns. Failure pattern is independent of type of infill and type of loading pattern but it is governed by diameter to thickness (D/t) ratio. Damage index of in-filled column decays with the type of in-fill and D/t ratio. Failure pattern observed for thinner tube was rupture of steel tube whereas for thicker tube it was outward buckling. It was observed that high amplitude cycles are more susceptible to number of inelastic cycles.

Wu *et al.* 2012 experimentally compared the cyclic behavior of thin walled square steel tubular columns filled with demolished concrete lumps (DCLs) and Fresh Concrete (FC). Local buckling observed within the plastic hinge occurred near the base stub. For thin wall CFST (2mm, 3mm) local buckling occurred before steel yielding whereas with thick wall CFST (6mm) no buckling before longitudinal yield was observed. For thin wall CFST bulging occurred at 4.11%-16.67% of length of the column from the bottom where as for the thick wall CFST it was about 6.25%. It was found that the lateral strength of the DCLs and FC has a tendency slightly lower than those filled with FC alone maintaining same axial ration and thickness of the tube. Energy dissipation increases with increase in the axial load ratio or the steel tube thickness up to a certain limit. The deformation capacity remains comparable with increasing the steel tube thickness maintaining same axial load ratio.

An experimental investigation was performed by Yin and Zhang 2012 on concrete-filled steel tubular column and steel beam joint under seismic loading. Specimens were designed to have strong member and weaker joint so that the damage of the joint is earlier than members and accordingly failure mode and mechanical behavior of the joint was studied.

Patel *et al.* 2014 developed numerical model for predicting the cyclic performance of high strength rectangular CFST slender beam-column under constant axial load and cyclically varying lateral load. The local and global buckling behavior of thin walled high strength rectangular beam-column was studied. It was reported that use of high strength concrete will not lead to significant increase in the cyclic lateral load capacity and flexural stiffness. Ultimate cyclic lateral load and stiffness of the CFST slender beam column decreases with the increase in the D/t ratio for the same size composite section. The lateral deflection at the ultimate cyclic lateral load increases with increase in the column slenderness ratio. By increasing the steel yield strength, the ultimate cyclic lateral load was found to be increased.

Qin *et al.* 2015 performed experimental study on concrete-filled steel tubular (CFST) columns to analyze their seismic performance and failure modes. Parameters considered were axial compression ratio, loading sequence and strength of concrete and steel. It was concluded that different axial load ratios and loading sequence have effects on the load carrying capacity, ductility, and energy dissipation capacity of the CFT columns. Failure patterns were categorized into two types such as local buckling of steel tube in compression zone and low cycle fatigue tearing rupture failure of steel tube. The failure region is found to be 30 cm (20% of the length, l/l_f=5, l is the column length and l_f is the failure length) from the bottom. It was also found that loading paths have different effect on hysteresis behavior. It was suggested that the failure height of the concrete core has correlation with diameter to thickness ratio. The small diameter to thickness ratio makes the height of core concrete increase. It was also said that the axial load level within limits has smaller effect on hysteresis behavior. Loading path has significant influence on the dissipated energy and the maximum is 40%. Dissipation energy is much closer when high strength steel and concrete is used. It was also concluded that the ductility and energy dissipation ability of the CFT column decreases with an increase of the Diameter to thickness ratio and increases with the enhancement of material properties. Failure mode and failure length of core concrete are related to the loading path and loading path is an important parameter affecting the cyclic energy dissipation of CFT column.

An analytical model was developed by Serras *et al.* 2016 for the cyclic behavior and strength capacity of circular concrete-filled steel tube (CFT) under axial load and cyclically varying flexural loading. A non-linear finite element model was created using ATENA software. Carried out an extensive parametric study to observe the hysteretic behavior of the circular CFT column.

Liao *et al.* 2017 performed experimental investigation on concrete-filled stainless steel tubular columns (CFSST) under constant axial load and cyclic lateral loading. Investigated the influence of axial load level, cross section type, and concrete type on the seismic behavior of CFSST column. The hysteretic behavior of the CFSST was compared with CFST. The cyclic behavior of specimens in-filled with recycled aggregate concrete is very similar to that of the specimen with normal concrete.

2.3 CONCRETE-FILLED DOUBLE SKIN STEEL TUBE (CFDST) AND CONCRETE-FILLED DOUBLE TUBE (CFDT)

Han *et al.* 2006 conducted experiments on concrete-filled double skin steel tubular (CFDST) column specimens under constant axial load and cyclically increasing flexural load. It was found that the lateral strength increases with increase in axial load level (n) till *n* is less than 0.3, beyond which lateral strength decreases with increase in axial load level. It was also observed that ductility coefficient decreases with increase in axial load level and decreases with the increase in hollow ratio. CFST model can be used to predict the behavior of CFDST member. An enhancement in ultimate lateral strength and energy dissipation capacity of maximum up 18% and 47% could be observed for circular CFDST columns, whereas, for the square CFDST columns it was maximum upto 19% and 48%, respectively compared to the counterpart CFST columns.

Han *et al.* 2009 carried out an analytical study on concrete-filled double skin steel tubular (CFDST) columns under constant axial load and cyclically increasing flexural load. Developed a mechanics model for predicting the behavior of CFDST columns and was found to have a good agreement with the test results.

Mathew *et al.* 2014 performed a comparative study between concrete-filled double skin steel tubular (CFDST) columns and concrete-filled steel tubular (CFST) columns under axial and varying lateral reversal load experimentally. It was found that the lateral load capacity and ductility of CFDST is enhanced by 79% and 12.8% respectively with respect to CFST.

Zhou and Xu 2016 investigated experimentally the structural performance of concrete-filled double skin stainless steel tubular (CFDSST) columns with outer square hollow section and inner circular hollow section under constant axial load and cyclically increasing flexural loading. The effect of the test parameters on the lateral load versus lateral displacement envelope curves, ductility coefficient, dissipated energy, and stiffness degradation have been investigated. It was concluded that the axial load level and thickness of outer tube have a primary influence on the behavior of the test specimens while the hollow ratio and concrete strength have a little effect when the axial load level is low. An outward bulging Failure mode/pattern was observed at the bottom of the specimen. It was also found that specimens with lower axial compressive load level dissipated more energy and had better ductility.

2.4 STRENGTHENING OF THE CFST COLUMNS

2.4.1 Longitudinally arranged strengthening technique for CFST columns

The seismic performance of CFST column with two type of internal longitudinal stiffener has been investigated experimentally; a) with a longitudinal stiffener on each inner face of the steel tube and b) with one longitudinal stiffener on two opposite faces of the steel tube (Zhang *et al.* 2007). The difference in ultimate lateral strength exhibited by the unstiffened column and the two-stiffener columns was not very significant. However, CFST columns with four- stiffener columns showed enhanced ductility and energy dissipation capacity compared to the unstiffened CFST.

Wang *et al.* 2017b studied the seismic performance of the CFST column stiffened with binding bars through experimental and analytical investigations. Local buckling of the steel tube was effectively restrained by the binding bar depending on the longitudinal spacing of the binding bar. As a result, the local buckling of the columns with binding bars are significantly delayed. CFST columns with binding bars exhibited higher lateral bearing capacity, higher stiffness and better energy dissipation capacity. With the decrease in the spacing of the binding bar, the ultimate lateral strength and the energy dissipation capacity was found to have improved. The ultimate deformation capacity of the CFST with binding bars were also found to be higher than the corresponding CFST column.

2.4.2 Internally strengthening technique at plastic hinge region

Hsu and Yu 2003 carried out an experimental investigation to study the seismic performance of square CFST with restrained plastic hinge region. The study comprised of using cross restraining rods at the plastic hinge region. A three dimensional finite element simulation was carried out in ABAQUS to determine the plastic hinge length of the member. It was reported that the major buckling zones of the unstiffened specimens located within 0.45D to 0.95D (D is the depth of the cross section). One and two layers of restraining rods were placed at either 0.25D or 0.25D and 0.5D respectively to study the influence of the restraining rods. Based on the experimental results it was found that the tie rods were effective in restraining the excessive plate deformation and delaying local buckling of the columns. The lateral strength and stiffness were not much influenced by the application of tie rods. However, the energy dissipation capacity was significantly enhanced. It was also found that tube with excessive width to thickness ratio should be avoided so that fracturing and tearing can be prevented. It was also observed that lesser width to thickness ratio exhibit higher energy dissipation enhancement.

Liu *et al.* 2021 studied the seismic behavior of square concrete filled steel tubular column internally stiffened with diagonal rib and circular liner through experimental and numerical simulation. The stiffener region was confined upto a height equivalent to the width of the outer section (1D). Seven square CFST columns were evaluated experimentally considering the parameters; stiffener type, width-to-thickness ratio of steel tube and axial load ratio. Based on the experimental results it was observed that the stiffened columns exhibited excellent seismic performance with higher lateral resistance, better ductility, and greater energy dissipation capacity compared to the unstiffened counterpart columns. It was seen that the columns with diagonal ribs suffered weld fracture at large drift angle however the circular liner stiffener was effective and showed ductile behavior at large drift angle. It was also reported that all the specimens failed due to severe buckling of steel tube and crush of concrete at the plastic hinge region. The ultimate lateral strength and energy dissipation capacity of the columns were found to have improved with a decrease in the width-to thickness ratio of the steel tube. Increasing the axial load ratio of circular liner stiffened columns upto 0.4, improves the lateral strength but reduces the ductility coefficient. However axial load ratio beyond 0.4 to 0.6 does not have much effect on the result discussed above.

Han *et al.* 2022 performed an experimental study on the CFST columns internally strengthened by a stiffener under cyclic lateral loading while subjected to constant axial loading. The proposed cruciform stiffener constituting two steel plates with trapezoidal cutout fixed to the steel tube by external welding at the potential plastic hinge region. The height of the stiffener was ~1B (B being the width of the outer square steel section). The stiffener could effectively delay the local buckling of the steel tube and change its local buckling mode. For the CFST column the local buckling was confined upto a length of about 0.5B whereas for the internally strengthened columns, buckling was also observed above the stiffened region. Lateral load capacity was also found to be significantly enhanced by introducing the stiffeners. It was reported that thinner the section, higher the effect of the stiffener on the ultimate lateral capacities.

2.4.3 Externally strengthening technique at plastic hinge region

Xiao *et al.* 2005 performed a series of tests on circular confined CFST column under seismic loading. It was aimed to control the local buckling of the steel tube at the potential plastic hinge region resulting to higher seismic performance. Carbon-fiber-reinforced plastic (CFRP) was used to provide additional confinement to the potential plastic hinge region of the columns. The length of the confinement zone was approximately taken as the diameter of the steel tube section which was approximately 20% of the length of the column from the bottom end. It was demonstrated that the seismic performance could be significantly improved and the local buckling and the subsequent rupture of the steel tube could be effectively delayed using additional CFRP confinement to the CFST column. The local buckling and the confinement mechanism was examined with a proposed simple analytical model.

Mao and Xiao 2006 performed an experimental investigation to study the seismic behavior of confined concrete-filled tubular column (CCFT) under combined constant axial and cyclic lateral loading. The confinement was provided externally using thick plate stiffeners, steel stripe stiffeners and steel angle stiffeners at the potential plastic hinge region (~0.85B, B being the width of the square steel section which is approximately 20% of the clear height of the column). The additional confinement enhanced the ductility of the column (~ 67%). However, no significant improve in the lateral strength or stiffness was observed.

Yu *et al.* 2016 performed an experimental study on fiber-reinforced polymer (FRP) wrapped circular CFST columns under seismic loading. CFST columns were wrapped with glass FRP (GFRP) and Carbon FRP (CFRP) upto a height of 1.5D (D, diameter of the outer steel tube). It was seen that FRP jacket could effectively delay the local buckling failure. Columns with relatively thick FRP jacket, the buckling deformation was forced by the FRP jacketing to appear above the FRP jacketed region. The seismic performance of the CFST columns in term of ductility and energy dissipation capacity could be significantly enhanced with the FRP confinement.

2.5 SUMMARY

Based on the literature review, it has been seen that, several studies have been made on CFST columns under combined axial compression and lateral cyclic loadings. However, studies on strengthening the plastic hinge region under cyclic loading is very limited and systematic study is lacking. The details of the studies on confining potential plastic hinge region has been summarized in Table 2.1. Studies reported confining the plastic hinge region externally may affect the aesthetics, outer column dimensions and indoor floor space, whereas confining plastic hinge internally may require additional welding/fastener (e.g. Liu *et al.* 2021) to hold the stiffener. Furthermore, investigation on retrofitting the damaged CFST columns were not reported in the public domain.

Table 2.1: Summary of studies on confining plastic hinge region

Authors	Study type	Section *B* or *D* (mm)	Thickness, *t* (mm)	f_y (MPa)	f_{ck} (MPa)	Parameters considered	Stiffener type	Plastic hinge length or confined length
Xiao et al. 2005	E'	C, (336, 326)	3, 6	303, 312	39.1, 28	t, with/without CFRP	External- CFRP	~ *0.89D*
Liu et al. 2021	E', N'	S, (326-365)	2.25-3.5	326-365	58	Stiffener type, width to thickness ratio	Internal- Diagonal rib, circular liner stiffener	~ *1.1B*
Xu et al. 2016	E'	H, (171, 307)	3.95, 7.50	262-718	52.5	Height of outer RC component	External- RC component	~ *2B, 3B*
Yu et al. 2016	E'	C, (318)	3	271	31-36	with/without CFRP, GFRP	External- GFRP, CFRP	~ *1.57D*
Hsu and Yu 2003	E'	S, (280)	6, 4.5, 3.2	321	34	Width to thickness ratio, single or double layer of tie rods	External- Tie rods	~ *0.25D, 0.5D*
Mao and Xiao 2006	E'	S, (350)	6	256	40	Stiffener type, thickness of stiffener	External- steel plate, steel strip, steel angle	~ *0.86B*

E'=Experimental, N'=Numerical, C=Circular steel section, S=Square steel section, f_y= Yield strength of steel, f_{ck}=cylinder compressive strength of concrete, CFRP=Carbon-fiber-reinforced polymers, GFRP=Glass-fiber-reinforced polymers, D=Diameter of the circular section, B=Width of the square section.

Chapter 3

Partially Confined Concrete-Filled Steel Tubular Square Columns under Lateral Cyclic Loading

3.1 INTRODUCTION

The column is an important structural element and carries the compressive load. However, under seismic loading, it is also acted upon by lateral cyclic loading. CFST columns are most suited structural member under lateral cyclic loading because of its various advantageous characteristics as mentioned in Chapter 1. Therefore, an extensive study on the CFST columns under lateral cyclic loading have been performed (e.g. Elchalakani and Zhao 2008; Fam *et al.* 2004; Gajalakshmi and Helena 2012; Liang *et al.* 2007b; Liu *et al.* 2008; Patel *et al.* 2014; Qin *et al.* 2015; Serras *et al.* 2016; Usami and Ge 1998; Varma *et al.* 2004 etc.) and presented in Chapter 2. It was observed that under lateral cyclic loading, the failure of the CFST column occurs due to the formation of a plastic hinge near the support of the column (e.g. Hsu and Yu 2003; Varma *et al.* 2002; Wu *et al.* 2012). Therefore, there is a need to confine the column at the plastic hinge region to delay the local buckling and inelastic deformation of the column. A very limited studies on confining the plastic hinge region (e.g. Hsu and Yu 2003; Liu *et al.* 2021; Mao and Xiao 2006; Xu *et al.*

2016; Yu *et al.* 2016 etc.) mostly confined externally have been reported so far (thereby affecting the aesthetics and outer column dimensions). Most of the confining techniques involves huge welding work which may affect the ductility and energy dissipation capacity of the columns.

Hence in the present chapter, an innovative, internally strengthening technique has been introduced to strengthen the plastic hinge region of the square CFST column using a circular hollow steel tube (see Figure 3.1). The structural performance of the strengthened square CFST named partially confined concrete-filled steel tubular (PCCFST) columns under constant axial and cyclic lateral loading has been assessed in terms of ultimate lateral strength, energy dissipation capacity and ductility. The parameters varied in the present study are: diameter and height of the inner circular steel tube. Based on the experimental results obtained, an eurocode (Eurocode 4 1994) based simplified design guideline has been proposed.

3.2 DESCRIPTION OF THE TEST CAMPAIGN

3.2.1 Specimen details

The experimental campaign consisted of 8 columns: 7 partially confined concrete-filled steel tubular (PCCFST) square columns and 1 concrete-filled steel tubular (CFST) column. All these specimens consisted of square hollow section (SHS) steel tubes with measured outer width (*D*) and thickness (*t*) of 114 mm and 4.06 mm, respectively. The clear height (*H*) of the specimens was 650 mm (length between the top of the stiff reinforced concrete footing (i.e. column end) to the location of lateral load application (i.e. column head)). All the 7 PCCFST specimens were provided with one inner circular hollow section (CHS) steel tube (having diameter, D_i, of 60 mm or 50 mm and thickness, t_i, of 3.2 mm) each, welded concentrically at the base plate. The height of inner CHS was taken as ~ 0.5D, 1D, 1.5D, and 2.5D from the column end. No inner steel tube was provided to the CFST specimen. Two separate batches of concrete mix were prepared, one for the RC footing and another for the CFST and PCCFST specimens. The concrete mix for the RC footing was designed for a higher grade (cube strength, f_{cu} of ~ 39 MPa) of concrete so that the footing (fixed support) does not fail during the test. All the specimens were subjected to combined constant axial compression and cyclically varying lateral loading. To maintain uniformity in comparison, all the specimens were provided with the same axial load level (n = 0.02). The axial load level (n) in this chapter is defined by equation 3.1.

$$n = \frac{N_0}{N_u} \tag{3.1}$$

where N_0 is the axial load applied to the specimen and N_u is the axial compressive capacity of the specimen. The value of N_u was determined by taking the average compressive strength of square CFST stub columns of the same cross-section tested in a 3000 kN hydraulic compression testing machine (CTM). The compressive strength test set-up and the results obtained have been shown in Figure 3.2 and Figure 3.3, respectively. The average N_u of the CFST stub column was found to be 1152 kN. The effect of partial confinement while determining the compressive capacity has been ignored, as the partial confinement length for PCCFST specimens was relatively smaller when compared to the column's length to be tested (H_i/H ~ 0.09-0.43). Nomenclature of the specimen follows the form Sx-cy-z, where ‘Sx’ represents square outer steel tube of ‘x’ width, ‘cy’ represents the circular inner steel tube of ‘y’ diameter, and ‘z’ represents the height of the inner steel tube. For example, S114-c60-1.5D means a square outer steel tube of 114 mm width provided with a circular inner steel tube of diameter 60 mm till 1.5D height from the column end. As mentioned before, the outer SHS and inner CHS steel tube thickness was 4.06 mm and 3.2 mm, respectively. The specimen with no inner steel tube was named S114-c0. Due to the limitation of the test set-up, only small-scale specimens could be tested.

3.2.2 Material properties

3.2.2.1 Steel tubes

Commercially available square hollow section (SHS) tubes and circular hollow section (CHS) tubes were procured from the local market. All the steel tubes used in the test campaign are cold-formed. The mechanical properties of all square and circular hollow section tubes were investigated through a standard tensile coupon test according to ASTM E8 2016. A series of coupon specimens were prepared from the extract of square and circular hollow tubes. All the coupon specimens were tested in a displacement-controlled method in a universal testing machine (UTM) of 250 kN capacity. The displacement rate of 0.05 mm/min in the elastic range and 0.4mm/min beyond that was maintained until failure, as recommended by Huang and Young 2014. The tensile test set-up for the coupon specimens has been shown in Figure 3.4. The engineering stress strain curve generated from the tensile coupon specimens have been shown in Figure 3.5 and Figure 3.6. The average mechanical properties based on the tensile coupon tests in terms of yield strength, f_y, and ultimate strength, f_u, are presented in Table 3.1. Based on the experimental results, the grades of the steel tubes used were YSt 210 for SHS (IS 4923, 2009) and YSt 210 for CHS (IS 1161 1998).

3.2.2.2 Concrete

Due to the limited testing capacities of the machines available, a normal strength (cube strength, f_{cu} of ~ 20-40 MPa) concrete was decided to be used for the experimental tests presented herein. A trial concrete mix was prepared (IS:10262 2009) with Portland pozzolana cement, river sand (medium coarse), and granite stones of specific gravity 2.92, 2.59, and 2.63, respectively, with a water-cement ratio of 0.52. Six 150 mm concrete cubes were prepared from the same mix, cured, and tested after 28 days. The trial mix resulted in an average compressive strength of ~ 31 MPa. However, the cubic compressive strength (f_{cu}) was converted into cylinder compressive strength (f_{ck}) by multiplying a factor of 0.8. The cylindrical compressive strength obtained was used in section 3.4, to calculate the ultimate lateral strength. The same concrete mix has been used to cast all the CFST and PCCFST specimens. A coarse aggregate of MSA (maximum size aggregate) 10 mm was used to facilitate the workability during compaction. The mix proportion of concrete used is shown in Table 3.2.

3.2.3 Preparation of test specimens

Procured square and circular steel tubes were originally of length 6 m. A length of 1300 mm was cut from the square steel tube (S-114), which provided a clear height of 650 mm. Inner CHS steel tubes (c-60 and c-50) of height H_i (~ 0.5D, 1D, 1.5 D and 2.5D) plus the depth of the footing was also cut from the 6 m length original pipe. The average geometrical dimensions of all the PCCFST and CFST specimens are shown in Table 3.3. D, t, and H are the outer diameter, thickness, and clear height of the outer square hollow section (SHS) steel tube, respectively. D_i, t_i, and H_i are the outer diameter, thickness, and height of the inner CHS steel tube, respectively. The ends of the cut specimens were machined to avoid any undulations. The insides of the steel tubes were brushed to remove any loose debris or rust present. A 200 mm × 200 mm square steel base plate of thickness 4 mm was welded at the bottom of the specimen for better grip of the specimen with the reinforced concrete (RC) footing. The inner CHS tube was first welded to the center of the base plate at the bottom. A steel ‘spacer’ was fabricated to be used between concentric tubes to ensure uniform spacing between them. The spacer connected with a wire was then placed on the inner tube, the outer tube was placed from the top, and both tubes were welded to the same square base plate. The spacer was then removed once the welding of the outer tube was completed.

Formwork for RC footing of length 1550 mm, width 400 mm, and depth 350 mm was made to support the bottom of the specimen (to achieve fixed end support). The embedded length of the specimens into the footing was 350 mm (~ 3D). A minimum embedded length of 0.75D-0.9D is suggested to avoid cone pull-out failure and allow ductile tearing of the CFST specimen (Lehman and Roeder 2012; Stephens *et al.* 2016). Two specimens were cast using a single footing (see Figure 3.7) because of the constraints associated with the availability of strong floor fixture slots to economize the cost and for the better frictional grip of the footing to the strong floor. Welded steel tubes were then placed and centered in the formwork of the footing to be cast. The square steel tube was placed in the formwork in such a way that the single line welding of the square tube was either in the front or in the backside of the set-up (the welding line lies neither in compression nor in tension side) to maintain the symmetricity of the member. The footing of the specimens was first cast, followed by concreting of the tubular specimens in 3 layers. Each layer was compacted using a 12 mm diameter steel rebar attached to a 40 mm vibrator needle. A typical specimen is shown in Figure 3.7(b). Three 150 mm cubes of each batch were also cast during the concreting to check the concrete strength. The cubes and the CFST were kept for 28 days of curing under ambient temperature. During curing, a very small amount of longitudinal shrinkage of about 1-2 mm occurred at the top surface of the column. Gypsum paste was used to fill this longitudinal gap before testing so that the concrete surface was flush with the steel tube at the top, to enable proper contact between loading plates and the specimen top.

3.2.4 Test set-up and instrumentation

All the specimens were tested at the Structural Engineering Laboratory of Indian Institute of Technology Guwahati. The schematic view and photograph of the test set-up are shown in Figure 3.8. A fixed end support to the CFST column specimen has been provided at the bottom with the help of a near rigid RC footing, whereas a hinge support at the top *via* the actuator head has been provided. The footing was then laterally restrained by two steel supports (lateral restraints) to ensure no lateral slippage condition during the test. Additionally, two modified steel I sections (press down support) were designed to press the footing down and avoid the footing overturning. At the top, the axial load was applied using four loading plates, stacked one above another on a thick plate having a square groove on the other face of the plate (total deadweight of the loading plates being 2208 Kg or 22 kN) to hold the specimen. The axial loading was maintained constant throughout the test. Along with constant axial loading, cyclic lateral loading was also applied following AISC 2016 loading protocol, which is discussed in the following section (i.e. section 3.2.5). To impose lateral cyclic displacement to the specimen, two separate halves of a highly stiffened steel box with a concentric square hole (holder) that perfectly grips the column were pushed against the column and connected together using four high-strength bolts. This holder connects the specimens to the MTS actuator (250kN capacity and 500 mm stroke length). The lateral displacement imposed and the lateral force of resistance was measured by an inbuilt transducer and a load cell in the actuator, respectively. One displacement laser sensor was also used externally to measure the displacement of the column head at the loading level. Additionally, one linear variable displacement transducer (LVDT) was used to monitor the lateral displacement of the RC footing. Moreover, to monitor the yielding of the outer steel tube at the plastic hinge region, strain gauges were fixed for each specimen at the height of 50 mm and 150 mm (on both the diametrically tension and compression side) from the column end, respectively. Figure 3.9 illustrates the layout of the instrumentation. All the specimens tested showed a very ductile behavior, and testing proceeded in a smooth and controlled manner.

3.2.5 Loading pattern

After fixing the specimen on the strong floor with all the supports connected, all the strain gauges, laser sensors, and LVDTs were fixed. Axial compression was applied and maintained constant throughout the test. Displacement controlled lateral cyclic loading as per AISC 2016 was applied at the column head of the specimen, following those in the literature for similar studies (Narendra and Singh 2017; Park *et al.* 2010; Silva *et al.* 2016). Six cycles were applied for each 0.00375, 0.005, and 0.0075 radians of drift angle (θ, where, $\theta=\Delta/H$, Δ is the lateral displacement at the column head and H is the clear height of the specimen measured between column head and column end), followed by four cycles of 0.01 and two cycles of each 0.015 and 0.02 radians drift angle respectively. For the rest of the test, two cycles for each 0.01 increase in drift angle were provided (see Figure 3.10). A constant loading rate of 1 mm/sec was applied to maintain a near quasi-static loading condition. Trial runs with a slower loading rate e.g. 0.25 mm/sec, did not result in a significant change in the hysteresis pattern. The test continued until the lateral load dropped to 80% of the peak lateral load or the specimen failed (indicated by significant visible local buckling or tearing of the steel tube near the column end support).

3.3 EXPERIMENTAL RESULTS

3.3.1 General

The experimental observations and results are presented and discussed here in this section. The actuator's pull direction is defined as the positive direction, while the push direction is the negative direction. The specimens with the outer diameter of inner CHS of 60 mm and 50 mm were named c-60 series and c-50 series specimens, respectively. Specimen with no inner steel tube termed as c0 specimen. Specimens with 0.5D, 1D, 1.5D, and 2.5D height of inner CHS are termed as 0.5D, 1D, 1.5D, and 2.5D specimens, respectively. For the ease of observation, a 10 mm ×10 mm white grid was plotted on the surface of the outer steel tube up to a height of 150 mm (or ~1.32D) from the column end.

3.3.2 Failure modes

The typical failure mode/pattern of the test specimens has been shown in Figure 3.11 (I, II, and III show the steel tube buckling, concrete crushing, and inner CHS member, respectively). Near the column end of all the specimens, the formation of plastic hinge (indicated by outward local buckling of the steel tube at the loading faces) could be seen. The formation of member's plastic hinge region may be directly related to the decrease of the lateral resistance for increasing level of deformation. For the c0 and 0.5D specimens, the visible initiation of the outward local buckling of the outer steel tube was observed at the drift angle of 3%, whereas, for 1D, 1.5D, and 2.5D specimens, the initial buckling of the outer steel tube appeared at 4% drift angle. The initial appearance of the visible buckling corresponds to the maximum lateral load. Immediately after the peak load was reached, the plastic hinge region appeared to have formed, as indicated by the appearance of local outward buckling of the outer steel tubes near the column end region. After reaching peak lateral load, with the gradual increase in drift angle, the buckling of the outer steel tube became more apparent and formed an outward (inward buckling was prevented by the presence of the inner concrete core) local buckled ring gradually at that region. The bulges on the steel tube grew rapidly at the moment when the specimen was close to failure. From the failure modes of all the specimens, it could be concluded that by providing an inner tube to the CFST specimen, the buckling phenomenon could be delayed.

Figure 3.11(II) shows the surface and the sectional cut-views of core concrete after the outer steel tube was removed. From the sectional cut views located at the base of the column, it could be seen that the desired compaction of the concrete core was achieved both inside and outside of the inner tube. It has been seen that for the 0.5D specimens, the concrete was seriously crushed at the location where the outer steel tube buckled (Level-1, region where outer steel tube buckling occurred near the column end), similar to c0 specimen. At the same time, no severe damage was observed in other parts of the specimen. But in addition to the concrete crushing at level-1, 1D and 1.5D specimens showed concrete crushing at the height of 1D and 1.5D region (level-2, region at the height of inner CHS) from the column end of the specimen, respectively. Unlike 1D or 1.5D specimens, 2.5D specimen showed crushing of concrete only at level-1. From the above discussion, it could be concluded that since the height of inner CHS of 0.5D specimens lies within the buckling region of the c0 specimen, therefore, the concrete crushing was at level-1 only (similar to c0 specimen). Whereas, the height of inner CHS for the 1D and 1.5D specimens, lies outside the buckling region of c0 specimen. Therefore, after the crushing of concrete at level-1, the inner CHS contributed to the desired stiffness, and the column end support is partially shifted to level-2, where crushing of concrete is observed in subsequent drift angles. But for 2.5D specimen, crushing of concrete was observed at level-1 only, possibly because it reached the optimum height of CHS (before 2.5D height), which could be provided to partially shift the column end support for the given CFST section. It could be seen from Figure 3.11(III) that the inner CHS in any specimen did not buckle locally.

3.3.3 Lateral load-displacement (P-Δ) hysteretic curves

The measured lateral load (P) versus displacement (Δ) at the level of lateral load, hysteretic curves for all the tested specimens have been shown in Figure 3.12. The hysteretic loops of the tested specimens were of plump type under cyclic loading and no obvious pinching effects were seen. It can also be clearly seen that there is an initial elastic response, and the lateral load-displacement relation can roughly be considered linear. The stiffness gradually degraded as the response entered the inelastic range.

3.3.4 Strength degradation

Under the same cyclic displacement, the loss of strength was observed at the successive loading loop and is termed as strength degradation, measured in terms of strength degradation coefficient (λ). The strength degradation coefficient for all the specimens was calculated as per equation 3.2 (e.g. (Xu *et al.* 2016).

$$\lambda_i = \frac{P_i^{j+1}}{P_i^j} \tag{3.2}$$

Where P_i^j is the peak load of the j^{th} cycle for the i^{th} drift angle. As six cycles were engaged for the first three drift angle and four cycles for the fourth drift angle, so, for the strength degradation coefficient calculation, the first two cycles of each drift angle were considered. For the rest of the drift angles, only two cycles were provided, so both the cycles were used for the calculation.

The average strength degradation coefficient (compression and tension side) has been plotted against the lateral displacement in Figure 3.13. It could be clearly seen that, for drift angle, less than 2% (stage-I), the strength degradation coefficient is almost constant, and close to unity. Whereas for drift angle ranging from 2% to 5% (stage-II), there is a sharp drop in strength degradation coefficient. For drift angle, greater than 5% (stage-III), the rate of strength degradation coefficient is reduced and remains approximately the same thereafter. The possible reason could be, at stage-I, there was no serious damage to the concrete, but during stage-II, severe concrete damage has occurred, and by the time stage-III has reached, maximum damage had already occurred, so there was no sharp drop at stage-III. Similar strength degradation pattern could be seen for all the specimens. However, from the figure mentioned above (Figure 3.13), strength degradation for the column with H_i equal to 0.5D, and column without inner CHS (H_i = 0) were found to be lower than those specimens with H_i equal to 1D, 1.5D or 2.5D height.

3.3.5 *P*-Δ envelope curves

P-Δ envelope curve for all the tested specimens have been depicted in Figure 3.14. Table 3.4 shows the ultimate lateral strength (P_u) obtained in all the tests, calculated as the average value of the positive and negative maximum lateral loads obtained from *P*-Δ envelope curves. The ultimate lateral strength of c-60 series specimens with the height of inner CHS as 0.5D, 1D, 1.5D, and 2.5D were found to have an enhancement of ~ 6.7%, 13.2%, 15.3%, and 16%, respectively with respect to the c0 specimen (Figure 3.14(a)). It could be seen from the above results that on increasing the height of inner CHS beyond 1.5D, does not exhibit much improvement in lateral strength (<1%). Since 2.5D height of inner CHS is likely to be higher than the expected plastic hinge region hence not contributing much to the lateral strength enhancement. Therefore, for the c-50 series, specimen with 2.5D inner CHS height was not included. The ultimate lateral strength of c-50 series specimens with the height of inner CHS as 0.5D, 1D, and 1.5D were found to have an enhancement of ~ 4%, 10.3%, and 12.3%, respectively with respect to c0 specimen (Figure 3.14(b)). From the above discussion, it could be stated that the enhancement in ultimate lateral strength was due to the increased confinement to the plastic hinge region as a result of the increase in inner tube height. The enhancement continued till the plastic hinge was entirely confined by the inner CHS. Once the plastic hinge region was entirely confined, further increase in the height of inner CHS does not significantly contribute to the strength enhancement.

The effects of the diameter of inner CHS on the overall performance of the PCCFST specimens were studied. One specimen from each of the c-60 series and c-50 series with 1.5D height of inner CHS was considered for the comparison (see Figure 3.14(c)). It has been observed that the diameter to width ratio of inner tube to outer tube (D_i/D = 0.44 & 0.53, for S114-c50-1.5D and S114-c60-1.5D respectively) has very minimal effect on the envelope curve, though specimen S114-c60-1.5D possess slightly higher (~ 2.6%) ultimate lateral strength compared to S114-c50-1.5D specimen. This indicates that the ultimate lateral strength could be enhanced by increasing the area of confinement. Possibly, to optimize the lateral strength, D_i/D

could be raised to a value such that the maximum size of aggregate could be easily placed and compacted. The ultimate lateral strength of both the c-60 series and c-50 series specimens have been plotted on the same graph with respect to H_i/D ratio (0-0.25) in Figure 3.15. It could be inferred that the use of partial double tube approach could improve the lateral strength by maximum ~ 15.3% for the specimen considered.

3.3.6 Stiffness degradation

The average stiffness (secant stiffness) has been used as a measure of the stiffness of the members at different lateral displacement levels. The average stiffness of members was calculated using equation 3.3 (Qian *et al.* 2014; Zheng *et al.* 2018).

$$K_i = \frac{|P_i| + |-P_i|}{|\Delta_i| + |-\Delta_i|} \tag{3.3}$$

where, P_i and Δ_i are the peak load and corresponding lateral displacement at the i-th displacement loading level (drift angle), respectively. + and – sign denote the push and pull directions, respectively.

The stiffness (K) versus lateral displacement (Δ) curves for all the tested specimens have been shown in Figure 3.16. It could be seen that the stiffness of all the specimens drops as the lateral displacement increases due to the cumulative damage occurring at the expected plastic hinge region near the support. Stiffness deterioration of all the specimens was found to follow a similar nonlinear pattern. It has been observed that on increasing the height of inner CHS, the stiffness also increases. It may be due to the increase in the height of the inner CHS, the confined region along the height increases, which contributes to the additional stiffness of the member. Therefore, the stiffness of PCCFST specimens was slightly higher compared to the CFST specimen (c0 specimen).

Figure 3.16(c) indicates that the diameter to width ratio of inner tube to outer tube (D_i/D) as a whole has little effect on the stiffness degradation. Specimen S114-c60-1.5D has slightly higher (~ 5.1%) initial secant stiffness corresponding to S114-c50-

1.5D specimen. This could possibly be because of higher steel confinement provided by the 60 mm diameter CHS at the plastic hinge region.

3.3.7 Energy dissipation capacity

The distribution of energy dissipation corresponding to each drift angle with respect to lateral displacement for all the tested specimens has been shown in Figure 3.17. It has been seen that for all the specimens, 15% drop in peak lateral load has occurred within 9% drift angle. Therefore, energy dissipated is calculated up-to the last cycle of the 9% drift angle to maintain uniformity in comparison. The cumulative energy dissipation capacity obtained from the test data has been summarized in Table 3.4. The cumulative energy dissipated by c-60 series specimens with the height of inner CHS as 0.5D, 1D, 1.5D, and 2.5D was found to have an enhancement of ~ 5.2%, 8.4%, 11.4%, and 13% respectively with respect to the c0 specimen (see Figure 3.17(a)). Similarly, the cumulative energy dissipated by c-50 series specimens with the height of inner CHS as 0.5D, 1D, and 1.5D was found to have an enhancement of ~ 4%, 6.8%, and 9%, respectively with respect to c0 specimen (see Figure 3.17(b)). This shows that on increasing the height of inner CHS, the energy dissipation capacity of the PCCFST specimen could be significantly enhanced. Energy dissipation capacity depends on the region where the plastic hinge is expected to form, and strengthening that region with additional steel confinement improves the property.

The distribution of energy dissipated by specimens S114-c60-1.5D and S114-c50-1.5D corresponding to each drift angle was found to be very similar (see Figure 3.17(c)). However, specimen S114-c60-1.5D is found to possess slightly higher (~ 2.2%) cumulative energy dissipation capacity with respect to S114-c50-1.5D. This could be because of the higher steel confinement provided by the 60 mm inner CHS tube. The cumulative energy dissipation capacity of both the c-60 series and c-50 series have been plotted on the same graph with respect to H_i/D ratio for comparison (Figure 3.18). From the above, it could be concluded that by providing an inner CHS member, the energy dissipation capacity of the CFST member could be enhanced. The data obtained from the LVDT reading showed a support slippage of approximately a maximum of 2 mm for higher displacement for the specimen S114-

c60-1D. A correction has been applied considering the corresponding support slippage to each individual cycle while calculating the energy associated with it.

3.3.8 Ductility coefficient

The displacement ductility coefficient (μ) of the specimens has been assessed as per the expression given in equation 3.4 (Han *et al.* 2006; Liao *et al.* 2017).

$$\mu = \frac{\Delta_u}{\Delta_y} \tag{3.4}$$

Where, Δ_y= yield displacement, Δ_u= displacement when the lateral load falls to 85 % of the ultimate lateral strength. The P-Δ envelope curve of the tested specimens did not exhibit an obvious yield point. Thus, the displacement corresponding to the intersection of the two tangents between the elastic segment line and peak loading tangent has been taken as yield displacement (see Figure 3.19). The μ value for each specimen has been taken as the average value from the push and pull direction of cyclic loading. It has been observed that there is an enhancement in ductility coefficient of ~ 8% - 10% for H_i/D ratio up to 1.5 with respect to c0 specimen. Computed ductility coefficients are listed in Table 3.4 and plotted in Figure 3.20.

The ductility coefficient of all the specimens is larger than 4.5, demonstrating that all the specimens have good seismic performance. Moreover, the ductility behavior of the CFST (c0) specimens could be enhanced by providing an inner CHS tube up to a height of 1.5D from the column end.

3.3.9 Strains

Typical lateral force versus outer SHS steel tube strain (P-ε) hysteretic loops of the tested specimens has been shown in Figure 3.21, where the positive and negative values of the strains correspond to tension and compression, respectively. The strains were measured by the strain gauges, mounted at the height of 50 mm and 150 mm (on both the diametrically tension and compression side) from the column end, respectively. B1 and B2 represent the strain gauge mounted diametrically at the height of 50 mm, whereas T1 and T2 represent the strain gauge mounted diametrically at the height of 150 mm from the column end. It has been seen that the significant outer steel buckling occurred near the column end, which was reflected in the strain corresponding to B1 and B2 of the (P-ε) hysteretic loops. The PCCFST columns with no inner tube and 0.5D height of inner CHS have not shown significant strain at 150 mm height. In contrast, the PCCFST column with 1D and 1.5D height of inner steel tube showed considerable strain at 150 mm height, which supports the observation reported in section 3.3.2.

From Figure 3.22, it can be clearly seen that the yielding of the outer steel tube of the PCCFST column with no inner tube and 0.5D height of inner CHS starts at 3% drift angle. In contrast, for the columns with 1D and 1.5D height of inner CHS, the yielding starts at 4% drift angle, which supports the observation reported in section 3.3.2.

3.4 SIMPLIFIED DESIGN RULE BASED ON EUROCODE

It has been observed from the failure modes and experimental results that by providing partial confinement to the CFST column, the effective clear height could be reduced. The effect is similar to the shifting of support fixity (as mentioned in section 3.3.2). A simplified design rule has been proposed to predict the ultimate lateral strength of the PCCFST columns with 1.5D height of inner steel tube based on the code provision, (Eurocode 4 1994) and the limited experimental results herein. The height of the inner steel tube has been taken as 1.5D, since it has been seen that for the height of the inner steel tube beyond 1.5D, the increase in ultimate lateral strength is not very significant (see Figure 3.15). As per the simplified design rule, the ultimate lateral strength could be calculated as per the expression given in equation 3.5.

$$P_u = \frac{M_{Euro}}{(\beta - 1.5D)\alpha} \tag{3.5}$$

where, α, β, and γ are the effective length ratio, effective length correction factor, and the normalized strength ratio of the CFST column, respectively (see equation 3.6-3.8). Where α is obtained empirically by fitting a linear curve ($R^2 = 1$) (refer Figure 3.23).

$$\alpha = \frac{\beta}{\beta - 1.5D} - 0.0033D_i \tag{3.6}$$

$$\beta = \frac{M_{Euro}}{P_{0,Euro}\gamma} \tag{3.7}$$

$$\gamma = \frac{P_{u0,Exp}}{P_{u0,Euro}} \tag{3.8}$$

M_{Euro} is the maximum moment capacity of the CFST column under N_0 applied axial load as per Eurocode 4 1994. M_{Euro} can be calculated as per the equation given in 3.9a, 3.9b or 3.9c, based on the limits of applied axial load.

If $N_0 \geq A_c f_{ck}$

$$M_{Euro} = \frac{N_u - N_0}{N_u - A_c f_{ck}} M_p \tag{3.9a}$$

If $0.5A_c f_{ck} < N_0 < A_c f_{ck}$

$$M_{Euro} = M_p + \frac{A_c f_{ck} - N_0}{0.5A_c f_{ck}} \left(M_{max} - M_p\right) \tag{3.9b}$$

If $N_0 \leq 0.5A_c f_{ck}$

$$M_{Euro} = M_p + \frac{N_0}{0.5A_c f_{ck}} \left(M_{max} - M_p\right) \tag{3.9c}$$

Where, N_0 , N_u, M_p, and M_{max} are the applied axial load, section capacity, plastic moment capacity and maximum bending capacity of the concrete-filled steel tubular column, respectively. All these values can be calculated from the equations given below (equation 3.10-3.15). Where, A_a and A_c are the area of steel tube and core concrete at the cross-section. f_y, and f_{ck} is the yield strength of steel tube and cylinder compressive strength of the concrete core, respectively.

$$N_u = A_a f_y + A_c f_{ck} \tag{3.10}$$

$$M_p = M_{RHS} + f_y t \frac{1}{2}(D - 2t)^2 (1 - F_{RHS})^2 + \frac{1}{2}(D - 2t) d_n^2 f_{ck} \tag{3.11}$$

$$M_{RHS} = f_y t\left[D(D-t) + \frac{1}{2}(D-2t)^2\right] \tag{3.12}$$

$$d_n = \left(\frac{D-2t}{2}\right)F_{RHS} \tag{3.13}$$

$$F_{RHS} = \frac{1}{1+\frac{1}{4}\frac{f_{ck}}{f_y}\frac{D}{t}} \tag{3.14}$$

$$M_{\max} = M_{RHS} + \frac{1}{2}(D-2t)\left[\frac{D-2t}{2}\right]^2 f_{ck} \tag{3.15}$$

The ultimate lateral strength (P_u) obtained from the tested specimens has been compared with the predicted values (P_{ue}) based on the proposed design rule (see Table 3.5). It should be noted that the code provision was for concrete-filled steel columns under constant axial load and monotonically increasing flexural loading. The purpose for which the comparison was made was to evaluate their accuracy in predicting the capacity of the concrete-filled steel specimens. From Table 3.5, it could be concluded that the proposed design rule can predict the ultimate lateral strength capacity of the PCCFST column accurately (Mean = 0.993, COV =0.0047).

3.5 CONCLUSIONS

In this chapter, the cyclic performance of PCCFST (partially confined concrete-filled steel tubular) specimens (i.e. short inner concrete core confinement near the support) were studied. The effect of height and diameter of inner confining CHS (circular hollow section, $H_i/D=0\text{-}2.5$ and D_i/D=0.44-0.53) on the ultimate lateral strength, strength degradation, stiffness degradation, energy dissipation capacity, and ductility coefficient was reported. The following conclusions have been drawn based on the experimental investigation of the PCCFST columns.

1) The ultimate lateral strength is found to increase with the increasing height of inner CHS. For a height of inner CHS, 1.5D, (where D is the width of the outer steel tube) the enhancement was found to be ~ 15.3% with respect to the CFST specimen.

2) The energy dissipation capacity has been found to have enhanced with increasing height of inner CHS. Approximately 11.4% enhancement with respect to the CFST (without inner CHS) specimen could be observed for the height of inner CHS up to 1.5D.
3) For 1.5D height of inner tube, a Ductility coefficient enhancement of ~ 9.6% has been observed with respect to the CFST specimen.
4) Beyond 1.5D height of the inner tube, the enhancement in the cyclic performance is found to be mild (<1 %).

Table 3.1: Average mechanical properties of hollow steel tubes used

Specimen ID	t (mm)	D/t	f_y (MPa)	f_u (MPa)
S-114	4.06	28.08	300.00	370.00
c-60	3.2	18.75	362.70	397.73
c-50	3.2	15.63	365.16	395.75

Table 3.2: Mix proportion of concrete

Materials	Cement	Fine aggregate	Coarse aggregate	Water
Quantity (kg/m^3)	400.0	916.1	792.4	208

Table 3.3: Average geometrical dimensions

Specimen ID	D (mm)	t (mm)	H (mm)	D_i (mm)	t_i (mm)	H_i (mm)	D_i/D	n	N_0 (kN)
S114-c0	114	4.06	650	-	-	-	-	0.02	22
S114-c60-0.5D	114	4.06	650	60	3.2	57	0.53	0.02	22
S114-c60-1D	114	4.06	650	60	3.2	114	0.53	0.02	22
S114-c60-1.5D	114	4.06	650	60	3.2	171	0.53	0.02	22
S114-c60-2.5D	114	4.06	650	60	3.2	285	0.53	0.02	22
S114-c50-0.5D	114	4.06	650	50	3.2	57	0.44	0.02	22
S114-c50-1D	114	4.06	650	50	3.2	114	0.44	0.02	22
S114-c50-1.5D	114	4.06	650	50	3.2	171	0.44	0.02	22

Table 3.4: Experiment findings

Specimen ID	P_u (kN)	E (kN.m)	μ
S114-c0	49.00	54.98	6.43
S114-c60-0.5D	52.28	57.83	6.62
S114-c60-1D	55.46	59.59	6.92
S114-c60-1.5D	56.47	61.23	7.05
S114-c60-2.5D	56.84	62.08	7.11
S114-c50-0.5D	50.96	57.20	6.49
S114-c50-1D	54.03	58.71	6.99
S114-c50-1.5D	55.02	59.90	6.99

Table 3.5: Comparison of the experimental values with the predicted values obtained from the simplified design rule

Specimen ID	Pu (kN)	Simplified design value	
		P_{ue} (kN)	$\frac{P_{ue}}{P_u}$
S114-c0	49.00	48.85	0.99
S114-c60-1.5D	56.47	56.42	0.99
S114-c50-1.5D	55.02	55.12	1.00
Mean			0.993
COV			0.0047

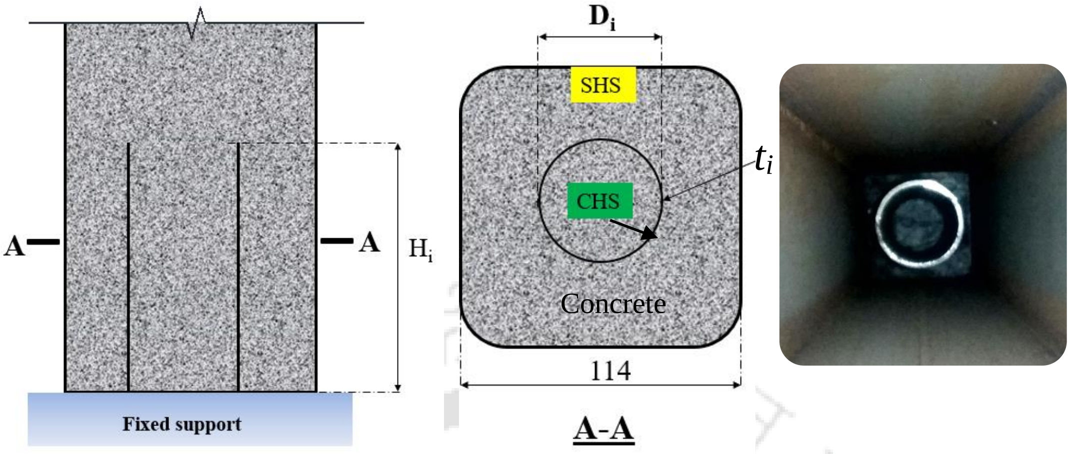

a) Front view b) Section A-A c) Inner view from top

Figure 3.1: Partially confined concrete-filled steel tubular square column (i.e. short inner concrete core confinement near the support)

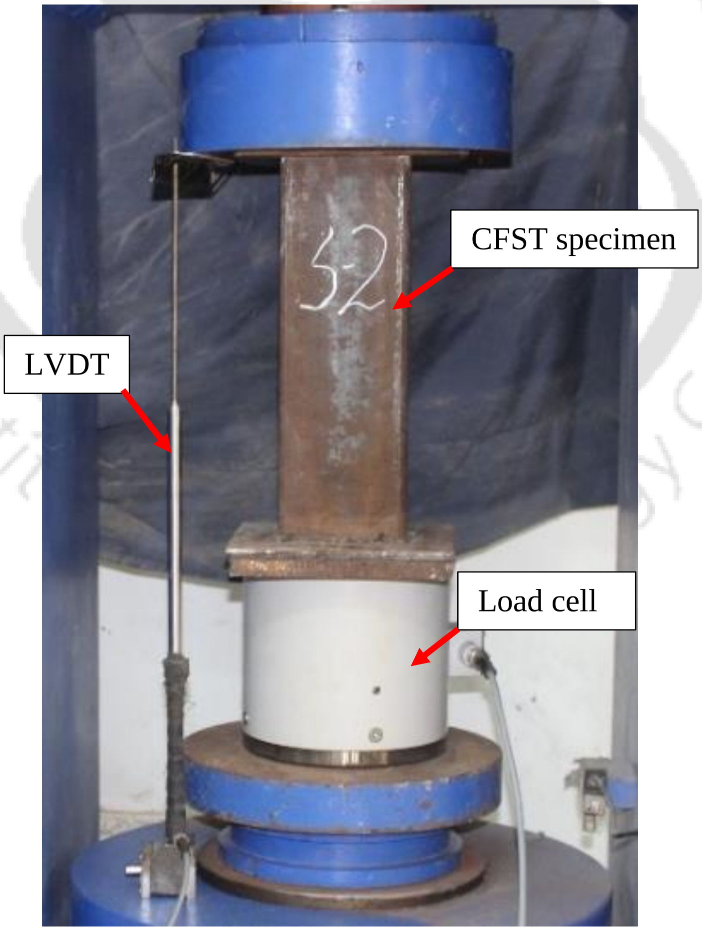

Figure 3.2: CFST specimen under axial compression

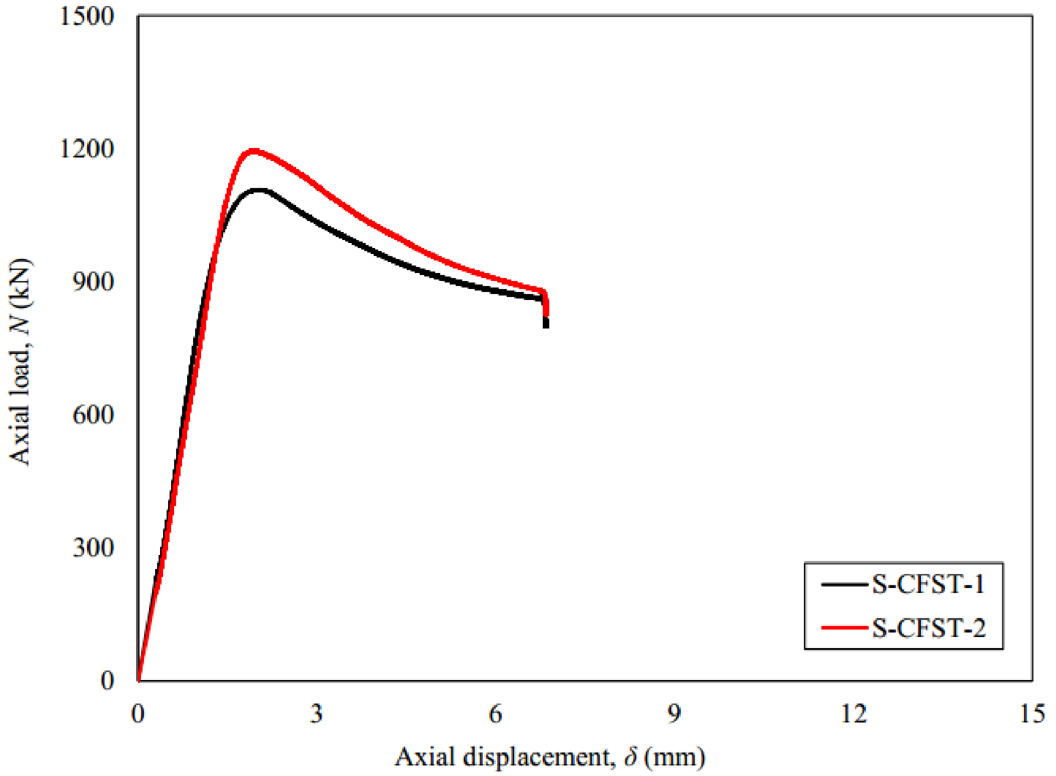

Figure 3.3: Load Vs Deformation curve of Square CFST

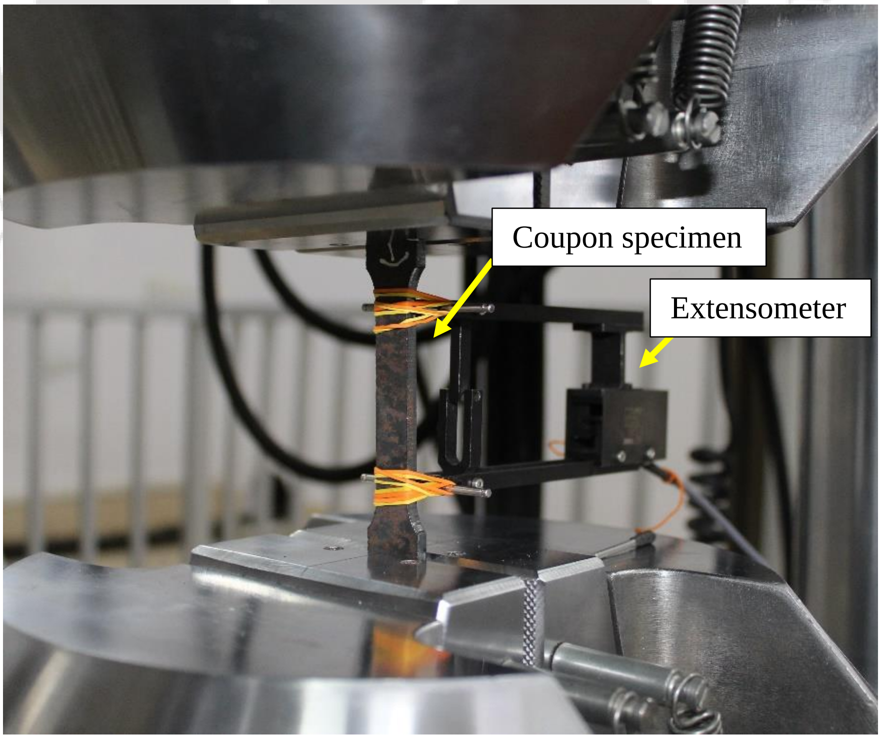

Figure 3.4: Tensile test set-up

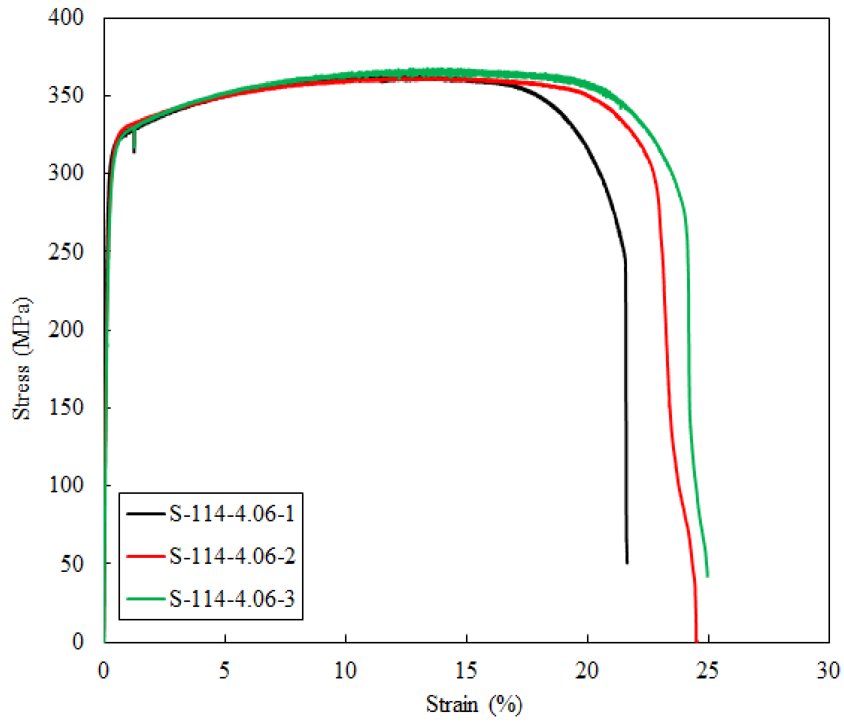

Figure 3.5: Engineering stress-strain curve generated from the tensile coupon test of outer square steel tube

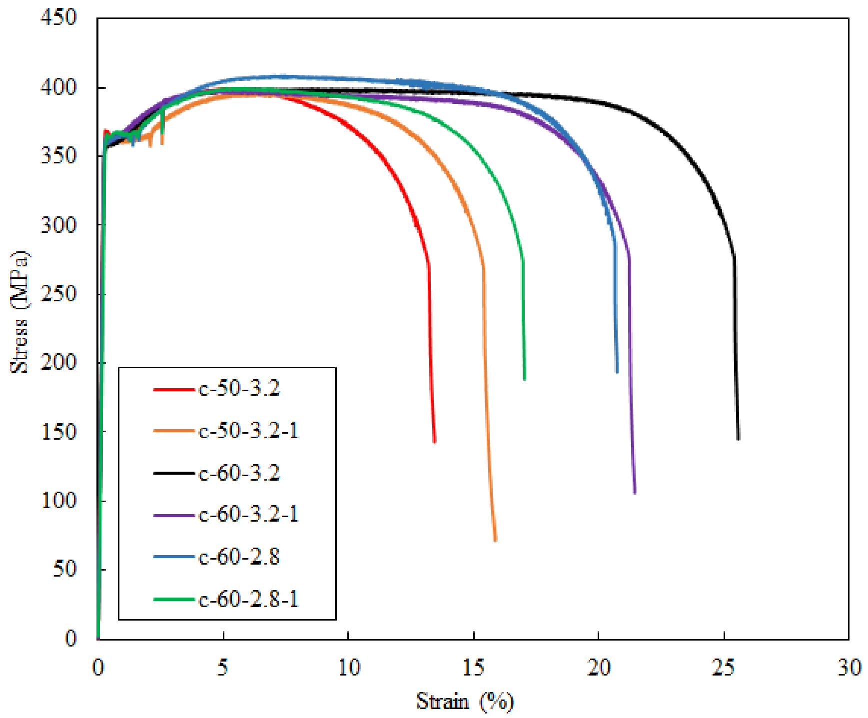

Figure 3.6: Engineering stress-strain curve generated from the tensile coupon test of inner circular steel tube

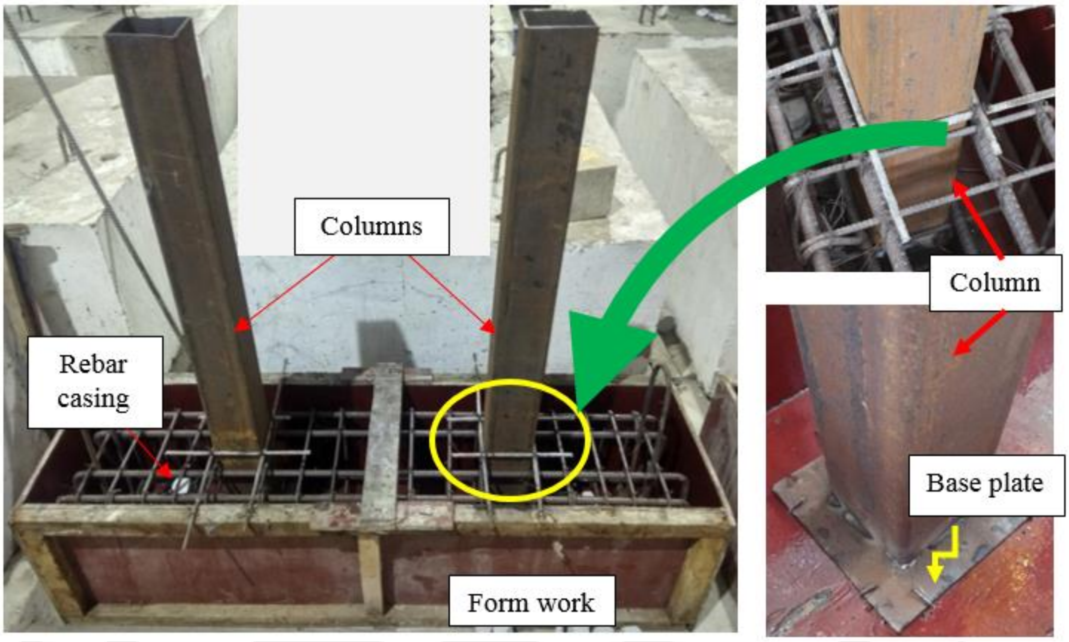

(a) Assembling of components

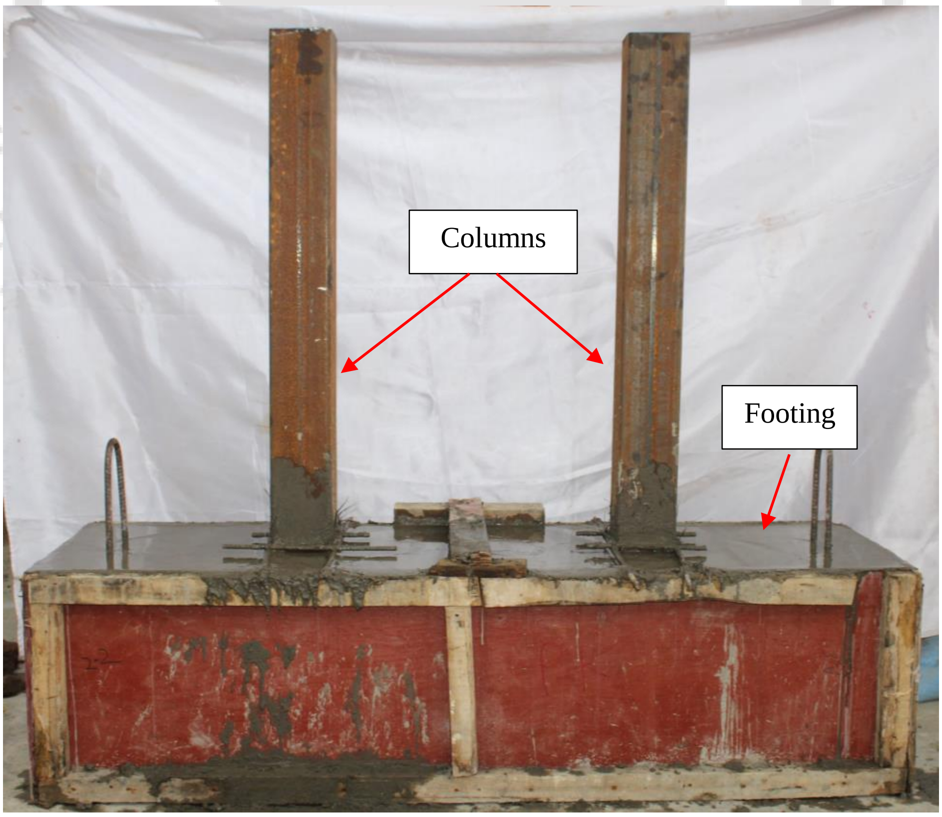

(b) Cast specimen

Figure 3.7: Specimen preparation

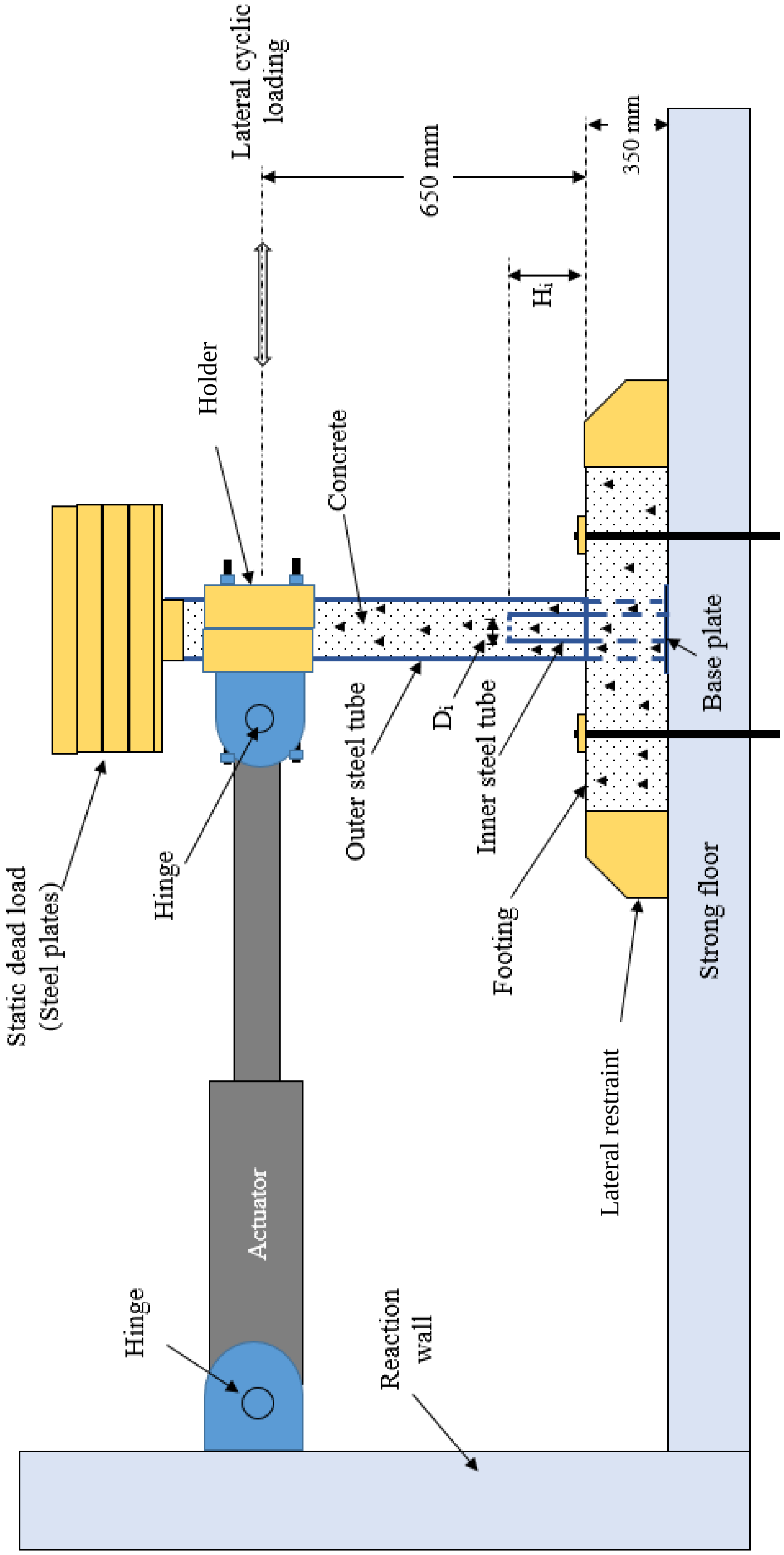

(a) Schematic view

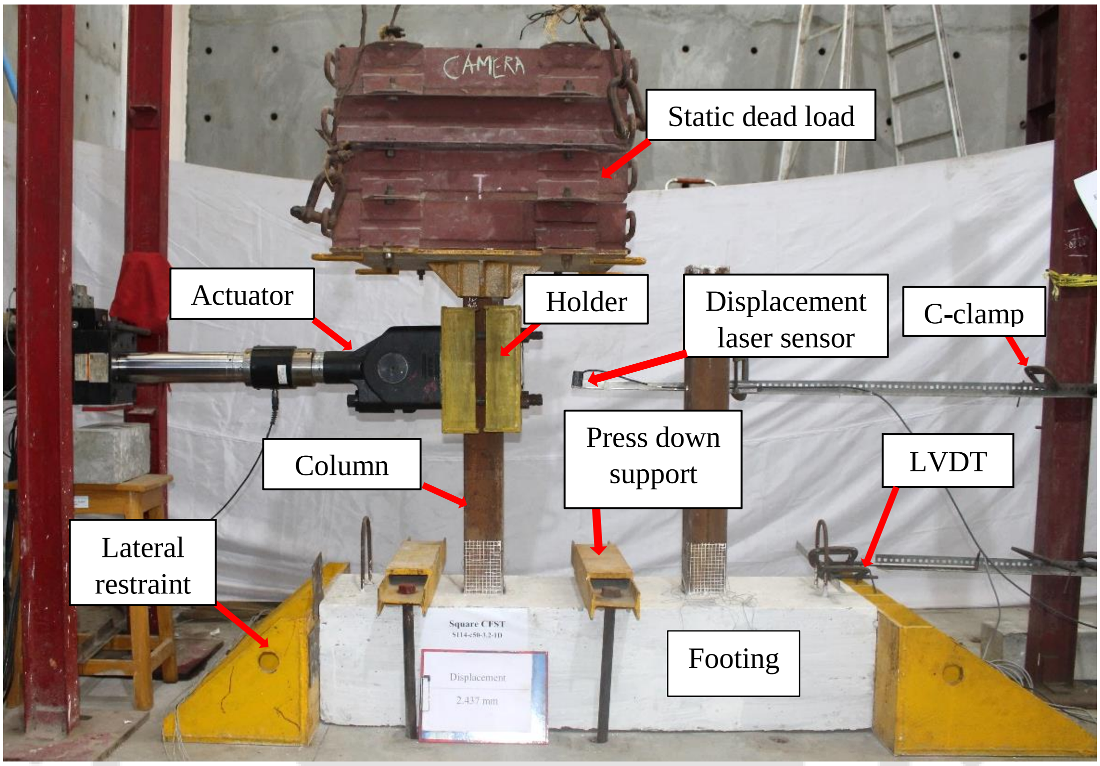

(b) Photograph

Figure 3.8: Lateral cyclic test set-up

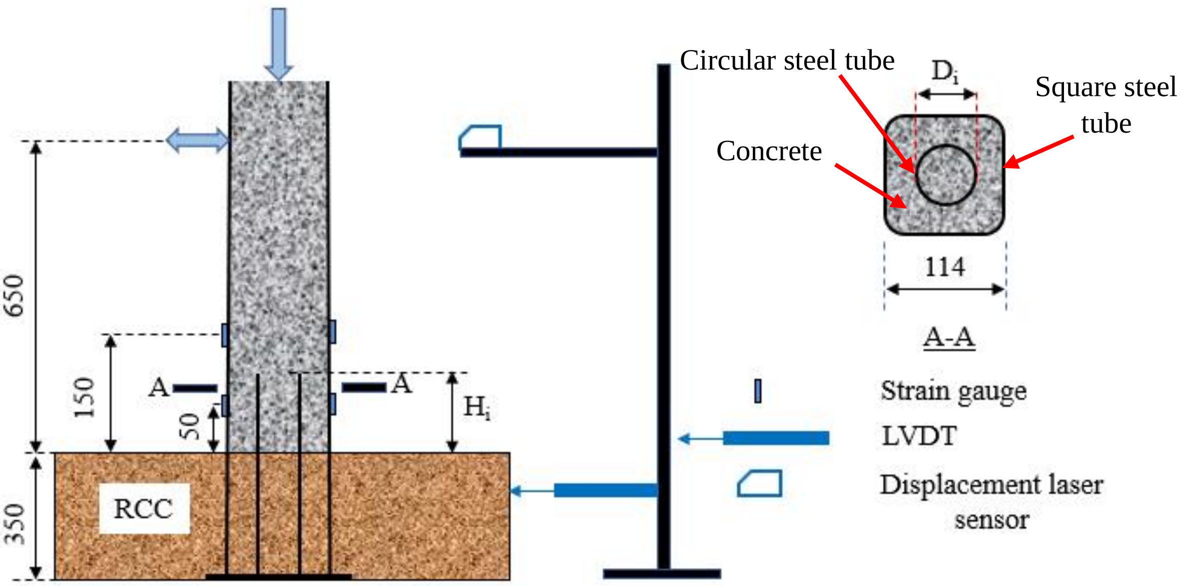

Figure 3.9: Configuration of typical specimen and instrumentation (unit: mm)

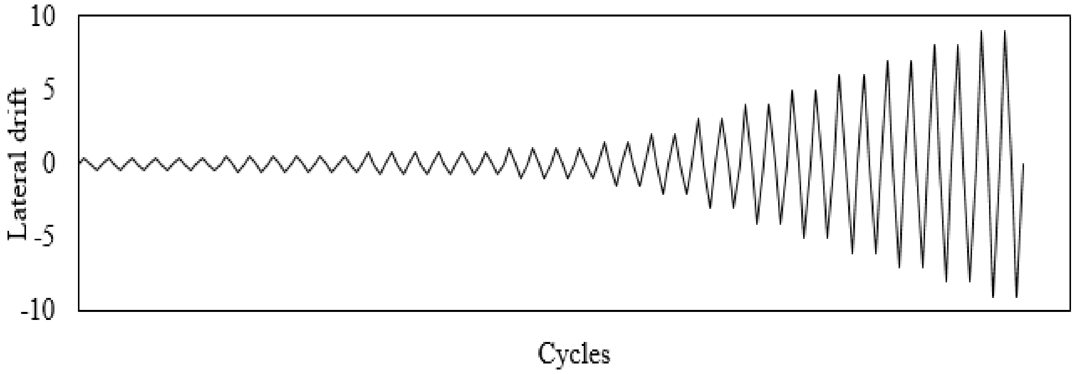

Figure 3.10: Cyclic loading protocol (AISC 341, 2016)

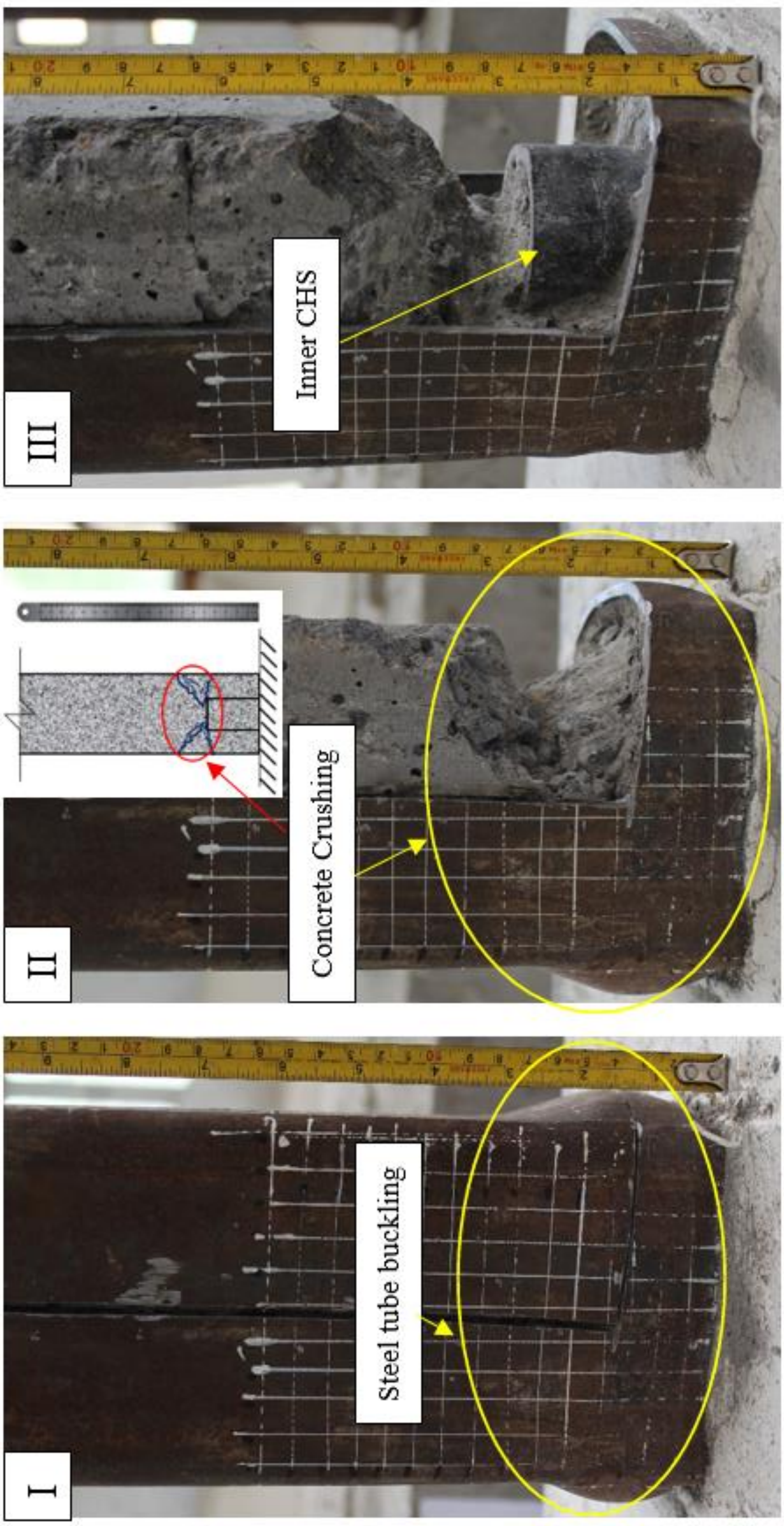

(a) S114-c60-0.5D

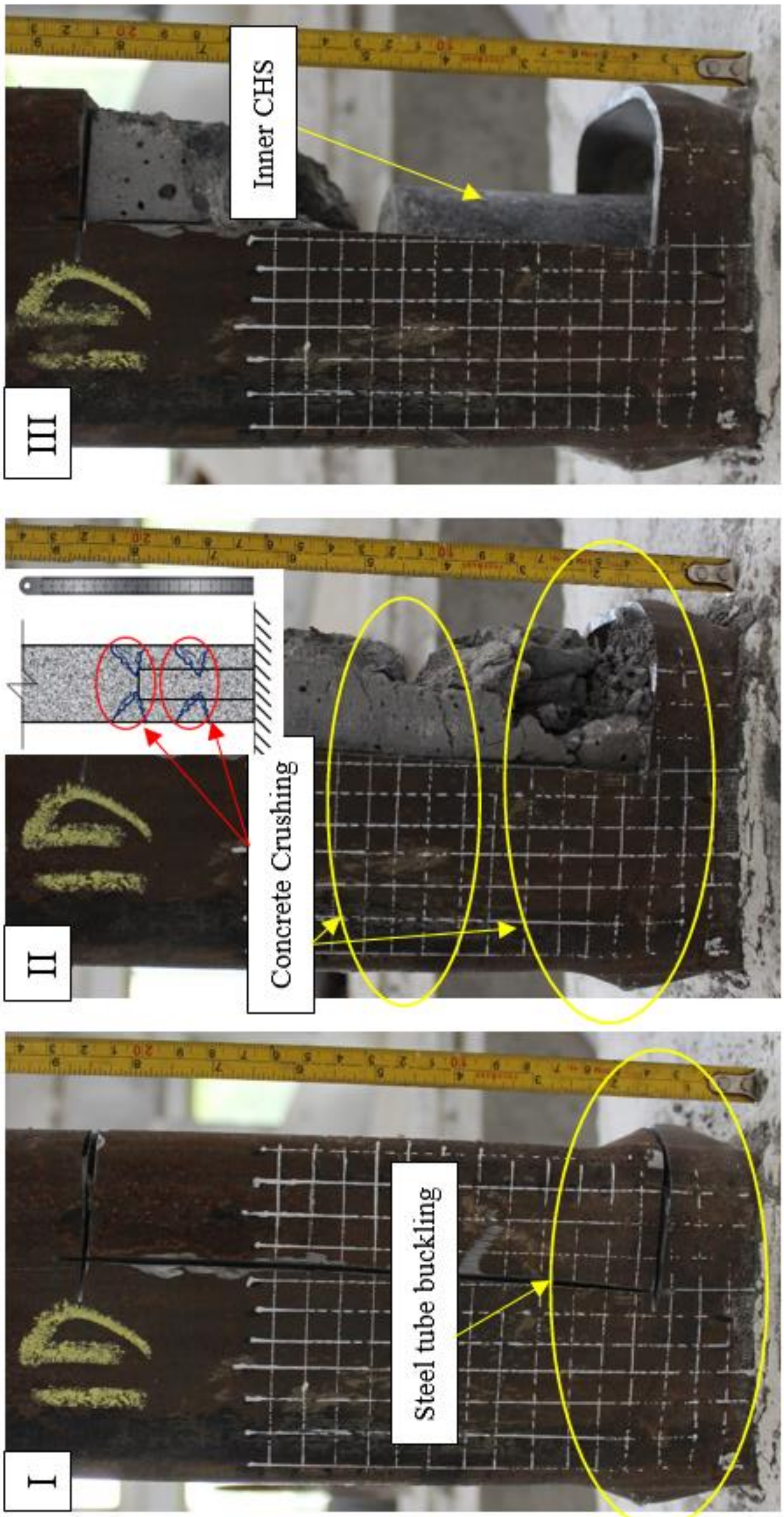

(b) S114-c60-1D

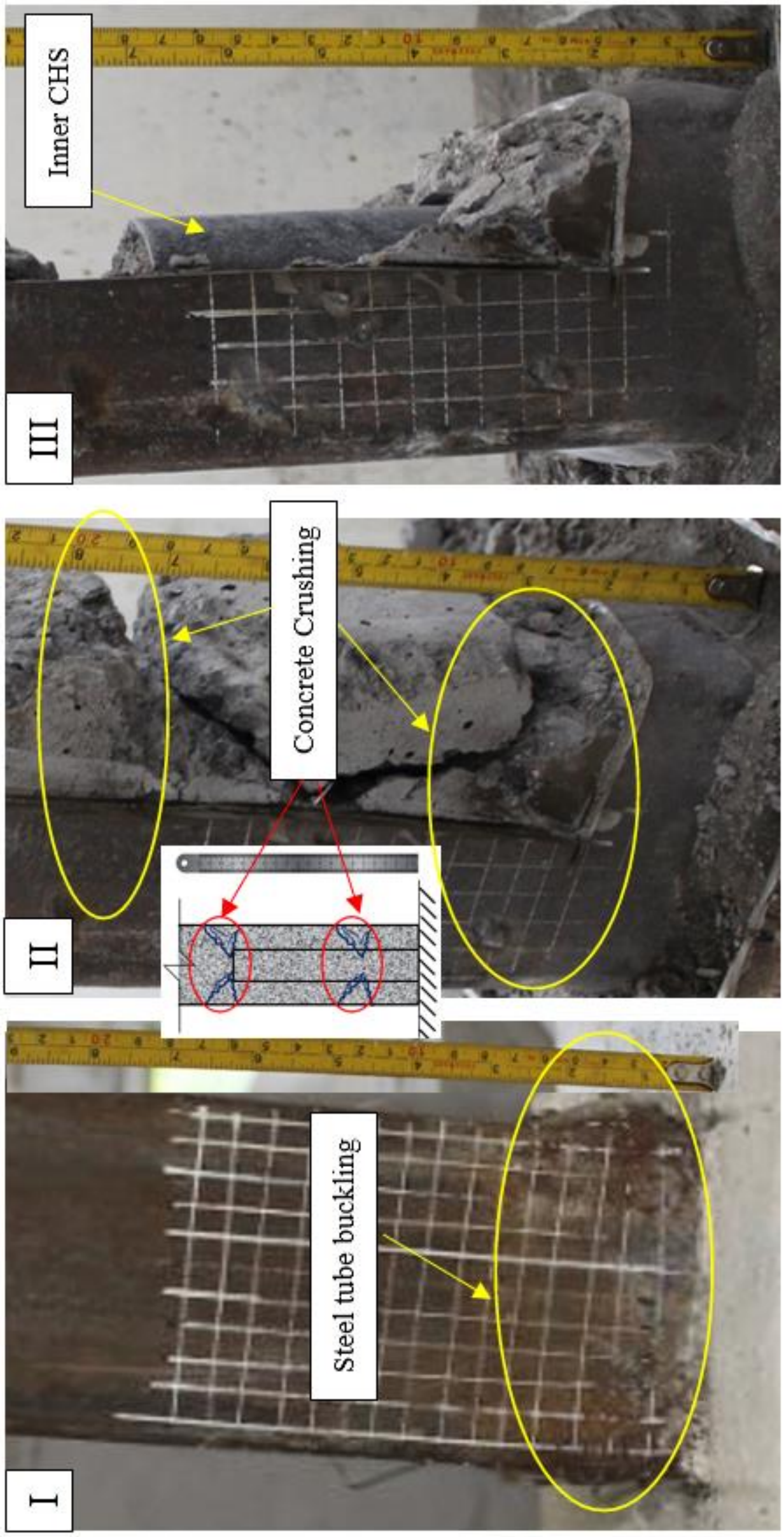

(c) S114-c60-1.5D

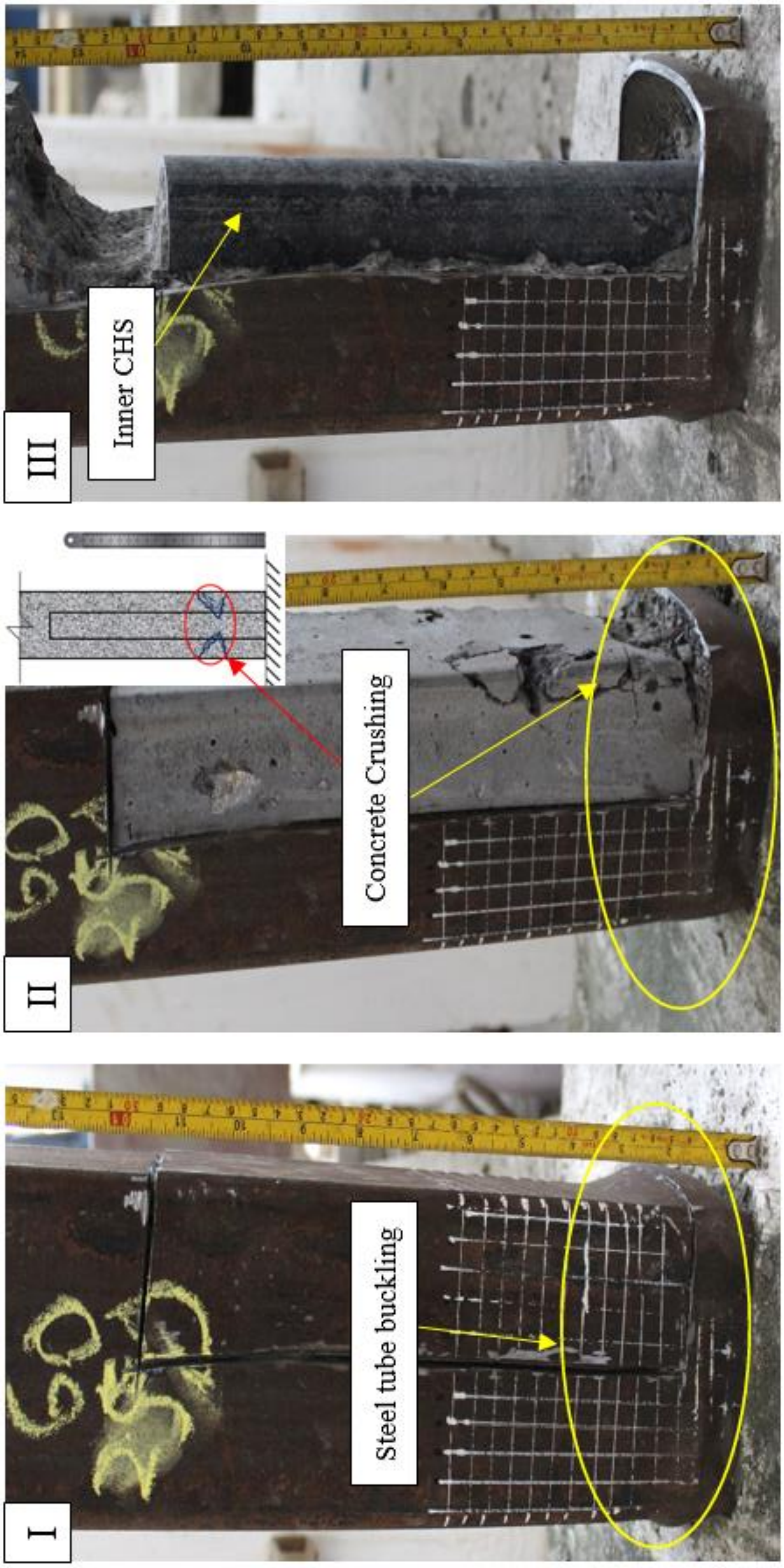

(d) S114-c60-2.5D

Figure 3.11: Typical failure mode of tested square PCCFST specimens

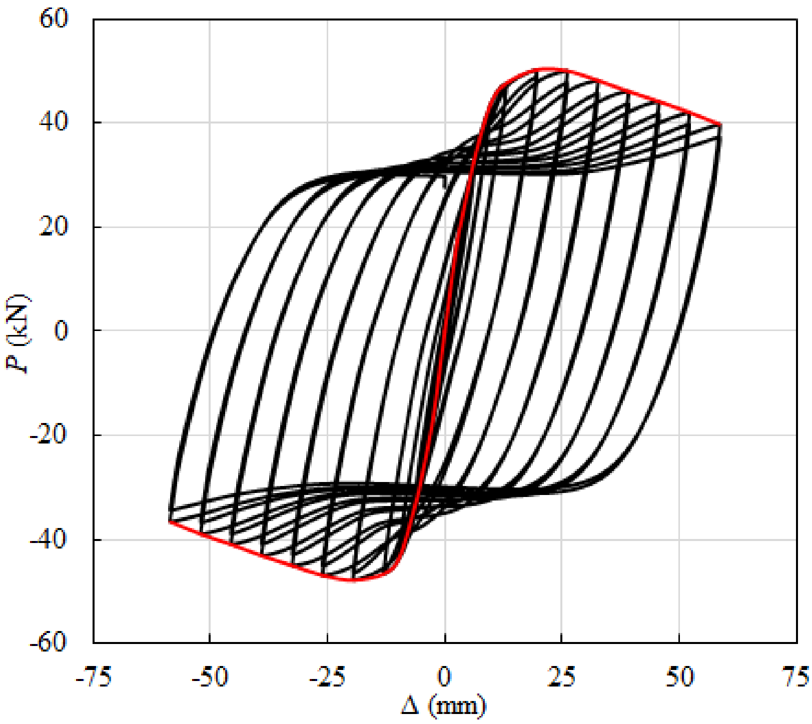

(a) S114-c0

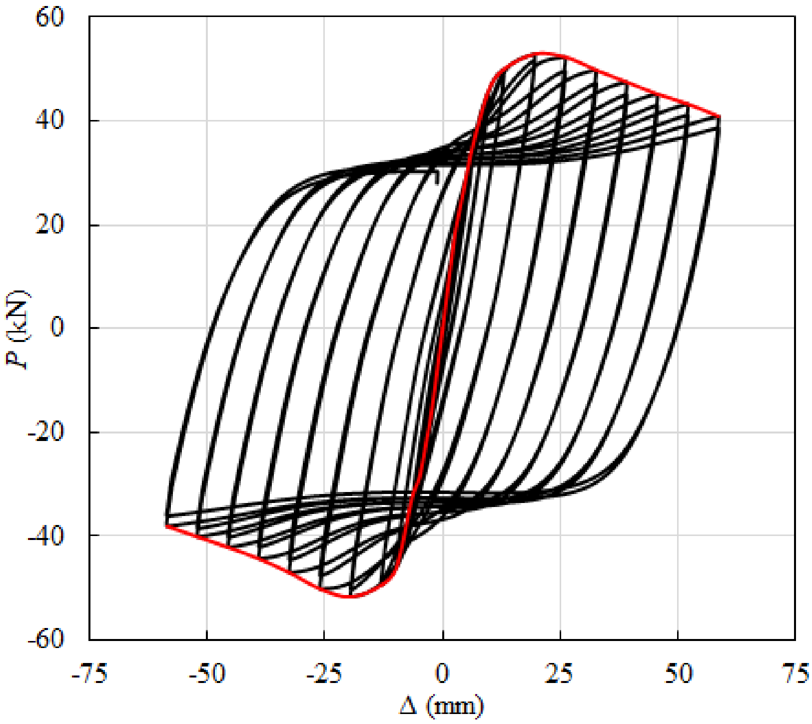

(b) S114-c60-0.5D

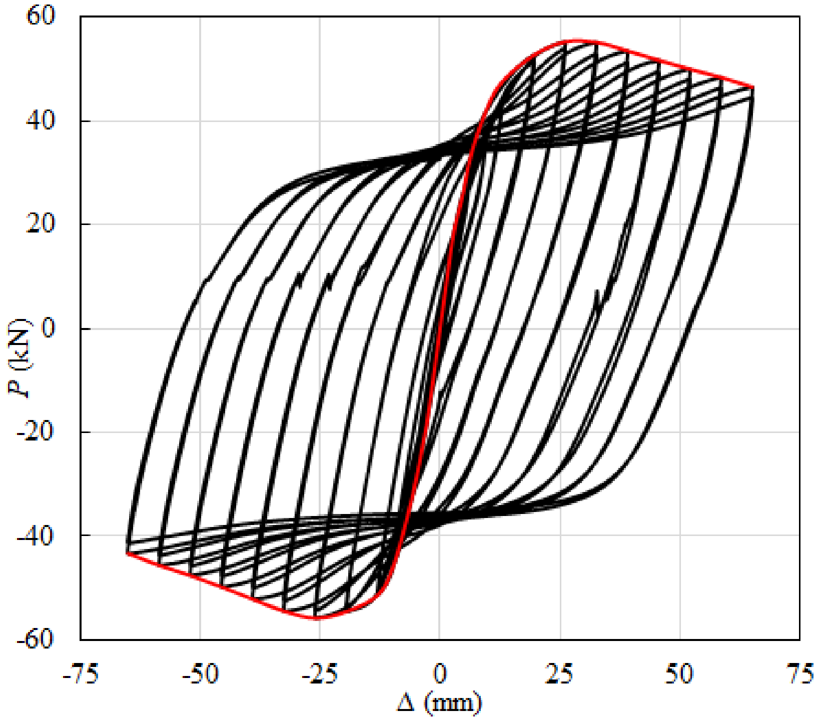

(c) S114-c60-1D

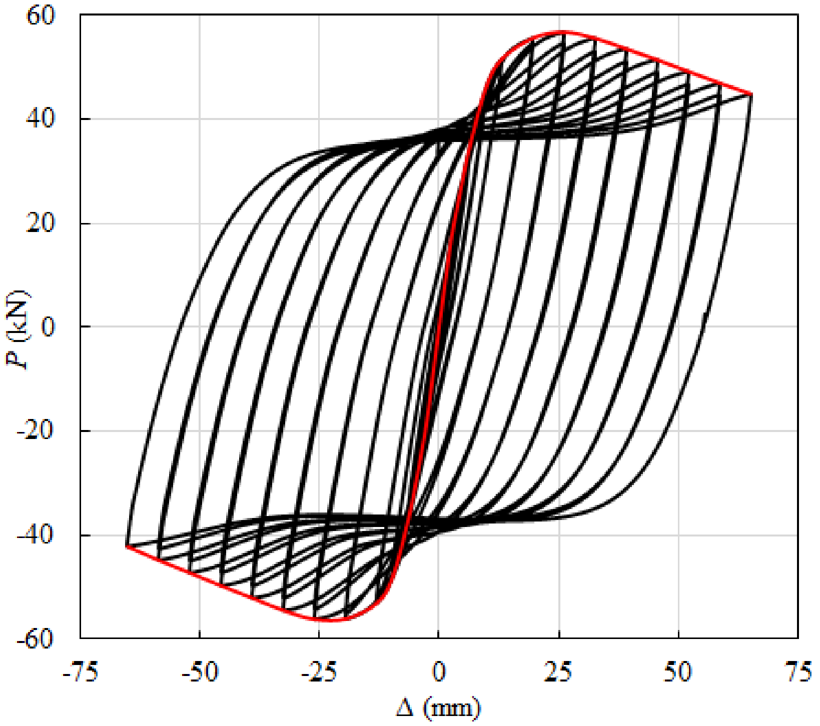

(d) S114-c60-1.5D

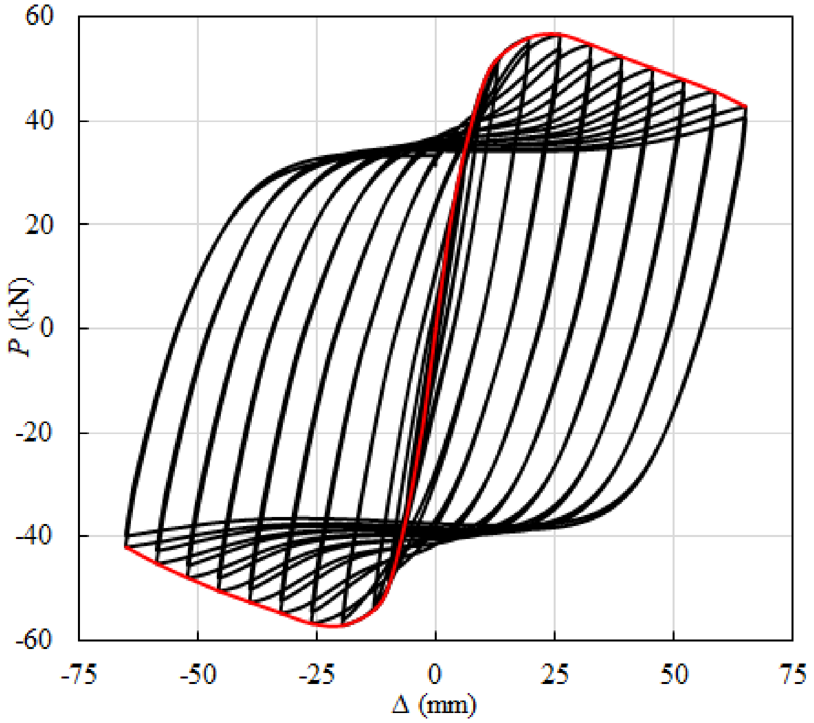

(e) S114-c60-2.5D

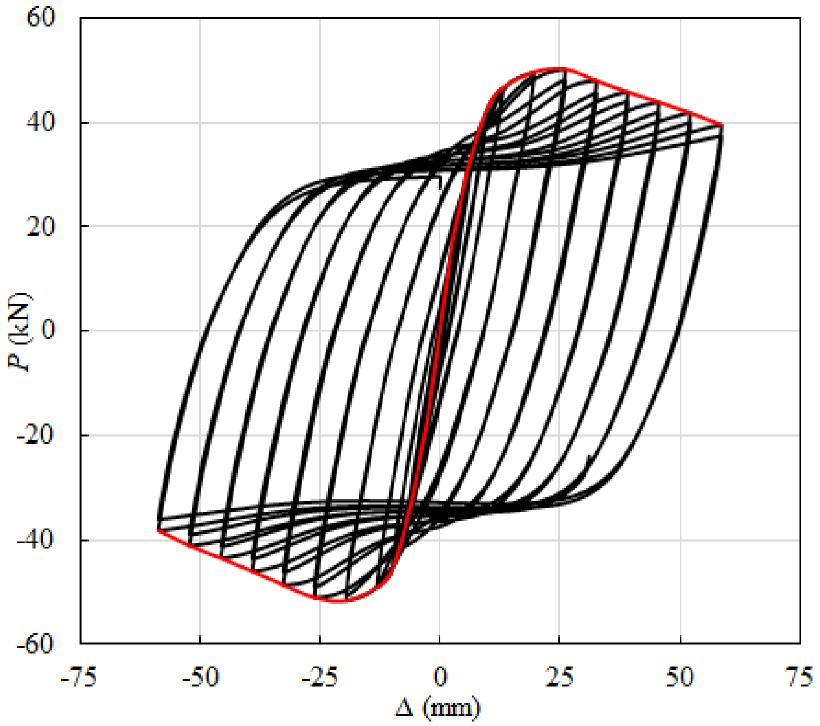

(f) S114-c50-0.5D

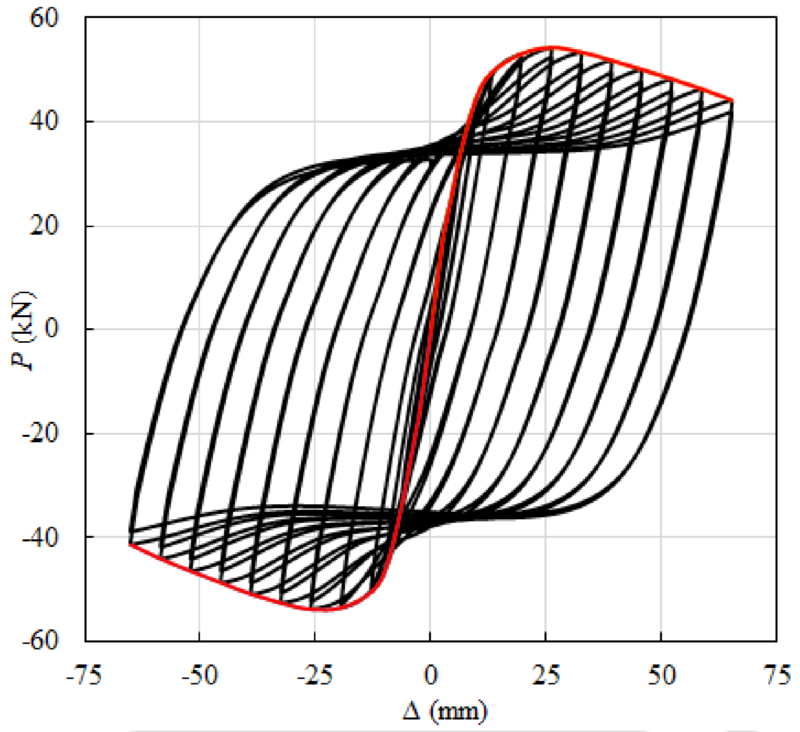

(g) S114-c50-1D

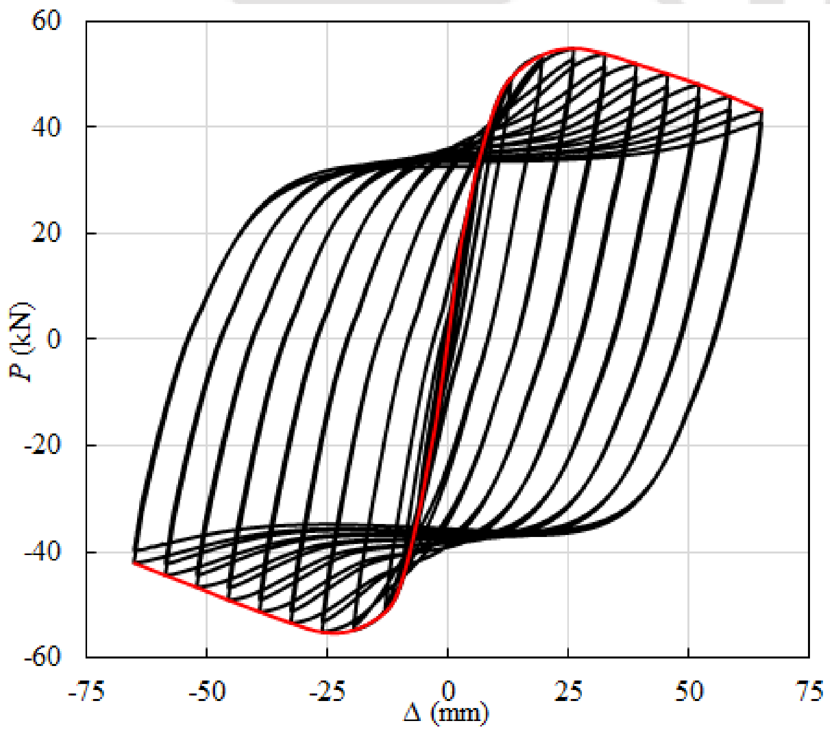

(h) S114-c50-1.5D

Figure 3.12: Lateral loads (*P*)- displacement *(*Δ*)* hysteretic curves of all tested specimens

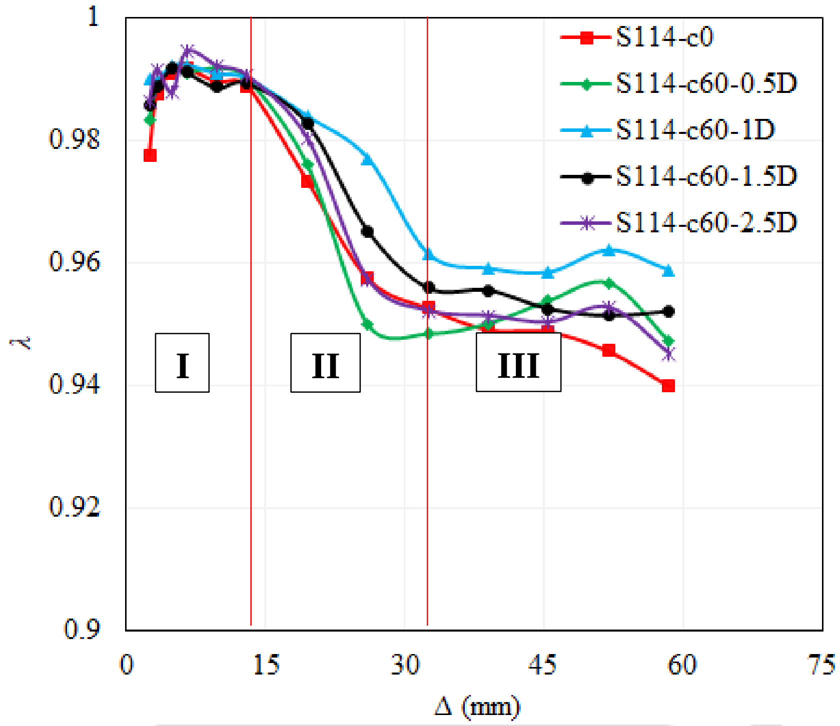

1
0.98
0.96
0.94
0.92
0.9
λ
0
15
30
45
60
75
Δ (mm)
S114-c0
S114-c60-0.5D
S114-c60-1D
S114-c60-1.5D
S114-c60-2.5D
I
II
III

(a)

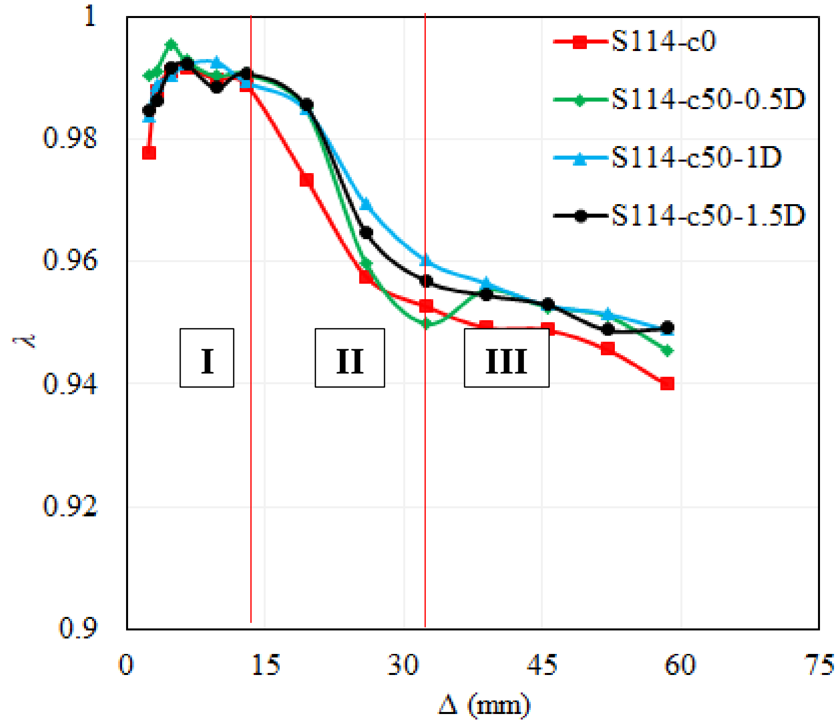

1
0.98
0.96
0.94
0.92
0.9
λ
0
15
30
45
60
75
Δ (mm)
S114-c0
S114-c50-0.5D
S114-c50-1D
S114-c50-1.5D
I
II
III

(b)

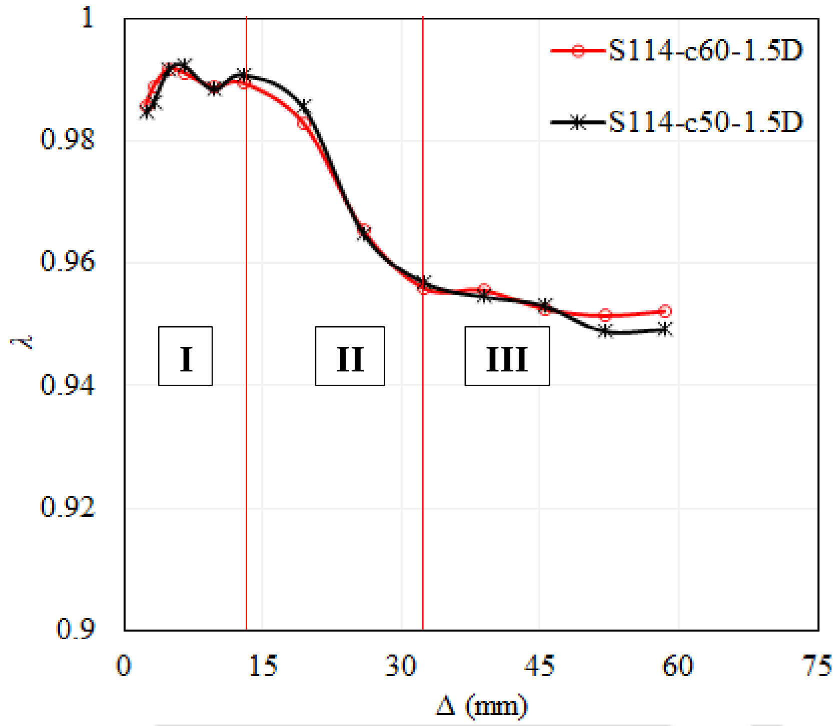

(c)

Figure 3.13: Strength degradation at different displacement peak level: (a) D_i/D=0.53, (b) D_i/D=0.44, (c) H_i/D=1.5

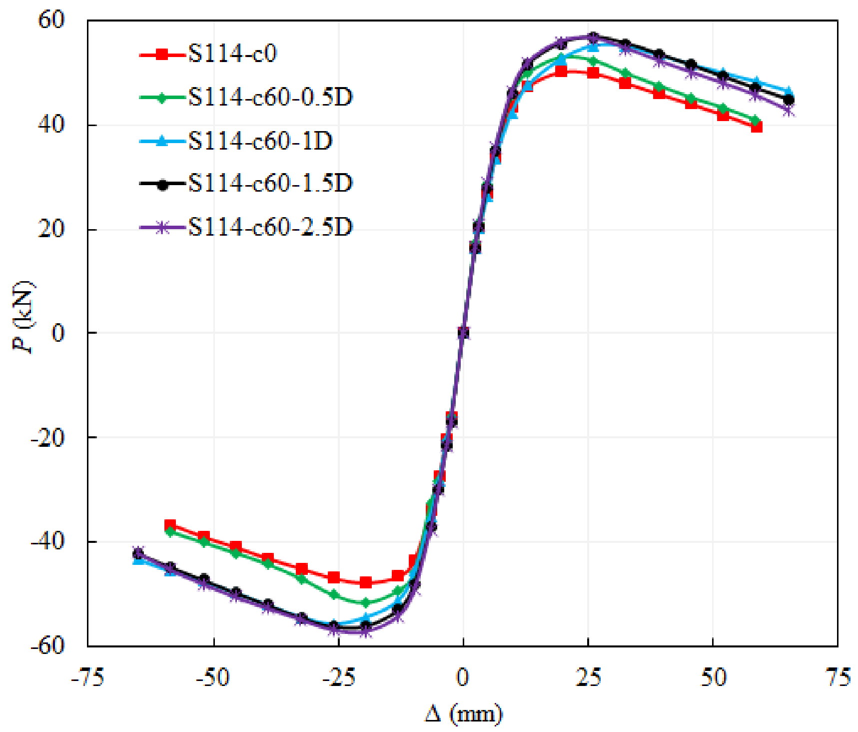

(a)

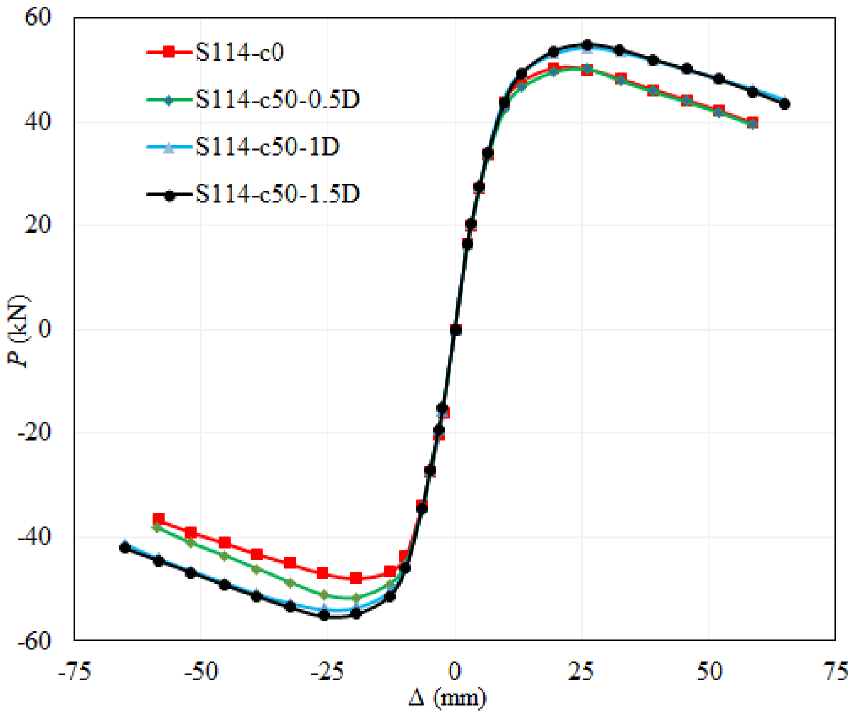

(b)

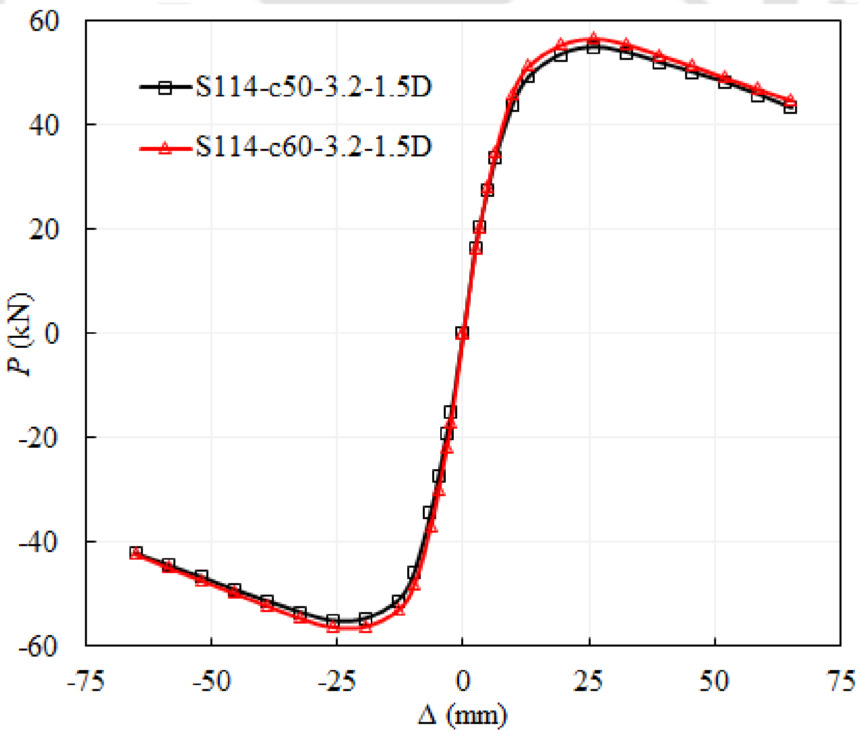

(c)

Figure 3.14: *P*-Δ envelope curves: (a) D_i/D=0.53, (b) D_i/D=0.44, (c) H_i/D=1.5

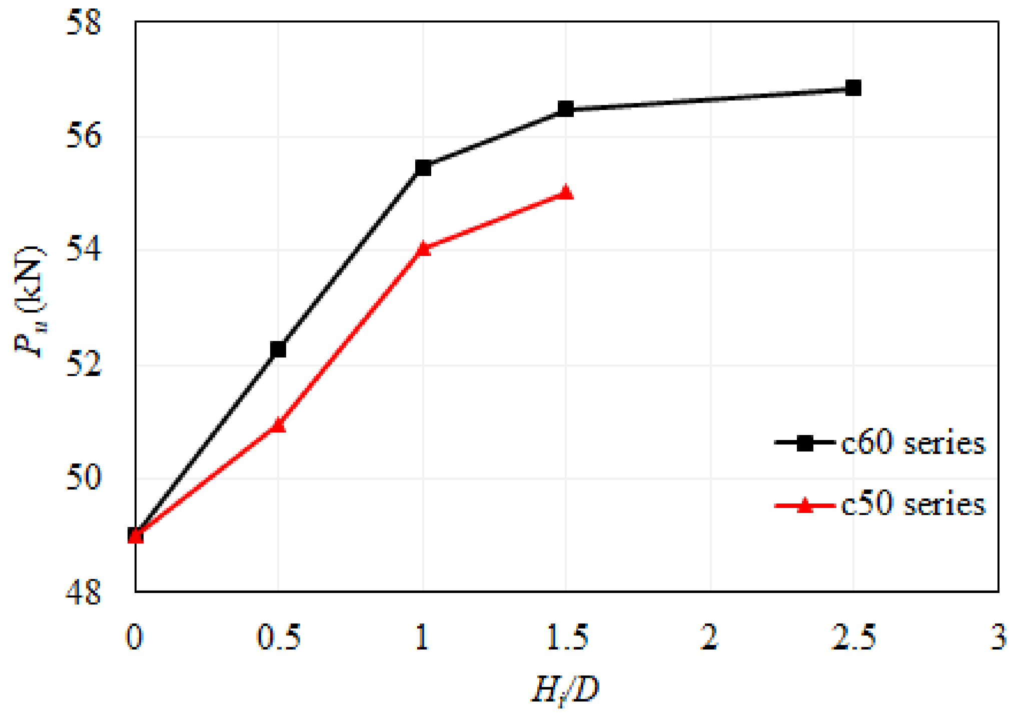

Figure 3.15: Effect of H_i/D ratio (0-2.5) on P_u

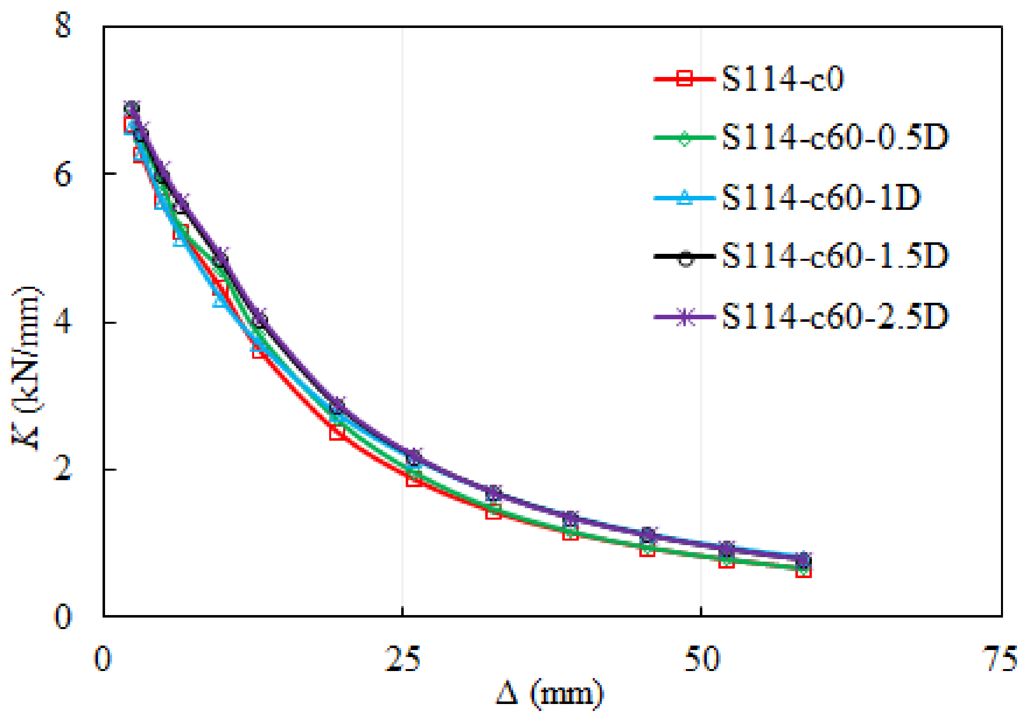

(a)

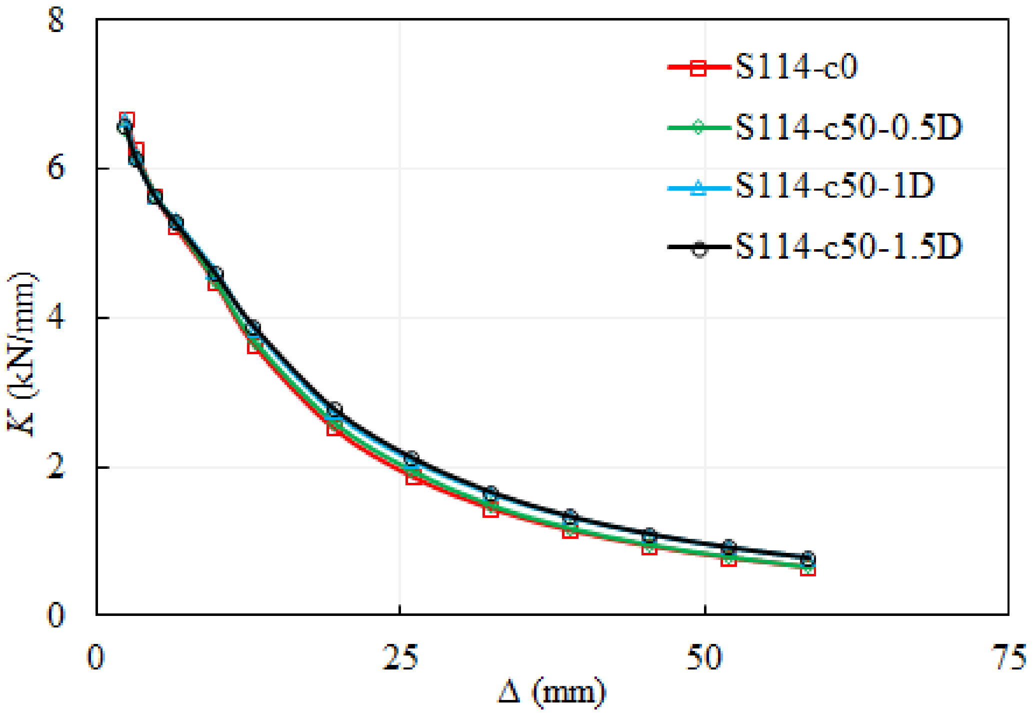

(b)

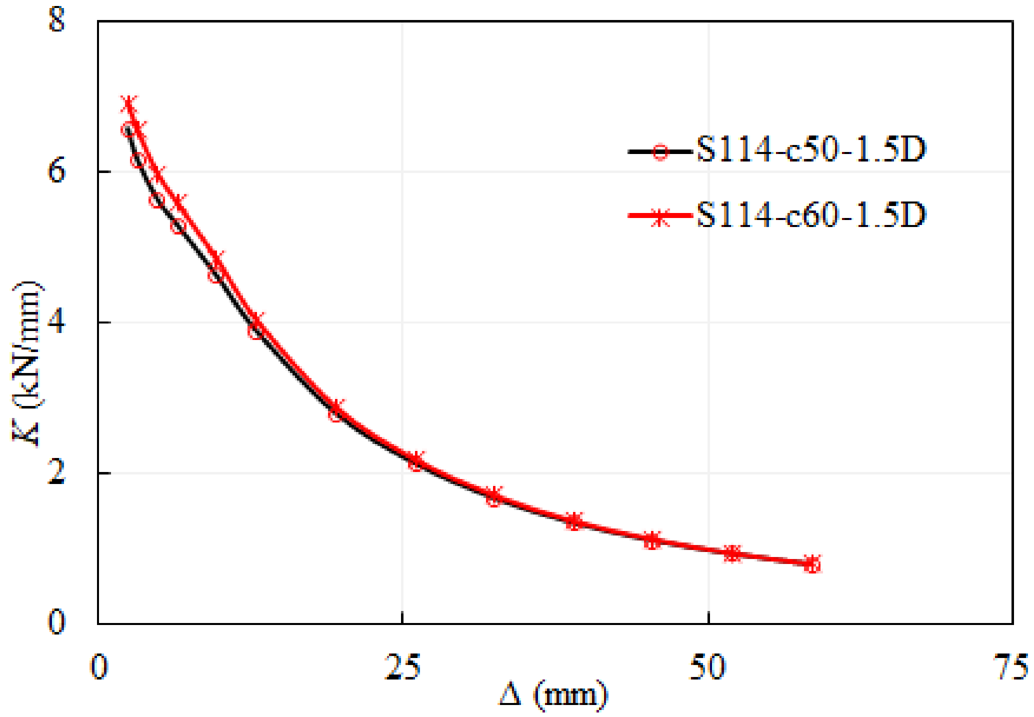

(c)

Figure 3.16: Stiffness degradation (K-Δ) curves: (a) D_i/D=0.53, (b) D_i/D=0.44, (c) H_i/D=1.5

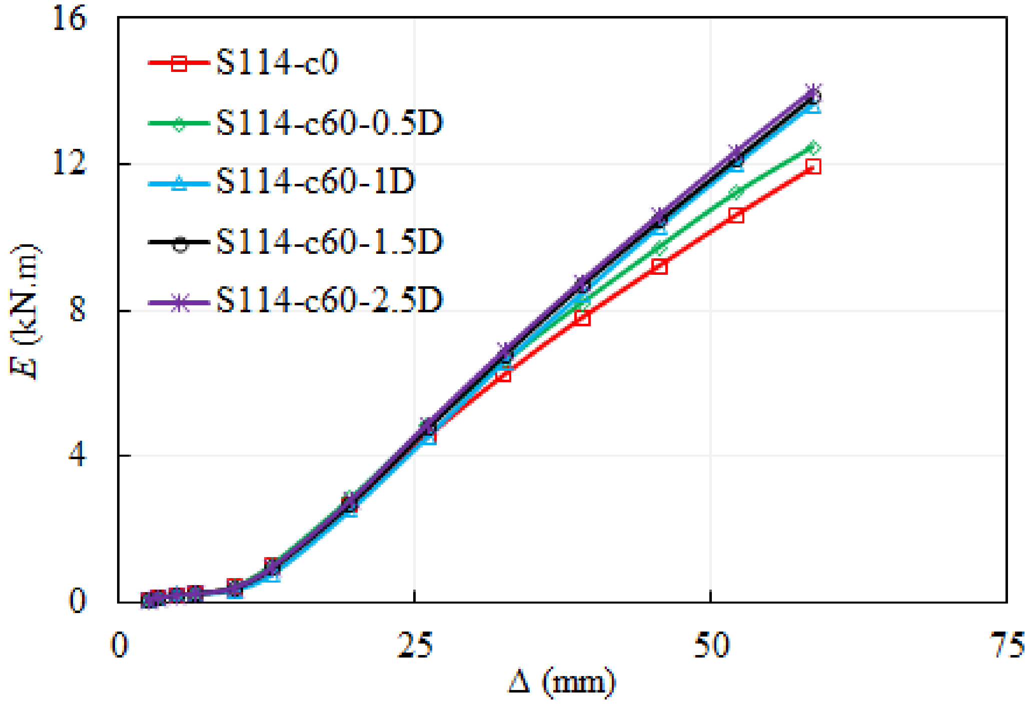

16
12
8
4
0
E (kN.m)
0
25
50
75
Δ (mm)
S114-c0
S114-c60-0.5D
S114-c60-1D
S114-c60-1.5D
S114-c60-2.5D

(a)

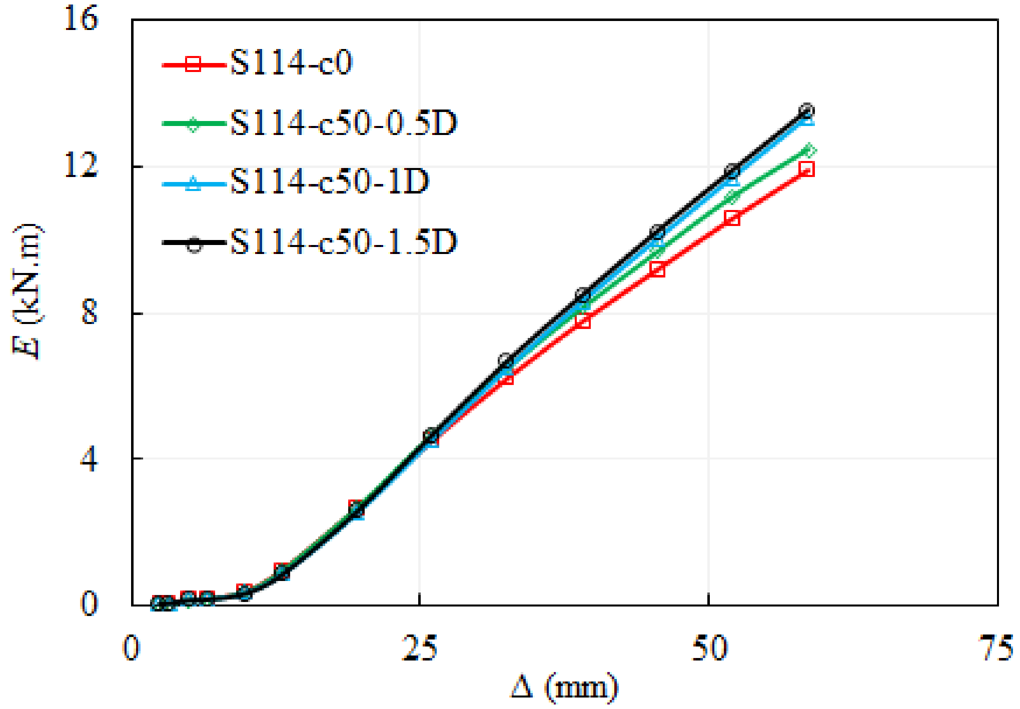

16
12
8
4
0
E (kN.m)
0
25
50
75
Δ (mm)
S114-c0
S114-c50-0.5D
S114-c50-1D
S114-c50-1.5D

(b)

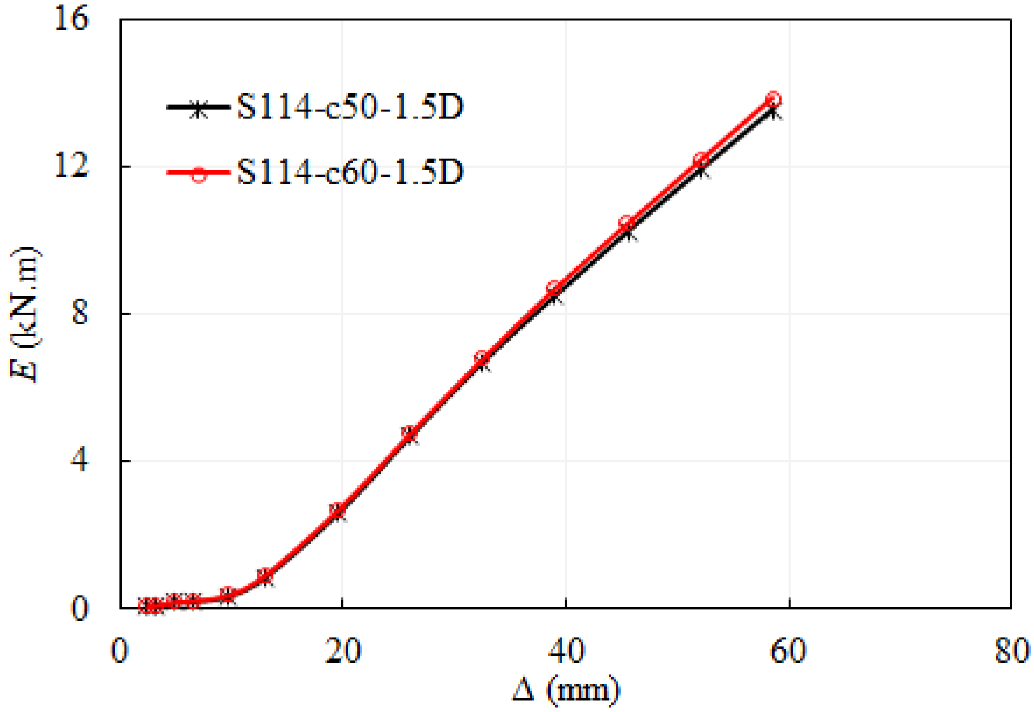

(c)

Figure 3.17: Energy dissipation (E-Δ) curves: (a) D_i/D=0.53, (b) D_i/D=0.44, (c) H_i/D=1.5

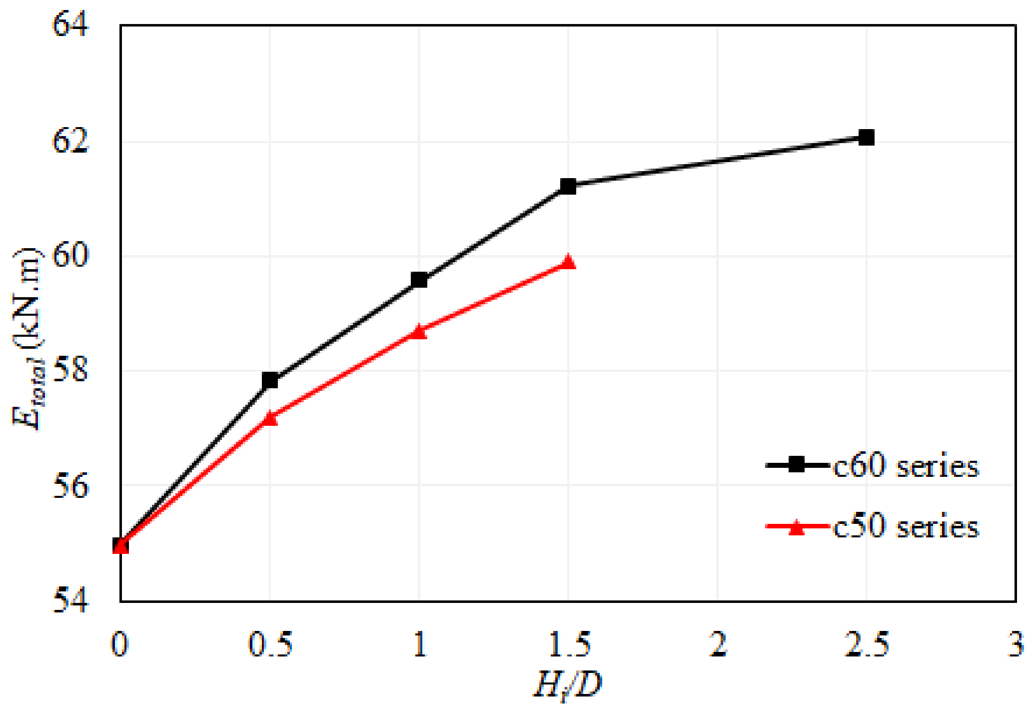

Figure 3.18: Effect of H_i/D ratio (0-2.5) on E_{total}

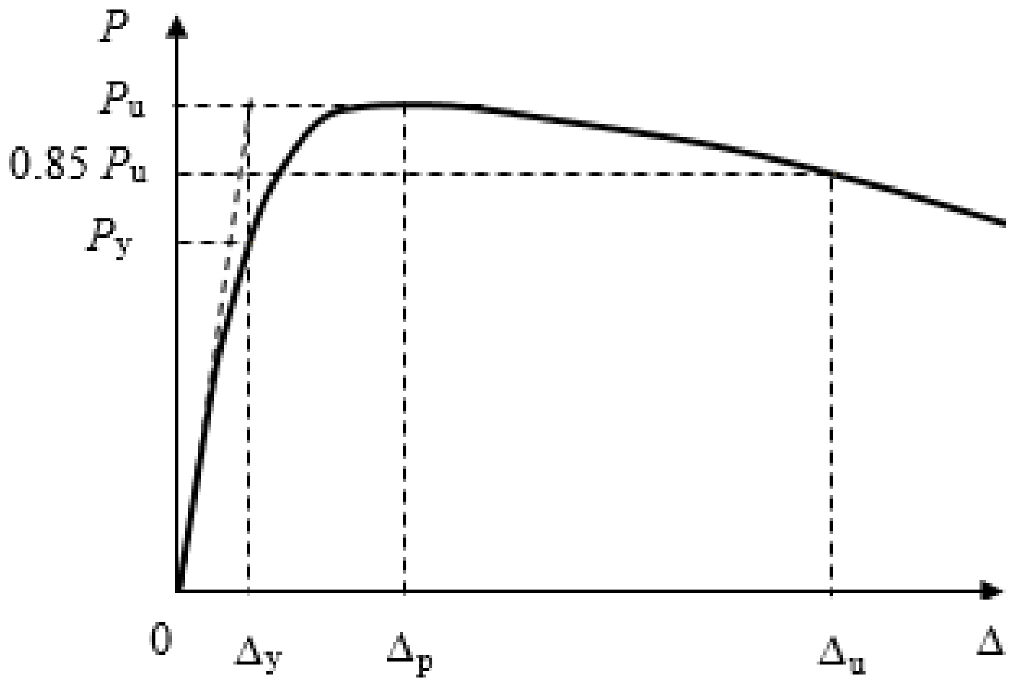

Figure 3.19: Typical *P*-Δ envelope curve

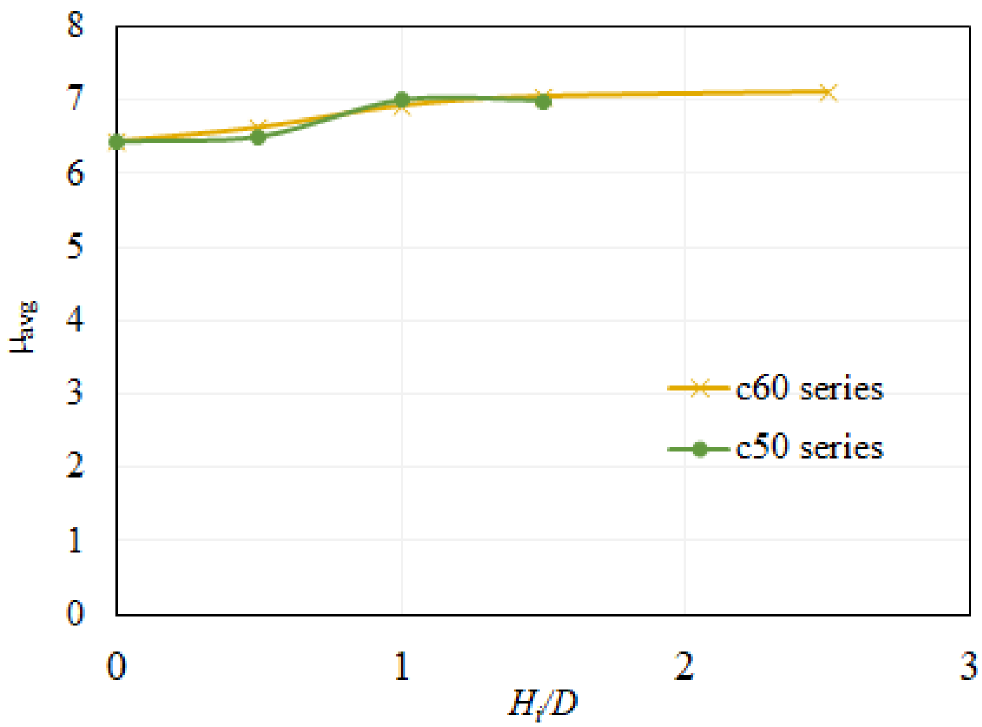

Figure 3.20: Ductility coefficient curve

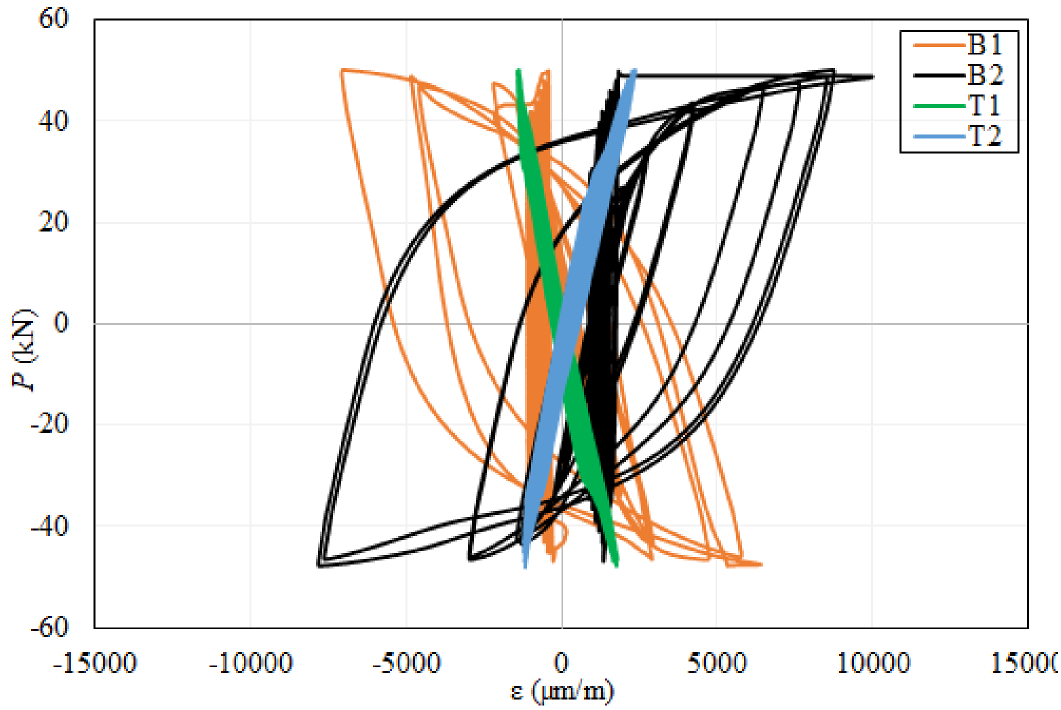

(a) S114-c0

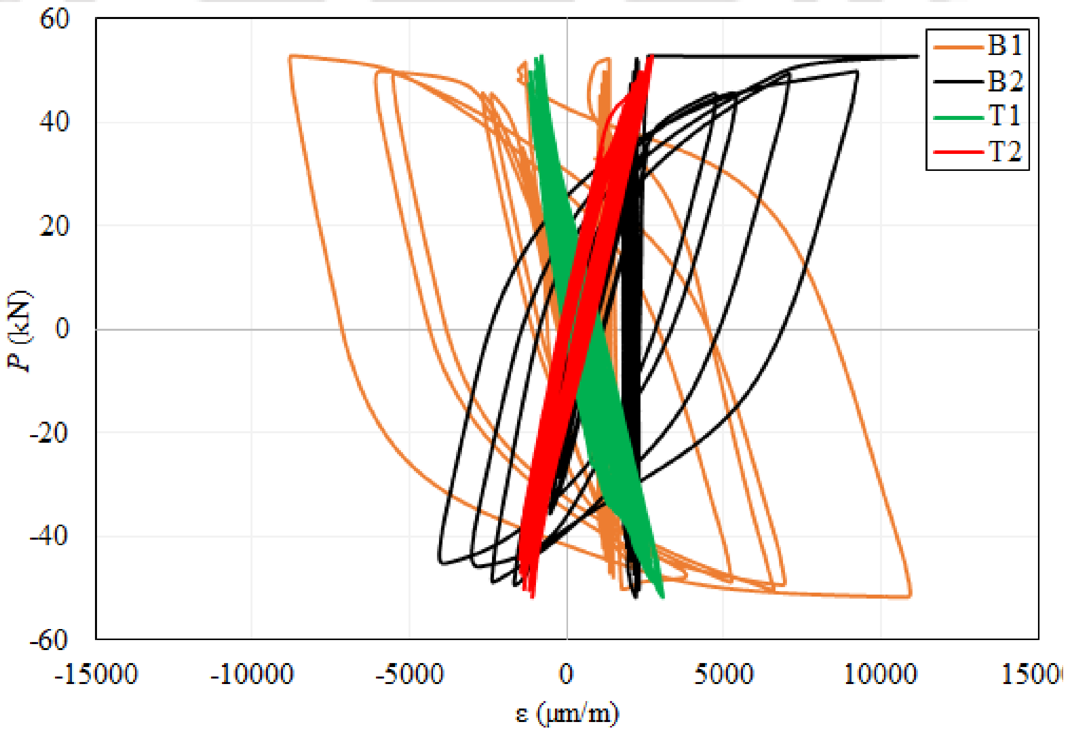

(b) S114-c60-0.5D

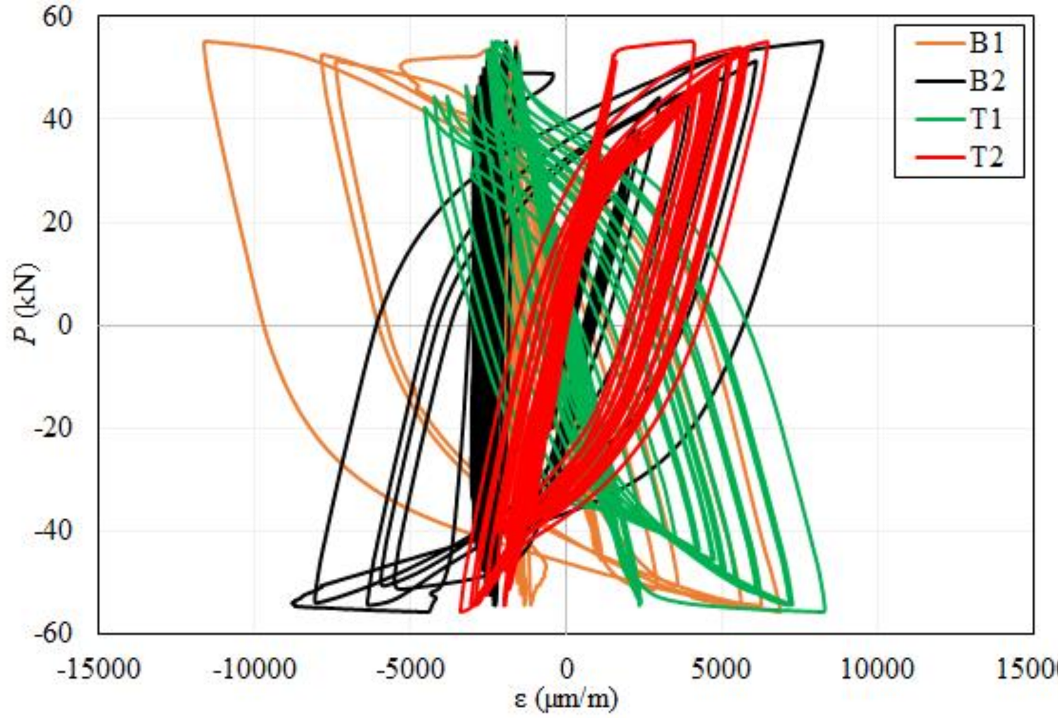

(c) S114-c60-1D

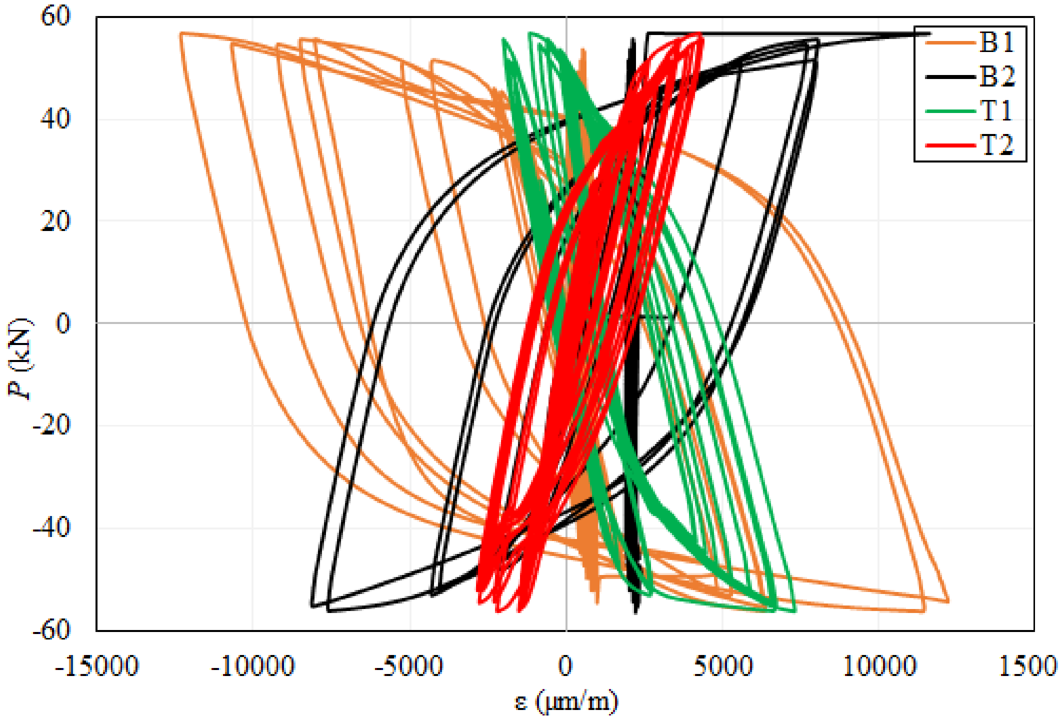

(d) S114-c60-1.5D

Figure 3.21: Typical lateral force versus outer SHS steel tube strain (P-ε) hysteretic loops (D_i/D=0.53)

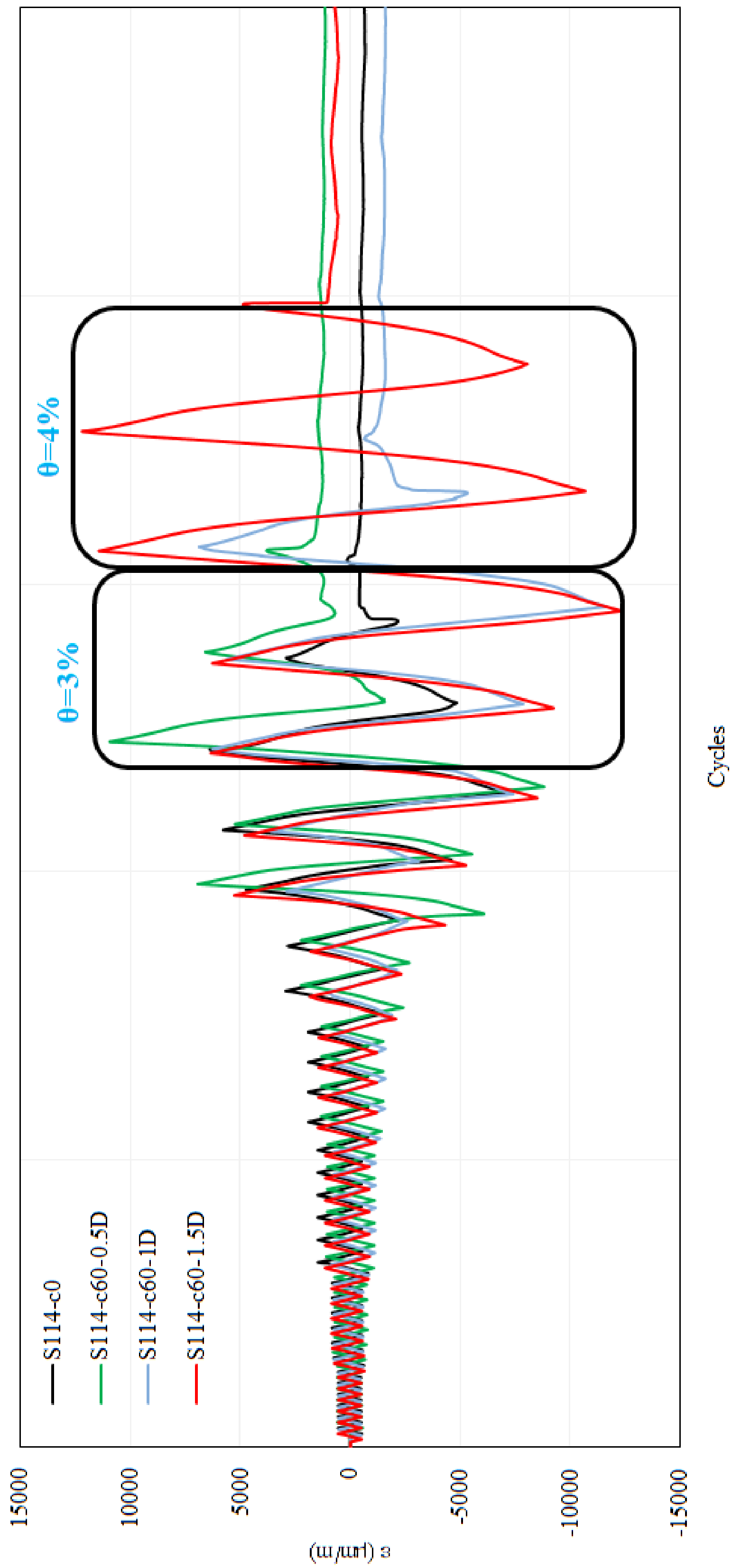

Figure 3.22: Typical vertical strain development of the outer SHS steel tubes

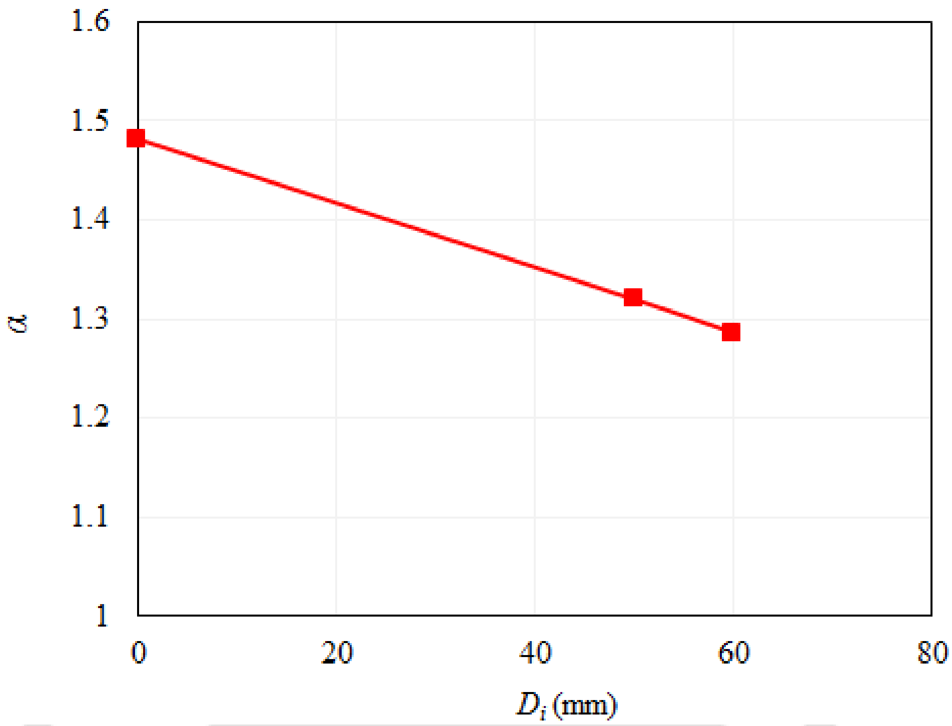

Figure 3.23: α *vs* D_i plot

Chapter 4

Partially Confined Circular CFST Columns under Cyclic Lateral Loading

4.1 INTRODUCTION

In the previous chapter (Chapter 3), an experimental investigation was carried out on square partially confined CFST columns under combined axial and lateral cyclic loadings. As an extension to the research performed in the previous chapter, circular partially confined CFST columns were investigated experimentally under same loading condition, in this chapter. Similarly, in the present chapter, the structural performance in terms of ultimate lateral strength, energy dissipation capacity, and ductility have been assessed varying the diameter and height of the inner circular steel tube. The proposed strengthening technique for circular CFST has been shown schematically in Figure 4.1. Based on the experimental findings, an Eurocode based (Eurocode 4 1994) simplified design guideline was also proposed for the circular partially confined CFST columns.

4.2 EXPERIMENTAL PROGRAM

4.2.1 Specimen details

Seven Circular columns were tested: 6 PCCFST columns and 1 CFST column under cyclic lateral loading while maintaining a constant axial load. Table 4.1 shows the average geometric dimensions of all the specimens. Each of these specimens consists of an outer circular hollow steel tube of 114 mm outer diameter (*D*) and a 3.2 mm thickness (*t*). The clear height (*H*) of 650 mm (measured between the location at which lateral load was applied (column head) and the top fiber of the footing (column end)). All 6 PCCFST specimens consisted of 1 inner steel tube having an outer diameter (D_i) of 50 mm or 60 mm and 3.2 mm thickness (t_i), welded to a thick base plate concentrically. The inner tube height was considered to be ~ 0.5*D*, 1*D*, and 1.5*D* from the top of the footing. The same axial load level (*n*=0.03) was maintained during the test of all the specimens to maintain uniformity. The axial load level (*n*) was calculated by using Equation 4.1.

$$n = \frac{N_0}{N_u} \tag{4.1}$$

Where, N_0 represents the applied axial load and N_u is the axial compressive capacity. The value of N_u was determined by testing a CFST stub column of the same sectional geometry under compression. The test set-up of the compressive strength test has been shown in Figure 4.2. Based on the axial load-deformation curve, the sectional capacity of the circular CFST stub column was found to be 834 kN (see Figure 4.3). The specimen is designated by the nomenclature Cp-cq-r, where ‘Cp’ stands for the circular outer tube of p diameter, ‘cq’ stands for the inner circular tube of q diameter, and r stands for the inner tube height. For instance, C114-c50-1.5D denotes a circular outer steel tube of diameter 114 mm consisting of a 50 mm diameter and 1.5D height inner circular steel tube. CFST specimen without any inner tube was named a c0 specimen. PCCFST columns with inner steel tube heights of 0.5D, 1D, and 1.5D were named 0.5D, 1D, and 1.5D specimens, respectively. Only small-scaled specimens could be evaluated due to the limitations of the test set-up.

4.2.2 Mechanical properties of materials

4.2.2.1 Steel

Locally available cold-formed circular hollow steel tubes were procured from the nearby market. The mechanical properties of all the steel tubes were evaluated based on the set of coupon specimens cut from the steel tubes. A standard tensile test was conducted on the cut coupon specimens as per ASTM standard (ASTM E8 2016). A 250 kN capacity, displacement-controlled universal testing machine (UTM) was used to test all the coupon specimens following the guidelines by Huang and Young 2014. Figure 4.4 shows the test set-up of the coupon specimens. The engineering stress-strain curves obtained from the tensile coupon test have been shown in Figure 4.5 (stress-strain curves of the inner steel tube have been shown in Chapter 3). The measured mechanical properties from the tensile coupon test have been summarized in Table 4.2, where f_y is the yield strength, and f_u, is the ultimate strength. Accordingly, the grade of the circular steel tubes was found to be YSt 210 as per (IS 1161 1998).

4.2.2.2 Concrete

The grade of concrete used in the previous chapter (Chapter 3) to cast the square partially confined CFST columns, following a concrete mix proportion, same grade of concrete has been used in the current chapter to cast the circular partially confined CFST columns. Six concrete cubes (150 mm) were also cast with freshly prepared concrete for the column specimens. Both the columns and the cubes set were cured for 28 days and then kept for surface drying for another 48 hours. On the day of testing the columns, the cubes were also tested under compression. The average cubic compressive strength of the cubes obtained was ~ 31 MPa. The cylinder compressive strength (f_{ck}) used in the calculation shown in section 4.4 below to predict the maximum lateral strength had been obtained by multiplying 0.8 to the cubic compressive strength (f_{cu}) (IS 516 1959; Xiao *et al.* 2005). All the specimens were cast with the same mix proportion.

4.2.3 Preparation of test specimens

The detail of the specimen preparation is shown in Figure 4.6. The procured steel tubes of diameter 114 mm were cut to a length of 1300 mm each to produce a 650 mm clear height. The inner tubes (c-60 and c-50) were cut into three sets each of height (H_i) ~ 0.5D, 1D, and 1.5 D) plus the footing depth. For improved grip between the specimen and the RC foundation, both the inner and outer tube was welded concentrically at the center of a 4 mm thick base plate of size 200 mm × 200 mm. Both the inner and outer tubes were welded concentrically at the center of the same base plate. The uniform spacing between the concentric tubes was ensured by placing a specially designed spacer between the tubes, which was removed when the outer tube's welding was complete.

As discussed in the previous chapter (Chapter 3), a similar formwork has been used in the present study. Three key considerations led to the casting of two columns on a single footing: (a) cost savings; (b) improved frictional grip on the strong floor, and (c) fitting into the strong floor fixture holes. The tubular columns were then concreted once the footing was cast. A representative cast specimen is displayed in Figure 4.6(b). At the top of the column, longitudinal shrinkage of ~ 1-2 mm was observed after curing. Before the test, the gaps were filled with gypsum in order to transfer the axial load uniformly across the column section.

4.2.4 Test set-up, instrumentation and loading protocol

At the Structural Engineering Laboratory of the Indian Institute of Technology Guwahati, all the specimens were tested. Figure 4.7 shows photograph of the test set-up. The test set-up and instrumentation discussed in Chapter 3, same test set-up and similar instrumentation have been used in the present testing (see Figure 4.8). However, a separate holder was fabricated for the circular outer steel tube used. The holder was fabricated in two equal halves with a semicircular groove in it, pressed and bolted against each other using four high-strength bolts that perfectly grip the specimen.

The loading protocol used in Chapter 3 (AISC 2016), same loading protocol has been used in the current chapter to apply displacement to the column head of all the circular columns. The lateral loading speed of 1 mm/sec was employed to sustain the quasi-static loading state. The test proceeded until either the column failed (either severe visible local buckling or outer steel tube tearing occurred) or the lateral load had fallen more than 20% of the maximum lateral load.

4.3 TEST RESULTS AND DISCUSSIONS

4.3.1 General

Here in this section, the experimental findings are presented and discussed. The actuator's pull and push direction is referred to as +ve and –ve direction, respectively. The specimens were designated as pertaining to the c-60 series and the c-50 series, depending on the inner tube diameter. For ease of viewing, a white square grid of size 10 mm was drawn near the base of the column upto 150 mm height from the footing top (within which the formation of the plastic hinge was anticipated) on the outer steel tube.

4.3.2 Description of failure modes

Figure 4.9 illustrates the typical CFST/PCCFST failure mechanism. Failure of the columns due to the plastic hinge formation could be seen in all the specimens (indicated by the outward buckling of the circular outer tube). The decrease of the lateral resistance after achieving the peak value for the increasing level of deformation may be directly linked to the formation of the plastic hinge of the column. The occurrence of plastic hinges was found to have formed at different locations for different sets of specimens. For specimen C114-c0, it has been found that the failure pattern (outward local buckling) near the base support of the specimen was similar to that reported by Qin *et al.* 2015. Whereas for the 0.5D specimens (C114-c60-0.5D and C114-c50-0.5D), the buckling has taken place at a region approximately 30-60 mm (at ~ 0.5D height) from the column end. For the 1D specimens (C114-c60-1D and C114-c50-1D), the buckling region was seen in 90-120 mm (at ~ 1*D* height) from the column end, whereas for 1.5*D* specimens (C114-c60-1.5D and C114-c50-1.5D) the buckling phenomenon was observed at two locations; one, near the base support of specimen and another, at around 170 mm (at ~ 1.5*D* height) from the column end. The local buckling region formed at ~ 170 mm from the support base was visible towards the end (during the last few cycles) of the test. A portion of the outer tube from the base of a 1D specimen (C114-c60-1D) has been cut, and the core concrete was exposed (see Figure 4.10). It was seen that both within and outside the inner tube, the core concrete had been compacted as desired. In the location at which the outer tube buckled, a serious crushing of concrete could be seen there. No significant inner CHS buckling was observed in any specimen.

From the above discussion, it could be inferred that the location at which the plastic hinge formation occurs could be shifted up according to the height of the inner CHS. Local buckling on the outer tube was evident at approximately 5% drift angle for all the specimens. After that, the outer tube's buckling became more evident with the progressive rise in the drift angle and gradually formed a buckled ring in that region.

4.3.3 Hysteretic curve

Figure 4.11 displays the measured lateral load (P) versus lateral displacement (Δ) relationships of all specimens. The hysteresis curves obtained were plump type showing no signs of pinching effect at any stage during the test because of the smaller D/t ratio of the steel tube. From the figures, it is obvious that for all the specimens, there exists an initial linear load-displacement relationship, and as the response moved towards the realm of inelasticity, the stiffness gradually declined. It was also seen that with the increase in cycle number, there is a degradation in peak lateral load. However, such a drop was not visible, in the ‘pull’ region, apparently due to some technical setting issue with the actuator set-up. Hence, the test lateral ultimate strength P_u from the push region was taken for ultimate load and ductility coefficient calculation.

4.3.4 Strength degradation

Each successive loading cycle of the same drift angle showed a reduction of strength called strength degradation. It is calculated using the strength degradation coefficient (λ). Equation 4.2 was used to compute the strength degradation coefficient for each specimen (e.g. Xu *et al.* 2016).

$$\lambda_i = \frac{P_i^{j+1}}{P_i^j} \tag{4.2}$$

Where P_i^j represents the maximum lateral load of the j^{th} cycle for the i^{th} drift angle. Since the initial three drift angles required six cycles, four cycles were required for the fourth drift angle; therefore, the strength degradation coefficient has been computed considering the initial two cycles of each drift angle. Only two cycles were offered for the remaining drift angles; hence both cycles were included in the computation.

The calculated strength degradation coefficient versus the measured lateral displacement has been plotted in Figure 4.12. The value of λ ranges between 0.92 to 1. It is evident that the λ is very close to unity for drift angles less than 1% (stage-I), whereas it rapidly decreases for drift angles between 1% and 3% (stage-II). The λ remains almost stable and the same for the drift angles between 3% and 6% (stage-III). The strength degradation coefficient deteriorates significantly at drift angles greater than 6% (stage-IV). The possible reason is that at stage-I, the concrete has not experienced any significant damage, but at stage-II, significant damage to the concrete has occurred. At stage-III, since the maximum damage had already occurred at stage –II, hence no sudden drop was seen at stage-III. At stage –IV, the tearing of the outer steel tube leading to total damage to the specimens, was observed.

4.3.5 Envelope curve

Envelope curve obtained from the P-Δ hysteresis plots of all the specimens tested has been shown in Figure 4.13. The ultimate lateral strength (P_u) obtained has been shown in Table 4.3. It was seen that the maximum lateral strength could be improved by increasing the height of the circular inner steel tube. The 1.5D specimen of the c-50 and c-60 series were found to show an enhancement in the maximum lateral strength by ~ 15.8% and ~ 16%, respectively, when compared with the c0 specimen. The possible reason for the enhancement in strength could be the partial confinement provided by the inner circular steel tube to the whole region where the plastic hinge was expected to form. The inner tube's height was restricted upto 1.5*D* only because the structural performance beyond 1.5*D* is not very significant (as per the results obtained in Chapter 3).

The effectiveness of the PCCFST specimens as a whole was examined in relation to the diameter of the inner tube. The results of the 1.5D specimens were displayed for comparison (see Figure 4.13(c)). It was seen that the D_i/D ratio ranged from 0.44-0.53 (D_i/D = 0.44 & 0.53, for C114-c50-1.5D and C114-c60-1.5D, respectively) has a negligibly little impact on the envelope curve. In order to optimize the maximum lateral strength, D_i/D value should be increased to the maximum possible value maintaining a sufficient gap for the concrete to be placed and compacted. Maximum lateral strength versus H_i/D ratio (0-1.5) of both the c-50 and c-60 series columns have been displayed on the same plot for comparison (Figure 4.14). It could be inferred from the above discussion that providing a concentric circular inner steel tube to the circular CFST could enhance the lateral strength by ~ 16% for the specimens being evaluated.

4.3.6 Stiffness degradation

At various drift angles, the stiffness of the specimen has been assessed using the average stiffness (secant stiffness). Using Equation 4.3, the average stiffness of the specimen was computed (Qian *et al.* 2014; Zheng *et al.* 2018).

$$K_i = \frac{|P_i| + |-P_i|}{|\Delta_i| + |-\Delta_i|} \tag{4.3}$$

where, P_i and Δ_i represents the maximum lateral load and the lateral displacement associated with the *i*-th drift angle, respectively. The pull and push direction is represented by +ve and –ve direction, respectively.

Figure 4.15 shows the stiffness-lateral displacement (K-Δ) plots of all the columns. It is evident that the cumulative damage accumulating at the potential plastic hinge area causes the stiffness to decrease as the lateral displacement advances. Stiffness deteriorations of all the specimens followed a similar nonlinear pattern. By increasing the height of the inner steel tube, no significant changes in the stiffness of the column could be observed. Figure 4.15(c) shows the effect of D_i/D on the stiffness of the columns. The stiffness degradation pattern exhibited by the two 1.5D specimens (C114-c60-1.5D and C114-c50-1.5D) was not very distinct.

4.3.7 Energy dissipation capacity

The cumulative energy dissipation capacity versus the displacement curves of the specimens tested has been shown in Figure 4.16. Within a 9% drift angle, the maximum lateral strength of all specimens dropped by 15% or more. As a result, energy dissipation was computed upto the final cycle of the 9% drift angle. Table 4.3 and Figure 4.17 provides a summary of the total energy dissipation capacity determined from the experimental results. It was evident from the plotted graphs that the energy dissipation ability of the circular PCCFST specimens could be substantially improved by increasing the height of the inner tube. The potential plastic hinge region determines the energy dissipation capacity, and by adding more steel confinement to that area, the property is improved.

The cumulative energy dissipated at each individual displacement by 1.5D specimens (C114-c60-1.5D and C114-c50-1.5D) were found to follow a similar pattern (see Figure 4.16(c)). The difference in the total energy dissipation upto 9% drift angle for the 1.5D specimens was not very significant. From the preceding, it may be inferred that adding an inner CHS member would enhance the CFST member's ability to dissipate energy. According to the results from the LVDT reading, the tested columns had a support slippage of nearly 1.5 mm at larger displacement. When calculating the energy dissipation ability, a correction has been made to each affected cycle of the P-Δ hysteresis curve considering the support slippage associated with it.

4.3.8 Ductility

The ductility of any structural element is quantified in terms of displacement ductility coefficient (μ). In the present study, the specimens' displacement ductility coefficient was calculated using the formula in Equation 4.4.(Han *et al.* 2006; Liao *et al.* 2017).

$$\mu = \frac{\Delta_u}{\Delta_y} \tag{4.4}$$

Where, Δ_y= yield displacement, Δ_u= displacement corresponding to a 15% post-peak drop. (details procedure to calculate the ductility coefficient has been illustrated in Chapter 3). A ductility enhancement of ~ 24% was observed for the 1.5D specimens when compared with the counterpart CFST specimen. The ductility coefficients computed are presented in Table 4.3 and plotted in Figure 4.18. All of the specimens' ductility coefficients are more than 4.5, which shows that they all have improved cyclic performance.

4.3.9 Strain development at the steel tube

Typical cyclic lateral load versus outer circular steel tube strain plots of the c-60 series columns are shown in Figure 4.19. The location of the stain gauges installed at two heights (50 mm (level-I) and 150 mm (level-II)) from the column end has been detailed in Figure 4.8. At each level, two strain gauges were installed diametrically on opposite sides. The strain gauges positioned at level-I are represented by B1 and B2, whereas the strain gauges fixed at level-II are represented by T1 and T2. For the CFST and the 0.5D specimens, the strain values corresponding to level-I exhibited a similar pattern; however, at level-II, strain values corresponding to 0.5D specimens showed slightly higher values compared to the c0 specimen. For 1D specimens, the strain corresponding to level-II was higher than level-I but Strains corresponding to level-I of the 1.5D specimens were higher than level-II. The possible reason for the above observation could be the occurrence of plastic hinge formation at different heights for different sets of PCCFST columns (as discussed in section 4.3.2), indicated by the buckling of the outer circular steel tube at that region.

4.4 EUROCODE-BASED SIMPLIFIED DESIGN RULE

To the best of the authors' knowledge, currently, there is 'no' formula to estimate the strength of circular partially confined CFST members as per any code provisions. However, an empirical equation was developed in the previous chapter (Chapter 3) to predict the maximum lateral strength of the square PCCFST column. Based on the data obtained from the limited test results and code provision, (Eurocode 4 1994), a simplified design guideline has been proposed here to estimate the maximum lateral strength of the circular 1.5D specimens. Since it was observed that the increase in maximum lateral strength for the inner steel tube height above 1.5D is not very significant, therefore 1.5D specimens were considered for the calculation. According to the simplified design rule, the formula given in Equation 4.5 could be used to compute the ultimate lateral strength.

$$P_u = \frac{M_{Euro}}{(\beta - 1.5D)\alpha} \tag{4.5}$$

where, α, γ, and β are the effective length ratio, the normalized strength ratio, and the effective length correction factor of the PCCFST column, respectively (Equations 4.6-4.8). Where α is an empirical value derived by a linear curve fitting ($R^2 = 0.97$) (refer Figure 4.20).

$$\alpha = \frac{\beta}{\beta - 1.5D} - 0.0036D_i \tag{4.6}$$

$$\beta = \frac{M_{Euro}}{P_{0,Euro}\gamma} \tag{4.7}$$

$$\gamma = \frac{P_{u0,Exp}}{P_{u0,Euro}} \tag{4.8}$$

Depending on the limits of the applied axial compression (N), the maximum moment capacity (M_{Euro}) can be computed as per the equations given below (Equations 4.9a-4.9c).

If $N_0 \geq A_c f_{ck}$

$$M_{Euro} = \frac{N_u - N_0}{N_u - A_c f_{ck}} M_p \tag{4.9a}$$

If $0.5A_c f_{ck} < N_0 < A_c f_{ck}$

$$M_{Euro} = M_p + \frac{A_c f_{ck} - N_0}{0.5A_c f_{ck}} \left(M_{\max} - M_p\right) \tag{4.9b}$$

If $N_0 \leq 0.5A_c f_{ck}$

$$M_{Euro} = M_p + \frac{N_0}{0.5A_c f_{ck}} \left(M_{\max} - M_p\right) \tag{4.9c}$$

Where M_p, and M_{max} , N, and N_u, are the plastic moment capacity, maximum bending capacity applied, axial load, and section capacity of the CFST column, respectively. From the equations listed below (Equations 4.10-4.22), all of these values can be computed. A_c and A_a are the area of the core concrete and the outer steel tube at the cross-section, respectively. f_{ck} and f_y are the cylinder compressive strength of the concrete core and yield strength of the steel tube, respectively.

$$N_u = A_a \eta_a f_y + A_c f_{ck} \left[1 + \eta_c \frac{t}{D} \frac{f_y}{f_{ck}}\right] \tag{4.10}$$

$$\eta_c = 4.9 - 18.5\bar{\lambda} + 17\bar{\lambda}^2 \tag{4.11}$$

$$\eta_a = 0.25\left(3 + 2\bar{\lambda}\right) \tag{4.12}$$

$$\bar{\lambda} = \sqrt{\frac{N_{pl,Rk}}{N_{cr}}} \tag{4.13}$$

$$N_{pl,Rk} = A_a f_y + A_c f_{ck} \tag{4.14}$$

$$N_{cr} = \frac{\pi^2 (EI)_{eff}}{(k_e L)^2} \tag{4.15}$$

$$(EI)_{eff} = E_a I_a + 0.6 E_c I_c \tag{4.16}$$

$$M_p = 4 f_y t r_m^2 \cos\gamma_0 + \frac{2}{3} f_{ck} r_i^3 \cos^3 \gamma_0 \tag{4.17}$$

$$r_m = \left(\frac{D - t}{2} \right) \tag{4.18}$$

$$\gamma_0 = \frac{\pi}{2} F_{CHS} \tag{4.19}$$

$$F_{CHS} = \frac{\frac{1}{8} \frac{f_{ck}}{f_y} \frac{D}{t}}{1 + \frac{1}{4} \frac{f_{ck}}{f_y} \frac{D}{t}} \tag{4.20}$$

$$r_i = \left(\frac{D - 2t}{2} \right) \tag{4.21}$$

$$M_{\max} = 4 f_y t r_m^2 + \frac{2}{3} f_{ck} r_i^3 \tag{4.22}$$

The estimated values (P_{ue}) based on the proposed design guideline were compared to the measured maximum lateral strength (P_u) obtained from the experiments conducted (Table 4.4). It is to be mentioned that the code provision discussed above was for CFST subjected to constant axial loads and monotonically increasing flexural loads only. The proposed design rule mentioned above could effectively estimate the maximum lateral strength of the 1.5D specimens (see Table 4.4, (Mean = 0.99, COV = 0.01)).

4.5 CONCLUSIONS

In the present study, a new and effective method has been proposed to enhance the structural performance of the circular CFST using a concentric inner circular steel tube at the potential plastic hinge zone under cyclic lateral loading. In addition to the experimental work, a Eurocode-based simplified design rule was developed to account for partial confinement. Based on the experimental observations of the circular PCCFST columns, the following conclusions can be drawn.

1) It has been noted that the location of the plastic hinge formation of the circular PCCFST columns could be effectively shifted up as per the height of the inner circular steel tube.

2) It was established that by employing inner circular hollow steel tubes upto a height of 1.5D, an enhancement in the ultimate lateral strength of approximately ~16% could be attained.
3) An enhancement in the energy dissipation capacity for PCCFST columns (1.5D specimens) was found to be approximate ~ 14% when compared with the counterpart CFST.
4) The PCCFST columns (1.5D specimens) were found to have an enhancement of approximately ~24% in the ductility coefficient with respect to the counterpart CFST.
5) The proposed design rule based on the Eurocode could effectively calculate the maximum lateral strength of the circular PCCFST columns.

Table 4.1 Geometrical parameters

Specimens	D (mm)	t (mm)	H (mm)	D_i (mm)	t_i (mm)	H_i (mm)	D_i/D	n	N_0 (kN)
C114-c0	114	3.2	650	-	-	-	-	0.03	22
C114-c50-0.5D	114	3.2	650	50	3.2	57	0.44	0.03	22
C114-c50-1D	114	3.2	650	50	3.2	114	0.44	0.03	22
C114-c50-1.5D	114	3.2	650	50	3.2	171	0.44	0.03	22
C114-c60-0.5D	114	3.2	650	60	3.2	57	0.53	0.03	22
C114-c60-1D	114	3.2	650	60	3.2	114	0.53	0.03	22
C114-c60-1.5D	114	3.2	650	60	3.2	171	0.53	0.03	22

Table 4.2 Summary of steel tube thickness and material properties

Specimens	t (mm)	D/t	f_y (MPa)	f_u (MPa)
C-114	3.2	35.63	312.00	374.00
c-50	3.2	15.63	365.16	395.75
c-60	3.2	18.75	362.70	397.73

Table 4.3 Experimental findings

Specimens	P_u	E_{total}	μ
C114-c0	27.00	32.97	7.90
C114-c50-0.5D	26.95	33.07	8.50
C114-c50-1D	27.54	36.18	8.69
C114-c50-1.5D	31.29	36.18	9.50
C114-c60-0.5D	27.96	33.21	8.30
C114-c60-1D	28.89	37.59	8.55
C114-c60-1.5D	31.30	37.66	9.76

Table 4.4 Comparison between experimental results and results obtained from the proposed guidelines

Specimens	Pu (kN)	Simplified design value	
		P_{ue} (kN)	$\frac{P_{ue}}{P_u}$
C114-c0	27.00	26.82	0.99
C114-c60-1.5D	31.30	31.38	1.00
C114-c50-1.5D	31.29	30.51	0.98
Mean			0.99
COV			0.01

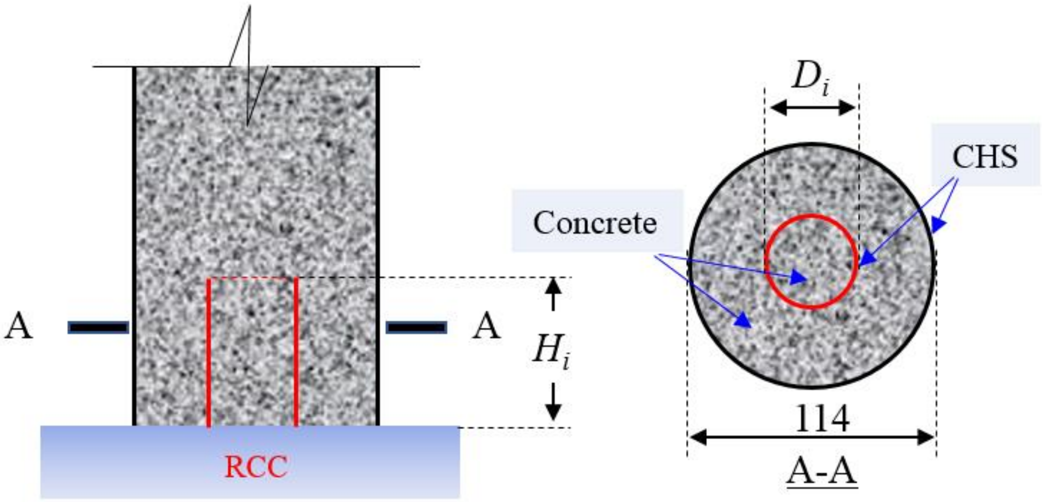

Figure 4.1 Proposed technique: Partially confined concrete-filled steel tubular circular column (i.e. core concrete confined at the potential plastic hinge region)

Figure 4.2 Circular CFST under compression

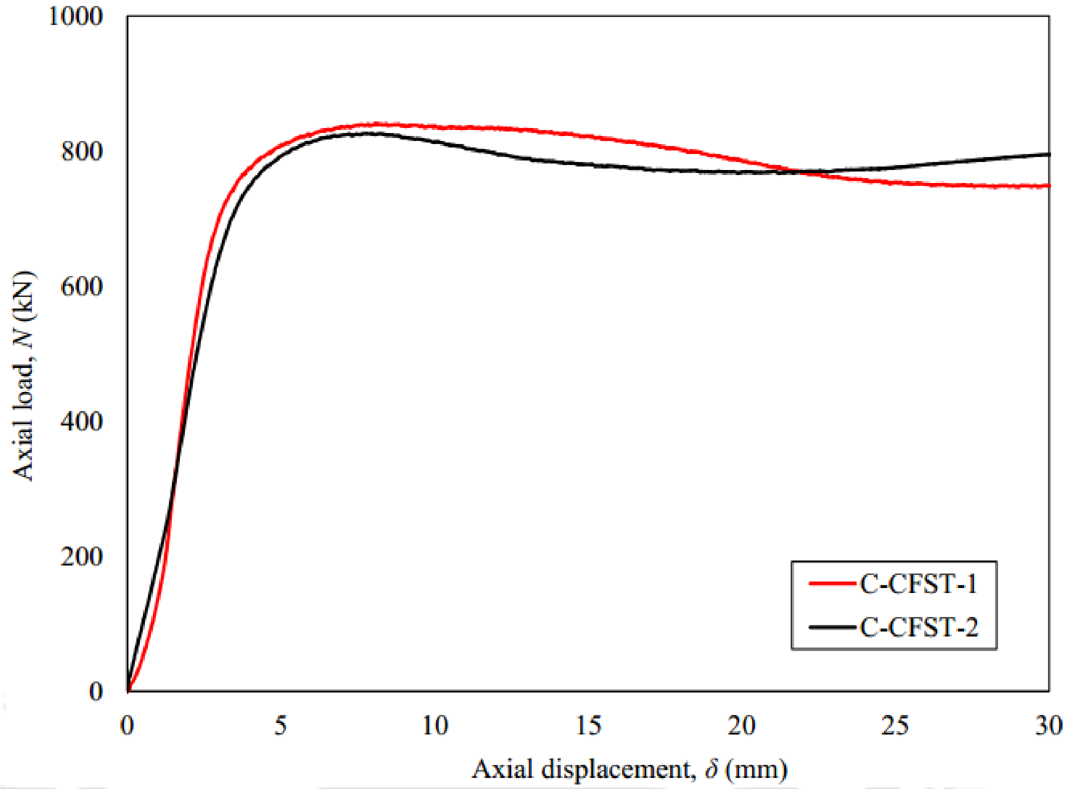

Figure 4.3: Load Vs Deformation curve of Circular CFST stub columns

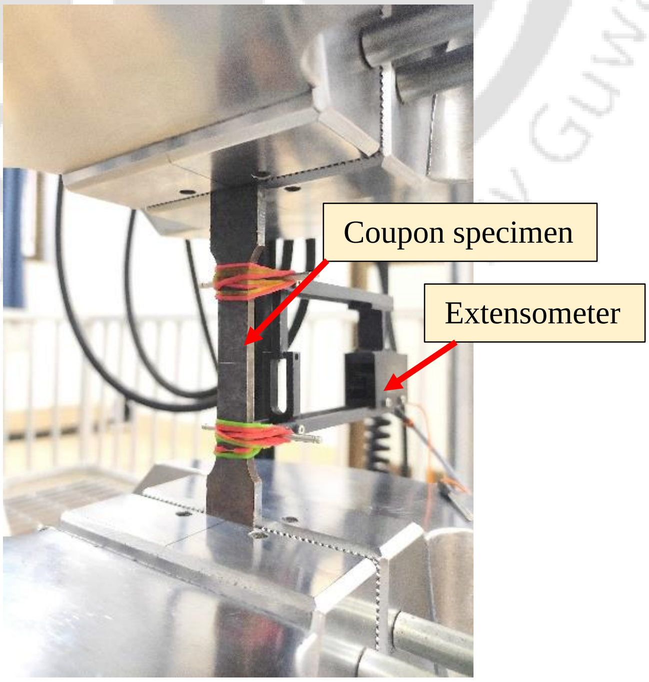

Figure 4.4: Tensile test set-up

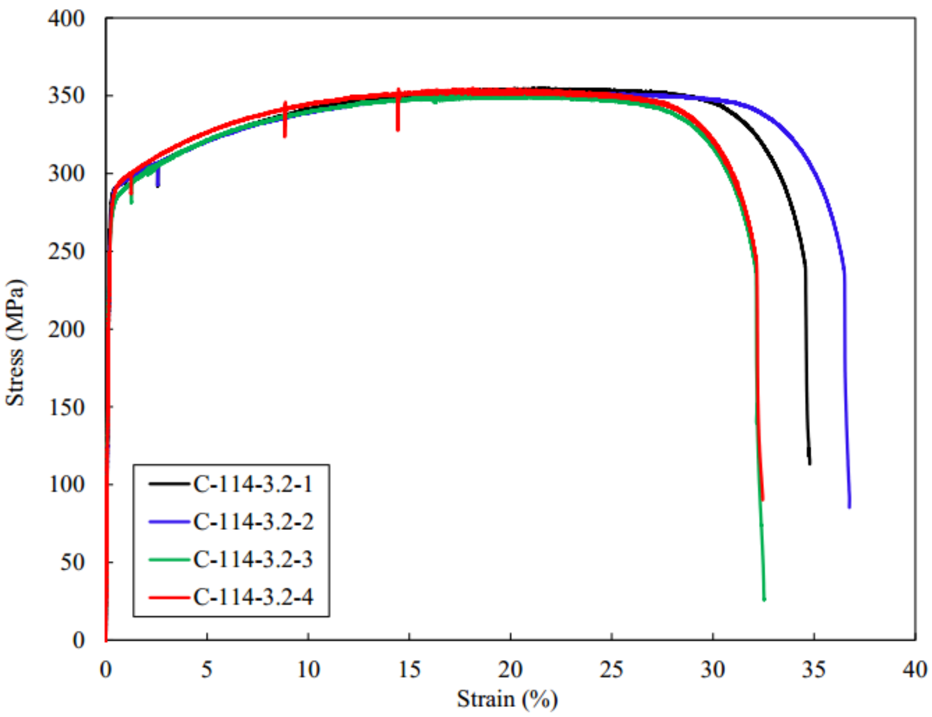

Figure 4.5: Engineering stress-strain curve generated from the tensile coupon test of outer circular steel tube

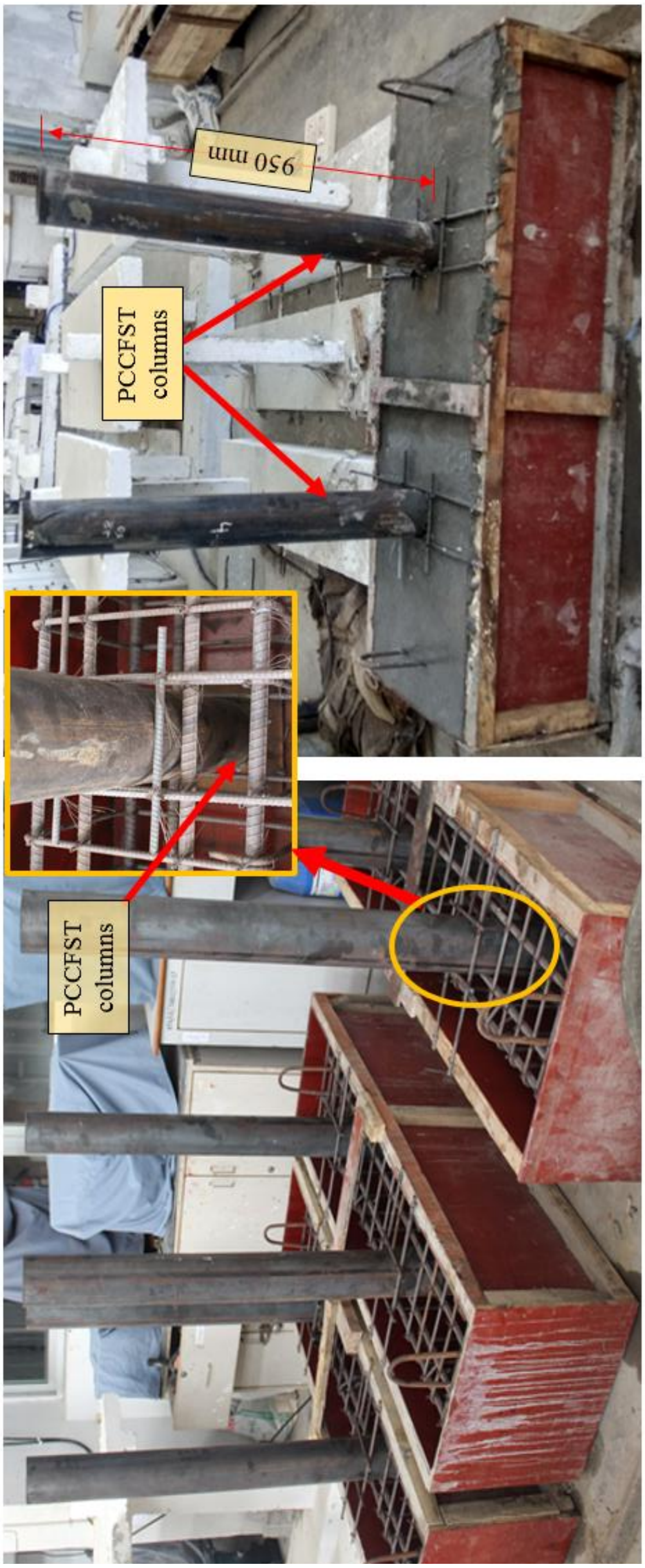

(a) Assembling of components

(b) Cast specimen

Figure 4.6: Specimen preparation

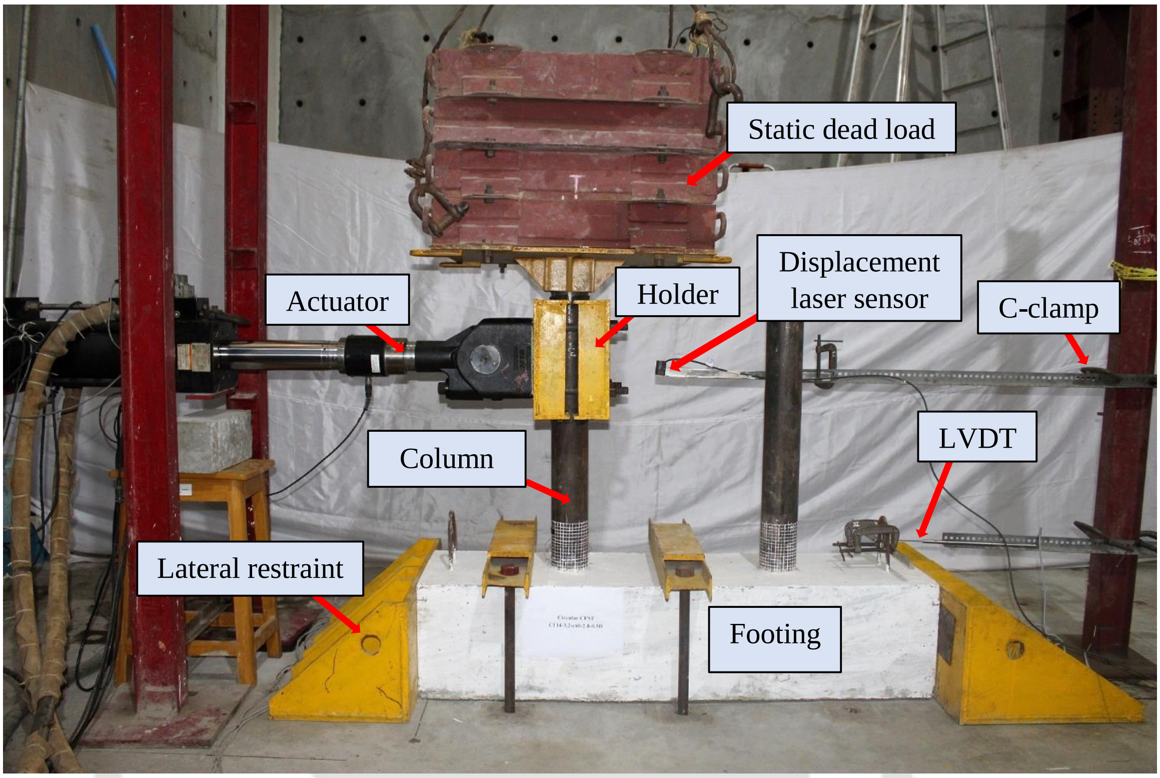

Figure 4.7: Lateral cyclic test set-up

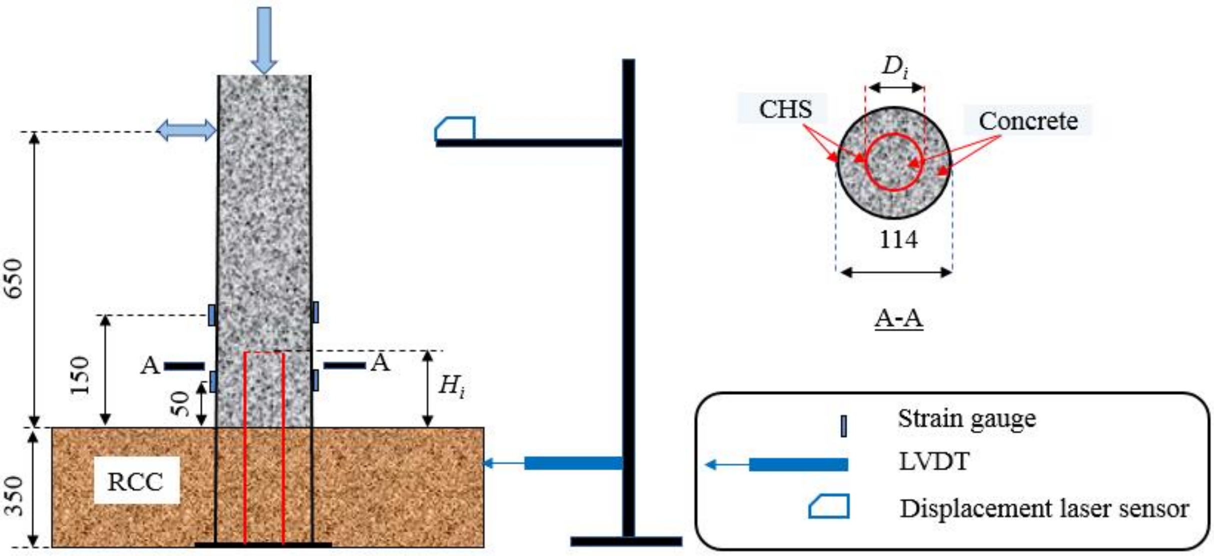

Figure 4.8: Specimen configuration and layout of instrumentation (unit: mm)

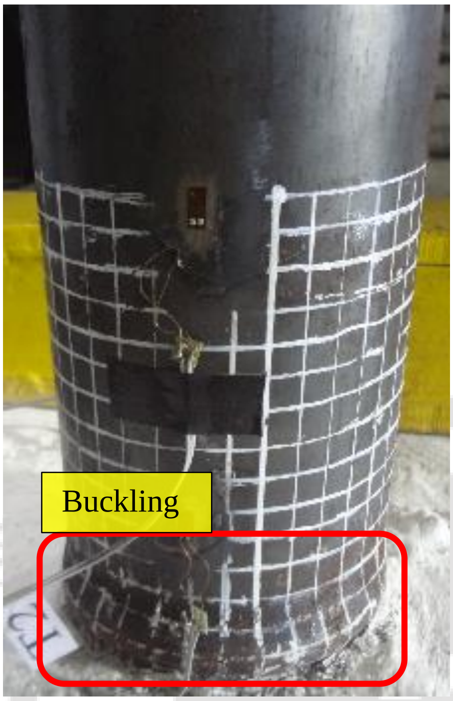

(a) C114-c0

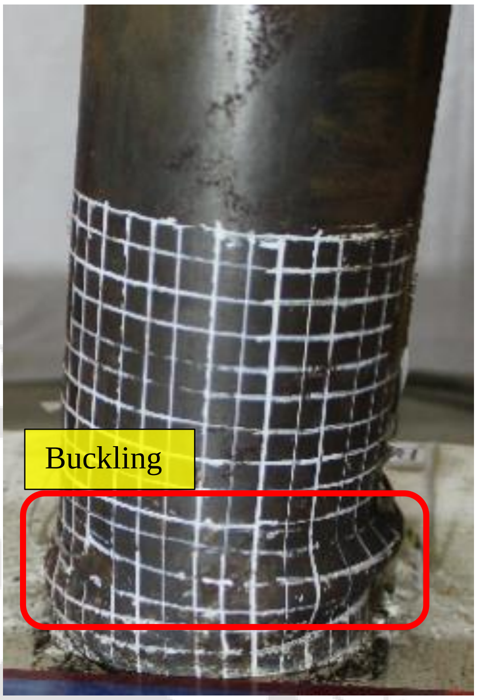

(b) C114-c60-3.2-0.5D

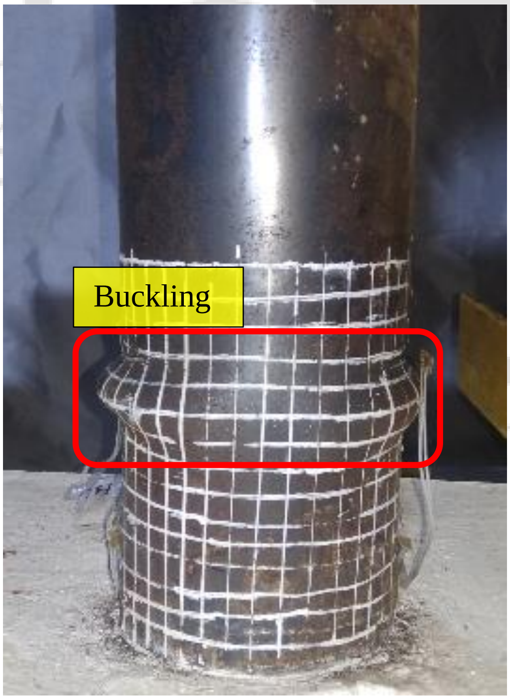

(c) C114-c60-3.2-1D

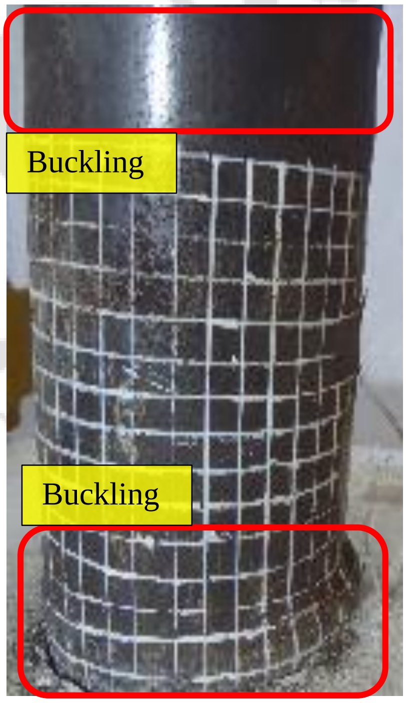

(d) C114-c60-3.2-1.5D

Figure 4.9: Typical failure pattern of the specimens

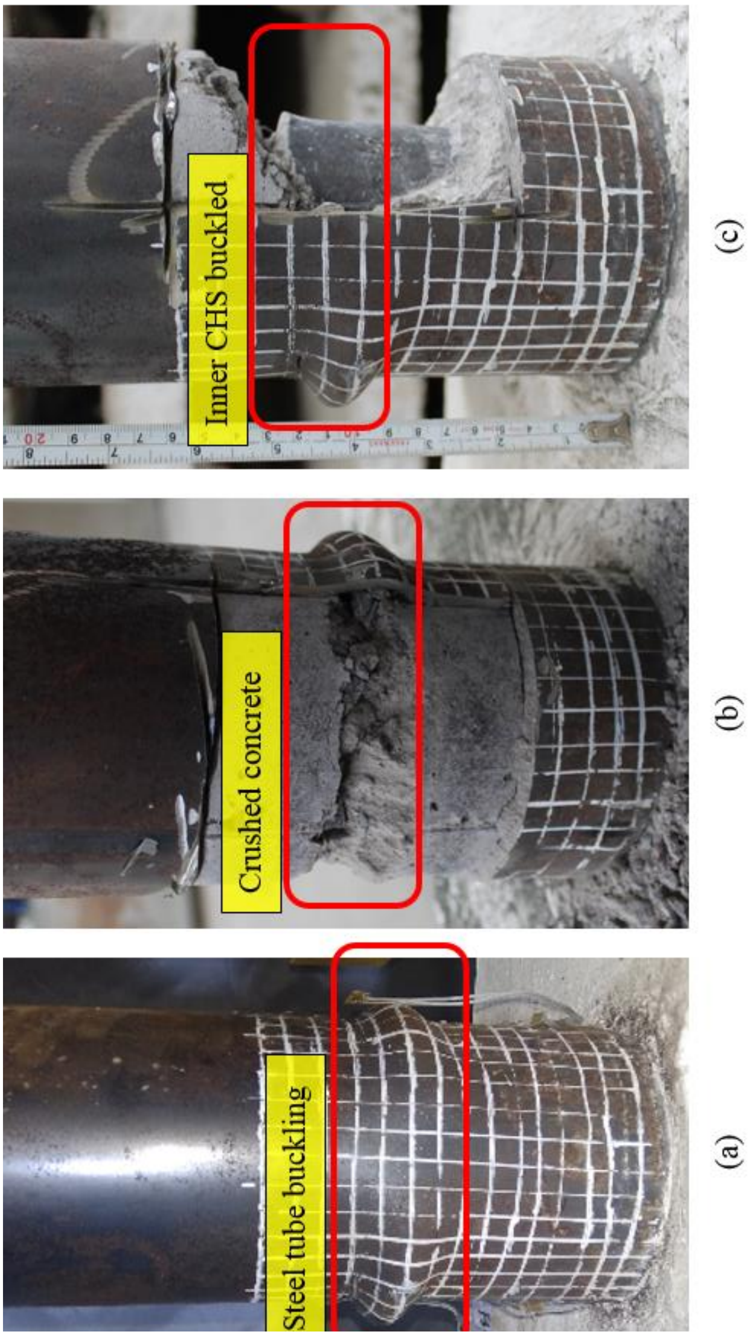

Figure 4.10: Typical failure mode of the 1D specimen

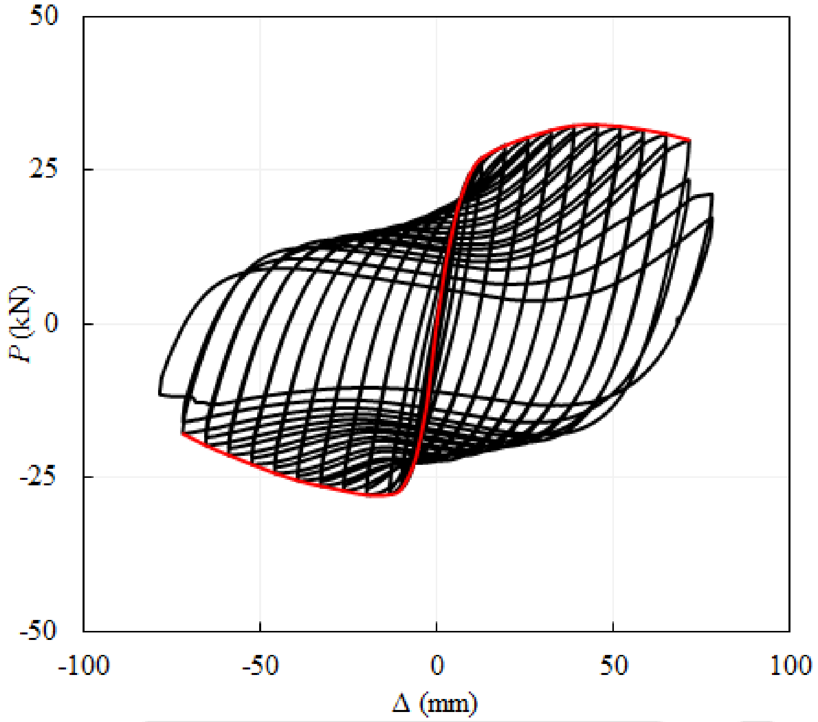

(a) C114-c0

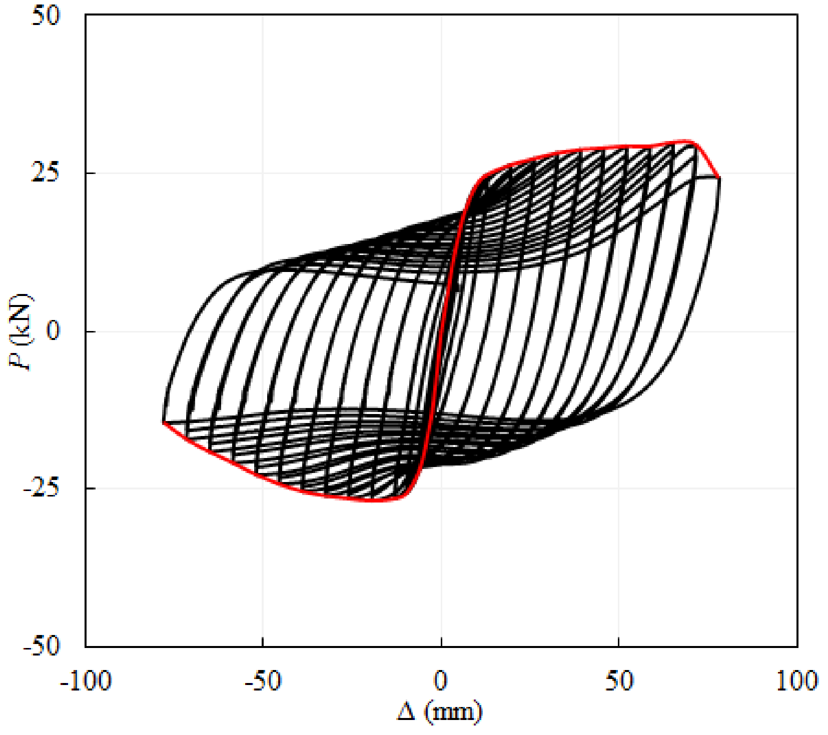

(b) C114-c50-0.5D

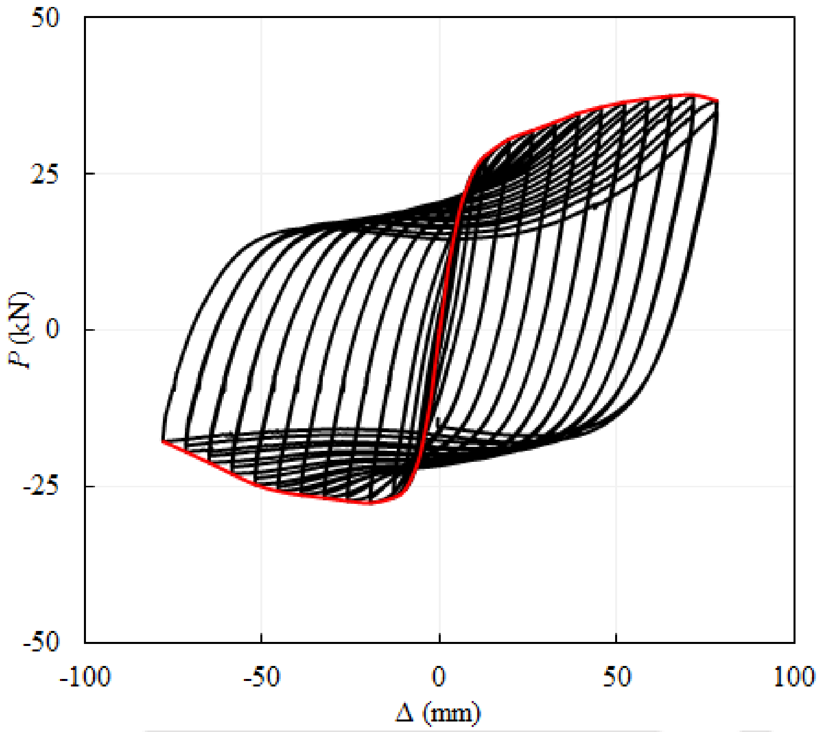

(c) C114-c50-1D

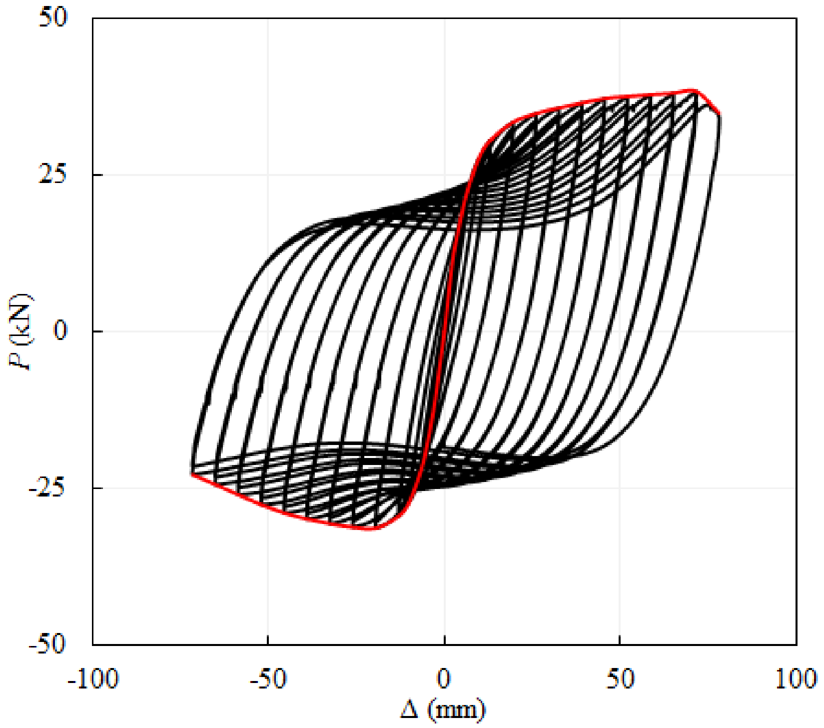

(d) C114-c50-1.5D

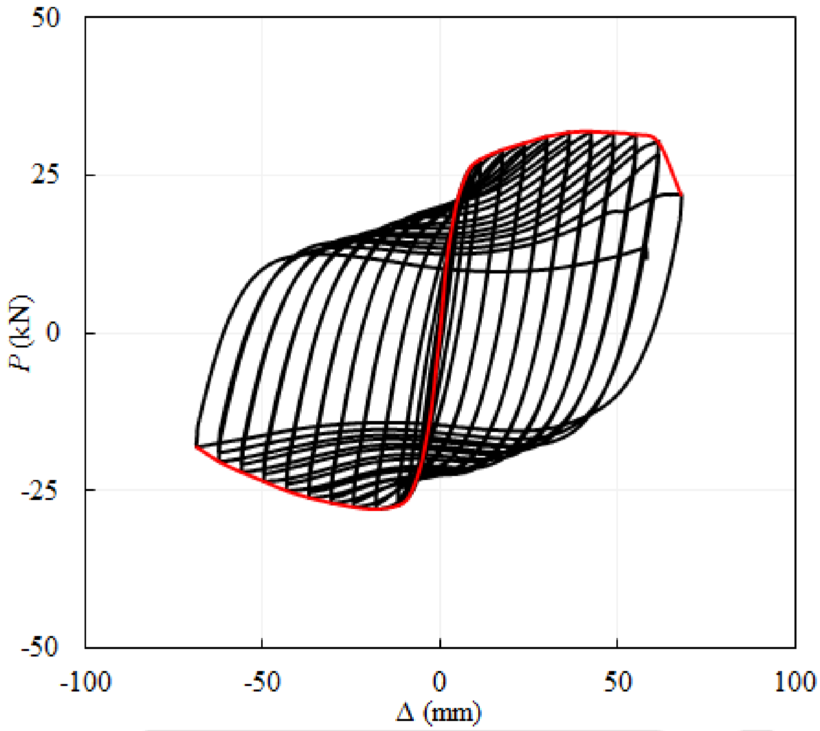

(e) C114-c60-0.5D

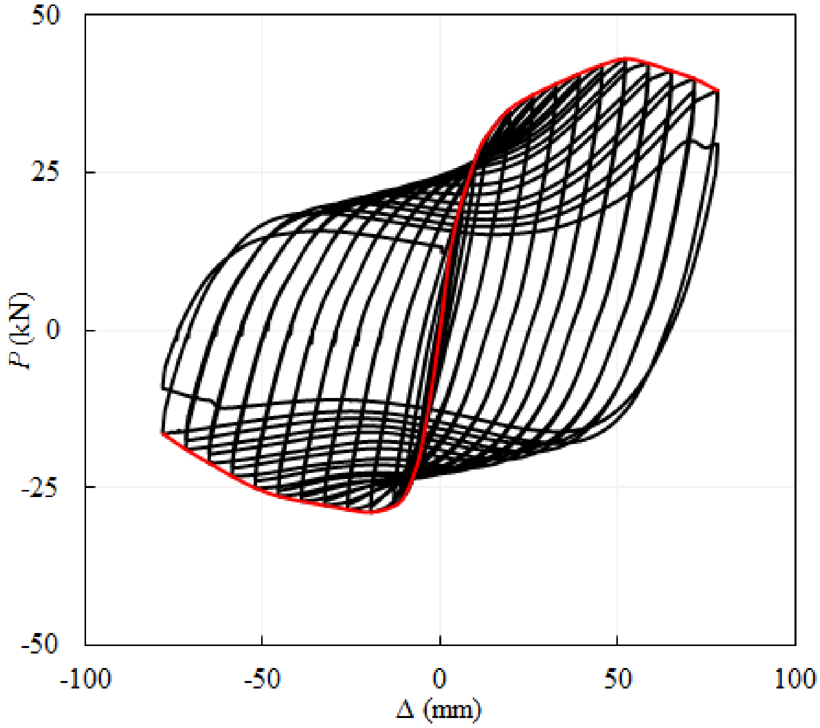

(f) C114-c60-1D

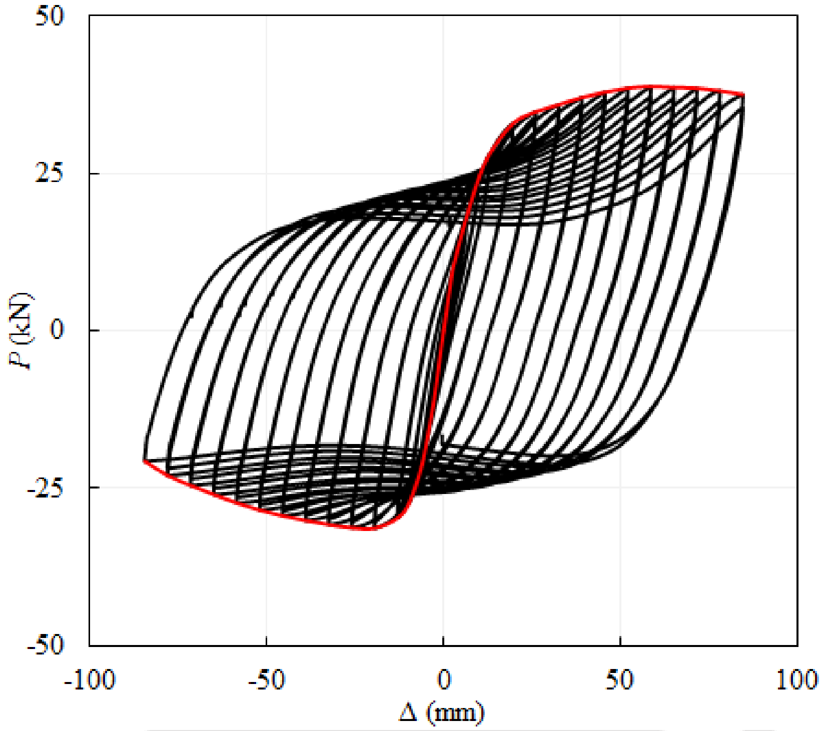

(g) C114-c60-1.5D

Figure 4.11: Lateral loads (P)- displacement (Δ) hysteresis curves

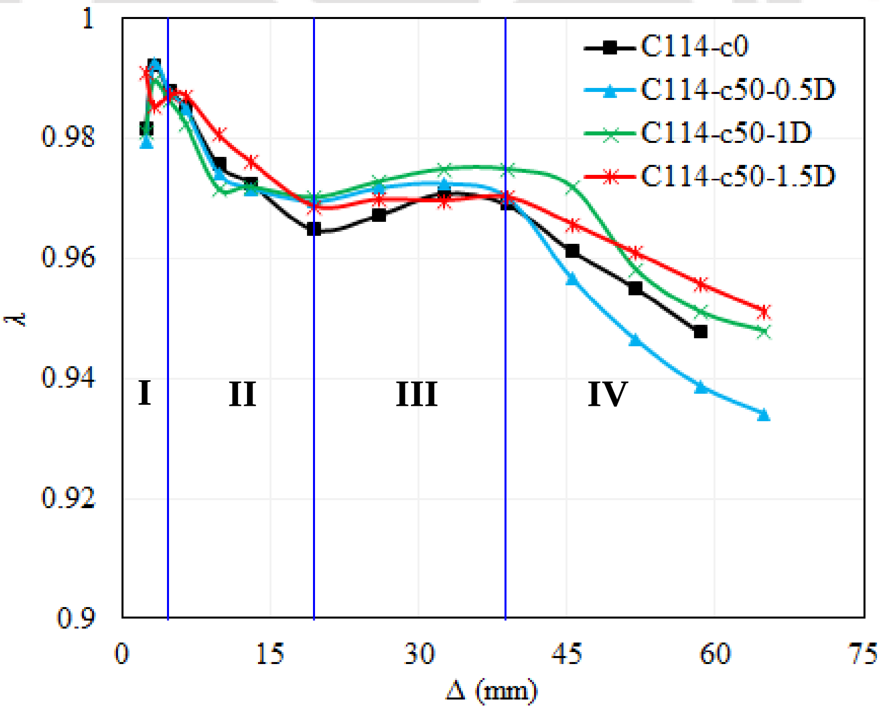

(a)

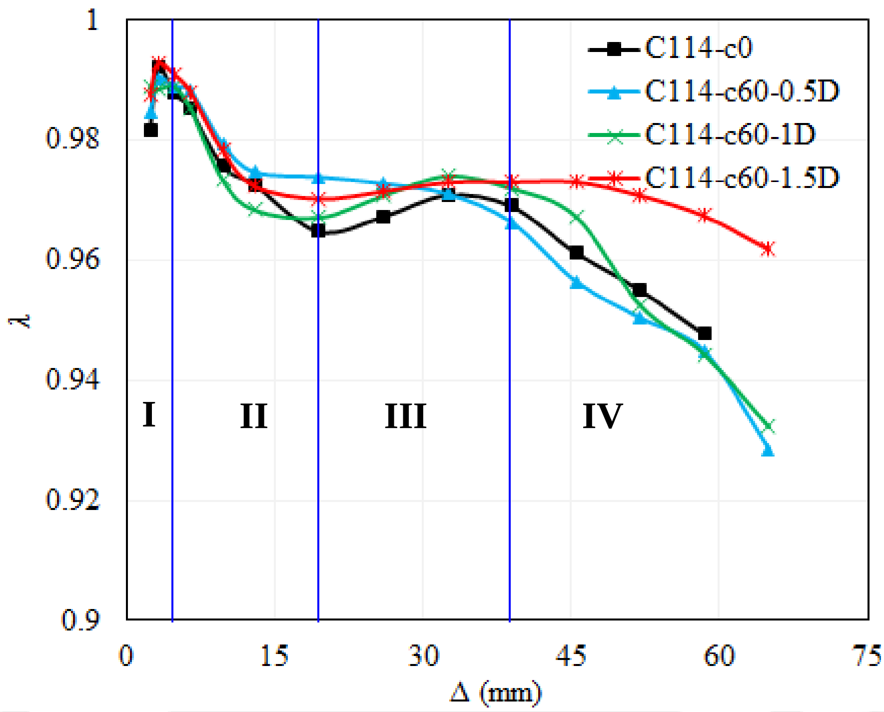

(b)

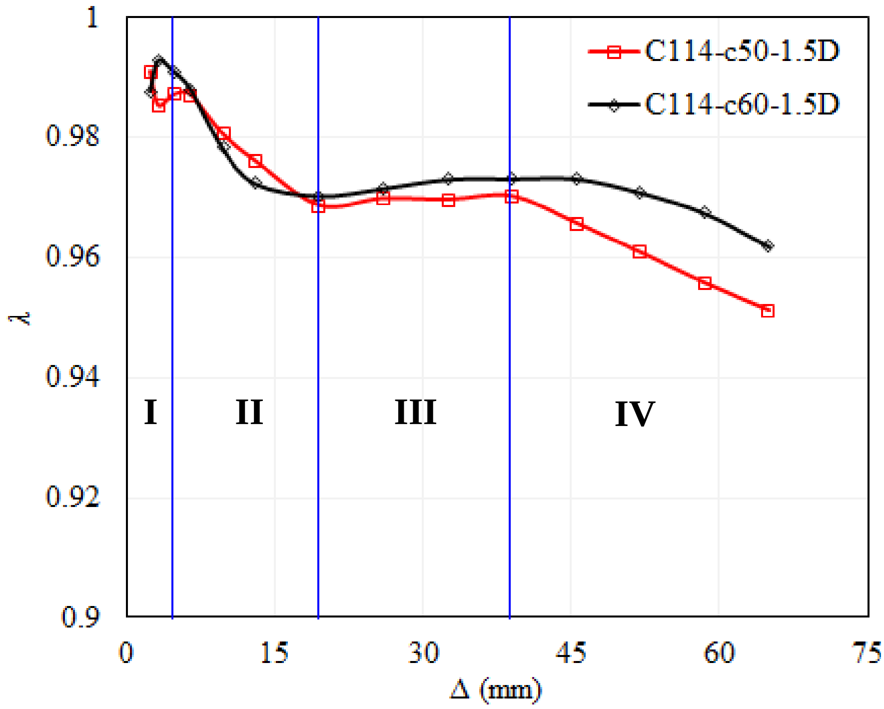

(c)

Figure 4.12: Strength degradation curve: (a) Di/D=0.44, (b) Di/D=0.53, (c) Hi/D=1.5

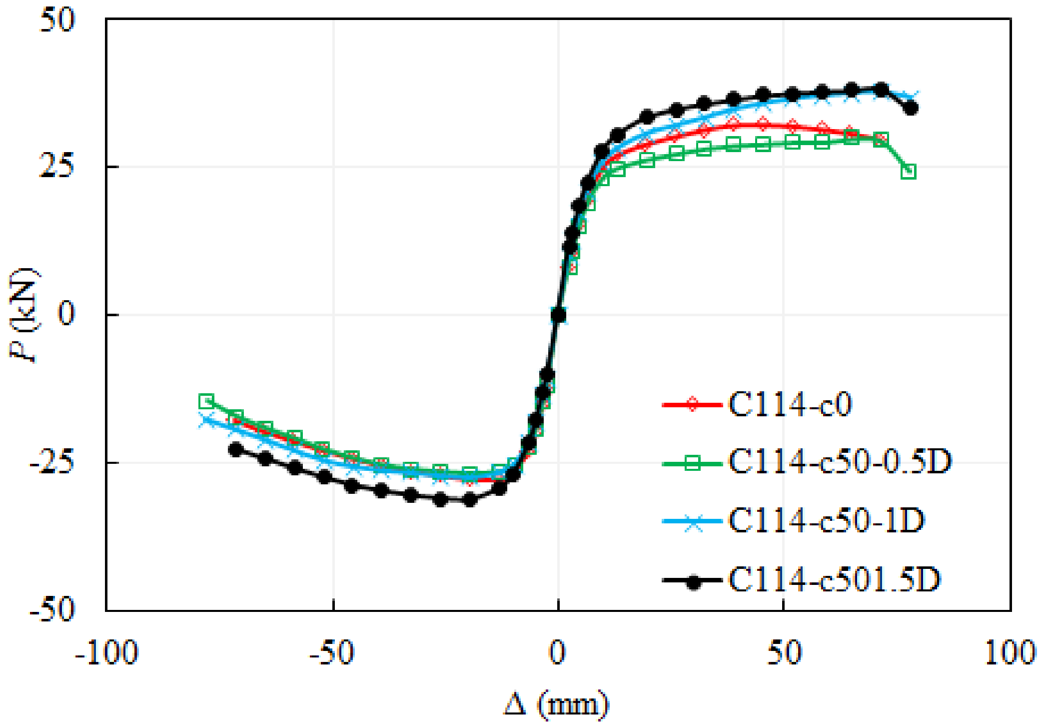
50
25
0
-25
-50
P (kN)
-100
-50
0
50
100
Δ (mm)
C114-c0
C114-c50-0.5D
C114-c50-1D
C114-c501.5D

(a)

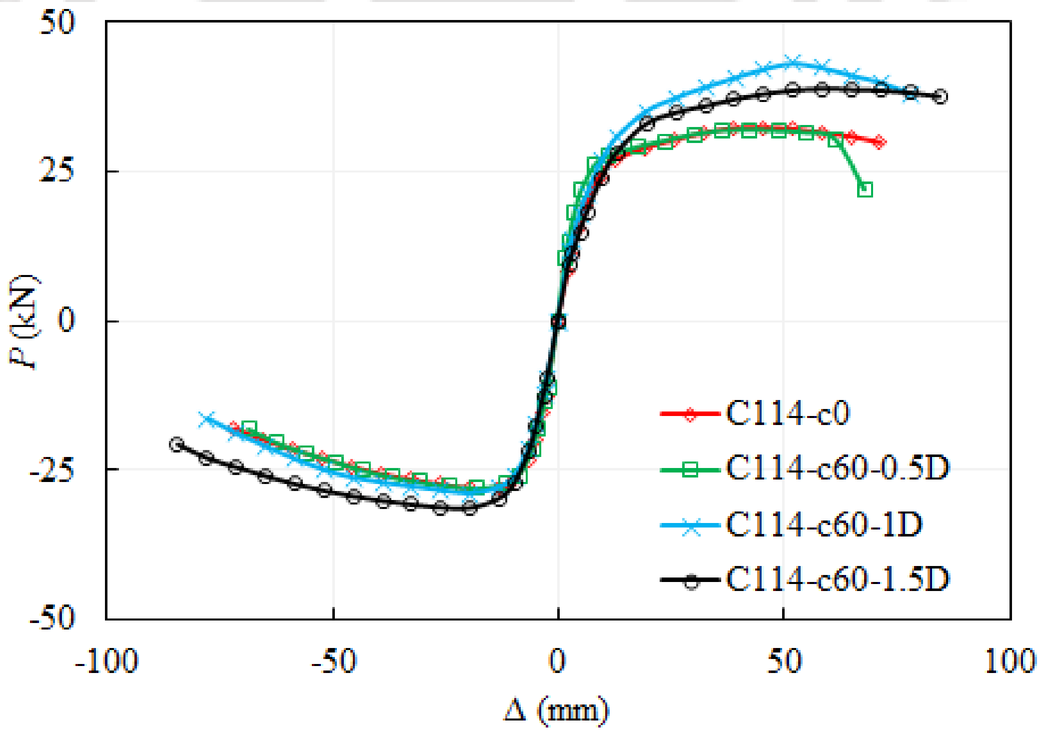
50
25
0
-25
-50
P (kN)
-100
-50
0
50
100
Δ (mm)
C114-c0
C114-c60-0.5D
C114-c60-1D
C114-c60-1.5D

(b)

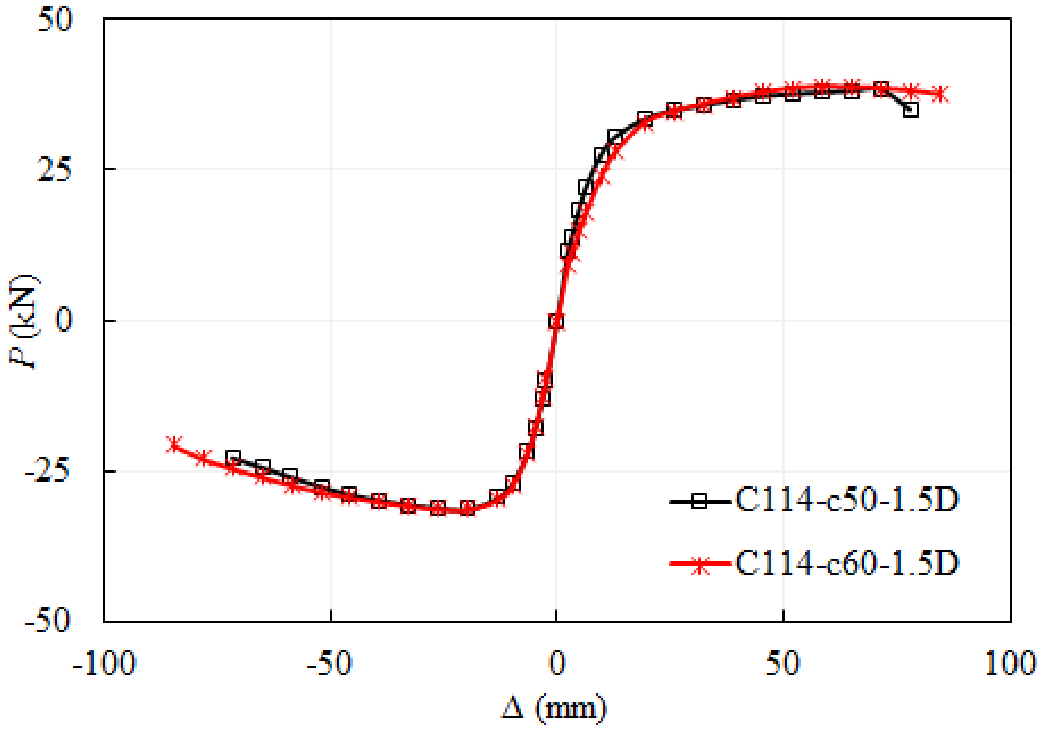

(c)

Figure 4.13: Lateral loads (P)- displacement (Δ) envelope curves: (a) Di/D=0.44, (b) Di/D=0.53, (c) Hi/D=1.5

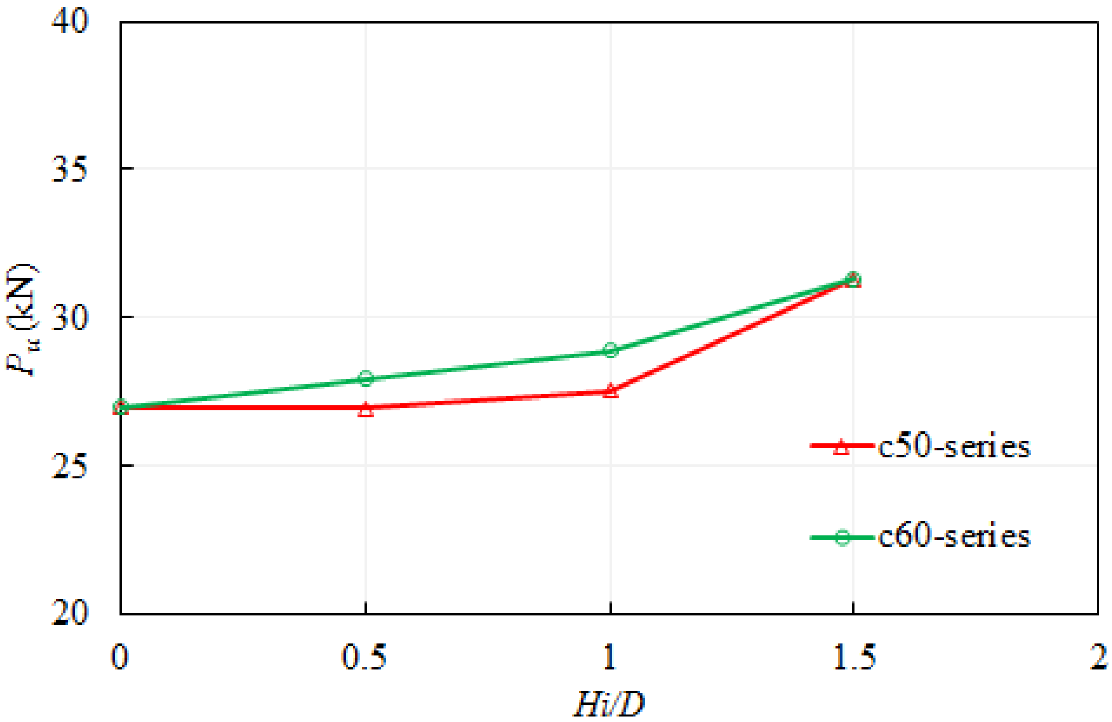

Figure 4.14: Maximum lateral strength (Pu) Vs Hi/D ratio

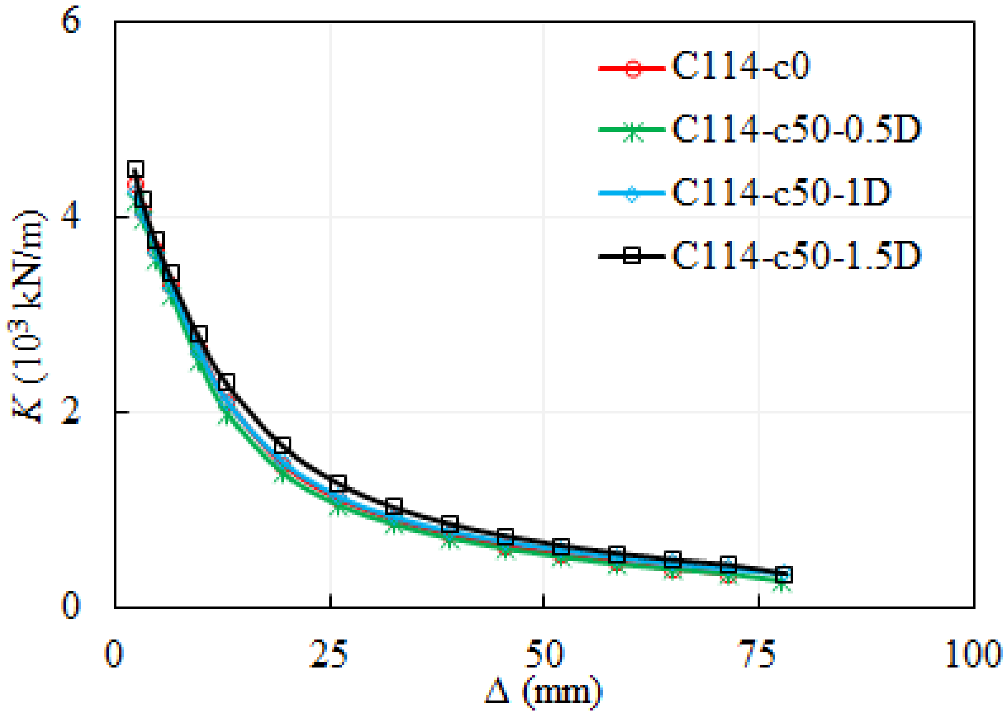
6
4
2
0
K (10³ kN/m)
0
25
50
75
100
Δ (mm)
C114-c0
C114-c50-0.5D
C114-c50-1D
C114-c50-1.5D

(a)

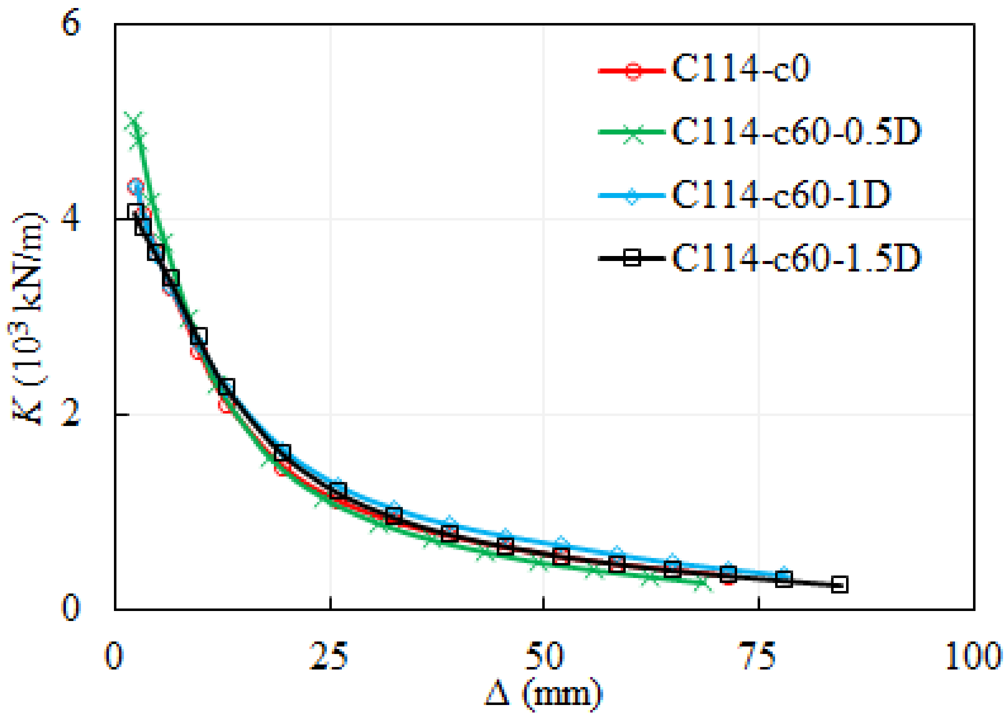
6
4
2
0
K (10³ kN/m)
0
25
50
75
100
Δ (mm)
C114-c0
C114-c60-0.5D
C114-c60-1D
C114-c60-1.5D

(b)

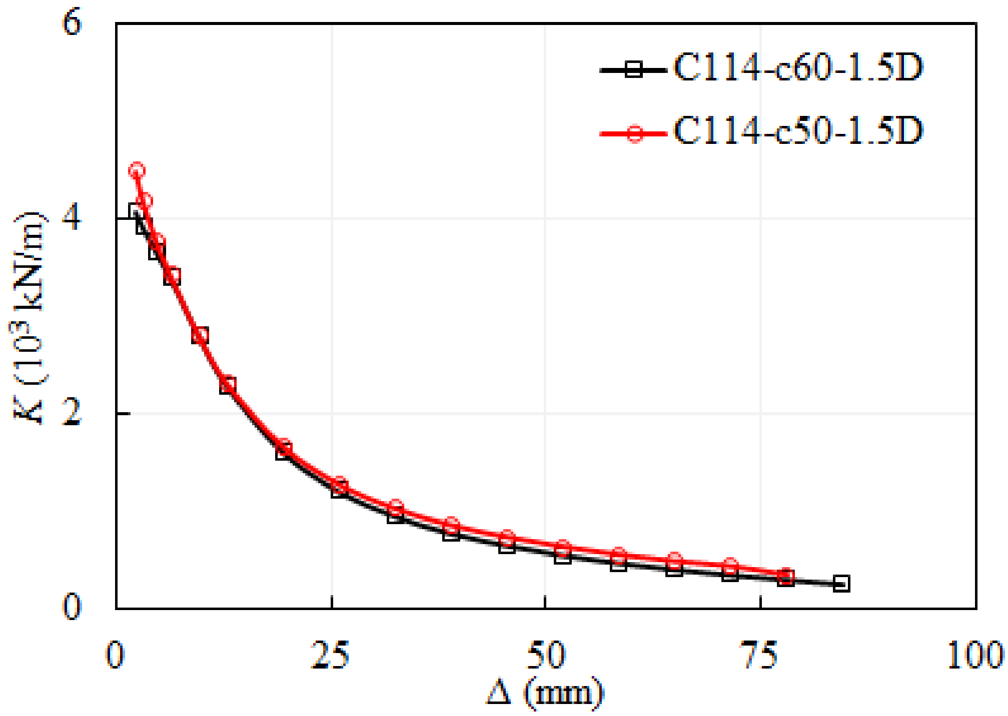

(c)

Figure 4.15: Stiffness degradation curves: (a) Di/D=0.44, (b) Di/D=0.53, (c) Hi/D=1.5

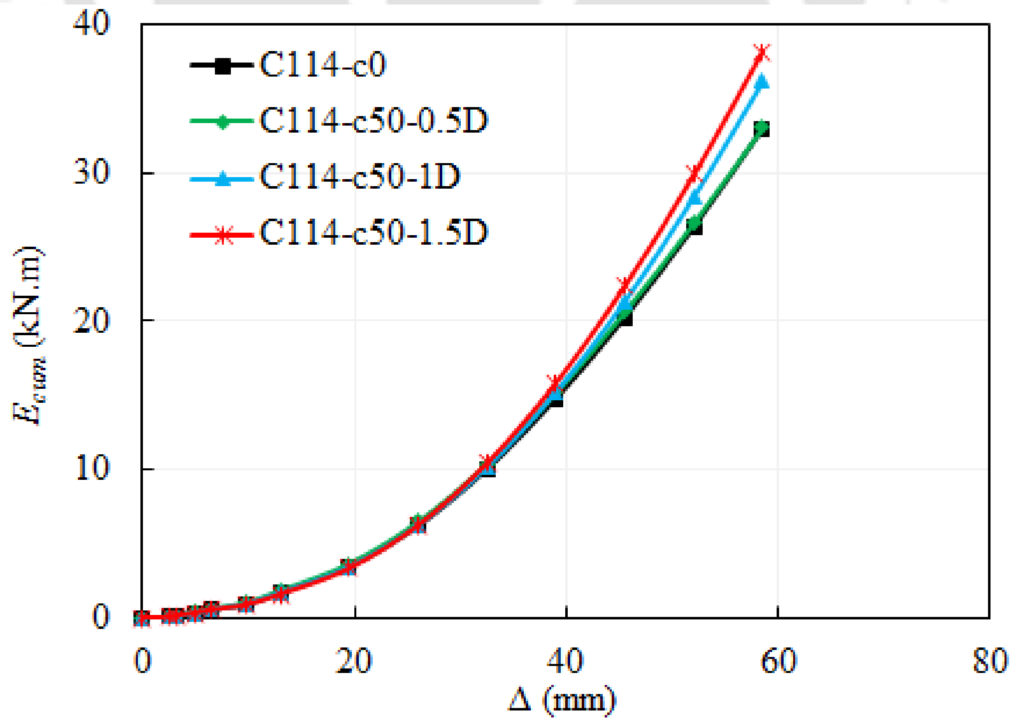

(a)

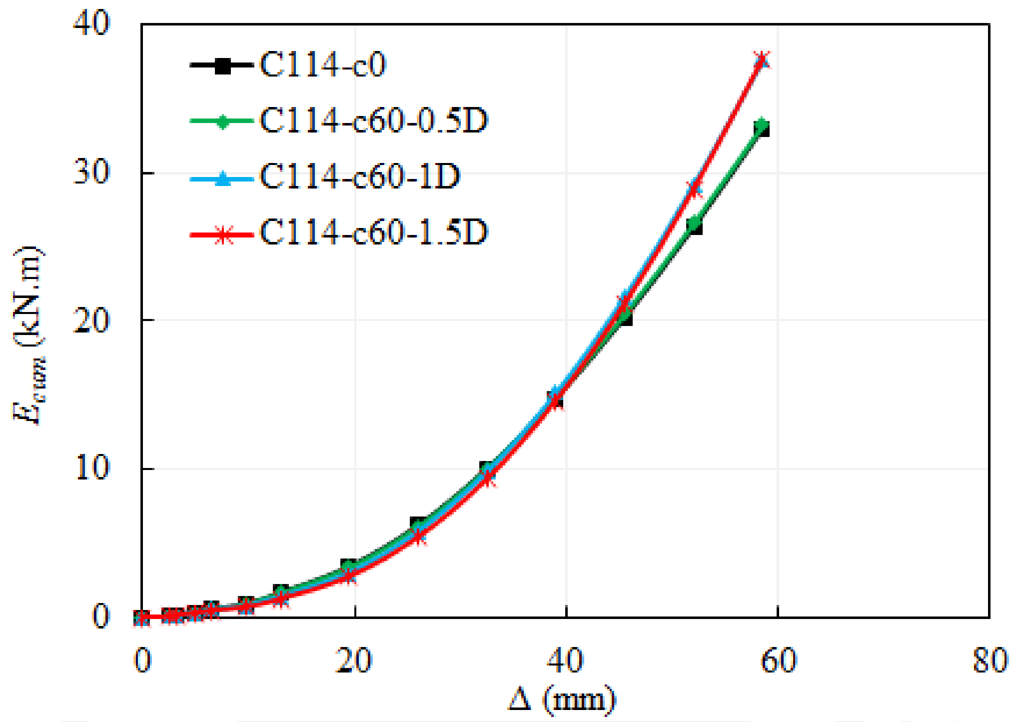

(b)

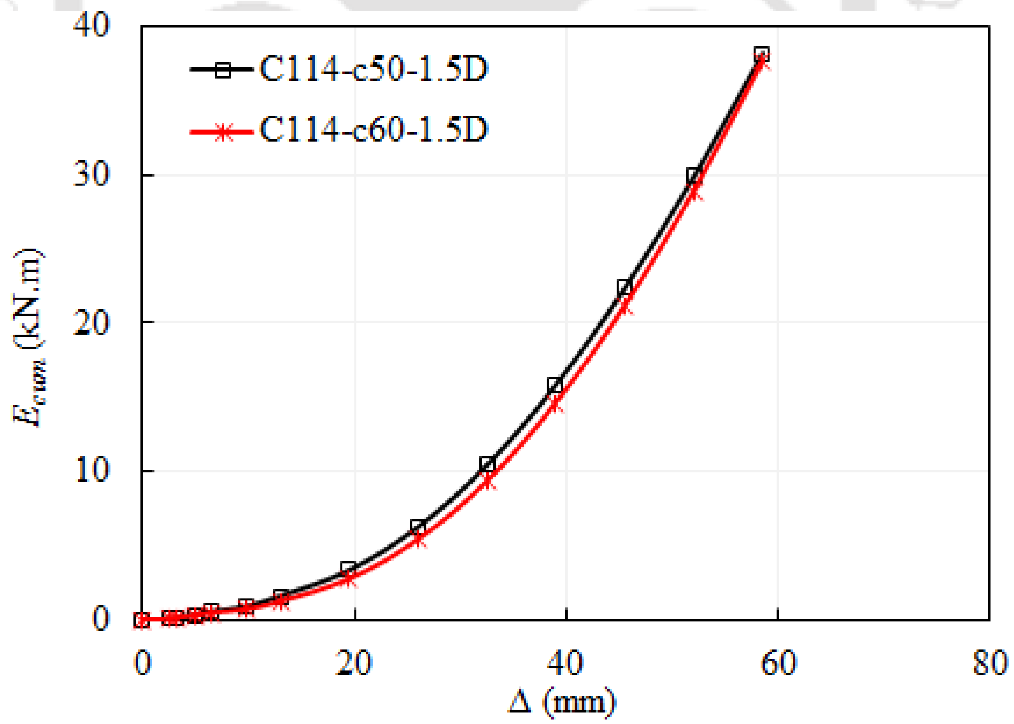

(c)

Figure 4.16: Cumulative energy dissipation (E_{cum}) versus lateral displacement (Δ) curves: (a) Di/D=0.44, (b) Di/D=0.53, (c) Hi/D=1.5

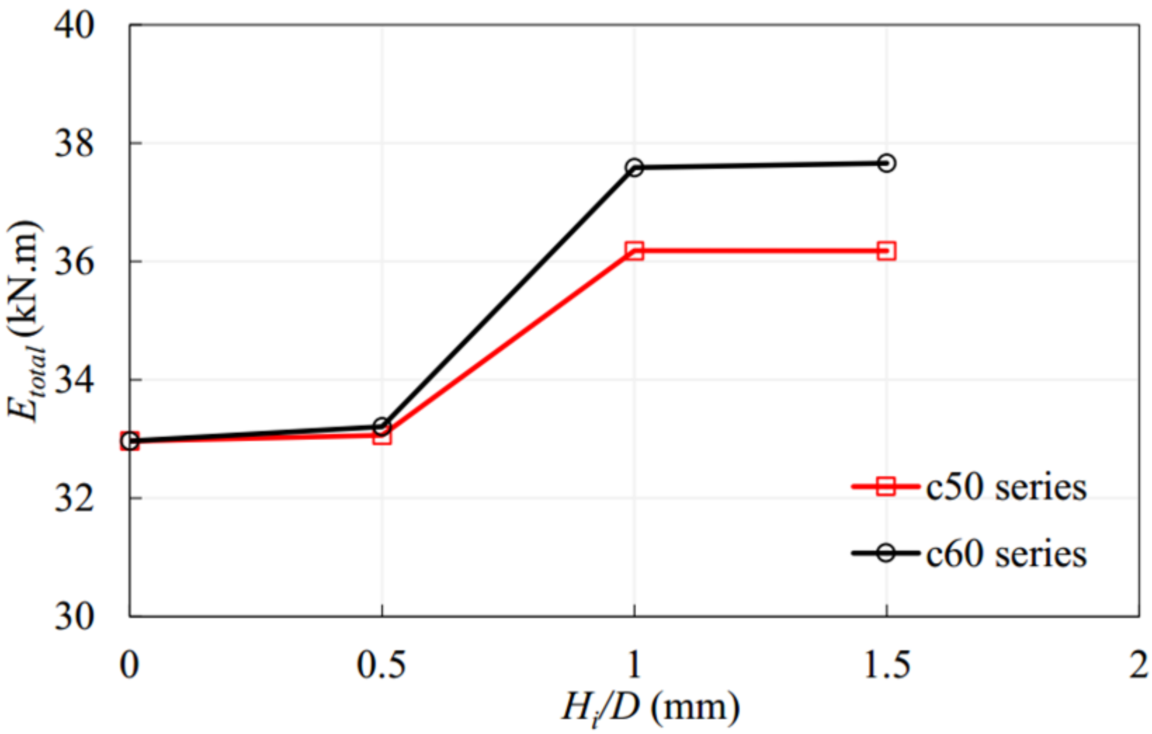

Figure 4.17: Effect of Hi/D ratio (0-1.5) on E_{total}

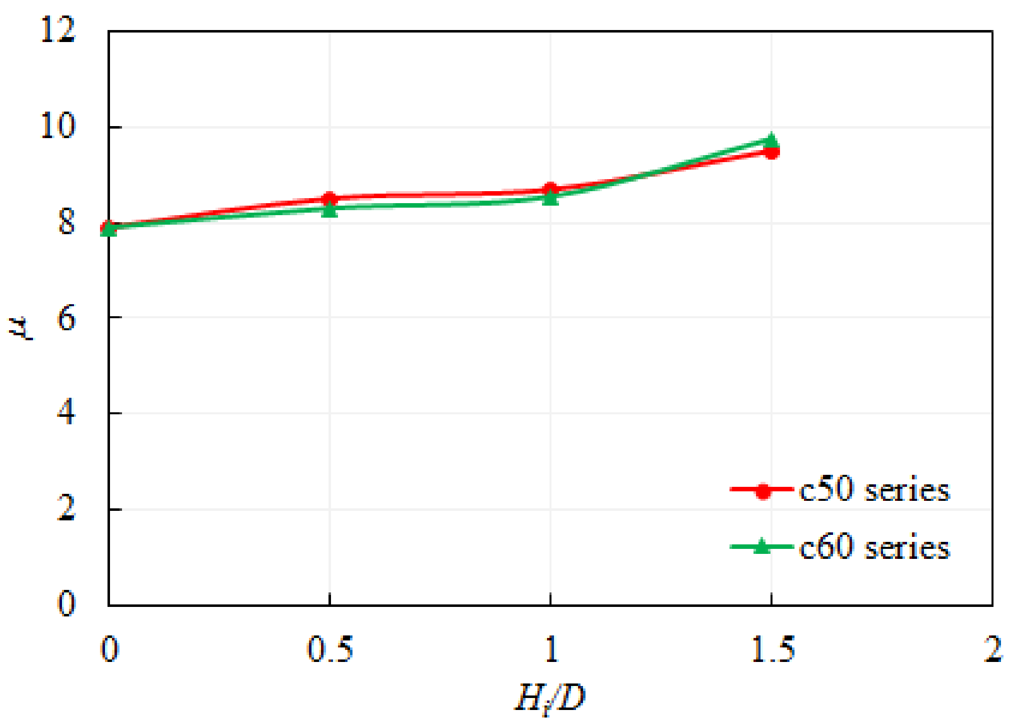

Figure 4.18: Ductility coefficient curve

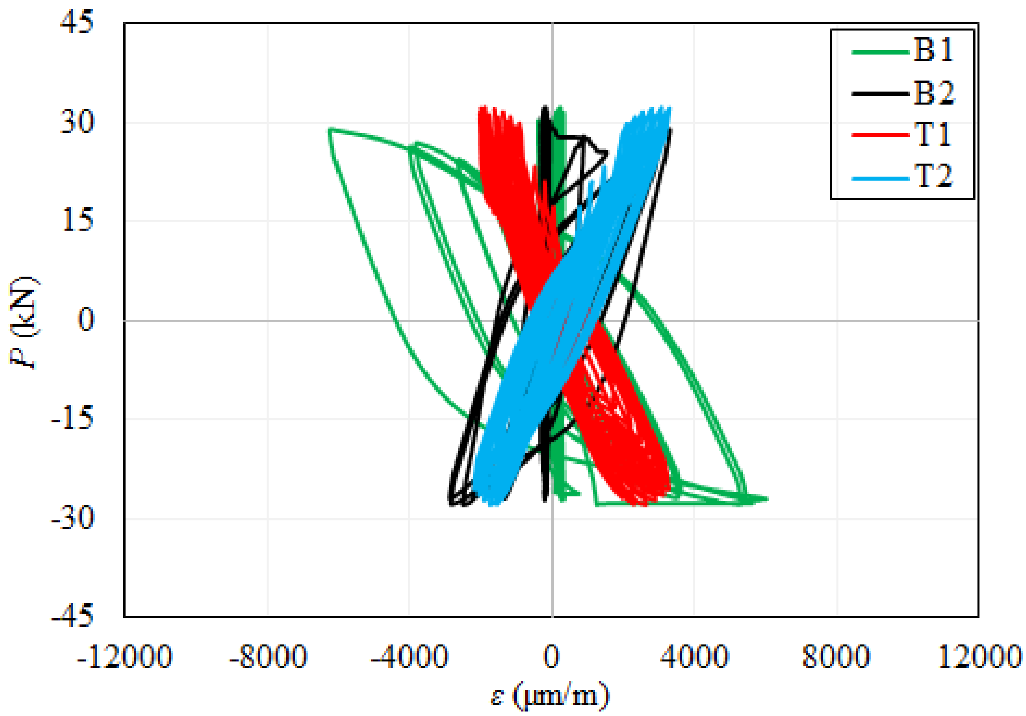

(a) C114-c0

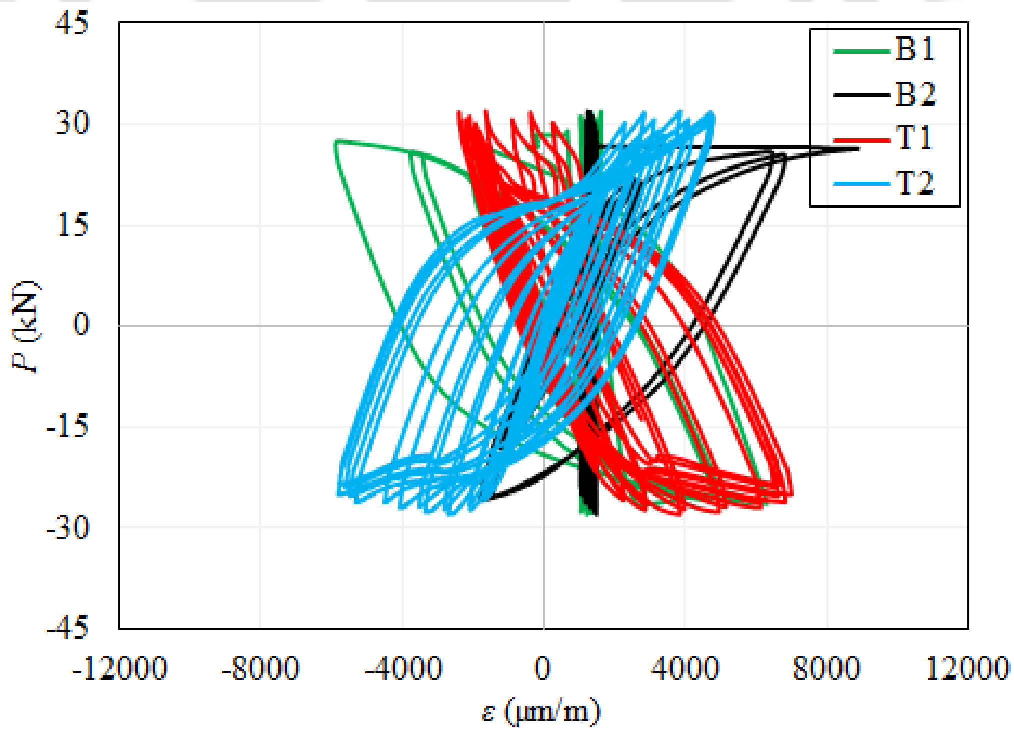

(b) C114-c60-0.5D

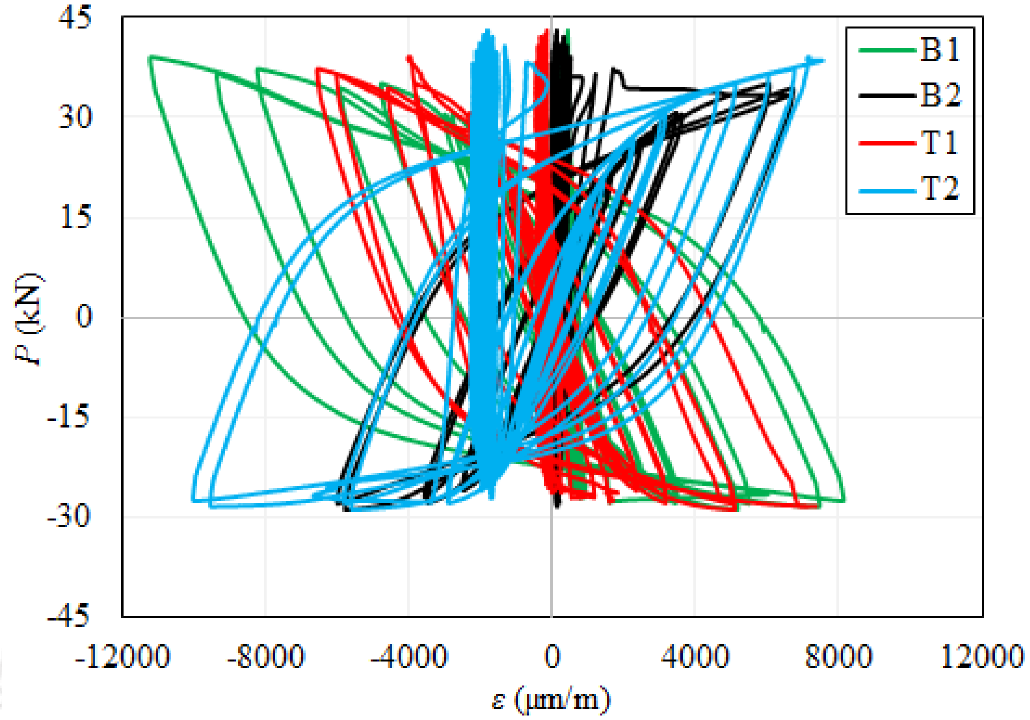

(c) C114-c60-1D

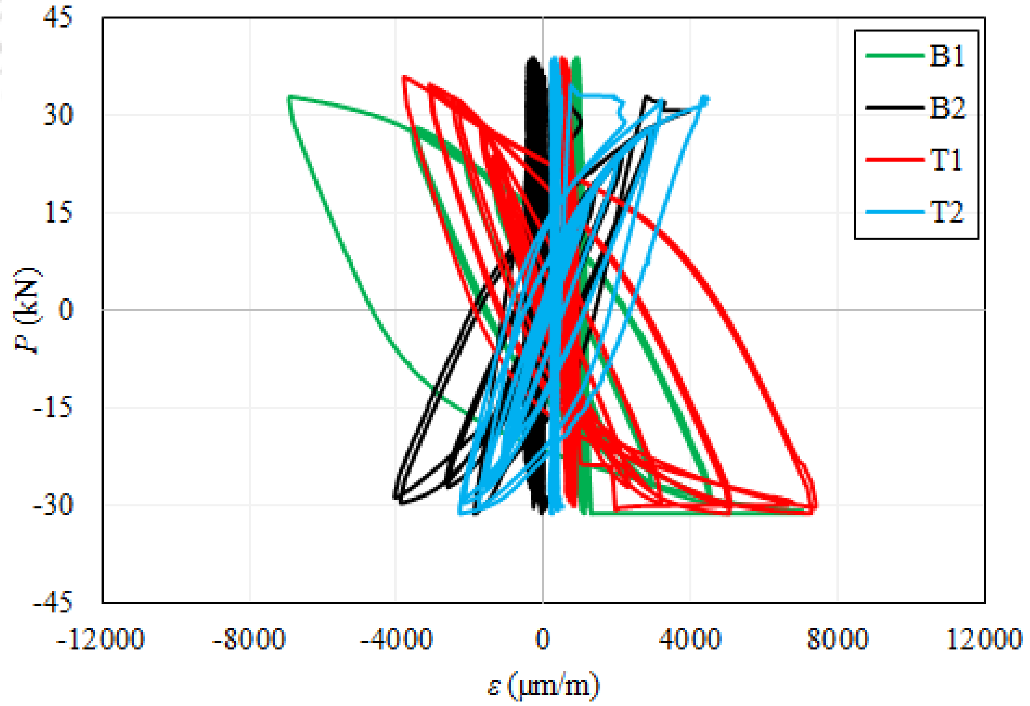

(d) C114-c60-1.5D

Figure 4.19: Lateral force (P) - outer circular steel tube strain (ε) plots (Di/D=0.53)

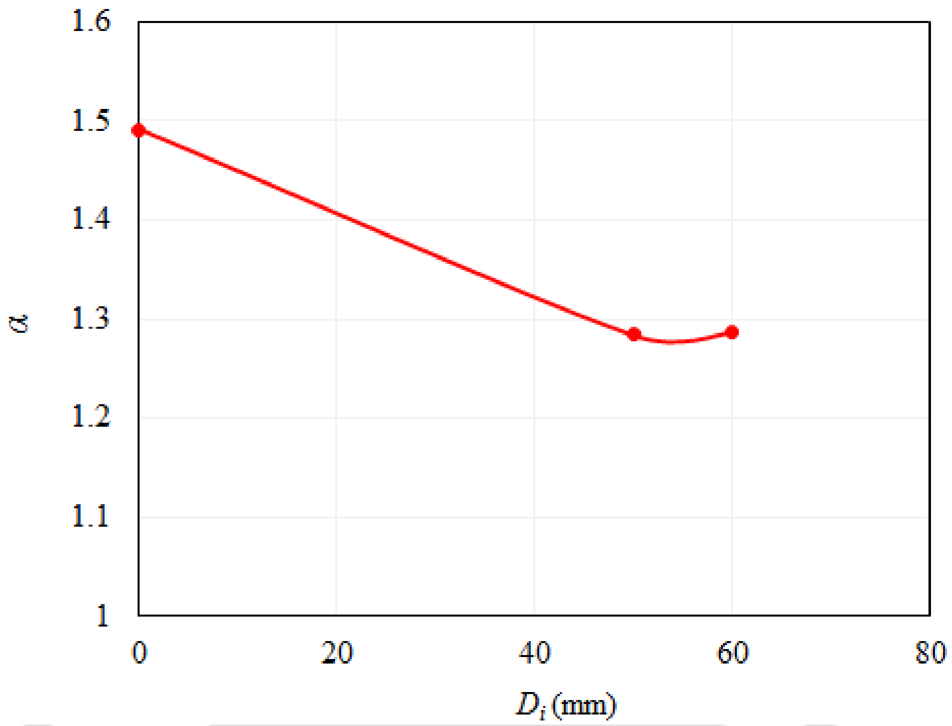

Figure 4.20: α vs D_i plot

This page is intentionally left blank

Chapter 5

Externally Retrofitted PC-CFST Square Columns under Cyclic Lateral Loading

5.1 INTRODUCTION

The structural performance of the square partially confined CFST columns have been assessed under combined axial and lateral cyclic loading in Chapter 3. In the present study, a novel retrofitting technique has been introduced to retrofit those damaged columns (CFST or plastic hinge strengthened-CFST) using square and circular CFST sections externally. The proposed retrofitting technique has been shown schematically in Figure 5.1. The effectiveness of using CFST as retrofitting element, the effects of the shape of the retrofitting element and the contribution of partial confinement to the retrofitted columns has been assessed experimentally. The hysteretic behavior, ultimate lateral strength, and energy dissipation capacity of the retrofitted specimens are reported in the current chapter.

5.2 DETAILS OF THE TEST PROGRAM

5.2.1 Specimens design

The experimental program consisted of 3 retrofitted columns: 1 CFST column externally retrofitted with square retrofitting element, 2 PCCFST columns consisting of 1.5D height of inner circular hollow section (CHS) externally retrofitted with square and circular retrofitting elements, respectively. A retrofitting element consisted of two parts: a) the retrofitting steel element and b) the sandwiched concrete. (See Figure 5.4(b); Hereafter, it would be referred to as a 'retrofitting element'. All these specimens were provided with a retrofitting element of height 1.75*D* above the stiff RC footing filled with concrete (sandwiched concrete). All the PCCFST specimens consist of one concentric CHS inner tube. The height of the circular inner tube was ~1.5*D* from the top of the rigid RC footing. The height (*H*) of all the columns was 650 mm (height of the column from the top of rigid RC footing (column end) upto the level at which lateral cyclic load was applied (column head)). The concrete mix prepared for the retrofitting element was the same (i.e. concrete cube strength, f_{cu} ~ 31 MPa) as that of CFST / PCCFST columns mentioned in Chapter 3. The constant axial loading for the current set of retrofitted columns was maintained same as it was mentioned in Chapter 3. All the experimental findings of the retrofitted specimens were compared with their corresponding original reference specimens.

The specimens were designated by the nomenclature Sp-cq-r-χ, where 'Sp' refers to the outer square steel tube of 'p' width, 'cq' to the inner circular steel tube of 'q' diameter, 'r' to the height of the inner circular steel tube, and 'χ' to the shape of the retrofitting element (where S and C refer to the square and circular sections, respectively). The specimen designated S114-c0 was devoid of an inner steel tube, and the specimens with no 'χ' are the reference set of specimens. Table 5.1 shows the average geometric dimension of the specimens.

5.2.2 Material properties

5.2.2.1 Steel and concrete

Flat steel sheets of 3.2 mm thickness were bought from the local market. All the sheets were then cold-formed to fabricate the desired steel sections (square and circular) to be used as retrofitting steel elements. The width/diameter (D_0) of the square and circular sections were taken to be 200 mm (~1.75D). The height (H_0) of the steel sections was considered to be 200 mm (~1.75D) so that the whole plastic hinge region could be merged within it. A standard tensile coupon test, in accordance with (ASTM E8 2016), was used to examine the mechanical characteristics of all the steel sections. A set of coupon specimens were cut from the fabricated steel sections (both square and circular). A 250 kN capacity universal testing machine (UTM) was used to test all the coupon specimens. The displacement rates of the test were followed as per the recommendation of (Huang and Young 2014). Similar tensile test set-up as mentioned in the previous chapter was used in the current chapter. The engineering stress-strain curves obtained from the tensile coupon test has been shown in Figure 5.2. The average mechanical properties thus obtained in terms of yield strength (f_y) and ultimate strength (f_u) are reported in Table 5.2. As per the mechanical properties, the used steel tubes were of grade YSt 210 for both square section(IS 4923 2009) and circular section (IS 1161 1998)). The grade of steel used to fabricate PCCFST columns has been shown in Chapter 3.

The grade of concrete used to cast the retrofitting element was the same as mention in the chapter 3 to cast the CFST or PCCFST columns. All the retrofitting elements were cast using the same concrete mix proportion.

5.2.3 Specimens preparation

The damaged square CFST and PCCFST columns of a clear height of 650 mm and outer width of 114 mm were considered for retrofitting purposes. The PCCFST specimens consisting of 1.5D height of inner circular steel tube were used. The testing of the PCCFST specimens was stopped once the 80% drop in the maximum lateral strength was achieved or the steel tube tearing occurred. The details of the retrofitted specimen preparation have been illustrated in Figure 5.3. Firstly, the concrete at the vicinity of the column end has been removed. The removal of the concrete went down up to approximately 25 mm down the top layer of 16 mm longitudinal rebar of the footing and laterally approximately 250 × 250 mm square area (see Figure 5.3). The deformed, damaged square specimens were vertically realigned by applying push and pull via an actuator on the strong floor. Fabricated retrofitting steel elements were provided with flat steel hooks welded internally at the mid-height. Damaged square specimens were provided with similar flat steel hooks welded externally but at a different level than the retrofitting steel. Flat hooks were provided to exhibit a composite action between the retrofitting element and the damaged square column. The retrofitting steel element was placed on the rebar of the footing in such a way that the welding line should lie in none of the loading faces so as to maintain the member's symmetry. To connect the retrofitting element to the footing and thereby to the damaged specimen, eight ‘U’ hooks were prepared using 8 mm rebar with the length of each leg to be approximately 70-80 mm, welded vertically with both the retrofitting steel and rebar of the footing together. A layer of cement slurry has been applied on the footing region to be cast as the retrofitting element to enhance the bonding between two layers of concrete. The freshly prepared concrete is then poured inside the retrofitting steel and compacted, followed by curing for 28 days. In order to test the concrete's strength, three 150 mm standard cubes were also cast during the concreting of the retrofitting element. During curing, no significant shrinkage of concrete could be seen. After 28 days of curing and drying for another 2- 3 days, the specimens are ready to be tested.

5.2.4 Testing frame, instrumentation and loading protocol

At the Indian Institute of Technology Guwahati (Structural engineering laboratory), all the specimens were tested. The typical experimental set-up is shown in Figure 5.4. All the supports mentioned in the previous chapters were used in the current chapter to offer fixed support to the retrofitted column specimens, while the actuator head has been used to provide hinge support at the column head. The axial load was applied at the top via a stack of four loading plates. The axial compressive load was maintained the same during the test. Lateral cyclic loading was also applied in addition to the axial loading, in accordance with (AISC 2016) protocol (discussed in previous chapters). Actuator of 250 kN (MTS) was used to transfer the lateral displacement to the retrofitted columns. The actuator's integrated load cell and transducer measured the lateral resistance and the lateral displacement, respectively. An external displacement laser sensor was also deployed to keep track of the displacement at the column head. An LVDT was further used at the footing level to track if there was any lateral shift to the RC footing. Additionally, for each specimen, two strain gauges were installed diametrically opposite in the compression and tension faces of the retrofitting steel element at the height of 50 mm from the column end to track the retrofitting steel yielding. One strain gauge was installed at the height of 50 mm above the retrofitting element to monitor the outer steel tube yielding at that region. The layout of the instrumentation is illustrated in Figure 5.5. The entire testing process was carried out without a hitch and under a controlled environment.

5.3 EXPERIMENTAL RESULTS AND DISCUSSION

5.3.1 General

Here in this section, the experimental findings and observations are presented and discussed. The pull direction of the actuator was considered to be positive, whereas the push direction was considered to be negative. The set of original reference columns has been named as ‘reference specimens’ and the set of retrofitted columns as ‘retrofitted specimens’.

5.3.2 Description of failure modes

The typical failure mode of the retrofitted specimens has been illustrated in Figure 5.6 (I and II show the damaged retrofitted specimen and cut out of the retrofitting steel, respectively). It has been seen that the specimen with a square retrofitting element was damaged, forming diagonal cracks at the sandwiched concrete portion of the retrofitting element. For specimens S114-c0-S and S114-c60-1.5D-S (specimens with square retrofitting element), the visible initiation of the diagonal cracks occurred at the drift angle (θ) of 1.5%. The widening of the cracks occurs with the increase in each drift angle. Along with the diagonal crack, simultaneously some gap was also observed along the compression and tension region of the retrofitting element. With the progress of the test, the width of the gap increased. The maximum gap width observed at the end of the test was approximately 15 mm and 5-7 mm for S114-c0-S and S114-c60-1.5D-S, respectively. At the same time, the bulging of the retrofitting steel wall at the top corners could be seen. However, no such diagonal cracks could be seen for the S114-c50-1.5D-C specimen, but with the progress of the test, a small gap between the retrofitting element and PCCFST column was seen at the later stage (~at θ =7%) at the same time very insignificant gap was also seen between the retrofitting element and the footing. The reason behind the small or insignificant gap width in the case of retrofitted PCCFST could be the stiffness imparted by the inner CHS. At a drift angle of 7%, specimen S114-c50-1.5D-C showed initiation of diagonal cracks at the footing, which gradually widened with higher drift angles. However, no trace of cracks on the footing was observed for S114-c0-S or S114-c60-1.5D-S. No visible significant buckling of the square CFST could be seen for S114-c0-S. Whereas, for S114-c60-1.5D-S and S114-c50-1.5D-C, visible significant buckling of the square CFST could be seen at the drift angle of 7% and 5%, respectively. The outer square steel tube's buckling became increasingly visible as the drift angle gradually increased.

Figure 5.6 (II) shows the sectional cut-views of retrofitting element after the retrofitting steel element was removed. It was evident from the sectional cut views at the column's base that the sandwiched concrete had been compacted to the desired degree. Horizontal cracks along the flat hook could be seen on the sandwiched concrete. Neither serious concrete crushing nor any damage to the retrofitted steel element at any sectional level was observed. The 'U' hook worked perfectly in connecting the retrofitting element with the footing and hence could be adopted for the same purpose in the future as well. It was evident from the specimens' failure modes that by retrofitting the PCCFST specimen, the structural performance could be enhanced effectively, and the buckling zone could be shifted up.

5.3.3 Lateral load-lateral displacement hysteretic curves

The lateral load versus lateral displacement (P-Δ) hysteretic curves of the retrofitted specimens at the column head were displayed in Figure 5.7. The hysteretic curves of all the specimens tested showed no sign of pinching effects. Furthermore, it was also clear that the relationship between the lateral load and the lateral displacement is initially linear elastic. As the response moved toward the inelastic range, the stiffness slowly deteriorated. The hysteretic responses are approximately symmetric along the compression and tension zone.

5.3.4 Strength degradation

As measured by the strength degradation coefficient (λ), strength degradation is the loss of strength seen at the subsequent loading cycle under the same displacement. The strength degradation coefficient was computed for each specimen using Equation 5.1 (e.g. (Xu *et al.* 2016)).

$$\lambda_i = \frac{P_i^{j+1}}{P_i^j} \tag{5.1}$$

Where P_i^j is the ultimate load of the j^{th} cycle for the i^{th} drift angle. For each drift angle, the first two cycles were taken into account when calculating the strength degradation coefficient since the first three drift angles engaged six cycles, while the fourth drift angle engaged four cycles. Only two cycles were offered for the remaining drift angles, so both cycles were incorporated into the calculation.

In Figure 5.8, the lateral displacement has been plotted against the average strength degradation coefficient obtained from the tension and compression side of both the retrofitted specimen and the corresponding reference specimens. It could be clearly seen that all the retrofitted specimens showed lower initial strength degradation values compared to their corresponding reference specimens at stage-I (θ <2%). At stage-I, all the specimens showed constant and highest strength degradation coefficient (close to unity). At stage-II (2% < θ < 5%), there was a substantial drop in the strength degradation pattern of all the specimens. However, the drop is low in the case of the retrofitted specimens compared to the reference specimens. At stage-

III (θ >5%), all the specimens showed a stable strength degradation pattern; however, λ for the retrofitted specimens was slightly higher than that of the reference specimens.

The damaged specimens already have crushed concrete and buckled steel at the plastic hinge region (as mentioned in Chapter 3) and hence showed lower initial strength degradation at stage-I. During stage –II, the retrofitting element contributed to the strength degradation, and hence the strength degradation coefficient didn't go much lower. At stage-III, the effect of retrofitting element played a key role in holding the strength degradation coefficient stable. For each of the retrofitted specimens, a similar pattern of strength degradation could be observed.

5.3.5 *P*-Δ envelope curves

The lateral load versus displacement (*P*-Δ) envelope curve of all the retrofitted specimens and their corresponding reference specimens have been shown in Figure 5.9. The ultimate lateral strength (P_u) resulting from all the tests was shown in Table 5.3, and it was computed as the average of the peak +ve and –ve lateral loads derived from *P*-Δ envelope curves. The retrofitted specimens could regain the ultimate lateral strength by 121%-134% with respect to their corresponding reference specimens (Figure 5.10). PCCFST specimens retrofitted with square element showed higher ultimate lateral strength compared to the CFST specimen retrofitted with square element, possibly because of the additional contribution of strength from the inner concrete-filled CHS for PCCFST specimen. The circular retrofitting element showed higher ultimate lateral strength when compared to the square retrofitting element, possibly because of the higher confinement imparted by the circular section retrofitting element at the plastic hinge region.

5.3.6 Stiffness degradation

The stiffness of the columns at various levels of lateral displacement has been measured using the average stiffness (secant stiffness). Equation 5.2 was employed to determine the members' average stiffness (Qian *et al.* 2014; Zheng *et al.* 2018).

$$K_i = \frac{|P_i| + |-P_i|}{|\Delta_i| + |-\Delta_i|} \tag{5.2}$$

where, P_i and Δ_i are the maximum lateral load and the associated lateral displacement at the i-th drift angle, respectively. The push and pull directions are denoted, respectively, by the + and – signs.

The degradation of average stiffness (K) versus the lateral displacement (Δ) for the retrofitted specimens were plotted corresponding to their reference specimens in Figure 5.11. It was evident that as the lateral displacement increased, the stiffness of each specimen decreased as a result of the specimen's accumulated damage. There was a consistent nonlinear pattern in the loss of stiffness across all of the specimens. It was observed that all the retrofitted specimens showed higher stiffness with respect to the corresponding reference specimens at every level of displacement. The reason may be the higher cross-sectional area of the retrofitted specimen at the potential plastic hinge zone. The average secant stiffness of S114-c50-1.5D-C was slightly higher at the drift angle ranging from 2%-7%, followed by S114-c60-1.5D-S and S114-c0-S. It may be due to the better confinement offered by the circular retrofitting element.

5.3.7 Energy dissipation ability

Figure 5.12 shows the energy dissipation associated with each drift angle. It was observed that for all the specimens, the maximum lateral load decreased by 15%, or the specimen was damaged within 9% drift angle. Hence, to ensure uniformity in comparison, energy dissipation is computed up until the second cycle of the 9% drift angle. Table 4 provides a summary of the total energy dissipation ability determined from the test results. The area where the plastic hinge is anticipated to develop determines the energy dissipation capacity, and retrofitting that area with a concrete-filled steel tube improves the property. All the retrofitted specimens were found to have higher energy dissipation capacity compared to the corresponding reference specimens. The regain in the energy dissipation capacity ranges from 110% to 115%

with respect to the reference specimens (see Figure 5.13). The possible reason could be providing an additional concrete-filled steel tubular retrofitting element at the damaged square columns. The cumulative energy dissipation ability of the retrofitted PCCFST specimen has been found to be higher than the retrofitted CFST specimen. The possible reason could be the presence of an additional concrete-filled circular steel tube at the potential plastic hinge region, which imparts enhancement in the energy dissipation ability. The PCCFST specimen retrofitted by the square element exhibits higher energy dissipation ability compared to the PCCFST specimen retrofitted by the circular element of the same outer dimension (the hysteresis curves of the PCCFST specimen retrofitted by the square element are relatively wider as compared to that of PCCFST specimen retrofitted with circular element). The probable reason could be the presence of more steel at the cross section of the columns retrofitted by square retrofitting element (for equal outer dimensioned circular and square hollow tube, the steel at the cross section of square tube is higher than the circular).

According to the LVDT reading, some of the specimens with higher displacement showed support slippage of around 1 to 1.5 mm. When calculating the energy dissipated by each individual cycle, a correction has been made to the affected cycles.

5.3.8 Strain development

Typical lateral force versus axial strain (P-ε) hysteretic curves has been illustrated in Figure 5.14, where compression and tension, respectively, are represented by the +ve and –ve values of the strains. The strain data were obtained from the strain gauges, installed at the height of 50 mm (diametrical tension and compression side; B1 & B2) on the retrofitting steel from the column end and 50 mm above the top fiber of the retrofitting element (T2) (See Figure 5.5). It has been seen that the retrofitting steel element showed no signs of buckling in any of the retrofitted specimens, which could be clearly illustrated from the strain data of B1 and B2. However, strain data corresponding to T2 showed a significant buckling of the outer square steel tube for S114-c60-1.5D-S and S114-c50-1.5D-C specimens. In contrast, strain data corresponding to T2 of the S114-c0-S specimen showed no significant buckling at that region.

5.4 CONCLUSIONS

In this chapter, a novel retrofitting technique using an external concrete-filled steel tube has been proposed. The cyclic performance of retrofitted CFST/PCCFST specimens was studied. The effect of the retrofitting element's shape and the presence of an inner circular steel tube of 1.5*D* height on the maximum lateral strength and energy dissipation ability has been assessed and reported. On the basis of the limited data obtained from the experimental analysis of the retrofitted columns, the following conclusions have been made.

1) The proposed retrofitting technique effectively regains the structural performance (ultimate lateral strength and energy dissipation capacity) of the damaged CFST/PCCFST columns.
2) The circular retrofitting element shows better ultimate lateral strength enhancement than the square retrofitting element.
3) The square retrofitting element showed higher energy dissipation capacity compared to circular retrofitting element.
4) In comparison to the retrofitted CFST specimen, the retrofitted PCCFST specimen performed better in terms of maximum lateral strength and energy dissipation capacity while maintaining a similar retrofitting element.

Table 5.1: Geometrical dimensions.

Specimens	D_0 (mm)	t_0 (mm)	H_0 (mm)	D (mm)	t (mm)	H (mm)	D_i (mm)	t_i (mm)	H_i (mm)	D_i/D	D_0/D	H_0/D	N_0 (kN)
S114-c0	-		-	114	4.06	650	-	-	-	-	-	-	22
S114-c0-S	200	3.2	200	114	4.06	650	-	-	-	-	1.75	1.75	22
S114-c60-1.5D	-			114	4.06	650	60	3.2	171	0.53	-	-	22
S114-c60-1.5D-S	200	3.2	200	114	4.06	650	60	3.2	171	0.53	1.75	1.75	22
S114-c50-1.5D	-			114	4.06	650	50	3.2	171	0.44	-	-	22
S114-c50-1.5D-C	200	3.2	200	114	4.06	650	50	3.2	171	0.44	1.75	1.75	22

Table 5.2: Properties of steel sections

Specimens	t (mm)	D/t	f_y (MPa)	f_u (MPa)
S-114	4.06	28.08	300.00	370.00
c-60	3.2	18.75	362.70	397.73
c-50	3.2	15.63	365.16	395.75
S-200	3.2	62.50	238.81	376.30
C-200	3.2	62.50	234.30	374.60

Table 5.3: Experiment findings

Specimens	P_u (kN)	E (kN.m)
S114-c0	49.00	54.98
S114-c0-S	64.07	60.54
S114-c60-1.5D	56.47	61.23
S114-c60-1.5D-S	68.42	70.28
S114-c50-1.5D	55.02	59.90
S114-c50-1.5D-C	73.59	65.98

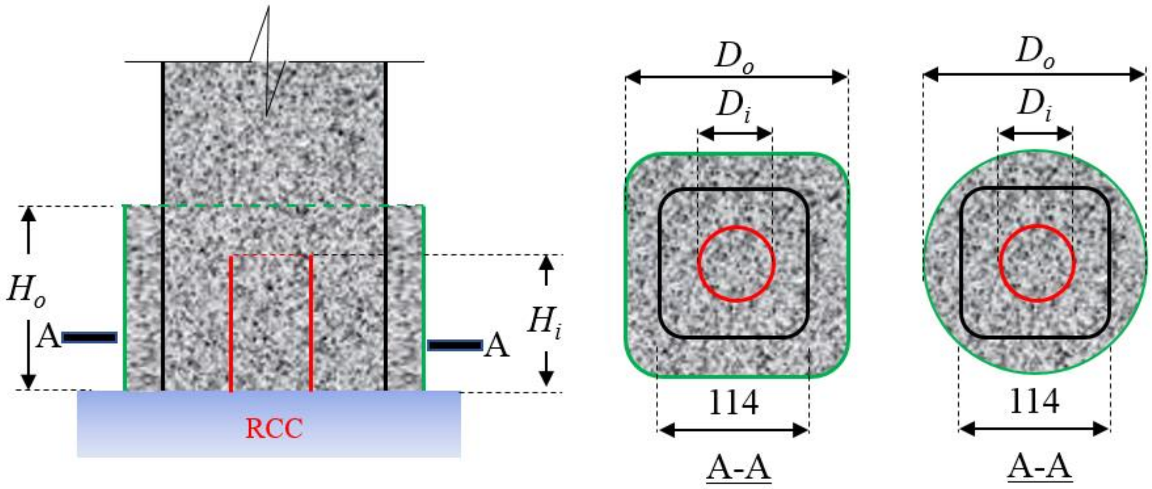

a) Front view
b) Section A-A

Figure 5.1: Novel Retrofitting technique for PCCFST columns (i.e. short external concrete-filled steel tubular retrofitting element near the support)

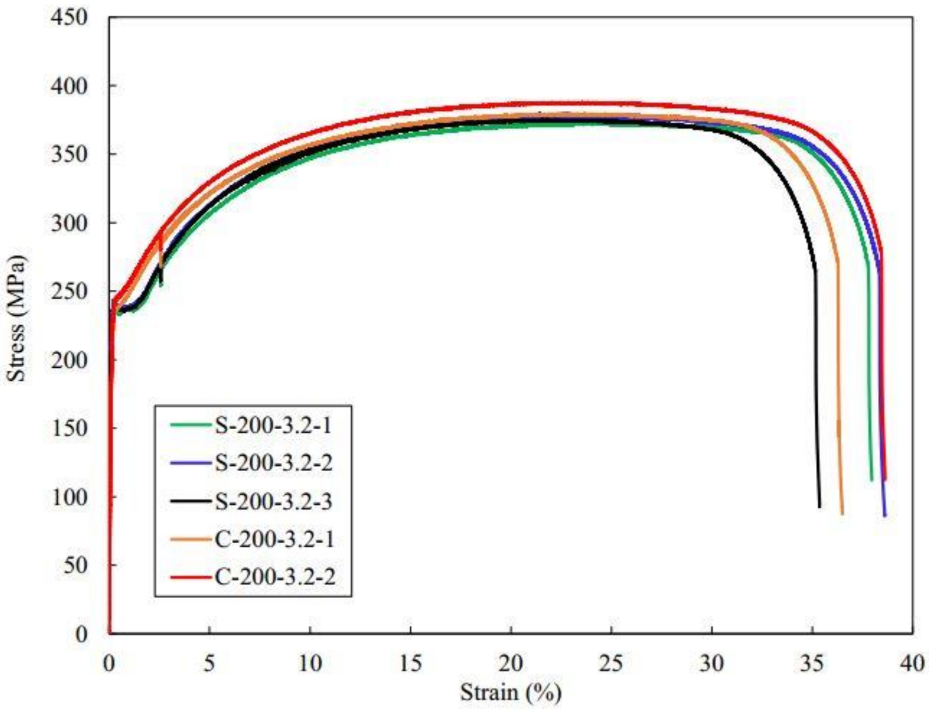

Figure 5.2: Engineering stress-strain curve generated from the tensile coupon test of retrofitting steel element

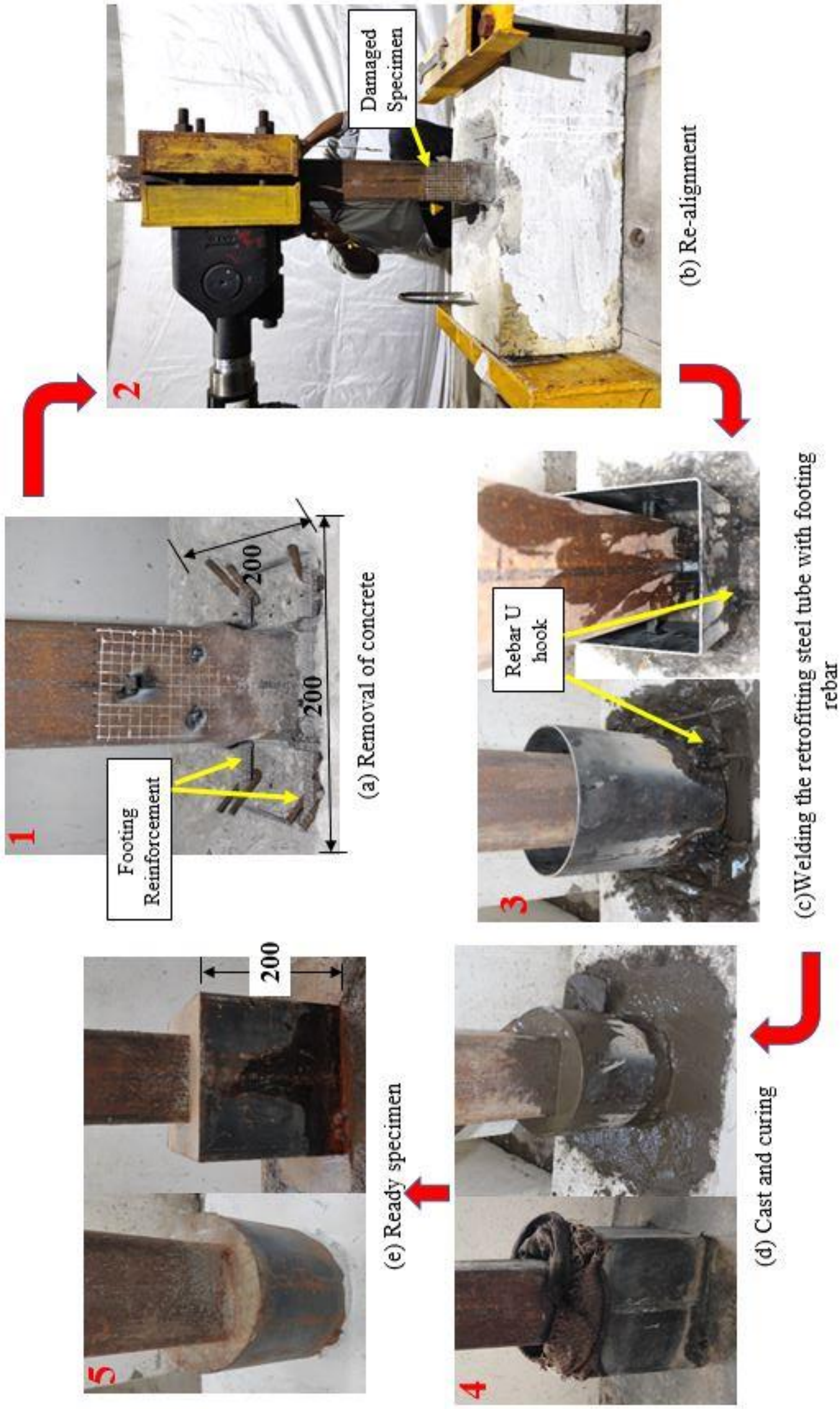

Figure 5.3: Specimen preparation (unit: mm)

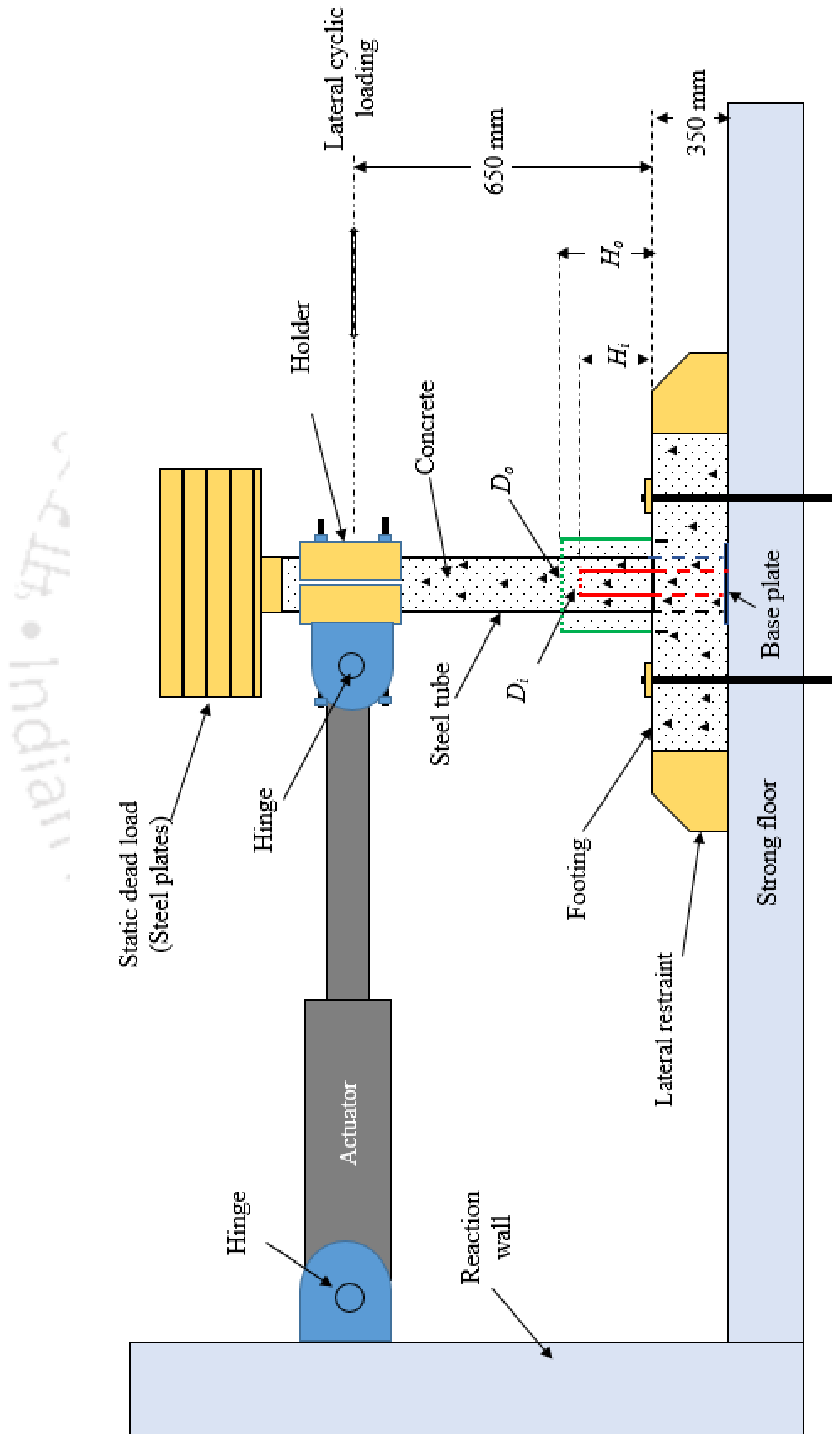

(a) Schematic view

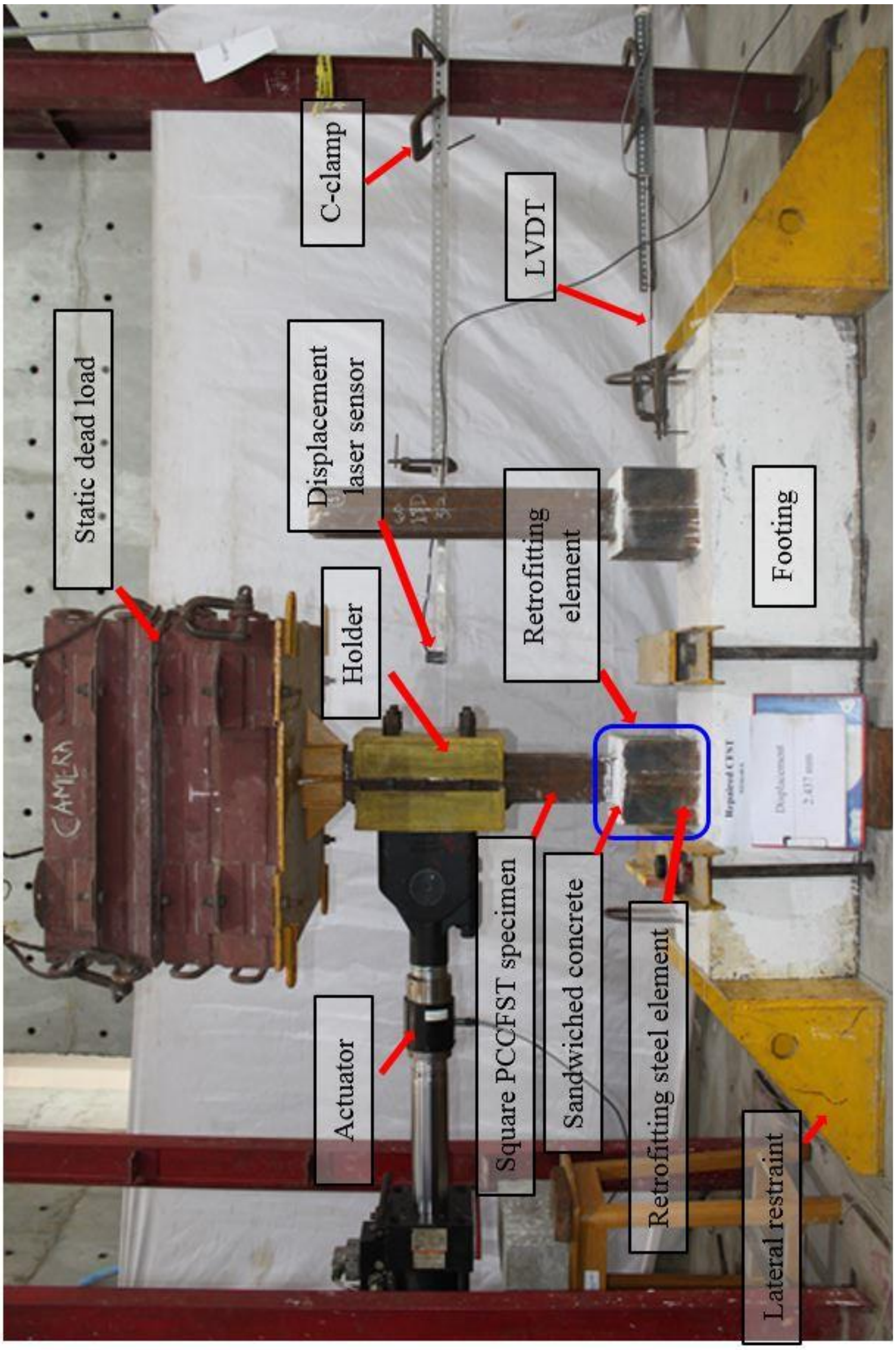

(b) Photograph

Figure 5.4: Test set-up

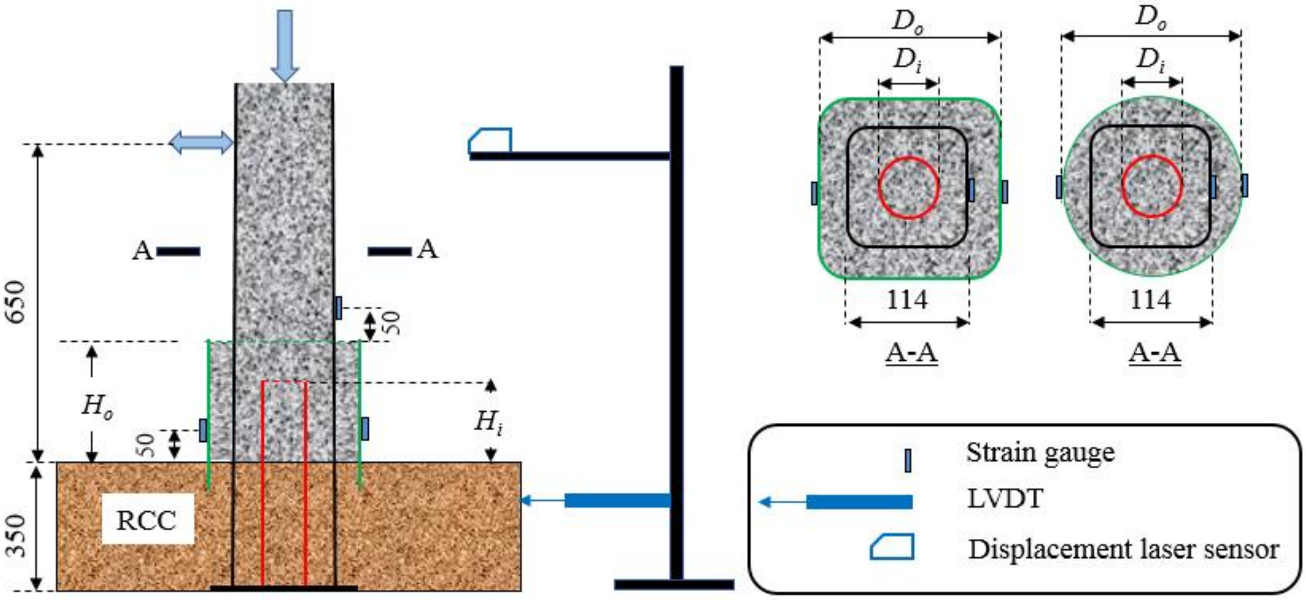

Figure 5.5: Specimen configuration and instrumentation (all units in mm)

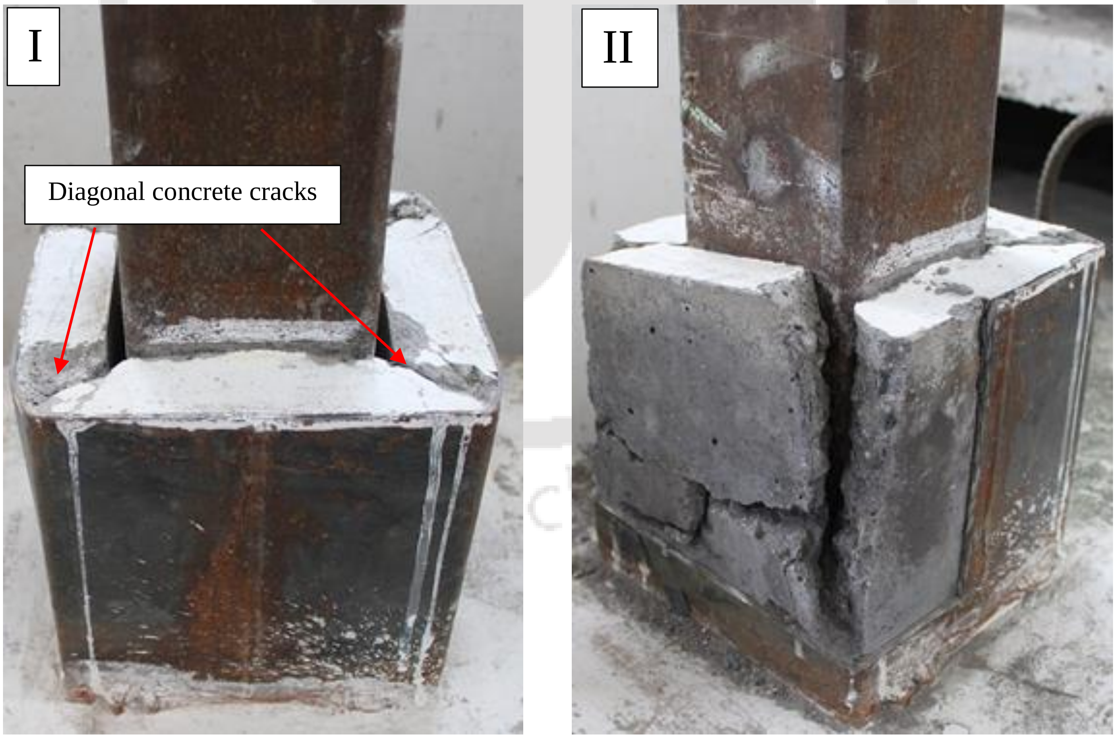

(a) S114-c0-S

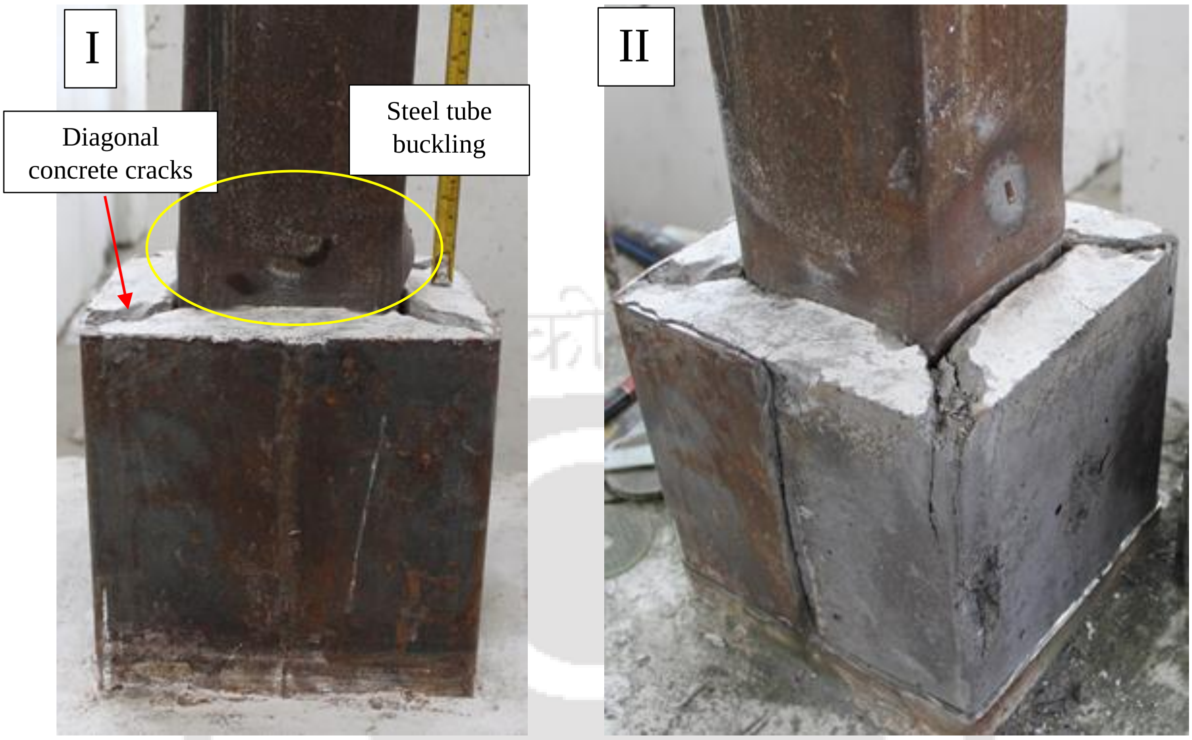

(b) S114-c60-1.5D-S

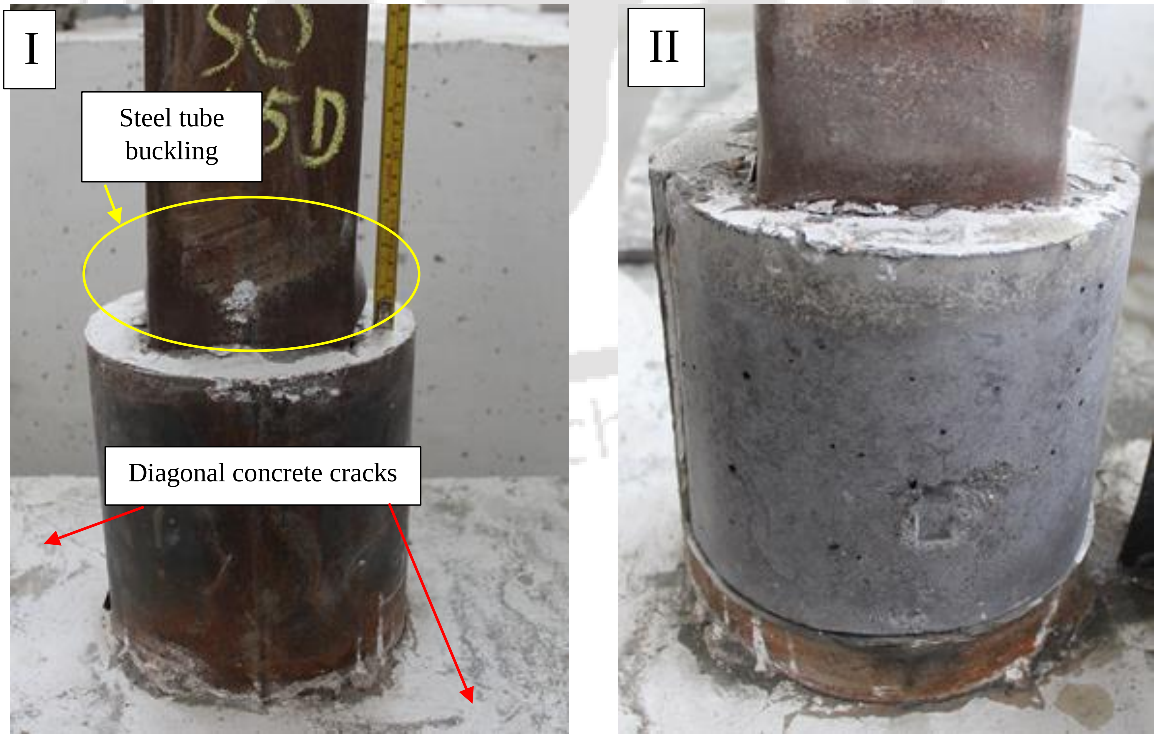

(c) S114-c50-1.5D-C

Figure 5.6: Failure modes of retrofitted specimens

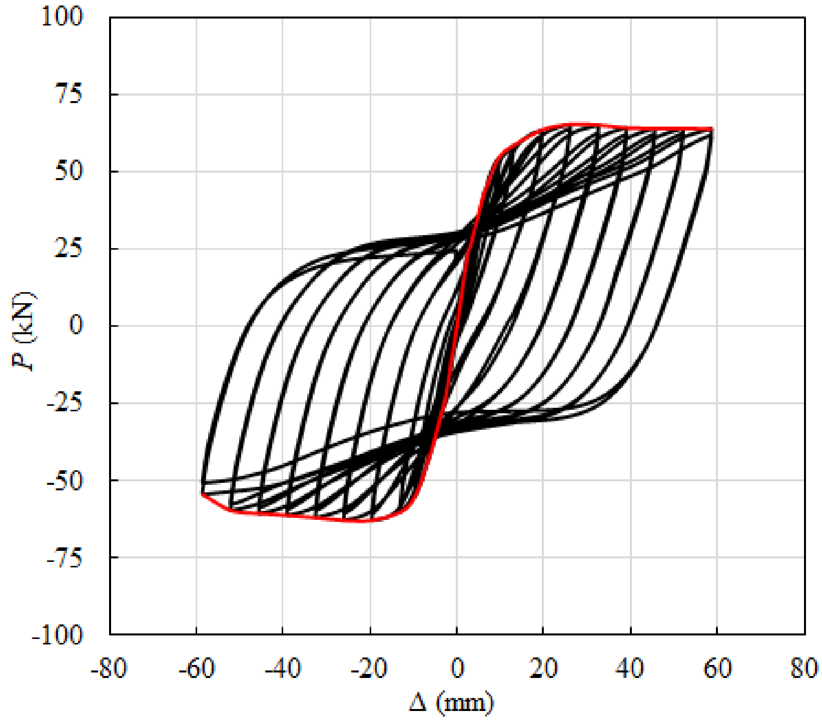

(a) S114-c0-S

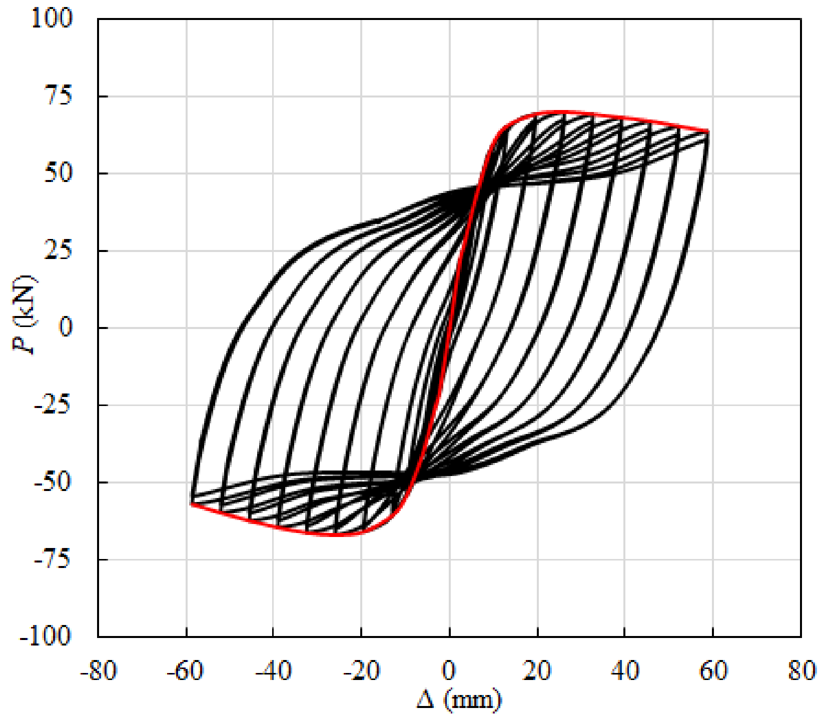

(b) S114-c60-1.5D-S

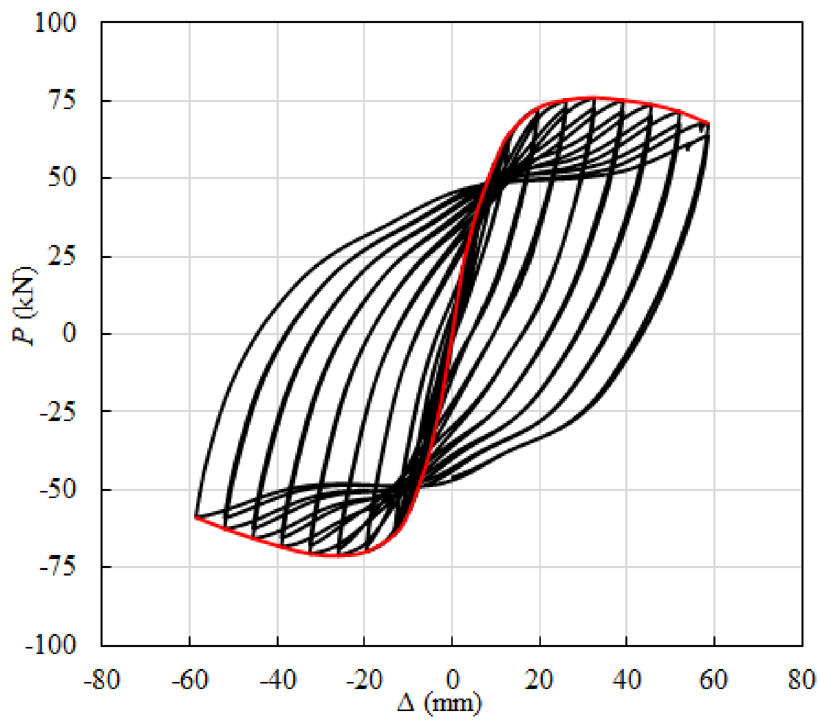

(c) S114-c50-1.5D-C

Figure 5.7: Lateral loads (P) versus lateral displacement (Δ) hysteretic curves

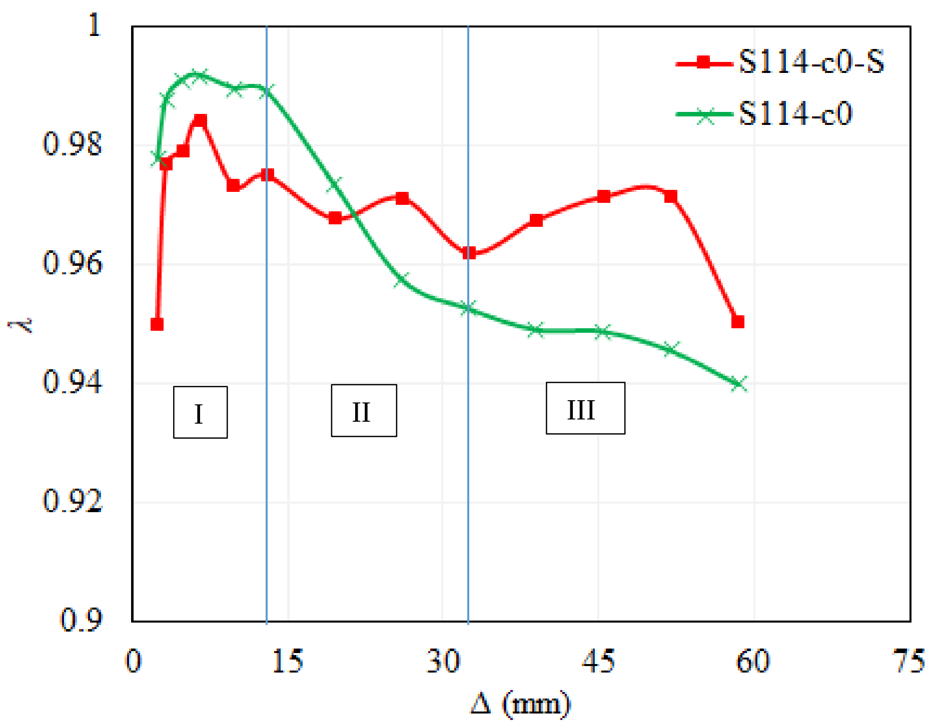

(a)

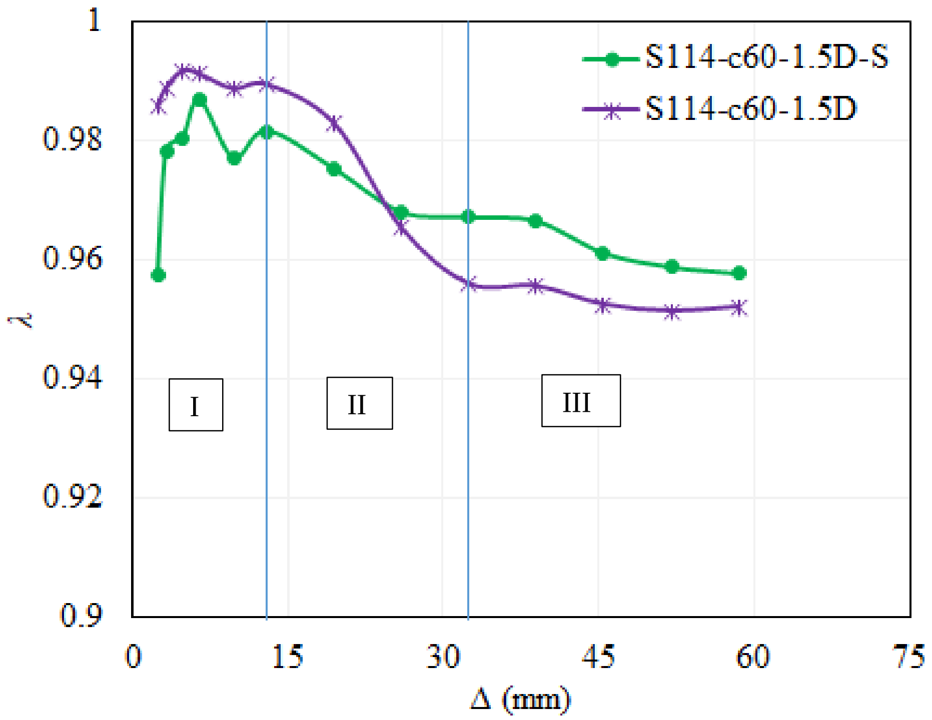
S114-c60-1.5D-S
S114-c60-1.5D
I
II
III
λ
Δ (mm)
1
0.98
0.96
0.94
0.92
0.9
0
15
30
45
60
75

(b)

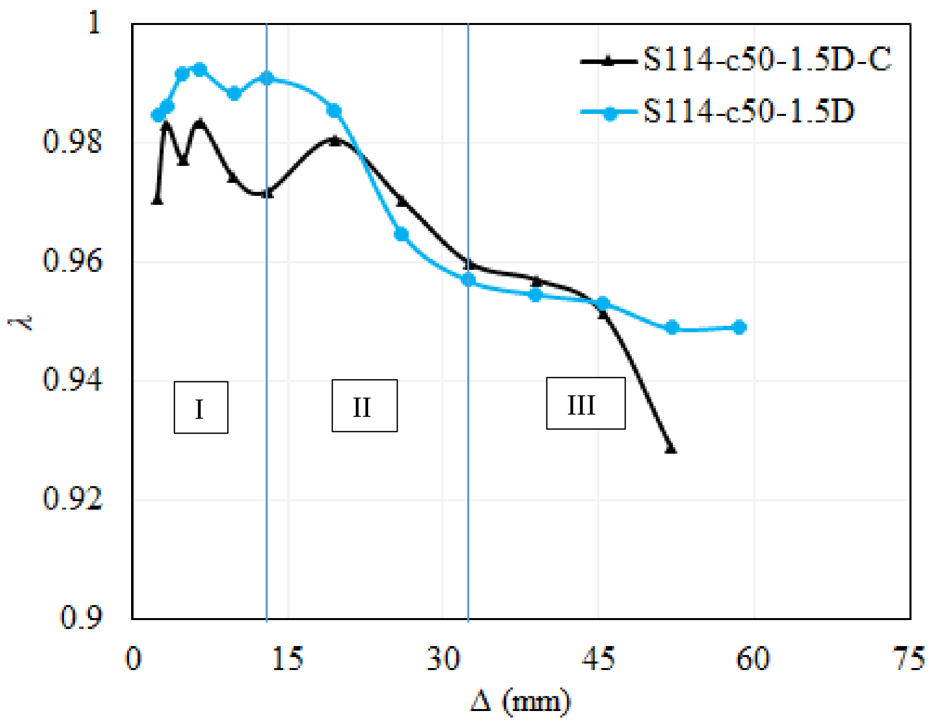
S114-c50-1.5D-C
S114-c50-1.5D
I
II
III
λ
Δ (mm)
1
0.98
0.96
0.94
0.92
0.9
0
15
30
45
60
75

(c)

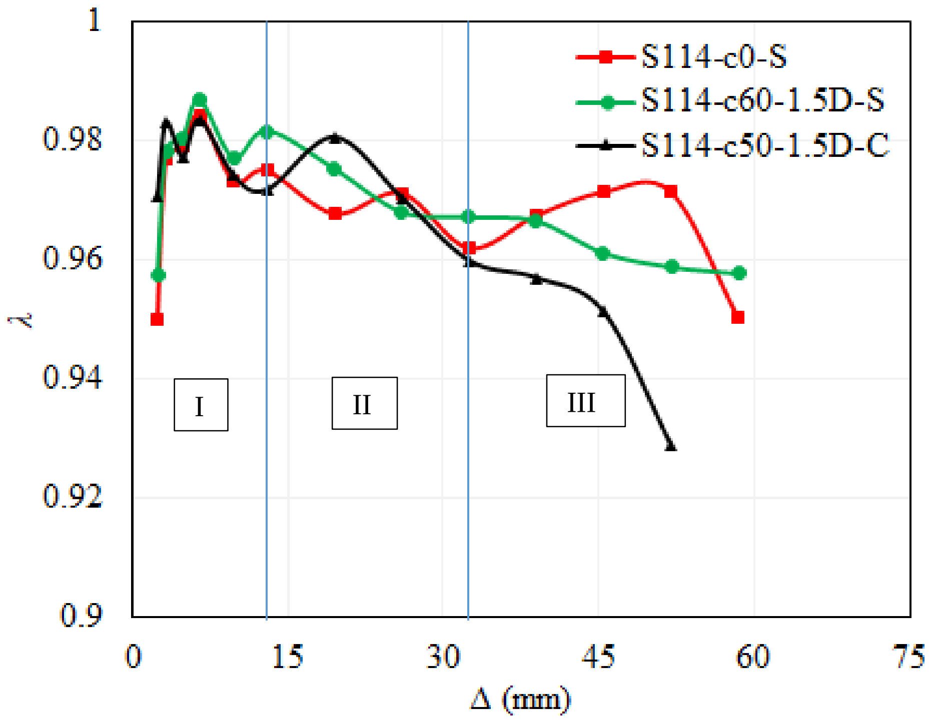

(d)

Figure 5.8: Strength degradation curve

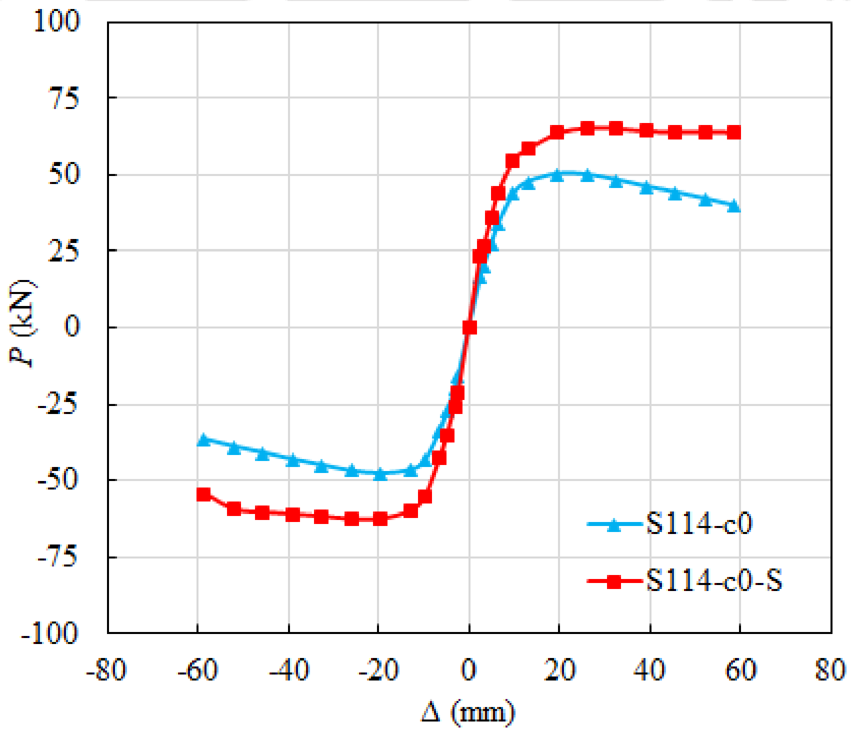

(a)

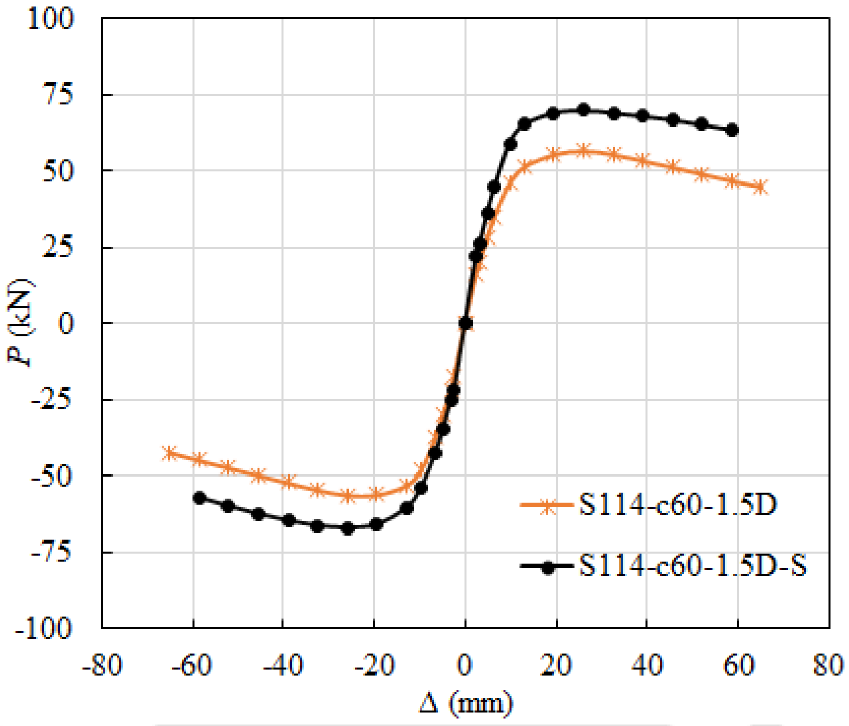
100
75
50
25
0
-25
-50
-75
-100
P (kN)
-80
-60
-40
-20
0
20
40
60
80
Δ (mm)
S114-c60-1.5D
S114-c60-1.5D-S

(b)

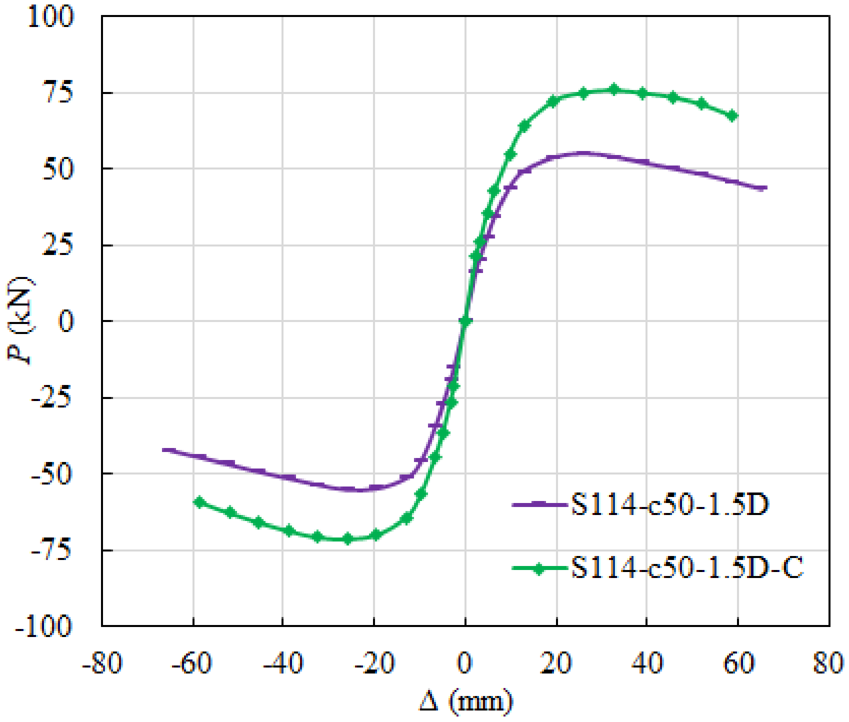
100
75
50
25
0
-25
-50
-75
-100
P (kN)
-80
-60
-40
-20
0
20
40
60
80
Δ (mm)
S114-c50-1.5D
S114-c50-1.5D-C

(c)

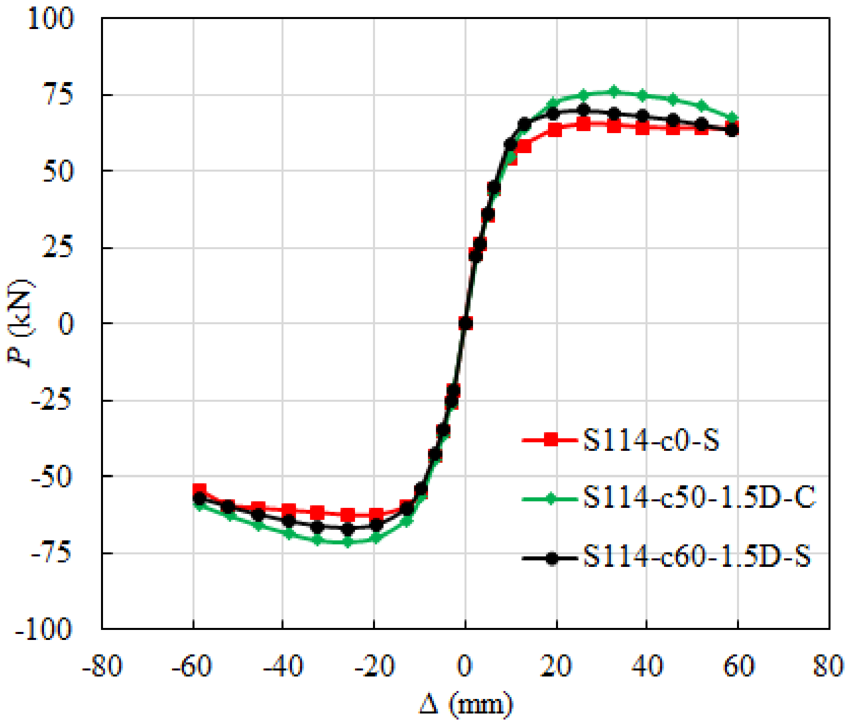

(d)

Figure 5.9: Lateral load versus lateral displacement (*P*-Δ) envelope curves

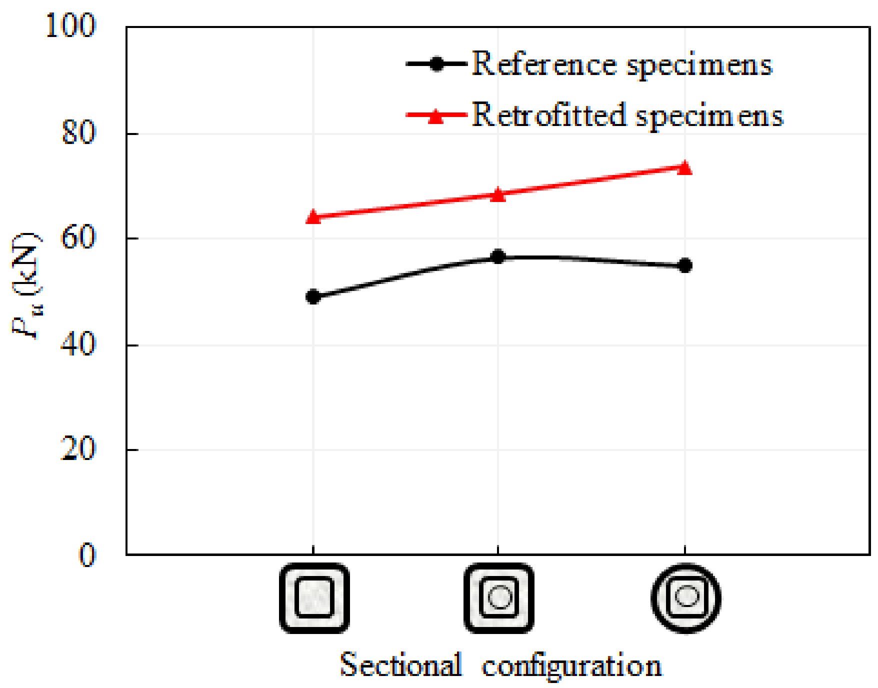

Figure 5:10: Effect of retrofitting element on P_u

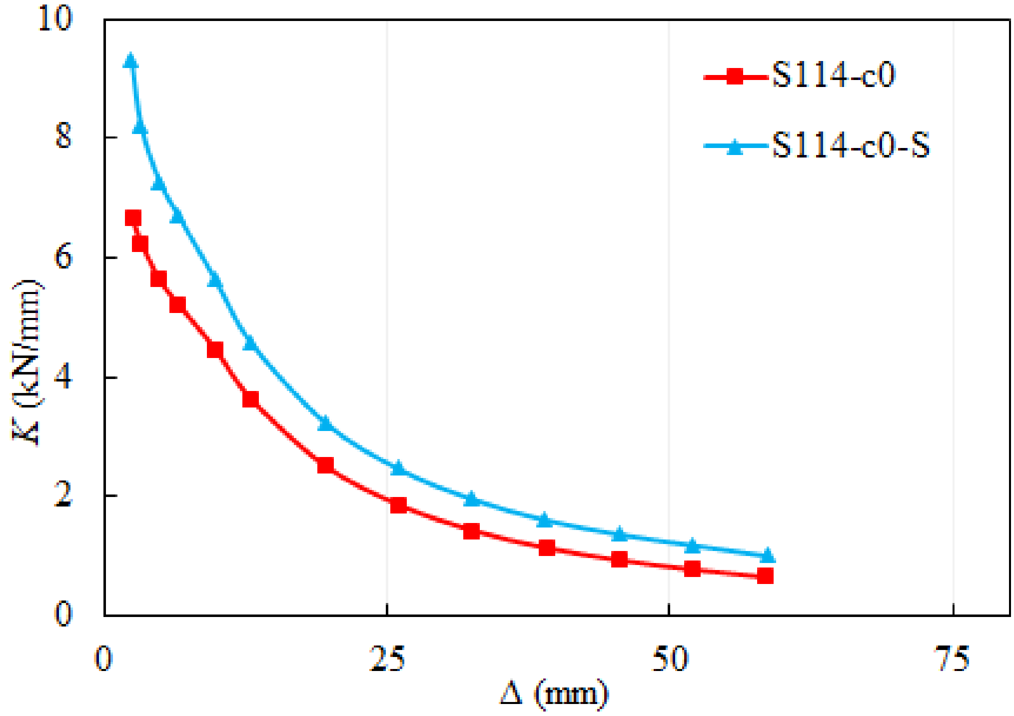
10
8
6
4
2
0
K (kN/mm)
0
25
50
75
Δ (mm)
S114-c0
S114-c0-S

(a)

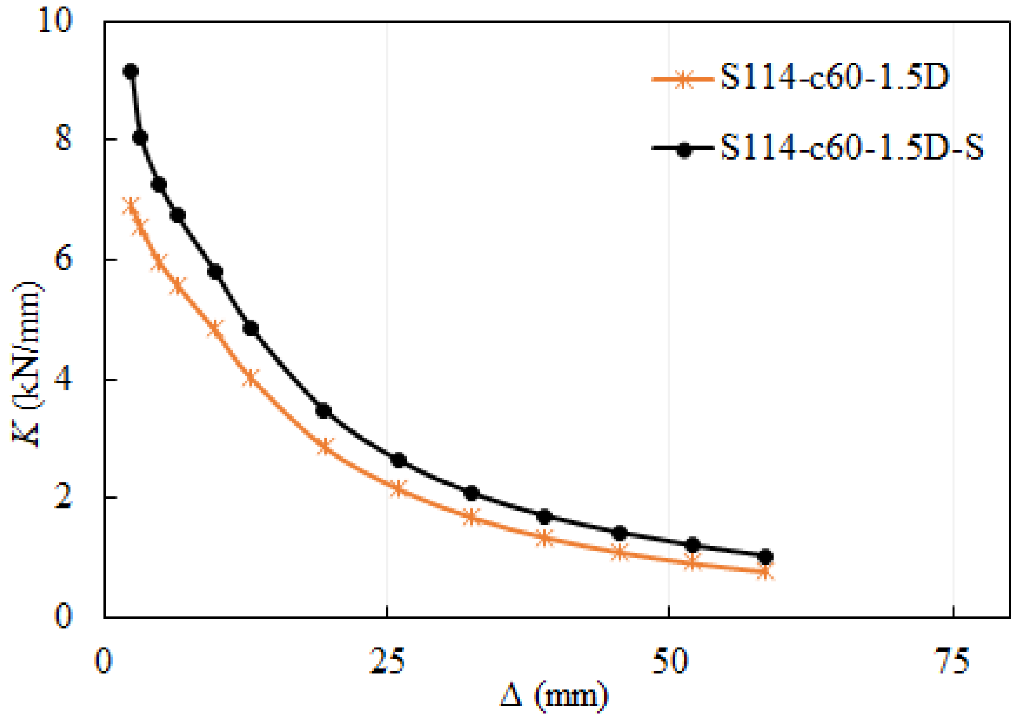
10
8
6
4
2
0
K (kN/mm)
0
25
50
75
Δ (mm)
S114-c60-1.5D
S114-c60-1.5D-S

(b)

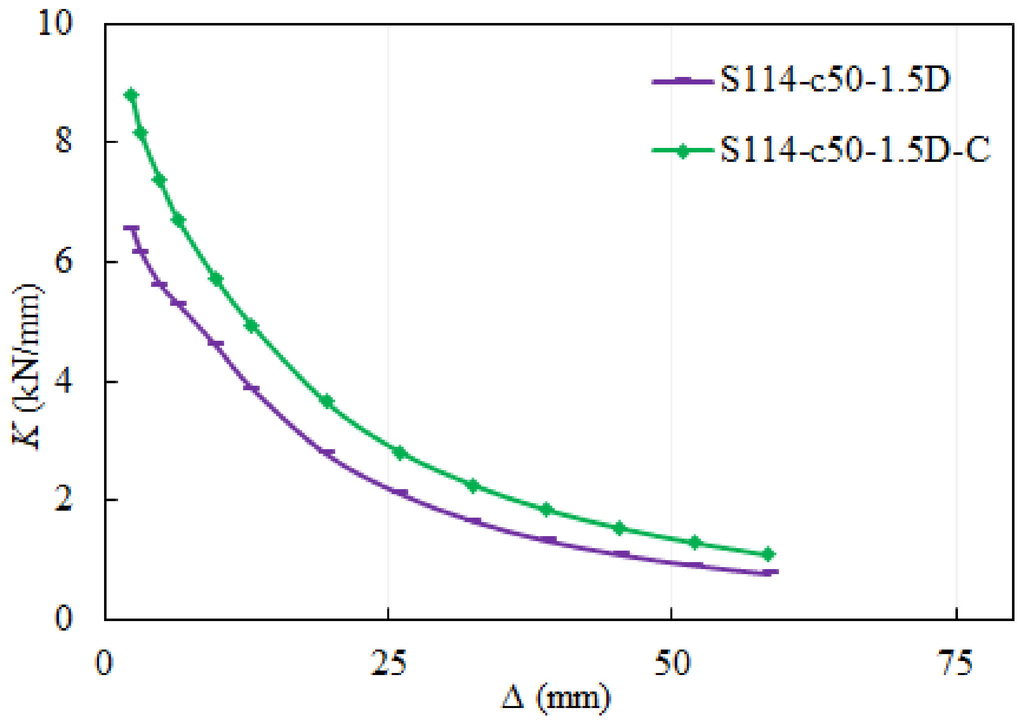

(c)

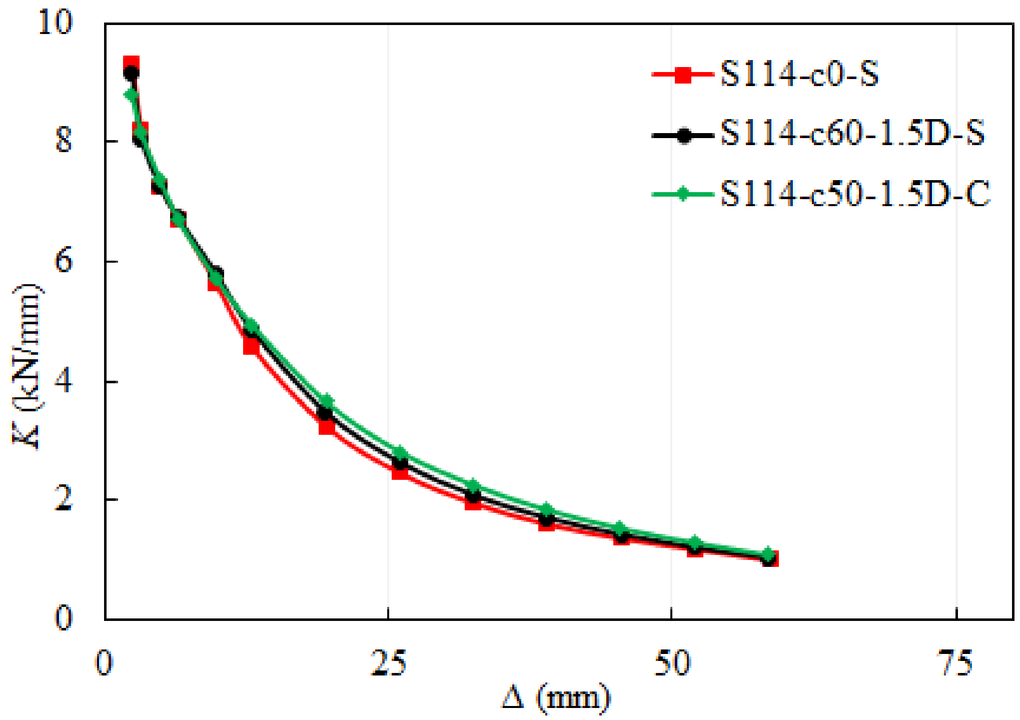

(d)

Figure 5.11: Stiffness degradation (K-Δ) curves

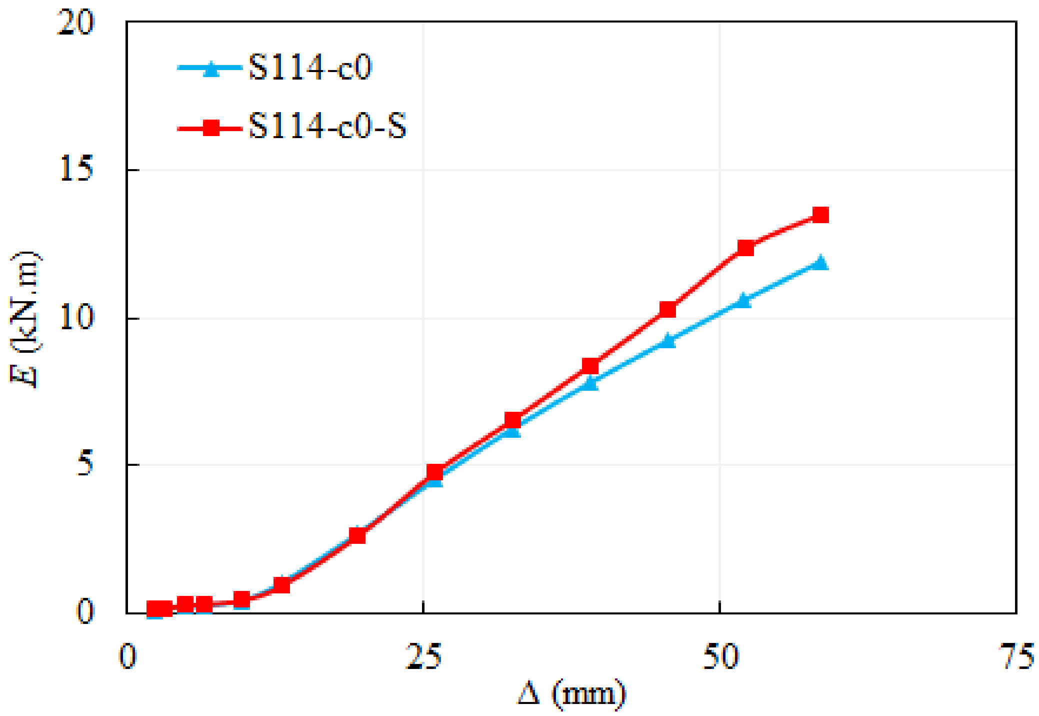
S114-c0
S114-c0-S
E (kN.m)
Δ (mm)
0
5
10
15
20
0
25
50
75

(a)

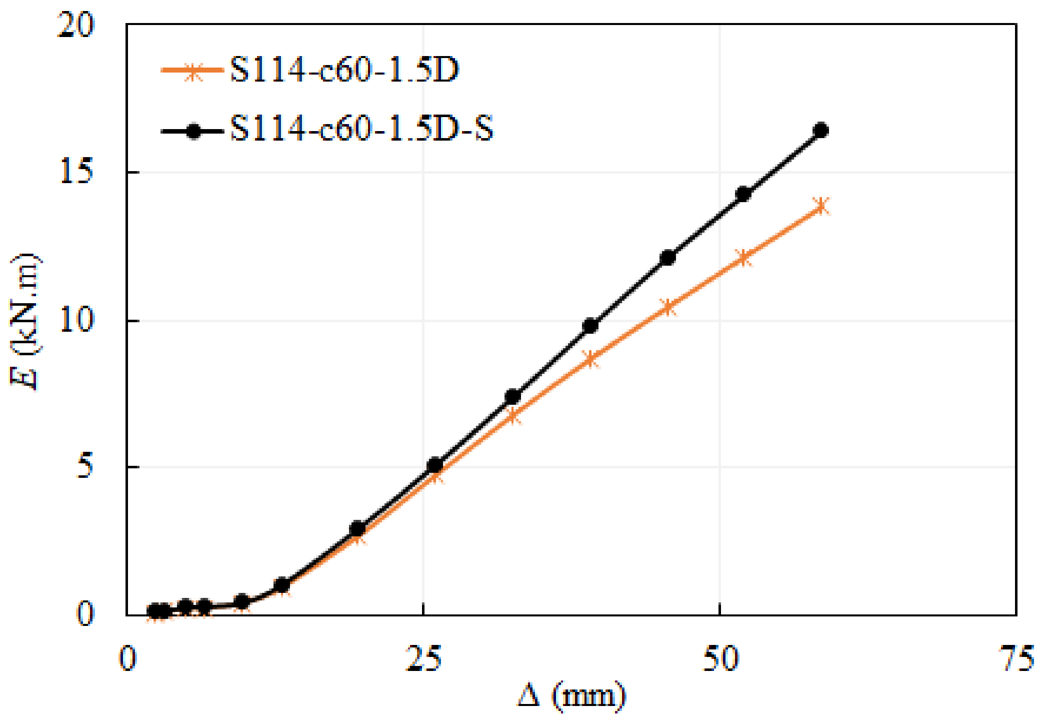
S114-c60-1.5D
S114-c60-1.5D-S
E (kN.m)
Δ (mm)
0
5
10
15
20
0
25
50
75

(b)

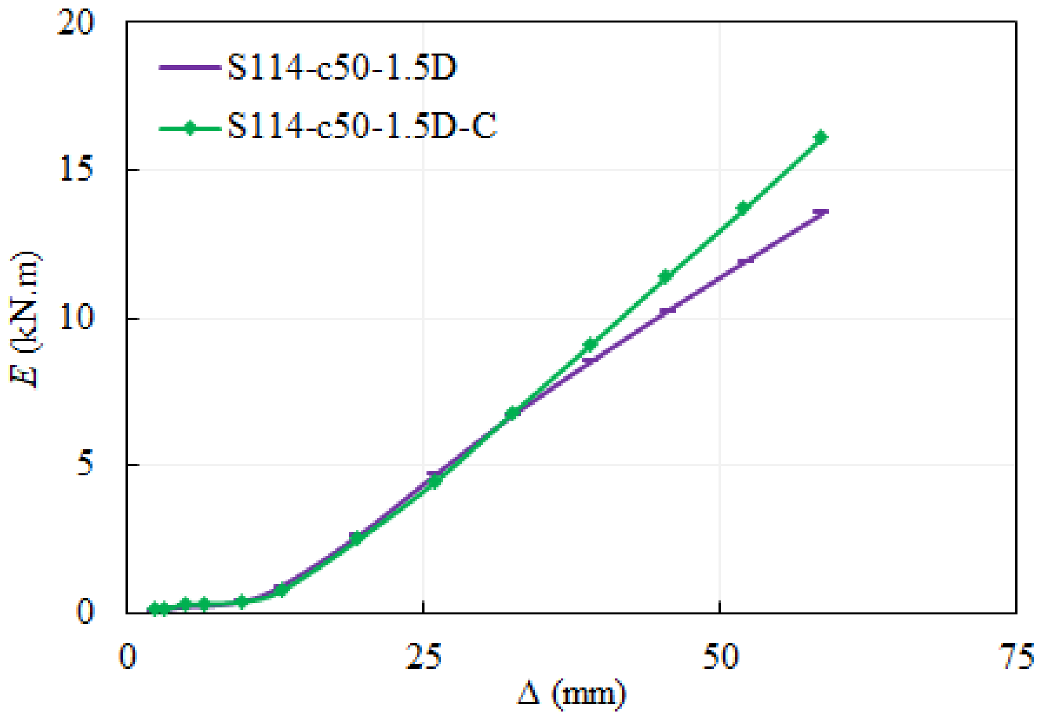

(c)

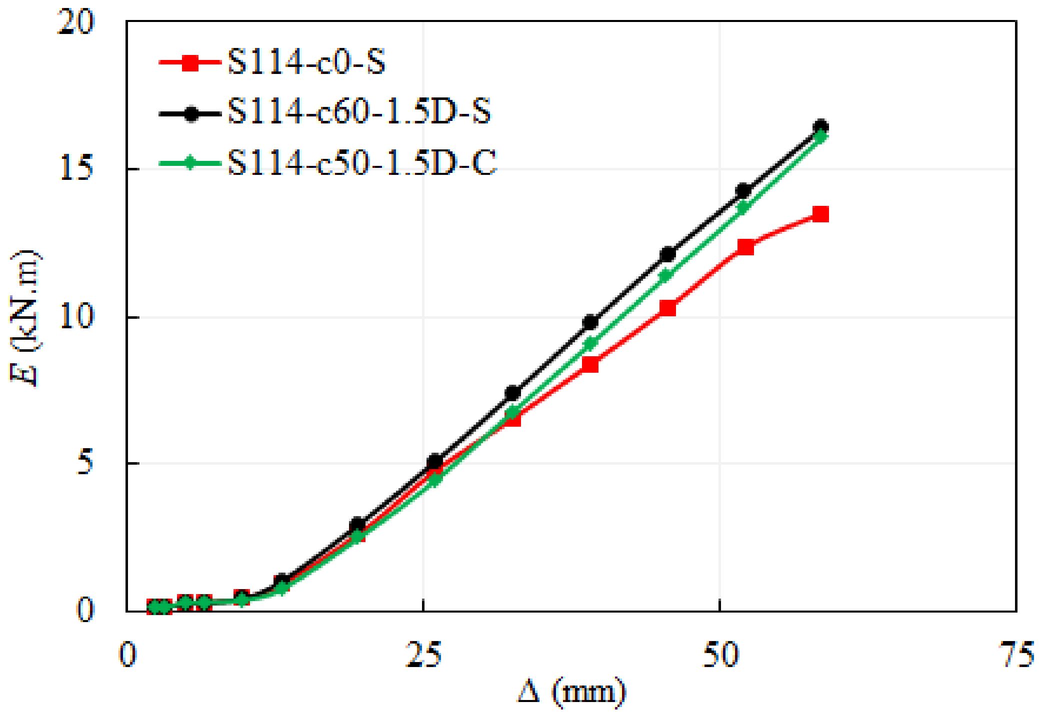

(d)

Figure 5.12: Energy dissipation (E-Δ) curves

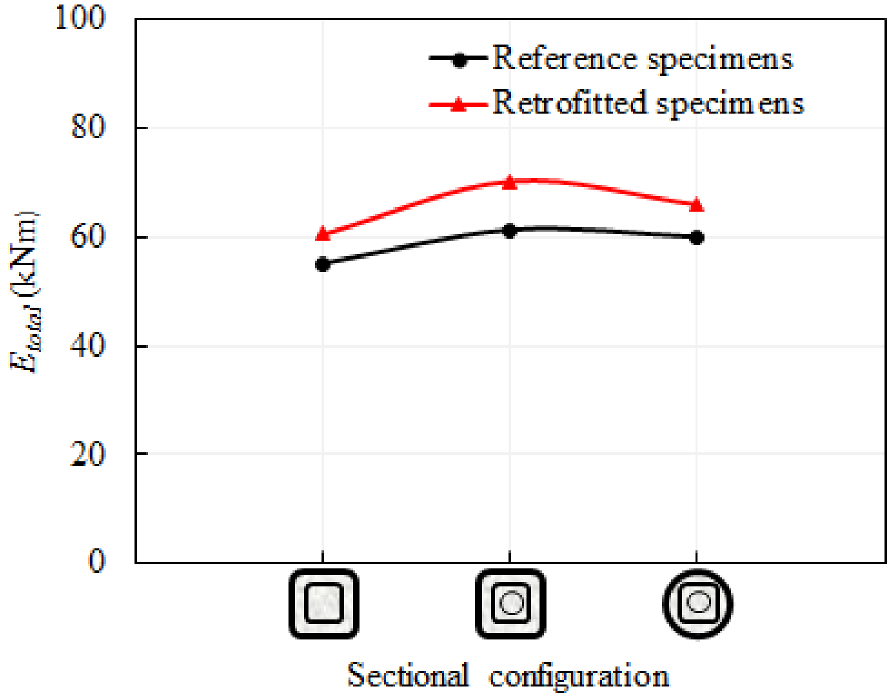

Figure 5.13: Effect of retrofitting element on E_{total}

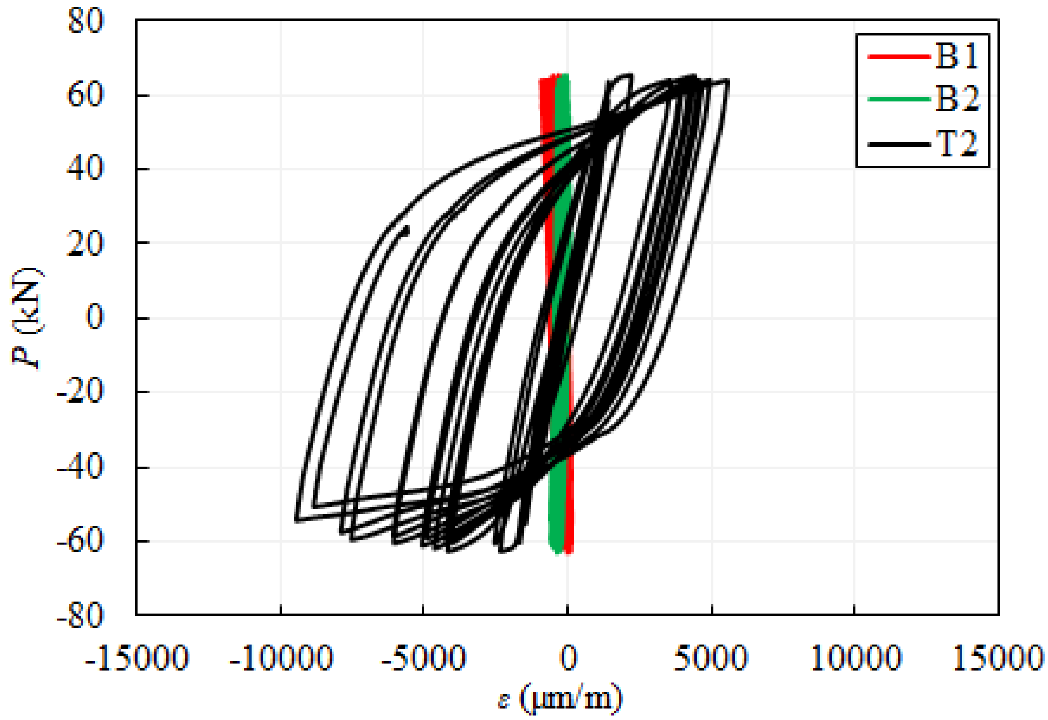

(a) S114-c0-S

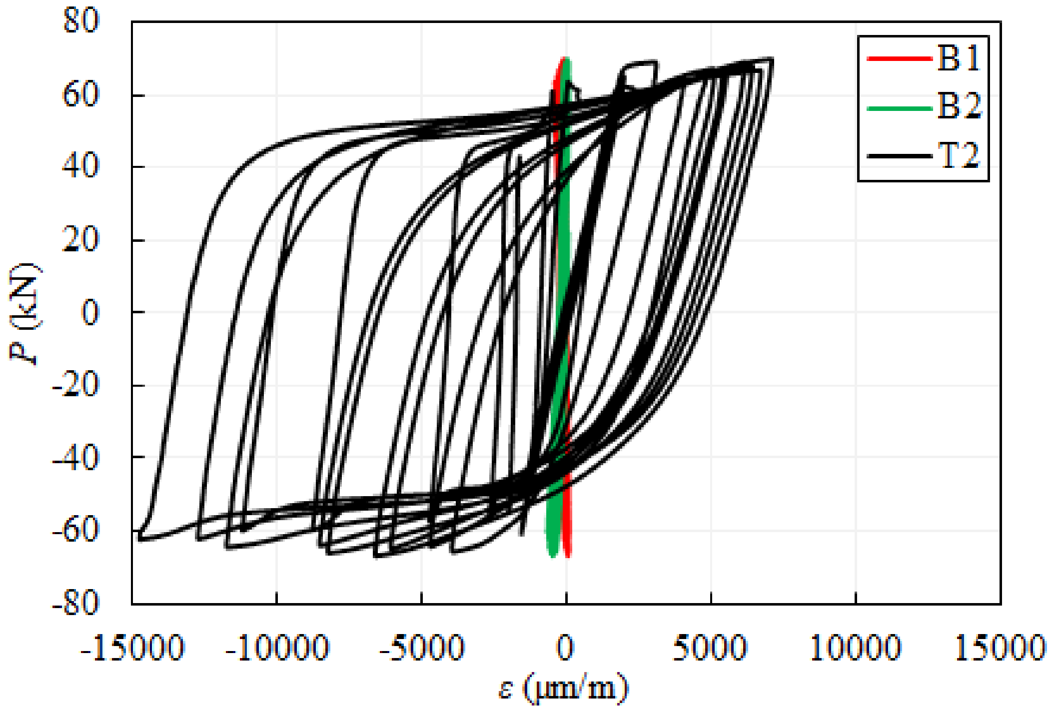

(b) S114-c60-1.5D-S

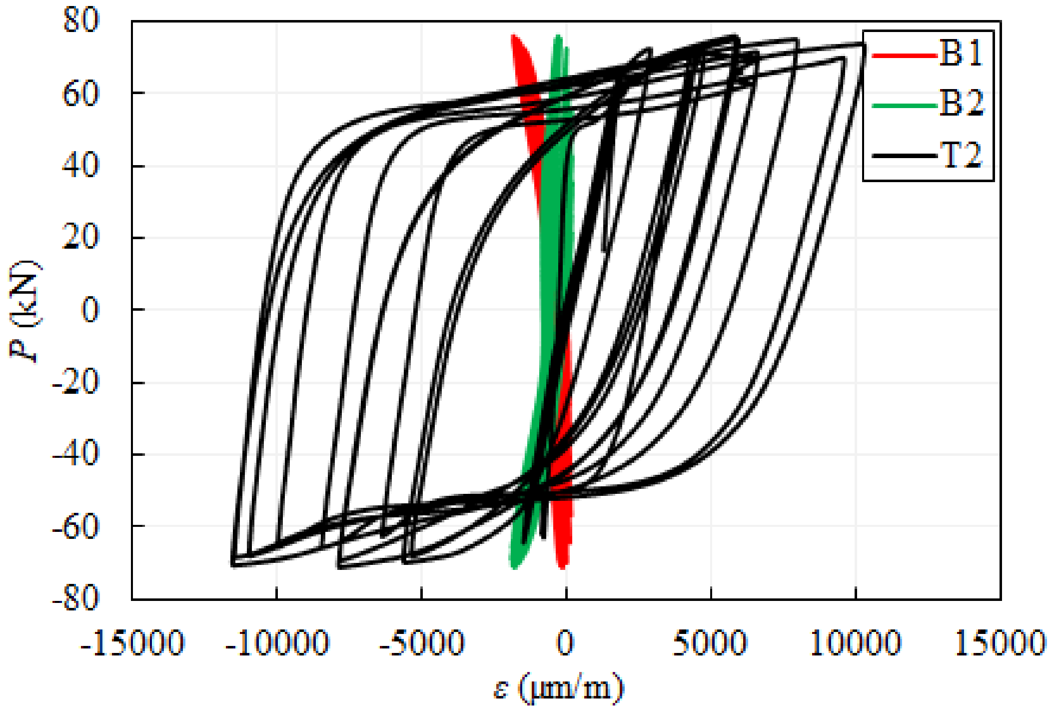

(c) S114-c50-1.5D-C

Figure 5.14: Typical lateral force versus strain (P-ε) hysteretic loops

This page is intentionally left blank

Chapter 6

Circular PC-CFST Columns Externally Retrofitted with Concrete-Filled Steel Sections

6.1 INTRODUCTION

The cyclic performance of circular partially confined CFST has been presented in Chapter 4. After the test was conducted, all the damaged columns were retrofitted using the technique proposed in Chapter 5. In order to see the effect of the thickness of the inner CHS on the overall performance of the retrofitted columns, an additional circular partially confined CFST column (diameter, thickness and height of inner CHS was ~ 60mm, 2.8 mm and 1.5D, where D is the diameter of outer circular steel tube) was also cast, cured and tested under similar loading condition (hysteretic curve shown in Figure 6.6), as mentioned in previous chapters followed by retrofitting of the same specimens using the proposed retrofitting technique. The schematic diagram of the retrofitted, circular partially confined CFST has been shown in Figure 6.1. Similar study as reported in Chapter 5 has been carried out in the current Chapter on the circular retrofitted columns varying the shape of the retrofitting element.

6.2. DETAILS OF THE TEST PROGRAM

6.2.1. Specimens design

The experimental program consisted of 4 retrofitted columns: 1 circular CFST column externally retrofitted with square retrofitting element, 3 PCCFST columns consisting of 1.5D height of inner circular hollow section (CHS): 2 PCCFST columns (c-60 series, inner CHS thickness 3.2 mm and 2.8 mm) were externally retrofitted with circular elements and 1 PCCFST column (c-50 series, inner CHS thickness 3.2 mm) was retrofitted with square element. Similar loading condition as mentioned in the previous chapters has been used in the current chapter to investigate the cyclic performance of the retrofitted columns in terms of ultimate lateral strength, and energy dissipation capacity.

The specimens were designated by the nomenclature Cp-cq-t-r-χ, where 'Cp' refers to the outer circular steel tube of 'p' diameter, 'cq' to the inner circular steel tube of 'q' diameter, 't' thickness of the inner circular steel tube, 'r' to the height of the inner circular steel tube, and 'χ' to the shape of the retrofitting element (where S and C refer to the square and circular sections, respectively). The specimens with no 'χ' are the reference set of specimens. Table 6.1 shows the average geometric dimension of the specimens.

6.2.2 Material properties

6.2.2.1 Steel and concrete

The retrofitting steel elements mentioned in the previous chapter have been used in the current chapter as well. The geometry of the retrofitting element is same as previous chapter (mentioned in section 5.2.2.1). The concrete used to cast the retrofitting element covering the plastic hinge region is same as that of the previous chapter (see section 3.2.2.2).

6.2.3 Specimens preparation

The tested and damaged CFST and PCCFST specimens were considered for the retrofitting purpose. The PCCFST specimens consisting of 1.5D height of inner circular steel tube were used. The testing of the specimens to be retrofitted were stopped after achieving 80% drop in the peak lateral load or the occurrence of steel tube tearing. The details of the preparation of the retrofitted specimen have been illustrated in Figure 6.2. A similar procedure has been followed in the current chapter as mentioned in the previous chapter (Chapter 5) to prepare the retrofitted columns.

6.2.4 Testing frame, instrumentation and loading protocol

The typical test set-up and specimen configuration have been shown in Figure 6.3 and Figure 6.4. In the present study, one strain gauge installed on the retrofitting steel element at the height of 50 mm from the column end to track the retrofitting steel yielding and another strain gauge installed at the height of 50 mm above the retrofitting element to monitor the outer steel tube yielding at that region. The layout of the instrumentation is illustrated in Figure 6.4. The testing process was conducted in a smooth and controlled environment. Similar loading protocol as mentioned in the previous chapters has been used in the current chapter.

6.3. EXPERIMENTAL RESULTS AND DISCUSSION

6.3.1 Failure mechanism

The typical failure mode of the retrofitted specimens has been shown in Figure 6.5 (I and II shows the failed specimen brought to initial position and the maximum deformation exhibited during the last cycle, i.e. at 52 mm, respectively). It has been seen that all the retrofitted specimens have shown similar failure pattern irrespective of the geometry of the retrofitting element. It may be concluded from the above that the size of the retrofitting element was sufficient enough to exhibit the optimum cyclic performance and shift the plastic hinge up for the given CFST /PCCFST columns. Usually for CFST column, under lateral cyclic loading, the plastic hinge formation occurs near the base (column end). But for the columns partially confined upto certain height may also shift the plastic hinge region up. Similarly, in the present study, the plastic hinge was formed above the retrofitting element (near the top fiber of the retrofitting element) and no sign of any significant deformation was seen at the retrofitting element of any specimen (strains corresponding to B2 strain gauge ranges from 100-500 µm/m, refer Figure 6.14). Hence it could be concluded that the retrofitting element has acted partially like a support, shortening the clear height of the CFST/PCCFST columns.

At the plastic hinge region, the crushing of core concrete and outward buckling of the outer hollow steel tube occurred (ring formation). The initiation of the steel tube buckling was observed at approximately 2-3% drift angle (θ). Drift angle is the ratio of the displacement at the column end to the clear height of the column. Steel tube buckling was not very distinct initially but with the progress of the test the buckling became more evident. At the top fiber of the retrofitting concrete, some minor concrete crushing at the circumferential region of the CFST/PCCFST column leading to a minor gap formation between the two was observed. The visible initiation of gap formation occurred at 4-5% drift angle. However, no significant damage to the retrofitting element has occurred. The maximum gap width observed at the end of the test was approximately 2-4 mm. No trace of any cracks or damage to the footing was seen during the test (see Figure 6.5(II)). Therefore, it could be concluded from the specimens' failure modes that by retrofitting the circular PCCFST specimens, the structural performance could be enhanced effectively, and the buckling zone could be shifted up.

6.3.2 Lateral load-lateral displacement relationships

Figure 6.7 shows the lateral load (P) versus lateral displacement (Δ) hysteretic curves of all the retrofitted specimens. The lateral cyclic load was applied at the column head. No sign of pinching effect was seen for any specimens and the hysteretic curves were fuller in size. The lateral load displacement relationship was initially linear elastic, however with the progress of the test, the stiffness gradually degraded leading to inelastic response.

6.3.3 Strength degradation

In Figure 6.8, the computed strength degradation coefficient versus lateral displacement graph has been plotted for all the specimens. It could be clearly seen that all the retrofitted specimens showed lower strength degradation coefficient compared to their corresponding reference specimens at stage-I (θ <1%) because of the presence of damaged plastic hinge from the reference specimens. At stage-II (1% < θ < 3%), there was a slight increase followed by a decrease in the λ for the retrofitted PCCFST specimens. However, for the retrofitted CFST specimens no such increase in λ was observed. The possible reason for the above could be the presence of inner circular steel tube imparting additional strength to the last cycle of the retrofitted PCCFST specimens. However, at stage-II, the λ for the retrofitted PCCFST specimens were higher than that of the corresponding reference specimens. The outer retrofitting element contributes in maintaining the higher λ at stage-II. At stage –III (3% < θ < 6%), the reference specimens showed approximately constant λ but for the retrofitted specimens the slope of degradation remains same as that of stage-II. Hence at stage-III, the strength degradation curve of both retrofitted PCCFST and the corresponding reference specimens most likely intersect each other. At stage-IV, (θ > 6%), the strength degradation coefficient deteriorates significantly for the retrofitted specimens compared to the corresponding reference specimens because of the damage of the retrofitted specimens above the retrofitting element in addition to the initial damage from the reference specimens. Figure 6.8(e) showed the Strength degradation coefficient of all the retrofitted specimens. It could be seen that all the retrofitted PCCFST specimens followed approximately similar path. However, the strength degradation curve for the retrofitted CFST was slightly lower than the retrofitted PCCFST because of the absence of the additional inner circular steel tube.

6.3.4 *P*-Δ envelope curves

Figure 6.9 shows the lateral load versus displacement envelope curve of all the retrofitted specimens and their corresponding reference specimens. The ultimate lateral strength (P_u) resulting from all the tests was shown in Table 6.2, and it was computed as the average of the peak +ve and –ve lateral loads derived from P-Δ envelope curves. The retrofitted specimens could regain the ultimate lateral strength by 113%-139% with respect to their corresponding reference specimens (refer Figure 6.10). All the retrofitted PCCFST columns have shown approximately 113 to 116% strength regain irrespective of the type of retrofitting element or thickness and diameter of inner CHS. Hence it could be concluded that the proposed geometry of the retrofitting element was sufficient enough to effectively shift the plastic hinge providing optimum possible strength enhancement using the proposed technique. The drift angle corresponding to the ultimate lateral strength of the retrofitted CFST was 3% whereas for the retrofitted PCCFST it was 4-5%. Hence it is evident that the presence of inner steel tube delayed the occurrence of steel tube buckling for the retrofitted specimens also.

6.3.5 Stiffness degradation

The degradation of average stiffness (K) versus the lateral displacement (Δ) for the retrofitted specimens were plotted corresponding to their reference specimens in Figure 6.11. It could be seen that with the increase in lateral displacement, the stiffness of the specimens decreased due to the damage accumulation. It was seen that all the retrofitted specimens showed higher stiffness initially with respect to the corresponding reference specimens (approximately 30-50%). However, at the higher level of displacement ($\theta \geq 6\%$), the stiffness degradation curve of the retrofitted specimens merges with the corresponding reference specimens.

6.3.6 Energy dissipation ability

Figure 6.12 shows the cumulative energy dissipation profile of all the specimens associated with the increasing drift angle. For all the retrofitted specimens, it was seen that the post peak drop of approximately 15% has occurred within 8% drift angle. Hence energy dissipation capacity of all the specimens have been computed upto the last cycle of the 8% drift angle. The energy dissipation capacity corresponding to each load-displacement hysteretic cycle was computed as the area enclosed in it. Table 6.2 provides a summary of the total energy dissipation ability obtained from the test results. For the columns under lateral cyclic loading, the potential plastic hinge region determined the energy dissipation capacity. Strengthening the plastic hinge region may enhance the overall performance of the column. In the present study, all the retrofitted columns were provided with additional CFST retrofitting element at the damaged region, hence were found to have exhibited higher energy dissipation capacity compared to the corresponding reference specimens. The regain in the energy dissipation capacity ranges from 116% to 135% with respect to the reference specimens (refer Figure 6.13 and Table 6.2). Furthermore, the energy dissipated by all the retrofitted columns were approximately same irrespective of the presence of inner circular steel tube. It may be concluded from the above that the retrofitting element was sufficient enough to exhibit the optimum seismic performance and shift the plastic hinge up.

6.3.7 Strain development

Typical lateral force versus axial strain (P-ε) hysteretic curves has been shown in Figure 6.14, where compression and tension, respectively, are represented by the +ve and –ve values of the strains. The strain data were obtained from the strain gauges, installed at the height of 50 mm (B2) on the retrofitting steel from the column end and 50 mm above the top fiber of the retrofitting element (T2). Detail instrumentation has been shown in Figure 6.4. The strain data obtained from the strain gauges installed on the retrofitting element near the column end (B2) showed no significant strains (strains ranges from 100 to 500 μm/m) whereas strain gauge installed above the retrofitting element (T2) showed strain ranging from 5000-10000 μm/m. Hence indicating that the significant buckling of the steel tube for all the specimens have occurred near the top fiber of the retrofitting element. Therefore, it is evident that by applying the proposed retrofitting technique for the circular CFST /PCCFST columns, the potential plastic hinge could be shifted up.

6.4 CONCLUSIONS

A novel CFST based retrofitting technique for circular CFST/PCCFST column has been proposed in the present chapter. The seismic performance of retrofitted

CFST/PCCFST specimens was investigated. The effect of the shape of the retrofitting element and the presence of an inner circular steel tube of 1.5*D* height on the maximum lateral strength and energy dissipation ability has been assessed and reported. On the basis of the limited data obtained from the experimental analysis of the retrofitted columns, the following conclusions have been made.

1) The proposed retrofitting technique is effective in regaining the structural performance (ultimate lateral strength and energy dissipation capacity) of the damaged circular CFST/PCCFST columns.
2) Maintaining the diameter and height of the CFST base retrofitting element as 1.75*D* could effectively delay the local buckling of the column.
3) With the proposed retrofitting technique, the plastic hinge could be shifted up effectively (i.e., the retrofitting element has most likely acted like a support to the CFST/PCCFST column leading to the occurrence of the plastic hinge immediate above the retrofitting element).
4) Irrespective of the shape of the retrofitting element, all the retrofitted specimens exhibited approximately same seismic performance.

Table 6.1: Geometrical dimensions

Specimens	D_0 (mm)	t_0 (mm)	H_0 (mm)	D (mm)	t (mm)	H (mm)	D_i (mm)	t_i (mm)	H_i (mm)	D_i/D	D_0/D	H_0/D	N_0 (kN)
C114-c0	-		-	114	3.2	650	-	-	-	-	-	-	22
C114-c0-C	200	3.2	200	114	3.2	650	-	-	-	-	1.75	1.75	22
C114-c50-3.2-1.5D	-			114	3.2	650	50	3.2	171	0.44	-	-	22
C114-c50-3.2-1.5D-S	200	3.2	200	114	3.2	650	50	3.2	171	0.44	1.75	1.75	22
C114-c60-3.2-1.5D	-			114	3.2	650	60	3.2	171	0.53	-	-	22
C114-c60-3.2-1.5D-C	200	3.2	200	114	3.2	650	60	3.2	171	0.53	1.75	1.75	22
C114-c60-2.8-1.5D	-			114	3.2	650	60	2.8	171	0.53	-	-	22
C114-c60-2.8-1.5D-C	200	3.2	200	114	3.2	650	60	2.8	171	0.53	1.75	1.75	22

Table 6.2: Experiment findings

Specimen ID	P_u (kN)	E (kN.m)
C114-c0	27.00	26.35
C114-c0-C	37.43	35.76
C114-c50-3.2-1.5D	31.29	29.88
C114-c50-3.2-1.5D-S	36.25	35.07
C114-c60-3.2-1.5D	31.30	29.92
C114-c60-3.2-1.5D-C	35.60	35.15
C114-c60-2.8-1.5D	29.2	29.8
C114-c60-2.8-1.5D-C	32.94	34.59

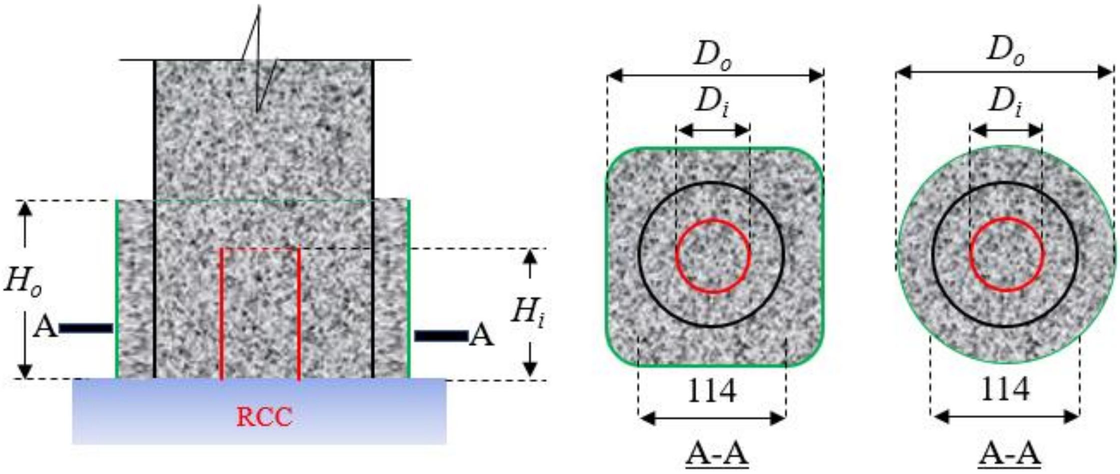

a) Front view b) Section A-A

Figure 6.1: Novel Retrofitting technique for circular PCCFST columns

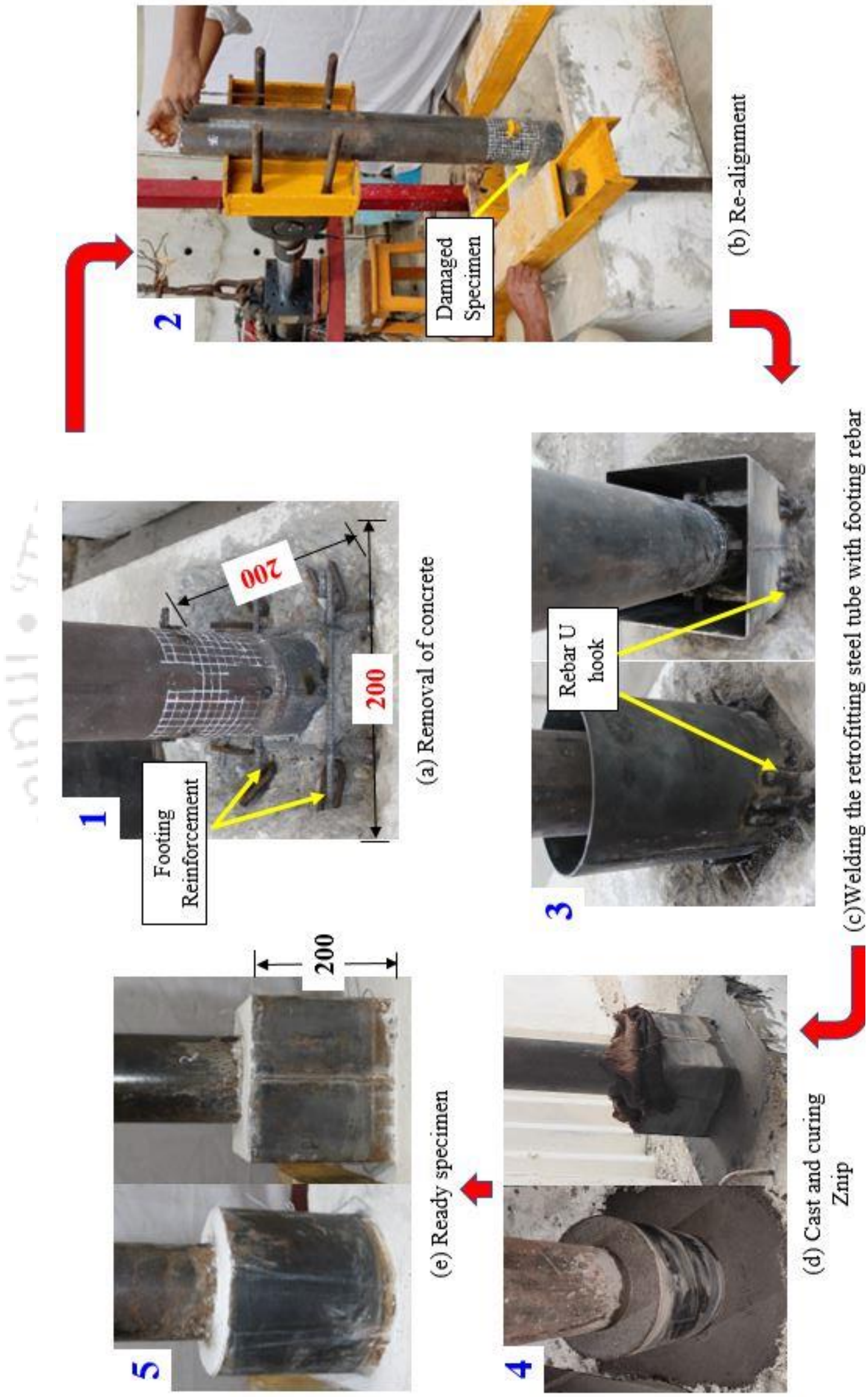

Figure 6.2: Specimen preparation (unit: mm)

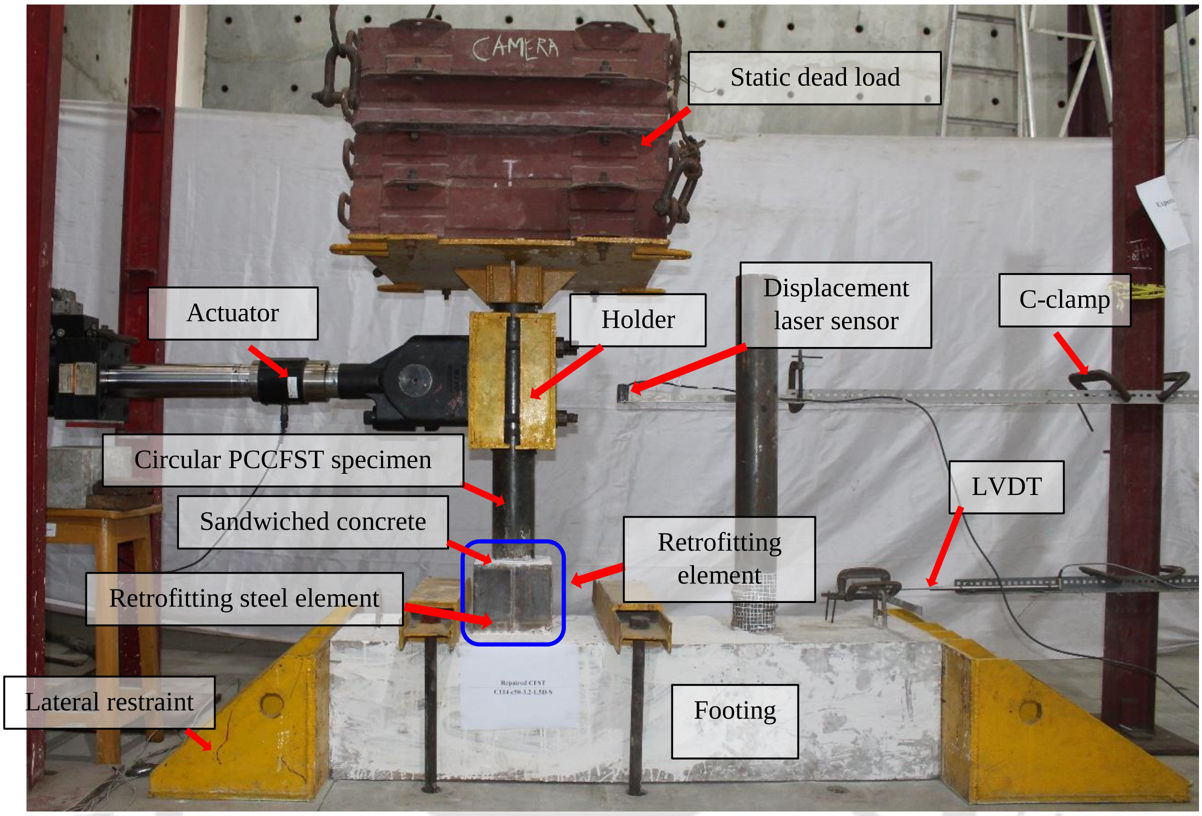

Figure 6.3: Test set-up

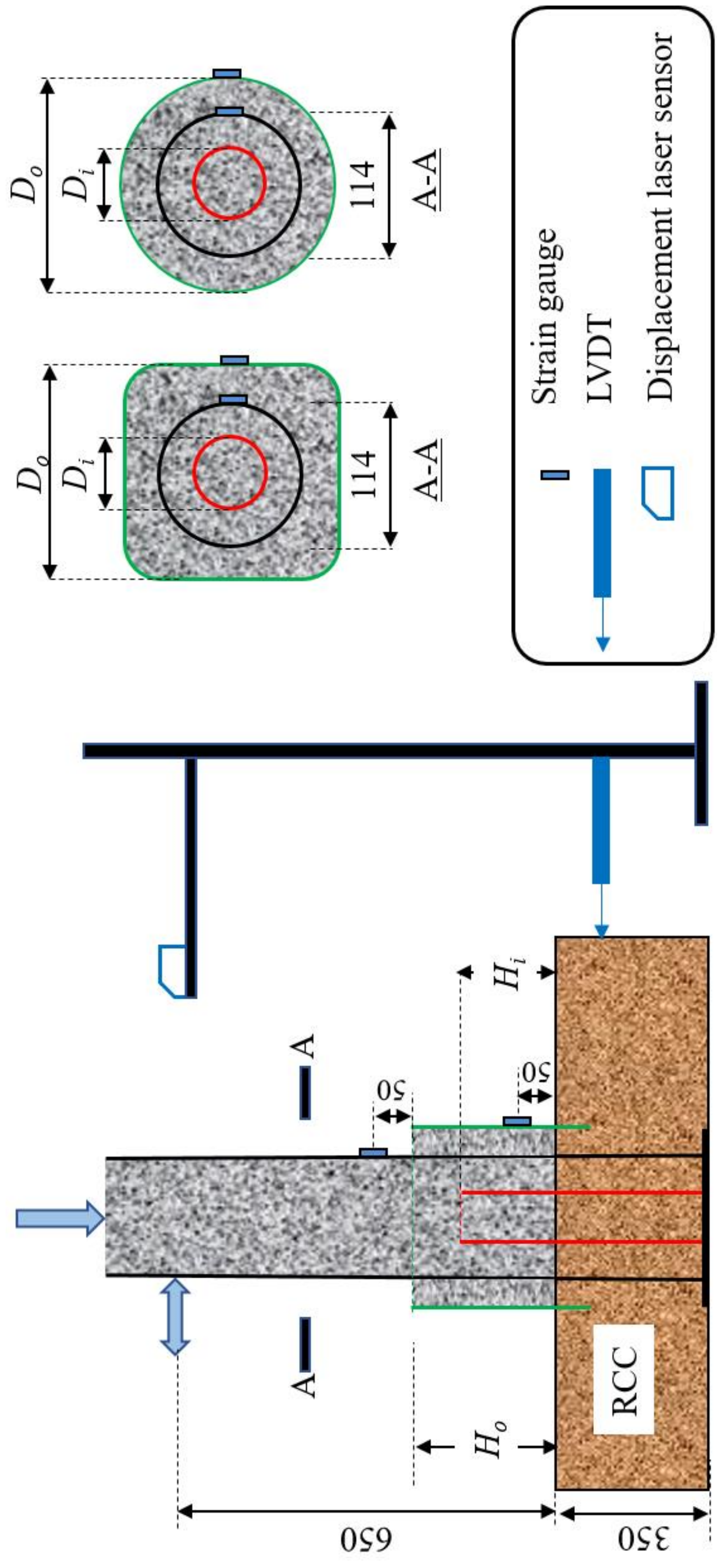

Figure 6.4: Specimen configuration and instrumentation (all units in mm)

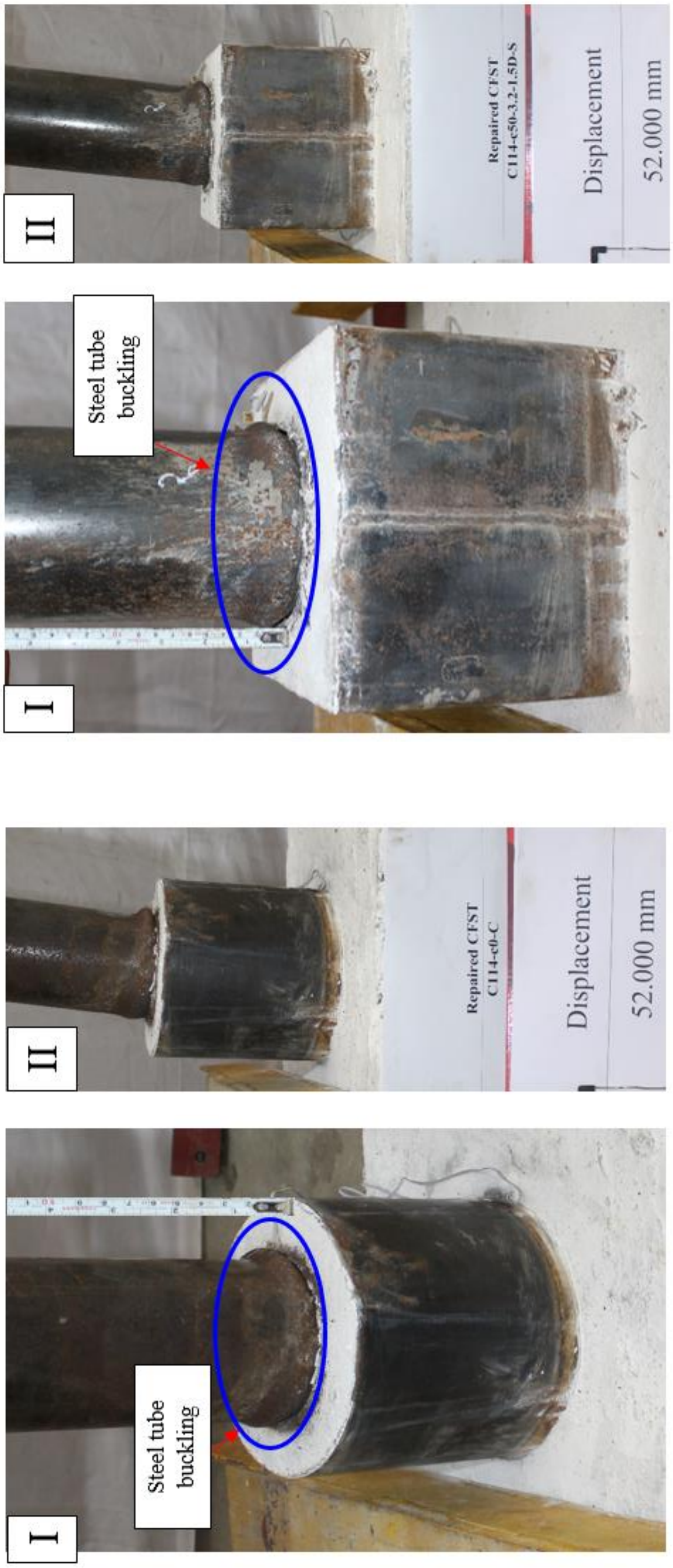

(b) C114-c50-3.2-1.5D-S

(a) C114-c0-C

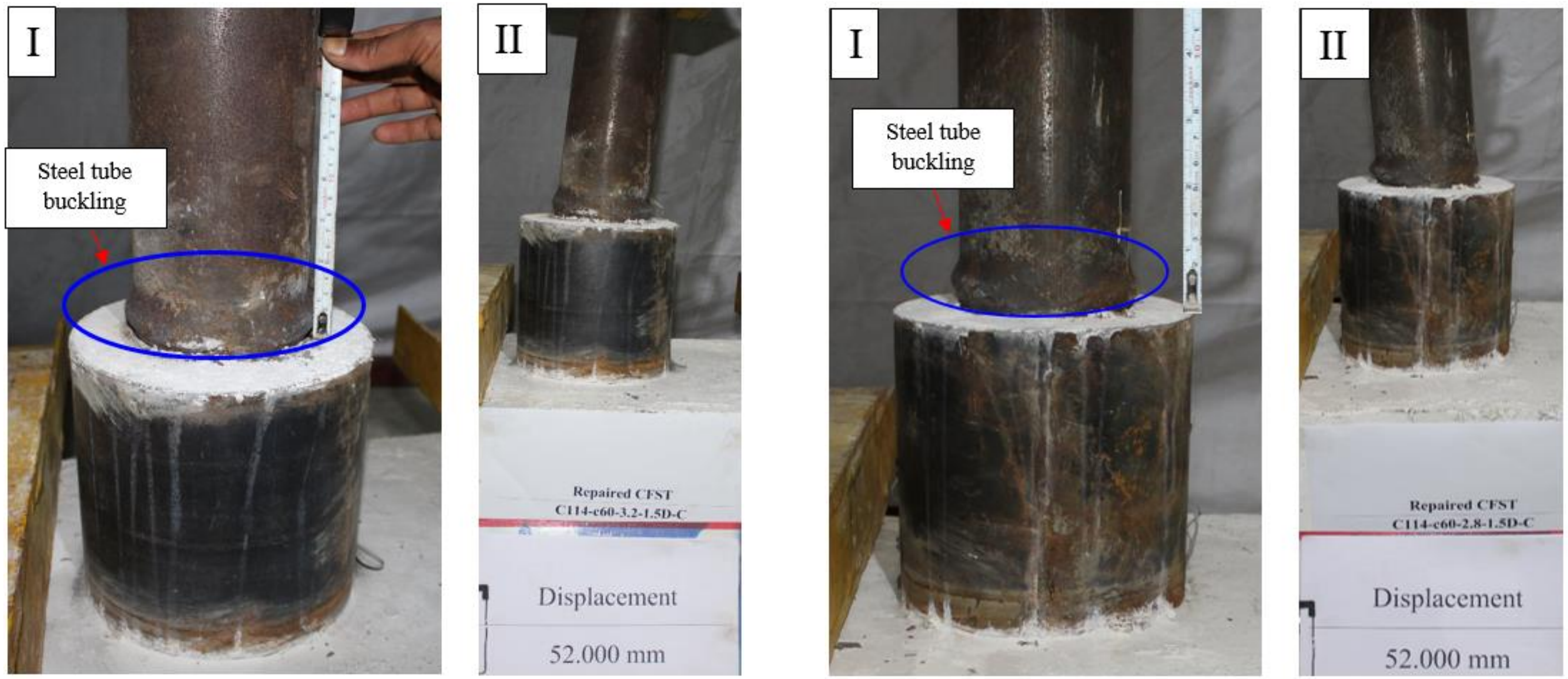

(c) C114-c60-3.2-1.5D-C (d) C114-c60-2.8-1.5D-C

Figure 6.5: Failure modes of retrofitted specimens

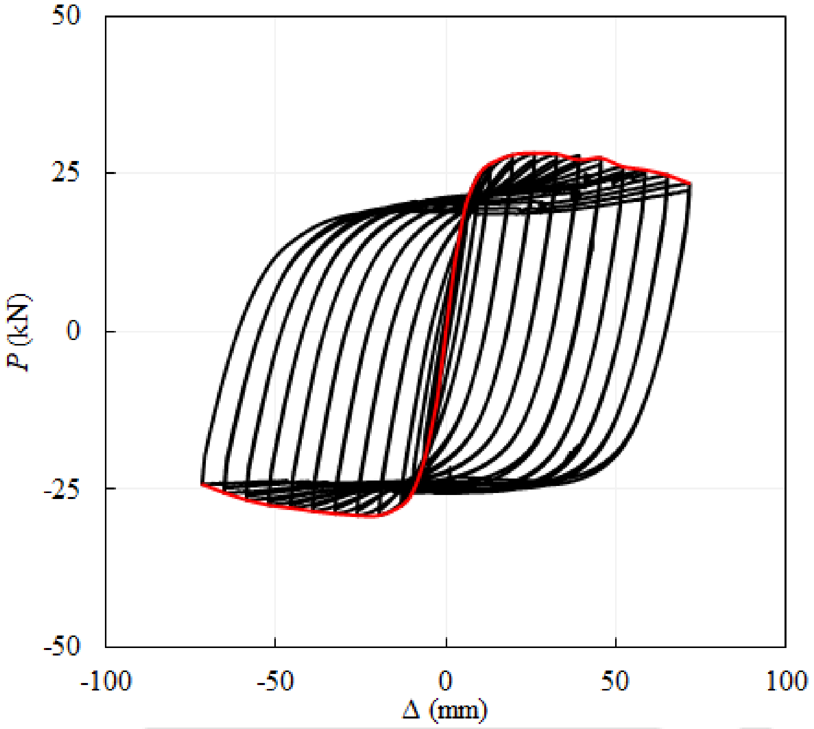

Figure 6.6: Lateral loads (P) versus lateral displacement (Δ) hysteretic curve of C114-c60-2.8-1.5D

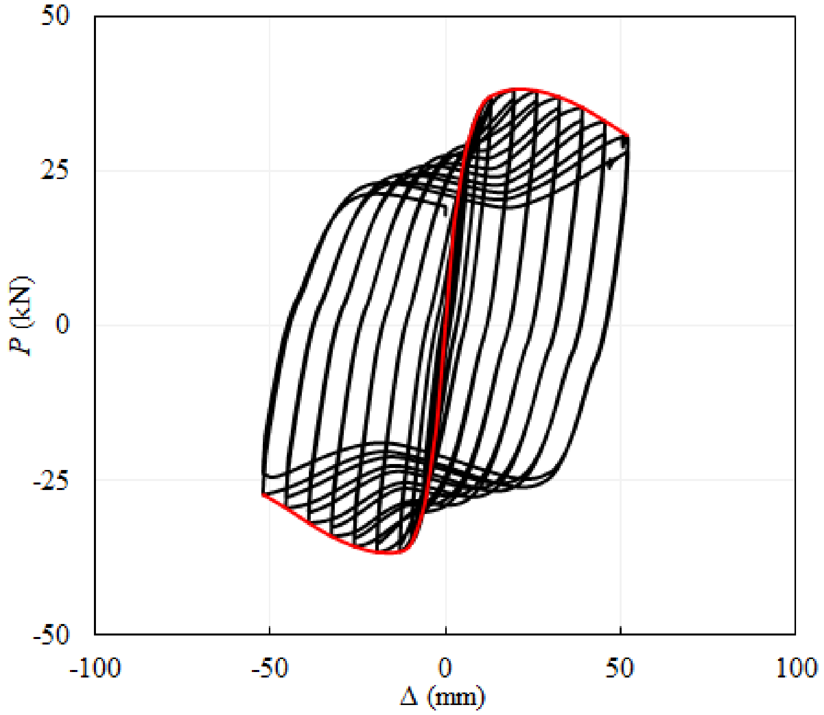

(a) C114-c0-C

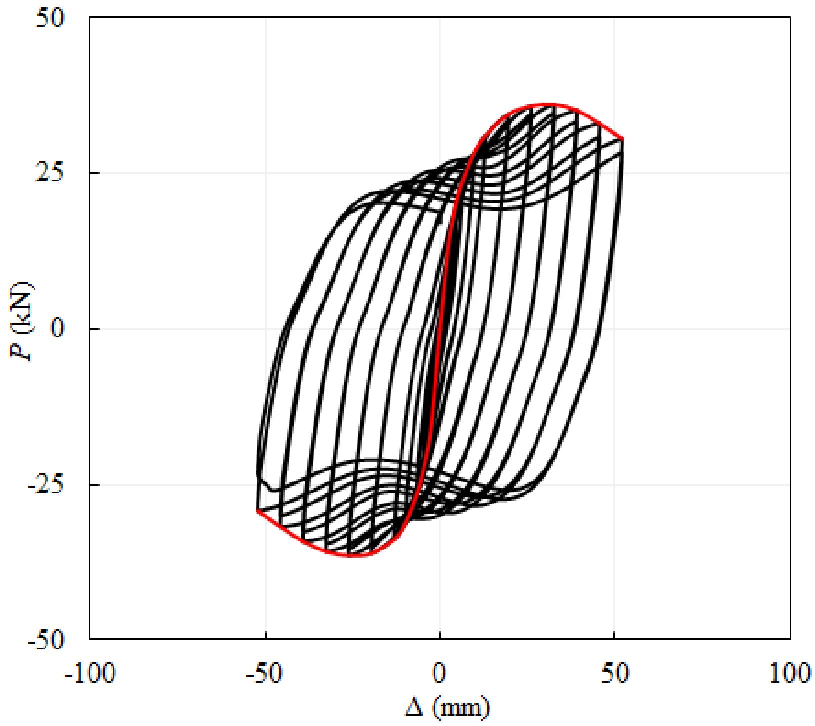

(b) C114-c50-3.2-1.5D-S

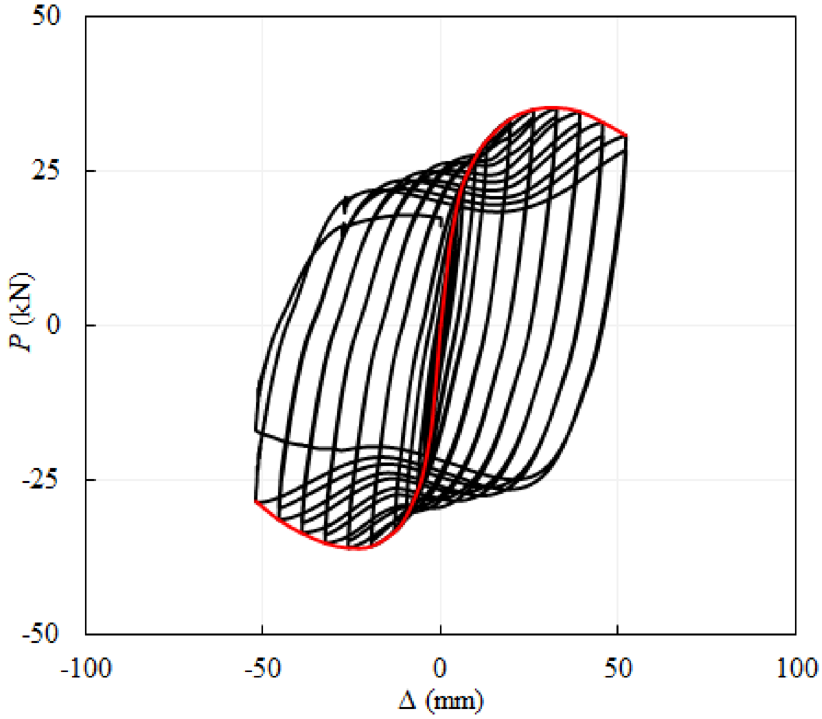

(c) C114-c60-3.2-1.5D-C

Figure 6.7: Lateral loads (*P*) versus lateral displacement (Δ) hysteretic curves of retrofitted columns

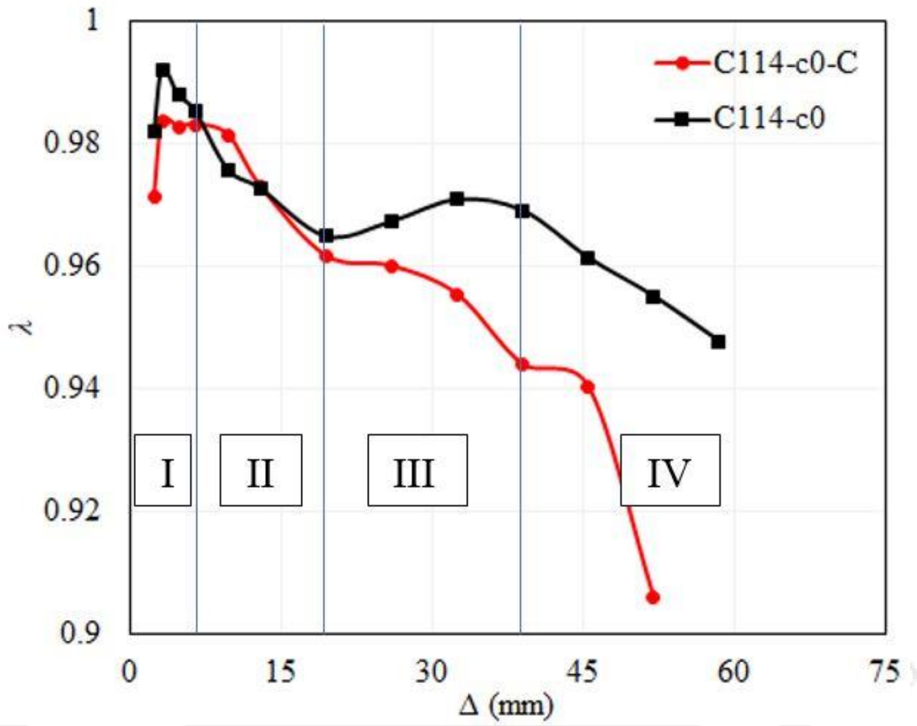
C114-c0-C
C114-c0
I
II
III
IV
λ
Δ (mm)
1
0.98
0.96
0.94
0.92
0.9
0
15
30
45
60
75

(a)

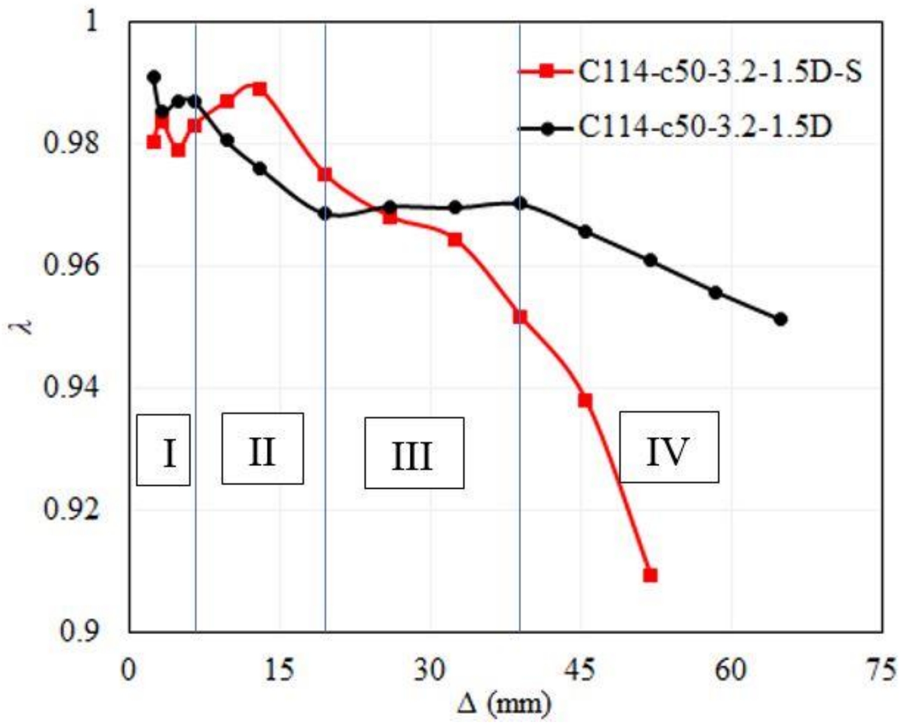
C114-c50-3.2-1.5D-S
C114-c50-3.2-1.5D
I
II
III
IV
λ
Δ (mm)
1
0.98
0.96
0.94
0.92
0.9
0
15
30
45
60
75

(b)

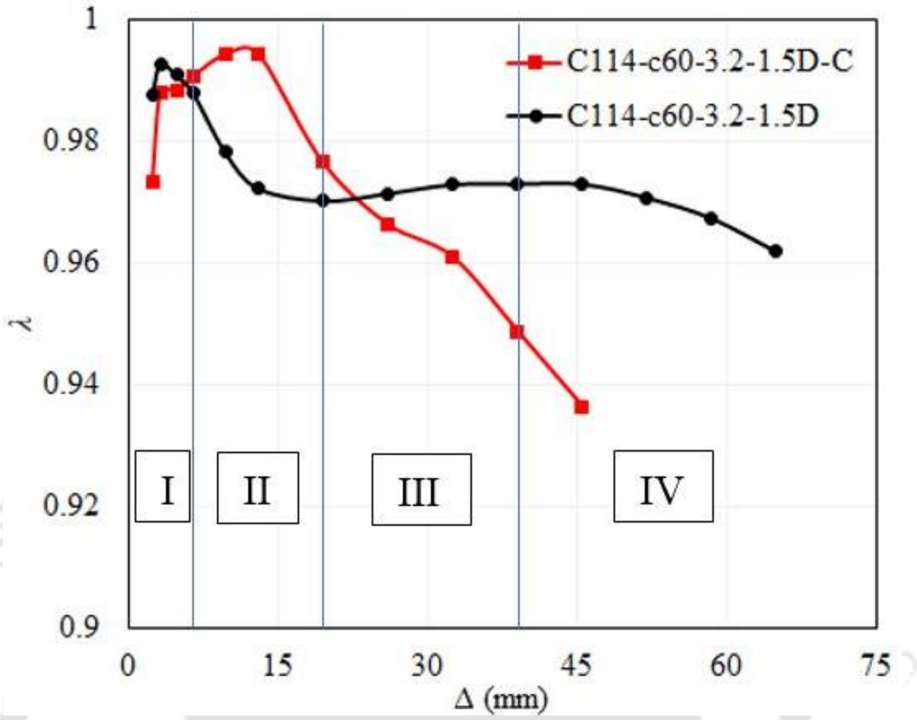
C114-c60-3.2-1.5D-C
C114-c60-3.2-1.5D
I
II
III
IV
λ
Δ (mm)
1
0.98
0.96
0.94
0.92
0.9
0
15
30
45
60
75

(c)

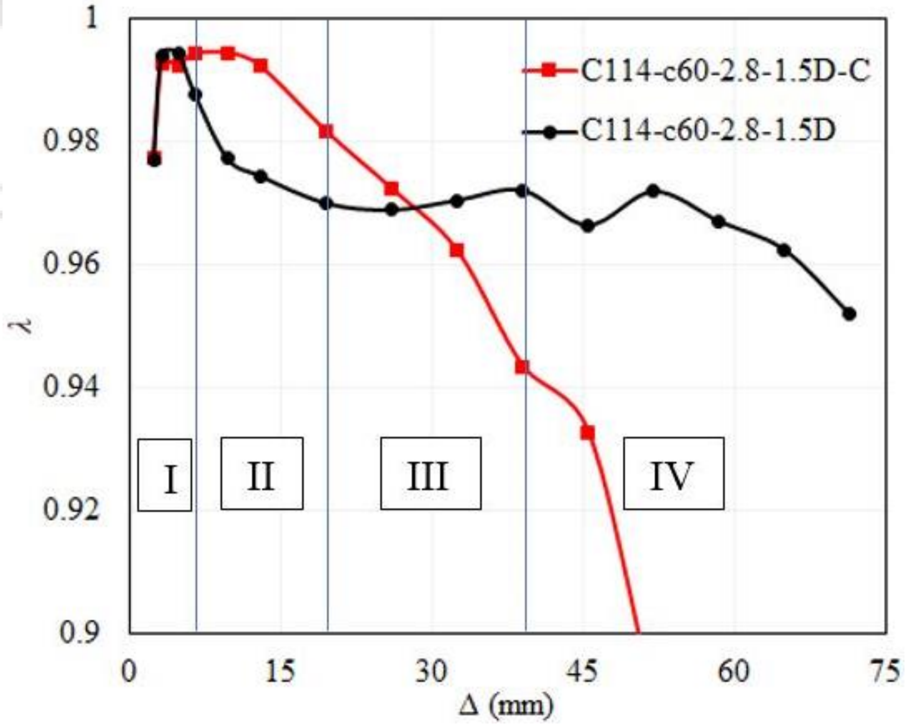
C114-c60-2.8-1.5D-C
C114-c60-2.8-1.5D
I
II
III
IV
λ
Δ (mm)
1
0.98
0.96
0.94
0.92
0.9
0
15
30
45
60
75

(d)

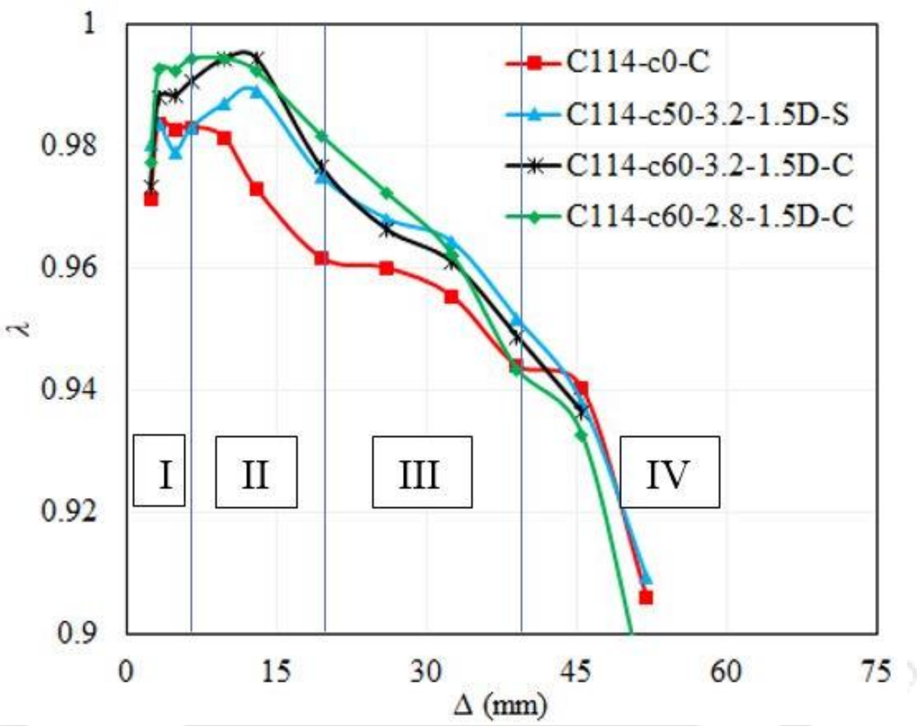

(e)

Figure 6.8: Strength degradation curve

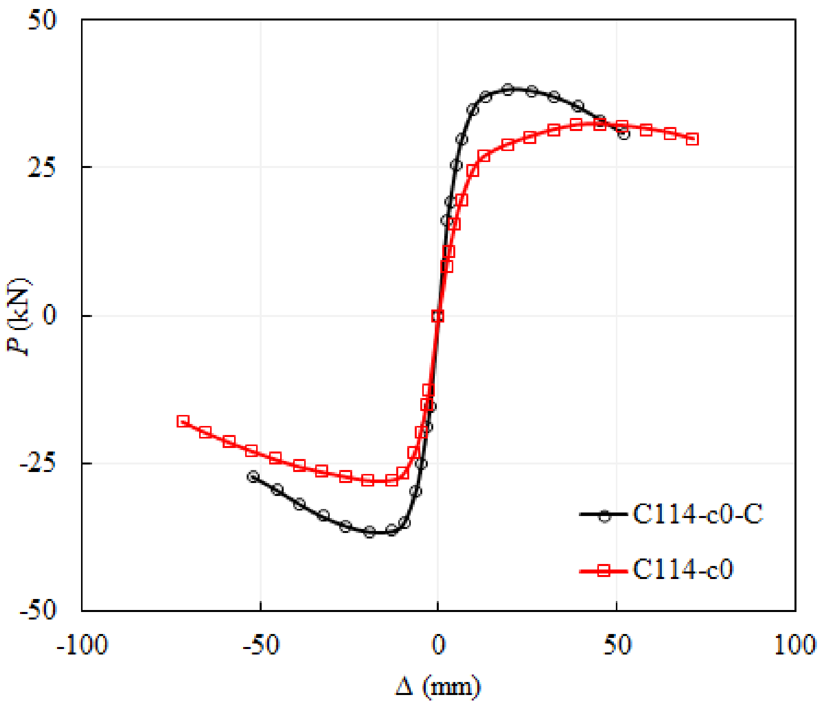

(a)

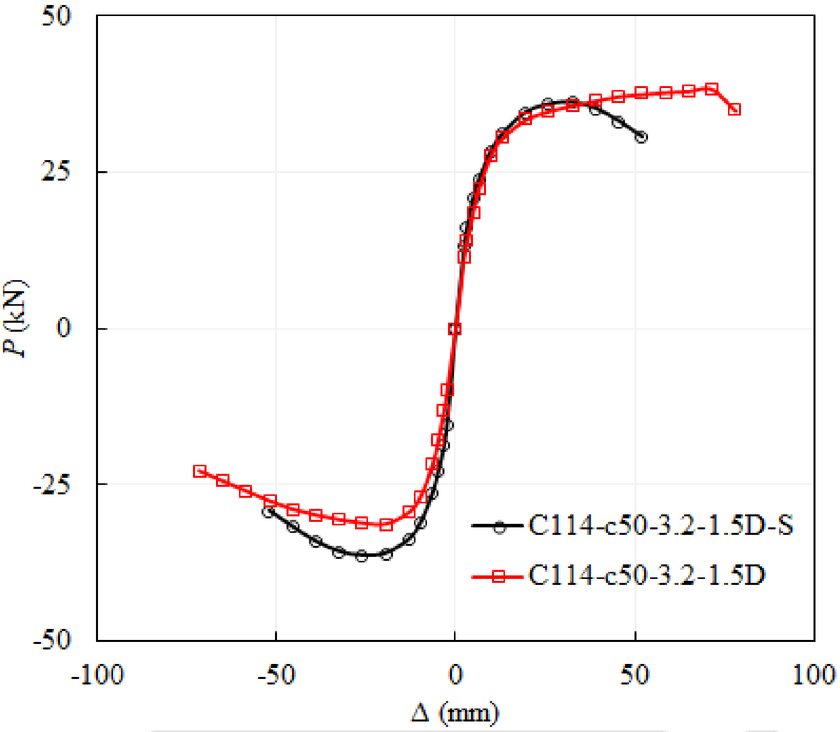
50
25
0
-25
-50
P (kN)
-100
-50
0
50
100
Δ (mm)
C114-c50-3.2-1.5D-S
C114-c50-3.2-1.5D

(b)

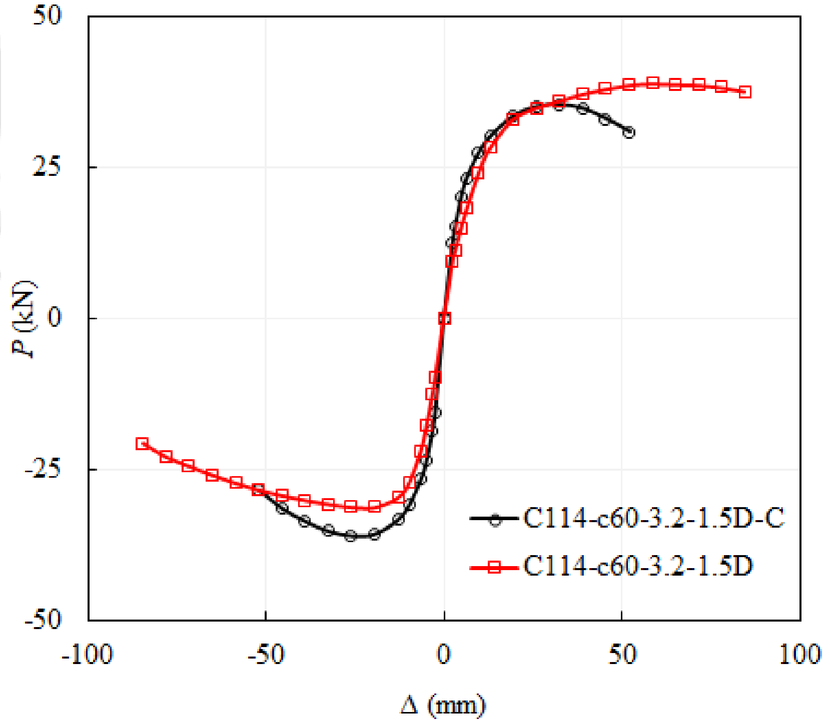
50
25
0
-25
-50
P (kN)
-100
-50
0
50
100
Δ (mm)
C114-c60-3.2-1.5D-C
C114-c60-3.2-1.5D

(c)

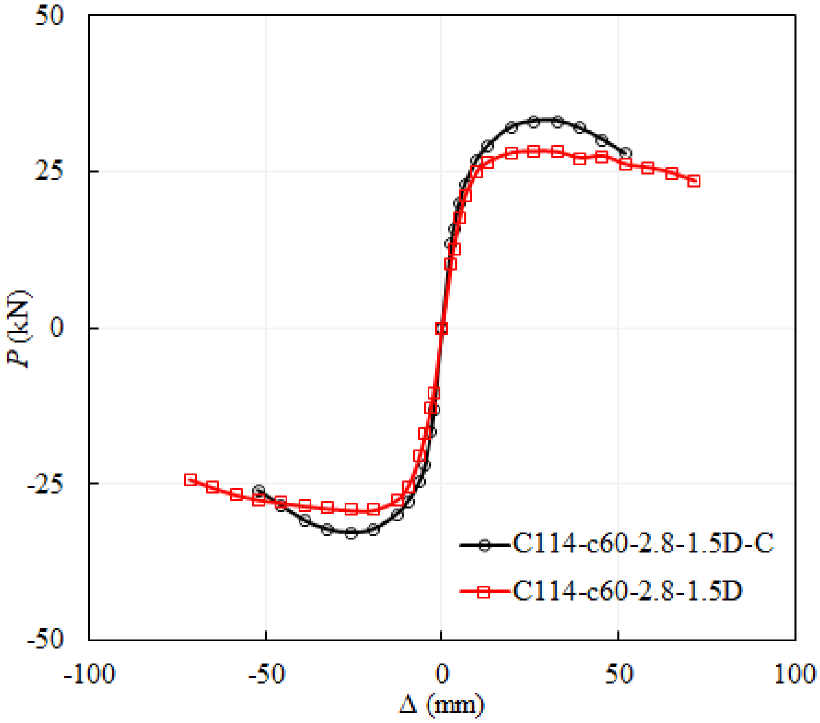

(d)

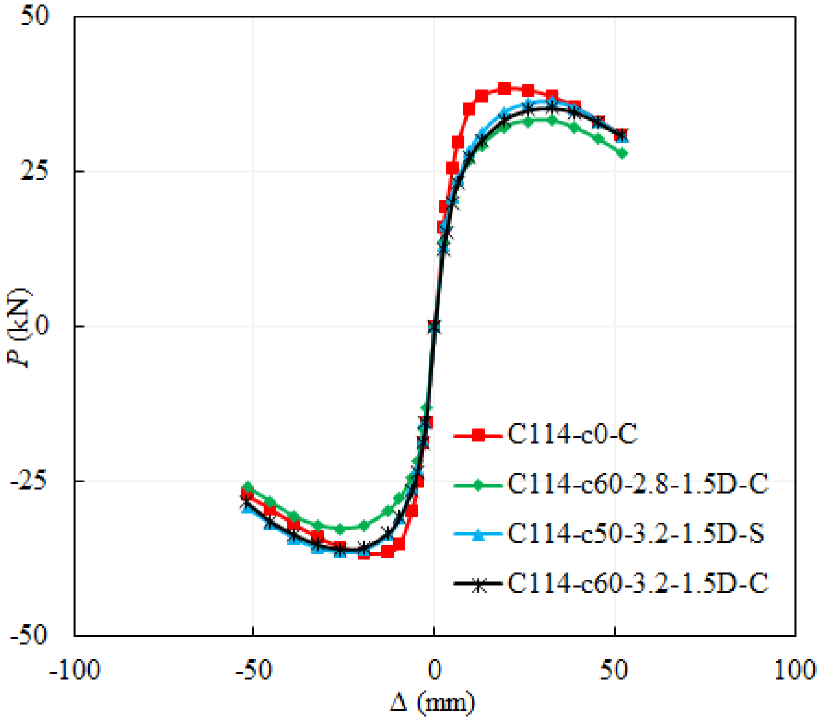

(e)

Figure 6.9: Lateral load versus lateral displacement (P-Δ) envelope curves

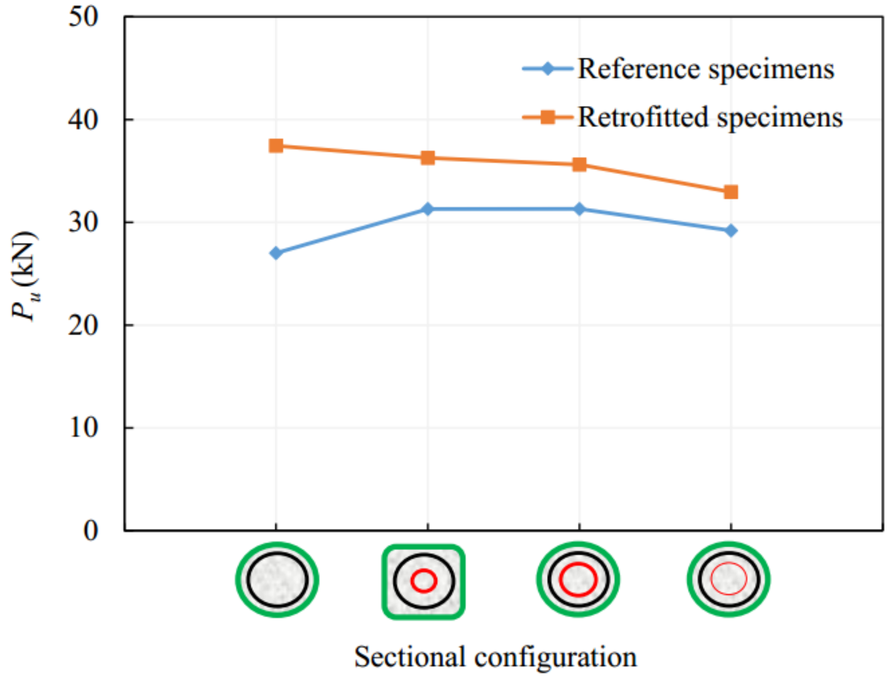

Figure 6.10: Effect of retrofitting element on P_u

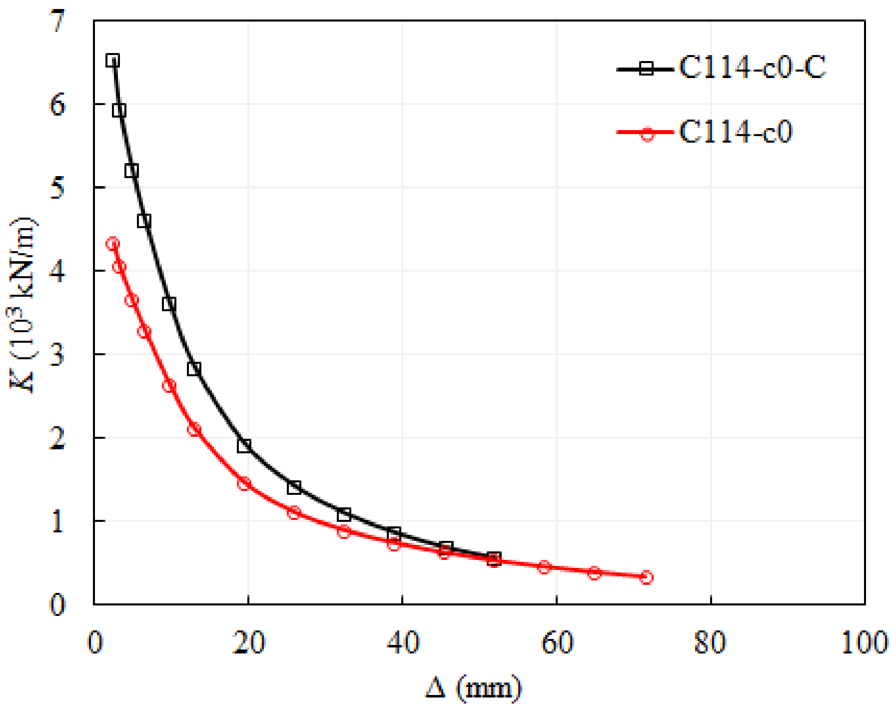

(a)

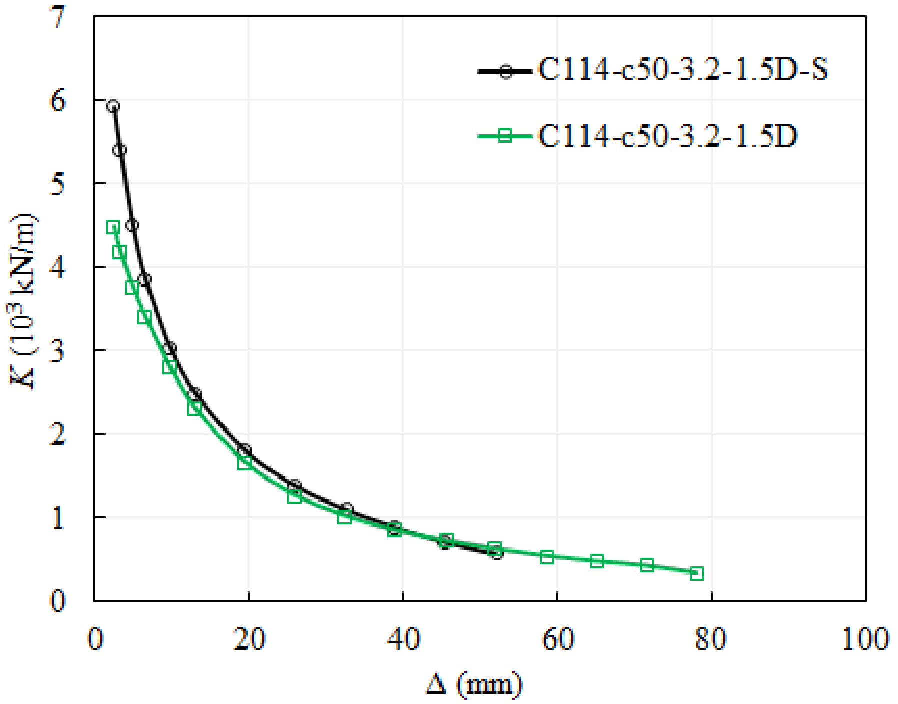
C114-c50-3.2-1.5D-S
C114-c50-3.2-1.5D
K (10^3 kN/m)
Δ (mm)
0
1
2
3
4
5
6
7
0
20
40
60
80
100

(b)

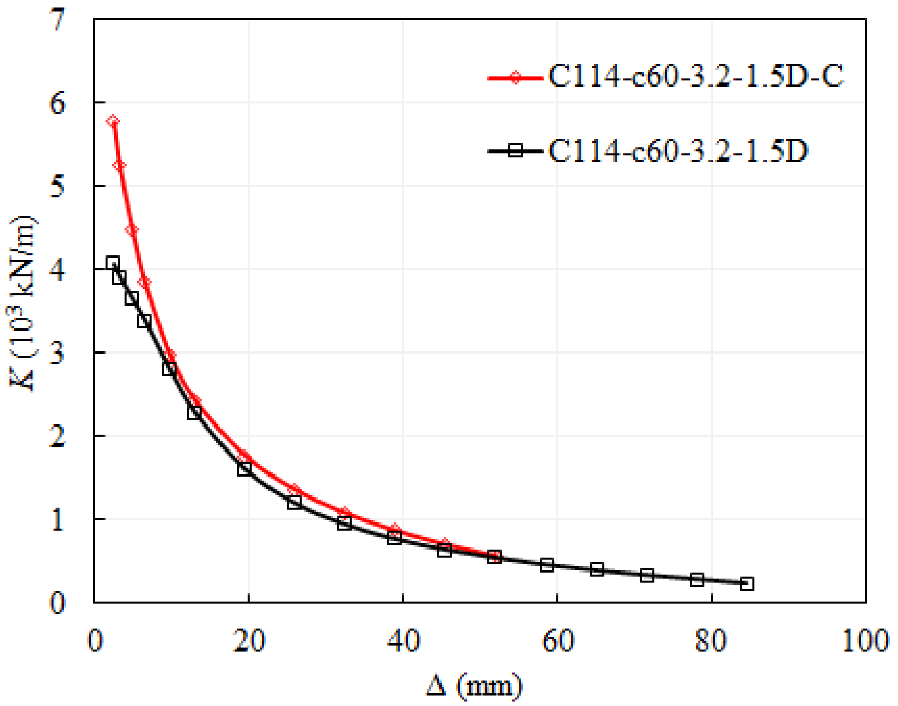
C114-c60-3.2-1.5D-C
C114-c60-3.2-1.5D
K (10^3 kN/m)
Δ (mm)
0
1
2
3
4
5
6
7
0
20
40
60
80
100

(c)

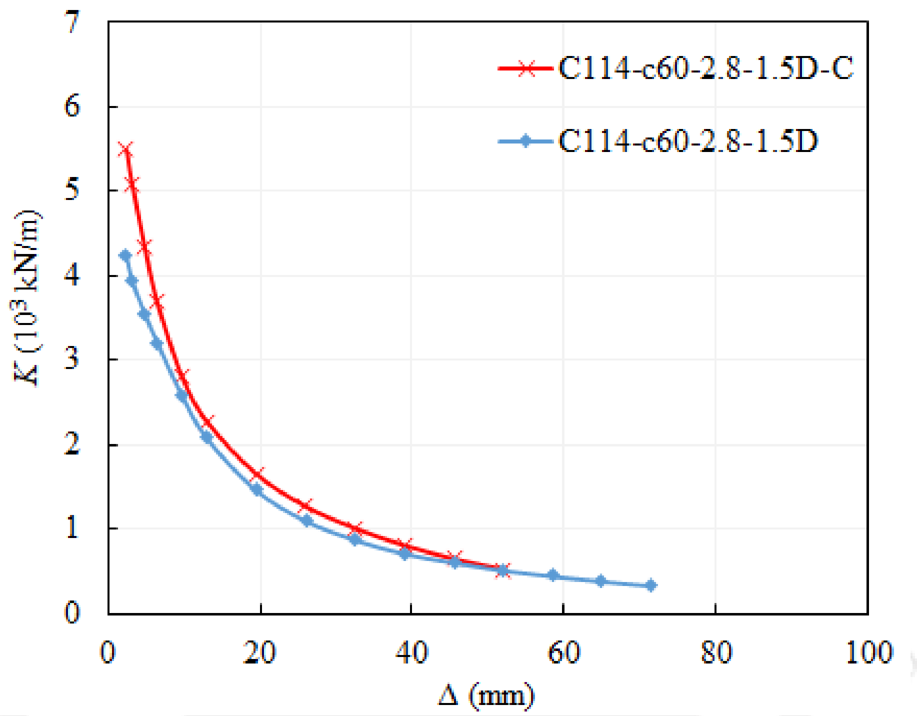

(d)

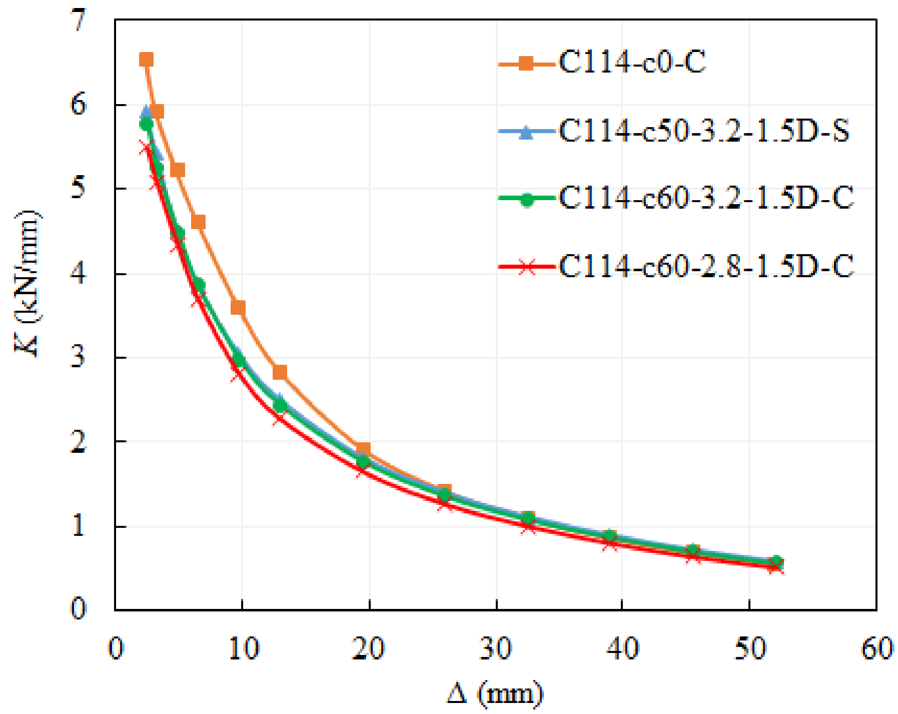

(e)

Figure 6.11: Stiffness degradation (K-Δ) curves

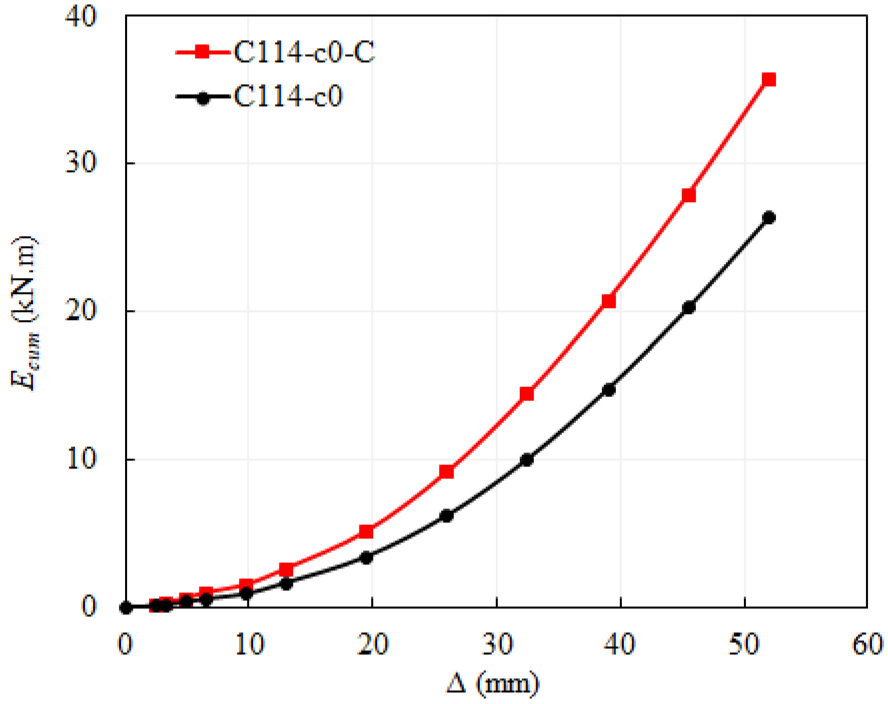

C114-c0-C
C114-c0
E_{cum} (kN.m)
Δ (mm)
0
10
20
30
40
50
60

(a)

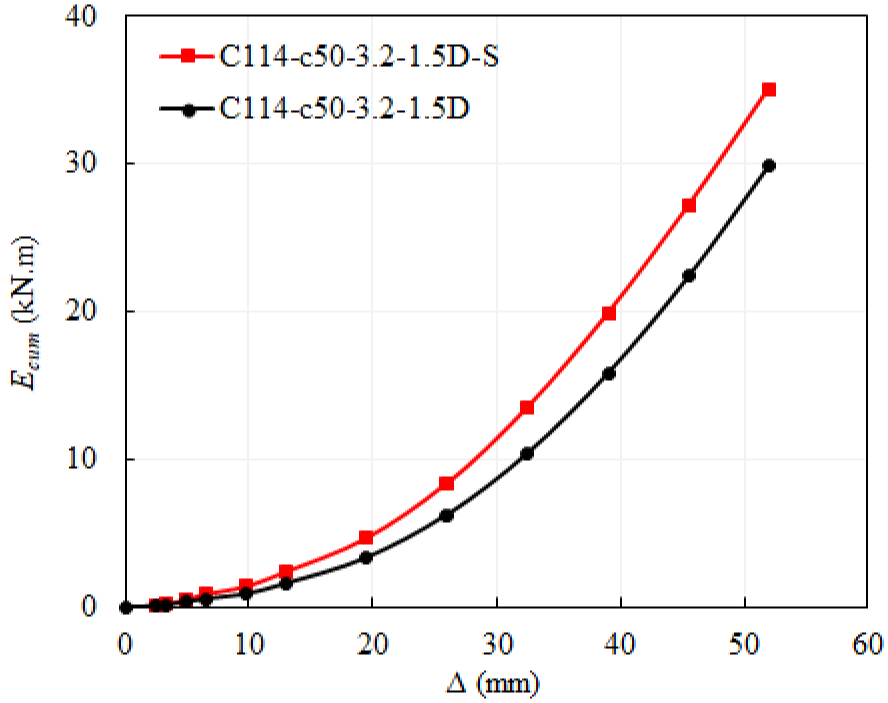

C114-c50-3.2-1.5D-S
C114-c50-3.2-1.5D
E_{cum} (kN.m)
Δ (mm)
0
10
20
30
40
50
60

(b)

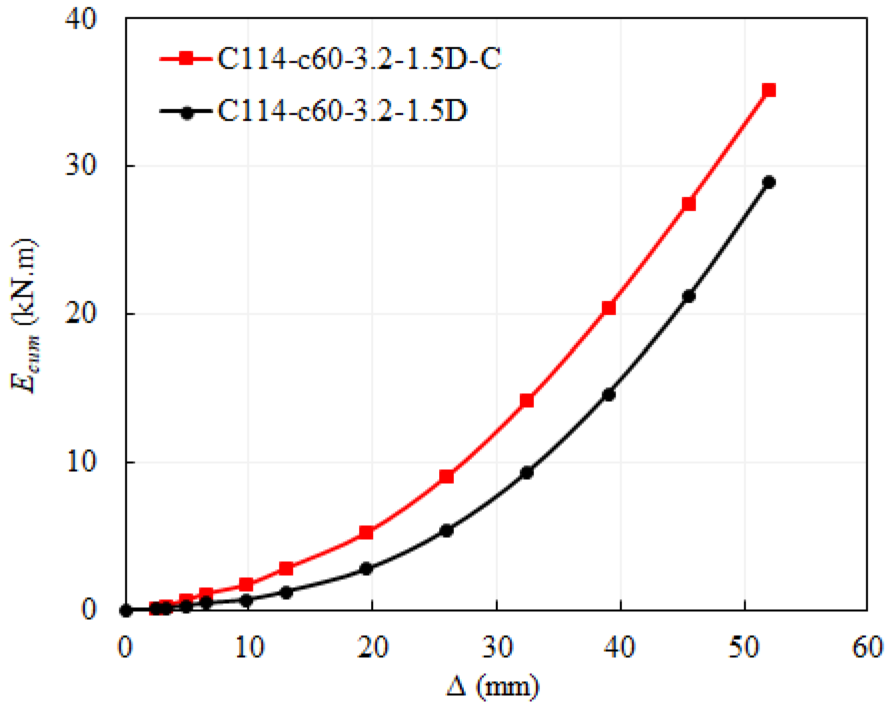
40
30
20
10
0
0
10
20
30
40
50
60
C114-c60-3.2-1.5D-C
C114-c60-3.2-1.5D
E_{cum} (kN.m)
Δ (mm)

(c)

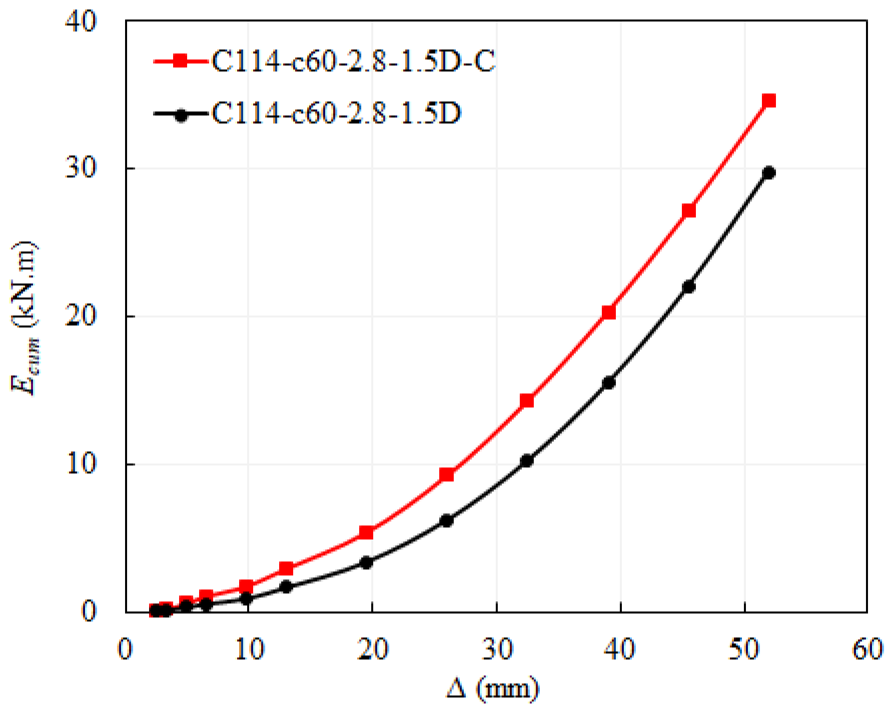
40
30
20
10
0
0
10
20
30
40
50
60
C114-c60-2.8-1.5D-C
C114-c60-2.8-1.5D
E_{cum} (kN.m)
Δ (mm)

(d)

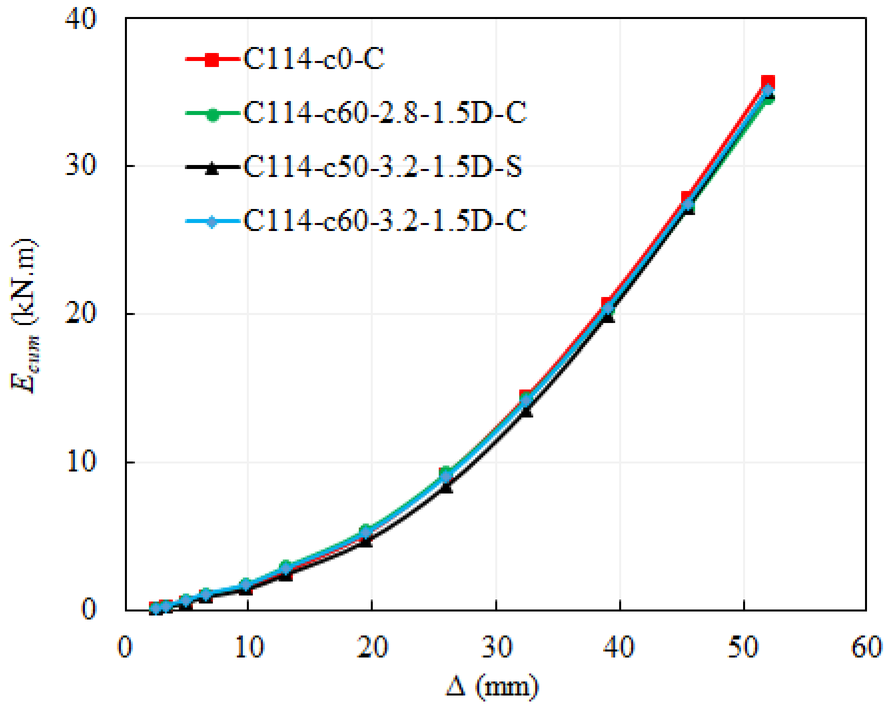

(e)

Figure 6.12: Energy dissipation (E-Δ) curves

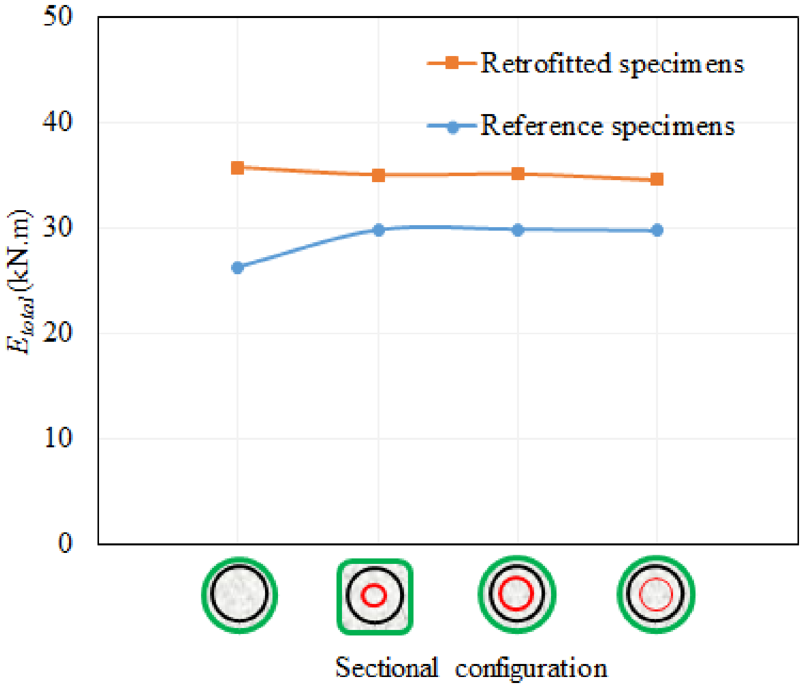

Figure 6.13: Effect of retrofitting element on E_{total}

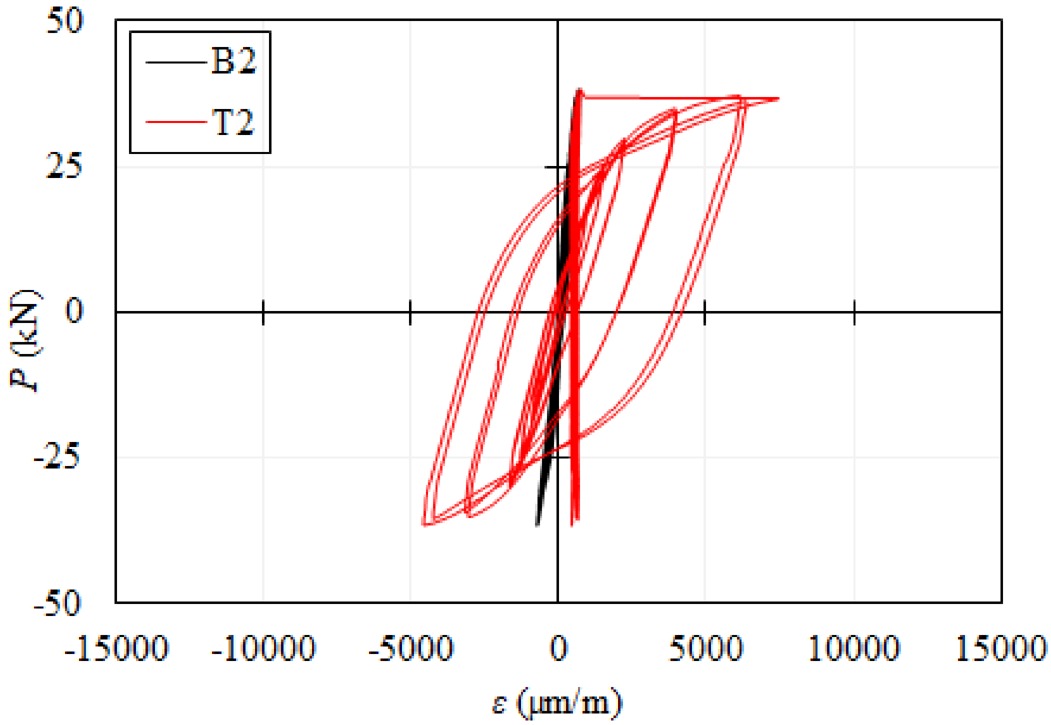

(a) C114-c0-C

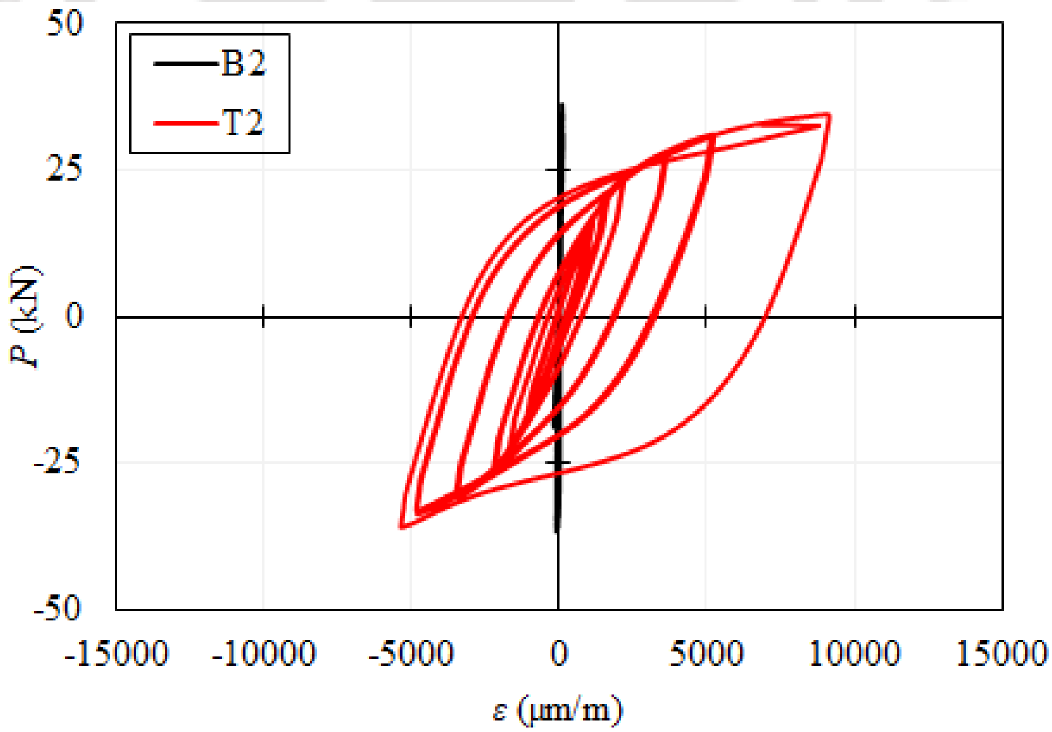

(b) C114-c50-3.2-1.5D-S

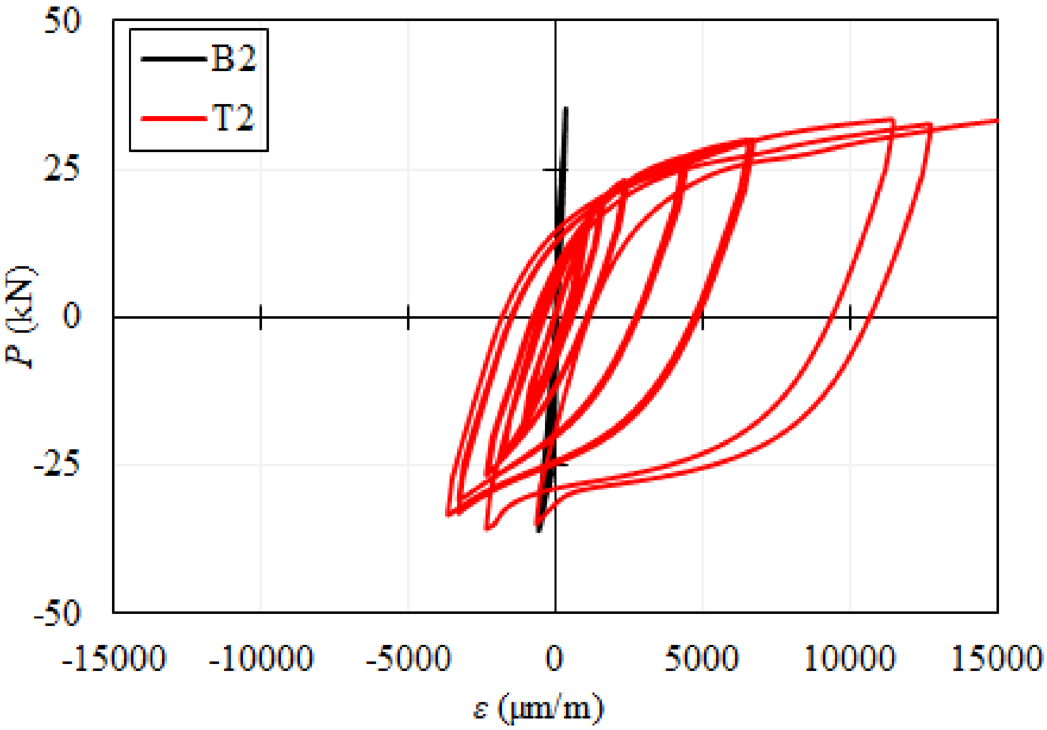

(c) C114-c60-3.2-1.5D-C

Figure 6.14: Typical lateral force versus strain (P-ε) hysteretic loops

This page is intentionally left blank

Chapter 7

Conclusions

7.1 RESEARCH SUMMARY

In the present thesis work, a novel, internally strengthening technique for the CFST columns (both square and circular) confining the potential plastic hinge region has been proposed named partially confined concrete-filled steel tubular column. In this technique, an inner circular hollow steel tube was provided concentrically to the CFST column at the potential plastic hinge region. A series of tests were conducted on the partially confined CFST columns under combined axial and lateral cyclic loadings. The structural performance (ultimate lateral strength, energy dissipation capacity, ductility, strength degradation, stiffness degradation etc.) of these columns were analyses based on the experimental data. Based on the experimental data, an Eurocode (Eurocode 4 1994) based simplified design guidelines has been proposed for both square and circular partially confined CFST columns. The test continued till the lateral resistance drops 20% of the ultimate lateral strength or the columns failed (indicated by the ductile tearing of the steel tube). The performance of these square and circular partially confined CFST columns have been presented in Chapters 3 and 4, respectively. After the tests were done, an innovative retrofitting technique was proposed to retrofit the damaged columns (both square and circular) externally using square and circular CFST elements. The feasibility and structural viability of the proposed retrofitting technique have been assessed under similar loading condition as mentioned above. The efficiency of the proposed technique on the square and circular damaged columns have been evaluated based on the data obtained from the series of tests and presented in Chapter 5 and 6, respectively.

The results obtained from the above experimental investigations were carefully analyzed and the main conclusions drawn from each chapter of this thesis has been presented here (sections 7.1.1 to 7.1.4). Furthermore, an insight of possible extension to the present work and future scope on strengthening and retrofitting the CFST columns have been briefly reported.

7.1.1 Square partially confined CFST columns

a) The proposed strengthening technique can effectively enhance the structural performance of the CFST columns.

b) For the square partially confined CFST column with 1D and 1.5D height of inner steel tube, the buckling of the outer steel tube has occurred at 2 locations: i) near the base of the footing and ii) height upto which partial confinement was provided. However, for the specimen with no inner tube, 0.5D and 2.5D height of inner tube, the buckling was restricted near the base of the column only.

c) Increasing the height of the inner circular steel tube increases the cyclic performance. However, beyond 1.5D height of the inner tube, the enhancement in the cyclic performance is found to be mild (<1 %).

d) With the increase in the diameter of the inner circular steel tube, the area of confinement increases across the cross section, hence the overall cyclic performance was enhanced.

e) An enhance in the structural performance of the partially confined CFST with 60 mm diameter and 1.5D height of inner circular steel tube in terms of ultimate lateral strength, energy dissipation capacity and ductility was found to be ~ 15.3%, 11.4% and 9.6%, respectively.

f) The simplified design guidelines presented in the chapter can effectively estimate the ultimate lateral strength of square partially confined CFST columns

7.1.2 Circular partially confined CFST columns

a) It was observed that the location of the plastic hinge formation of the circular CFST could be effectively shifted up using the partial confinement technique proposed in the chapter.

b) For the partially confined CFST columns, with the height of the inner circular steel tube upto 1D, the plastic hinge formation was found to have shifted to the height equivalent to the height of the inner tube.

c) The structural performance of the circular CFST was found to have enhanced using the proposed strengthening technique.

d) The ultimate lateral strength, energy dissipation capacity and ductility coefficient of the partially confined circular CFST columns with 60 mm diameter and 1.5D height of the inner circular steel tube, were found to have enhanced by ~16%, ~ 14% and ~24%, respectively.

e) The proposed design rule based on the Eurocode could effectively calculate the maximum lateral strength of the circular partially confined CFST columns.

7.1.3 Retrofitted square CFST and partially confined CFST columns

a) The proposed retrofitting technique could effectively regain the structural performance (ultimate lateral strength and energy dissipation capacity) of the damaged CFST and partially confined CFST columns.

b) The ultimate lateral strength and energy dissipation capacity regain of the retrofitted columns ranges from 121%-134%, and 110%-115%, respectively.

c) The square columns retrofitted by the square retrofitting element have showed severe diagonal cracks on the retrofitting element leading to the failure of the retrofitting element. However, no such diagonal cracks were seen for the column retrofitted with circular retrofitting element.

d) For all the retrofitted columns, the buckling of the outer square steel tube was observed above and near the retrofitting element.

e) The circular retrofitting element showed better ultimate lateral strength regain compared to the square retrofitting element.

f) The partially confined CFST column with square retrofitting element showed higher energy dissipation capacity in comparison to the circular cross section retrofitting element.

g) In comparison to the retrofitted CFST column, the retrofitted partially confined columns performed better in terms of maximum lateral strength and energy dissipation capacity while maintaining a similar retrofitting element.

7.1.4 Retrofitted circular CFST and partially confined CFST columns

a) The proposed retrofitting technique is effective in regaining the structural performance (ultimate lateral strength and energy dissipation capacity) of the damaged circular CFST and partially confined CFST columns.

b) The regain in the ultimate lateral strength and energy dissipation capacity, retrofitting the damaged circular CFST and partially confined CFST columns were 113%-139% and 116%-135 %, respectively.

c) Maintaining the diameter and height of the CFST base retrofitting element as 1.75*D* could effectively delay the local buckling of the column.

d) With the proposed retrofitting technique, the plastic hinge could be shifted up effectively (i.e., the retrofitting element has most likely acted like a support to the CFST/PCCFST column leading to the occurrence of the plastic hinge immediate above the retrofitting element).

e) The energy dissipation capacity exhibited by all the retrofitted specimens was same, irrespective of the shape of the retrofitting element.

f) In comparison to the retrofitted CFST specimen, the retrofitted partially confined CFST columns performed better in terms of maximum lateral strength and energy dissipation capacity while maintaining a similar retrofitting element.

7.2 FUTURE SCOPES

7.2.1 Extension to the present research work

In the present work, through an experimental investigation, an attempt has been made on strengthening the concrete-filled steel tubular column internally using circular inner hollow steel tube to be tested under constant axial compression and lateral cyclic loading. A numerical simulation can be performed on the same and parametric studies can be carried out to expand the data set.

In the present study, the height of the inner circular steel tube was limited to 1.5D. In continuation to the same, the height of the inner circular steel tube could be further increased gradually upto the actual height of the column making it concrete-filled double tube column and tested under same condition.

In the present study D_i/D ratio of the column was restricted from 0.44 to 0.53. Hence a study comprising of possibly minimum D_i/D ratio to the maximum D_i/D ratio could be performed to study the complete strength variation profile in consideration to the height of the inner Circular steel tube.

In the current study, an innovative retrofitting technique has been presented. For the retrofitted columns, the height and diameter of the retrofitting element was constant for all the specimens (~ *1.75D*). Therefore, a series of studies considering the thickness and strength of steel element, strength of concrete, width of sandwiched region, height of the retrofitting element could be performed for better understanding of the proposed retrofitting scheme.

The performance of the retrofitted specimens was examined through experimental investigation only. A numerical model could be prepared and parametric studies considering various key parameters could be performed for better understanding of the proposed retrofitting scheme.

The axial load ratio in the present research study was considerably low. However, present research work was focused on evaluating the cyclic performance of partially confined CFST columns and comparing with CFST under same loading condition. A similar study with the enhanced axial load ratio could be performed to understand the structural behavior under higher axial load ratio.

Further studies on partially confined CFST and retrofitted CFST columns considering different grades of steel and concrete with different steel thickness and steel type could be performed to enrich the CFST data set.

7.2.2 Other thoughts

In the current research programme, the lateral loading is restricted to quasi static loading condition only. Hence the structural performance of such CFST, partially confined CFST and retrofitted CFST columns under blast, impact and fire loading needs to be examined.

In case of partially confined CFST columns, the initial strength and stiffness of the column was enhanced because of the introduction of inner circular steel tube. However, introducing perforation to the CFST reduced the overall capacity of the column. Hence a study on CFST with inner circular steel tube and perforation could be investigated under lateral cyclic loading.

A study on the development of CFST based beam column joint under lateral cyclic loading may develop a better understanding of load transfer mechanism in case of a CFST construction. Furthermore, the seismic performance of frame structure made up of strengthened column and steel sections/CFST could be explored.

The performance of the partially confined CFST and retrofitted partially confined CFST columns under actual earthquake data needs to be explored.

`

References

AISC. (2016). "AISC 341. Seismic provisions for steel structural buildings, AISC." *Seismic Provisions for Structural Steel Buildings*, (1), 402.

ASTM E8. (2016). "ASTM E8/E8M standard test methods for tension testing of metallic materials 1." *Annual Book of ASTM Standards 4*, (C), 1–27.

Elchalakani, M., and Zhao, X. L. (2008). "Concrete-filled cold-formed circular steel tubes subjected to variable amplitude cyclic pure bending." *Engineering Structures*, 30(2), 287–299.

Elremaily, A., and Azizinamini, A. (2002). "Behavior and strength of circular concrete-filled tube columns." *Journal of Constructional Steel Research*, 58(12), 1567–1591.

Eurocode 4. (1994). "Design of composite steel and concrete structures, Part 1.1: General rules and rules for buildings."

Fam, A., Qie, F. S., and Rizkalla, S. (2004). "Concrete-filled steel tubes subjected to axial compression and lateral cyclic loads." *Journal of Structural Engineering*, 130(4), 631–640.

Gajalakshmi, P., and Helena, H. J. (2012). "Behaviour of concrete-filled steel columns subjected to lateral cyclic loading." *Journal of Constructional Steel Research*, 75(March), 55–63.

Han, L. H., Huang, H., Tao, Z., and Zhao, X. L. (2006). "Concrete-filled double skin steel tubular (CFDST) beam-columns subjected to cyclic bending." *Engineering Structures*, 28(12), 1698–1714.

Han, L. H., Huang, H., and Zhao, X. L. (2009). "Analytical behaviour of concrete-filled double skin steel tubular (CFDST) beam-columns under cyclic loading." *Thin-Walled Structures*, 47(6–7), 668–680.

Han, L. H., Li, W., and Bjorhovde, R. (2014). "Developments and advanced applications of concrete-filled steel tubular (CFST) structures: Members." *Journal of Constructional Steel Research*, Elsevier Ltd, 100, 211–228.

Han, L. H., Yang, Y. F., and Tao, Z. (2003). "Concrete-filled thin-walled steel SHS and RHS beam-columns subjected to cyclic loading." *Thin-Walled Structures*, 41(9), 801–833.

Han, R., Zhao, H., Sun, Y., Ju, N., and Zhao, S. (2022). "Cyclic behavior of concrete-filled square tubular columns with stiffened plastic hinge region." *Journal of Constructional Steel Research*, Elsevier Ltd, 190(February), 107152.

Hanbin Ge, and Usami, T. (1996). "Cyclic tests of concrete-filled steel." *Journal of Structural Engineering*, 122(October), 1169–1177.

Hsu, H. L., and Juang, J. L. (2000). "Performance of thin-walled box columns strengthened with internal braces." *Thin-Walled Structures*, 37(3), 241–258.

Hsu, H. L., and Yu, H. L. (2003). "Seismic performance of concrete-filled tubes with restrained plastic hinge zones." *Journal of Constructional Steel Research*, 59(5), 587–608.

Huang, Y., and Young, B. (2014). "The art of coupon tests." *Journal of Constructional Steel Research*, Elsevier Ltd, 96, 159–175.

Ichinose, L. H., Watanabe, E., and Nakai, H. (2001). "An experimental study on creep of concrete filled steel pipes." *Journal of Constructional Steel Research*, 57(4), 453–466.

Irfani, M. M. A., and Vimala, A. (2019). "Collapse mechanism of strong column weak beam buildings of varying heights." *International Journal of Engineering* *and Advanced Technology*, 9(1), 4144–4148.

IS:10262. (2009). “Guidelines for concrete mix design proportioning.” *Bureau of Indian Standards, New Delhi*, 1–14.

IS 1161. (1998). “Steel Tubes for Structural Purposes–Specification.” *Bureau of Indian Standards, New Delhi*.

IS 4923. (2009). “Hollow steel sections for structural use –Specification.” *Bureau of Indian Standards, New Delhi*.

IS 516. (1959). “Method of Tests for Strength of Concrete.” *Bureau of Indian Standards*, New Delhi, 1-30.

Lehman, D. E., and Roeder, C. W. (2012). “Foundation connections for circular concrete-filled tubes.” *Journal of Constructional Steel Research*, Elsevier Ltd, 78, 212–225.

Liang, Q. Q., Uy, B., and Liew, J. Y. R. (2007a). “Strength of Concrete-Filled Steel Box Columns with Buckling Effects.” *Australian Journal of Structural Engineering*, 7(2), 145–155.

Liang, Q. Q., Uy, B., and Richard Liew, J. Y. (2007b). “Local buckling of steel plates in concrete-filled thin-walled steel tubular beam-columns.” *Journal of Constructional Steel Research*, 63(3), 396–405.

Liao, F. Y., Han, L. H., Tao, Z., and Rasmussen, K. J. R. (2017). “Experimental Behavior of Concrete-Filled Stainless Steel Tubular Columns under Cyclic Lateral Loading.” *Journal of Structural Engineering (United States)*, 143(4), 1–15.

Liu, J., Zhao, Q., Xia, Z., Wang, X., Xu, H., Ding, Y., and Wang, X. (2021). “Seismic behavior of thin-walled square CFST columns with diagonal rib / circular liner stiffeners.” *Journal of Constructional Steel Research*, Elsevier Ltd, 179, 106519.

Liu, J., Zhou, X., and Zhang, S. (2008). “Seismic behaviour of square CFT beam-columns under biaxial bending moment.” *Journal of Constructional Steel*

Research, 64(12), 1473–1482.

Mao, X. Y., and Xiao, Y. (2006). "Seismic behavior of confined square CFT columns." *Engineering Structures*, 28(10), 1378–1386.

Mathew, D., T.S, P., Joanna, P. S., and Sakaria, P. E. (2014). "Cyclic behavior of concrete filled double skinned tubular columns (inner and outer square light gauge tubes)." 3(11), 802–804.

Narendra, P. V. R., and Singh, K. D. (2017). "Elliptical hollow section steel cantilever beams under extremely low cycle fatigue flexural load – A finite element study." *Thin-Walled Structures*, Elsevier Ltd, 119(March), 126–150.

Park, S. H., Choi, S. M., Kim, Y. S., Park, Y. W., and Kim, J. H. (2010). "Hysteresis behavior of concrete filled square steel tube column-to-beam partially restrained composite connections." *Journal of Constructional Steel Research*, Elsevier Ltd, 66(7), 943–953.

Patel, V. I., Liang, Q. Q., and Hadi, M. N. S. (2014). "Numerical analysis of high-strength concrete-filled steel tubular slender beam-columns under cyclic loading." *Journal of Constructional Steel Research*, Elsevier Ltd, 92, 183–194.

Qian, J., Li, N., Ji, X., and Zhao, Z. (2014). "Experimental study on the seismic behavior of high strength concrete filled double-tube columns." *Earthquake Engineering and Engineering Vibration*, 13(1), 47–57.

Qin, P., Tan, Y., and Xiao, Y. (2015). "Low cyclic fatigue performance of concrete-filled steel tube columns." *Journal of Central South University*, 22(10), 4035–4042.

Schneider, S. P., and Alostaz, Y. M. (1998). "Experimental Behavior of Connections to Concrete-Filled Steel Tubes." *Journal of Constructional Steel Research*, 45(3), 321–352.

Serras, D. N., Skalomenos, K. A., Hatzigeorgiou, G. D., and Beskos, D. E. (2016). "Modeling of circular concrete-filled steel tubes subjected to cyclic lateral loading." *Structures*, Elsevier B.V., 8, 75–93.

Silva, A., Jiang, Y., Castro, J. M., Silvestre, N., and Monteiro, R. (2016). "Experimental assessment of the flexural behaviour of circular rubberized concrete-filled steel tubes." *Journal of Constructional Steel Research*, 122, 557–570.

Stephens, M. T., Lehman, D. E., and Roeder, C. W. (2016). "Design of CFST column-to-foundation/cap beam connections for moderate and high seismic regions." *Engineering Structures*, Elsevier Ltd, 122, 323–337.

Usami, T., and Ge, H. B. (1998). "Cyclic behavior of thin-walled steel structures - Numerical analysis." *Thin-Walled Structures*.

Varma, A. H., Ricles, J. M., Sause, R., and Lu, L. W. (2002). "Seismic behavior and modeling of high-strength composite concrete-filled steel tube (CFT) beam-columns." *Journal of Constructional Steel Research*, 58(5–8), 725–758.

Varma, A. H., Ricles, J. M., Sause, R., and Lu, L. W. (2004). "Seismic behavior and design of high-strength square concrete-filled steel tube beam columns." *Journal of Structural Engineering*, 130(2), 169–179.

Wang, H., Wu, C., Zhang, F., Fang, Q., Xiang, H., Li, P., Li, Z., Zhou, Y., Zhang, Y., and Li, J. (2017a). "Experimental study of large-sized concrete filled steel tube columns under blast load." *Construction and Building Materials*, 134, 131–141.

Wang, J. H., He, J., and Xiao, Y. (2019). "Fire behavior and performance of concrete-filled steel tubular columns: Review and discussion." *Journal of Constructional Steel Research*, 157, 19–31.

Wang, Y. T., Cai, J., and Long, Y. L. (2017b). "Hysteretic behavior of square CFT columns with binding bars." *Journal of Constructional Steel Research*, Elsevier Ltd, 131, 162–175.

Wu, B., Zhao, X. Y., and Zhang, J. S. (2012). "Cyclic behavior of thin-walled square steel tubular columns filled with demolished concrete lumps and fresh concrete." *Journal of Constructional Steel Research*, 77, 69–81.

Xiao, Y., He, W., and Choi, K. K. (2005). "Confined concrete-filled tubular columns." *Journal of Structural Engineering*, 131(3), 488–497.

Xu, W., Han, L. H., and Li, W. (2016). "Seismic performance of concrete-encased column base for hexagonal concrete-filled steel tube: Experimental study." *Journal of Constructional Steel Research*, 121, 352–369.

Yin, Y., and Zhang, Y. (2012). "Research on the seismic behavior of concrete-filled steel tubular column and steel beam joint." *Applied Mechanics and Materials*, 204–208, 2528–2532.

Yu, T., Hu, Y. M., and Teng, J. G. (2016). "Cyclic lateral response of FRP-confined circular concrete-filled steel tubular columns." *Journal of Constructional Steel Research*, 124, 12–22.

Zhang, B., Teng, J. G., and Yu, T. (2015). "Experimental behavior of hybrid FRP-concrete-steel double-skin tubular columns under combined axial compression and cyclic lateral loading." *Engineering Structures*, 99, 214–231.

Zhang, Y., Xu, C., and Lu, X. (2007). "Experimental study of hysteretic behaviour for concrete-filled square thin-walled steel tubular columns." *Journal of Constructional Steel Research*, 63(3), 317–325.

Zheng, Y., He, C., and Zheng, L. (2018). "Experimental and numerical investigation of circular double-tube concrete-filled stainless steel tubular columns under cyclic loading." *Thin-Walled Structures*, Elsevier Ltd, 132(August), 151–166.

Zhou, F., and Xu, W. (2016). "Cyclic loading tests on concrete-filled double-skin (SHS outer and CHS inner) stainless steel tubular beam-columns." *Engineering Structures*, Elsevier Ltd, 127, 304–318.

Zubydan, A. H., and Elsabbagh, A. I. (2011). "Monotonic and cyclic behavior of concrete-filled steel-tube beam-columns considering local buckling effect." *Thin-Walled Structures*, Elsevier, 49(4), 465–481.

`

Publications

Journals:

1. **Kar, P.**, Borsaikia, A.C. and Singh, K.D., 2023. Experimental investigation of partially confined concrete-filled steel tubular square columns under lateral cyclic loading. ***Journal of Constructional Steel Research***, 201, p.107751.

2. **Kar, P.**, Borsaikia, A.C. and Singh, K.D., Structural behavior of partially confined circular CFST columns under cyclic lateral loading (*Ready to be submitted*).

3. **Kar, P.**, Borsaikia, A.C. and Singh, K.D., Experimental investigation on externally retrofitted partially confined square CFST columns: cyclic lateral loading (*Ready to be submitted*).

4. **Kar, P.**, Borsaikia, A.C. and Singh, K.D., Structural behavior of externally retrofitted circular partially confined CFST columns under cyclic lateral loading (*Under preparation*).

Conferences:

1. **Kar, P**., Borsaikia, A.C., and Singh, K.D., Structural performance of partially confined concrete-filled steel circular tubular columns under cyclic lateral loading. ***Indian Structural Steel Conference 2022 (ISSC 2022)***, IIT Hyderabad; 6th -8th January 2022, ISSCP10071/2022.

2. **Kar, P**., Borsaikia, A.C., and Singh, K.D., Structural performance of retrofitted partially confined concrete-filled steel circular tubular columns under cyclic lateral loading. ***Socio-Technological Aspects of Seismic Disaster and Mitigation (STASDM 2022)***, IIT Guwahati; 23rd -24th June 2022.

3. **Kar, P**., Borsaikia, A.C., and Singh, K.D., Experimental investigation on externally-retrofitted concrete-filled steel tubular square column under cyclic lateral loading. ***18th International Symposium on Tubular Structures (ISTS 18)*** (*Abstract accepted*).

Appendix A

EUROCODE BASED SIMPLIFIED DESIGN GUIDELINES TO ESTIMATE THE ULTIMATE LATERAL STRENGTH OF PARTIALLY CONFINED CONCRETE-FILLED STEEL TUBULAR COLUMNS

Problem A.1: To estimate the ultimate lateral strength of square partially confined concrete-filled steel tubular columns, diameter and height of inner steel tube is 60 mm and 1.5D respectively.

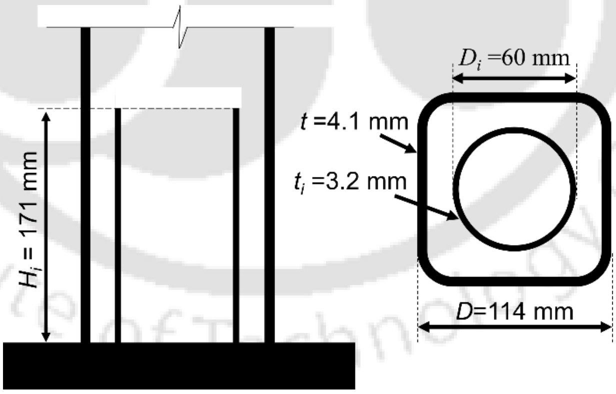

Figure A.1.1: Partially confined square CFST columns

<u>Mechanical and geometric properties:</u>

N_0= 22 kN

n=0.025

D=114 mm

D_i = 60 mm (inner CHS diameter)

t= 4.1 mm

f_{cu}= 31 MPa

f_y= 312 MPa

L= 650 mm

Solution:

f_{ck} = 0.8 ×f_{cu} =24.8 MPa

A_c = (114-(2×4.1)) × (114-(2×4.1)) = 11193.64 mm^2

A_a = (114×114) - (105.8×105.8) =1802.36

As per the Eurocode provisions (**Eurocode 4 1994**), following data has been obtained:

N_u = f_y× A_a +f_{ck}×A_c= (300×1802.36) + (24.8×11193.64) =839.94 kN

$$M_{RHS} = f_y t\left[D(D-t)+\frac{1}{2}(D-2t)^2\right] = 312\times4.1[(114(114-4.1) + 0.5(114-2\times4.1)^2]$$

= 23186037.3 Nmm

$$F_{RHS} = \frac{1}{1+\frac{1}{4}\frac{f_{ck}}{f_y}\frac{D}{t}} = \frac{1}{1+\frac{1}{4}\frac{24.8}{312}\frac{114}{4.1}} = 0.6441$$

$$d_n = \left(\frac{D-2t}{2}\right)F_{RHS} = \left(\frac{114-2\times4.1}{2}\right)0.6441 = 34.073$$

$$M_p = M_{RHS} + f_y t\frac{1}{2}(D-2t)^2(1-F_{RHS})^2 + \frac{1}{2}(D-2t)d_n^2 f_{ck}$$

$$= 23186037.3 + 312\times4.1\frac{1}{2}(114-2\times4.1)^2(1-.6441)^2 + \frac{1}{2}(114-2\times4.1)34.073^2\times24.8$$

= 25.6159 kNm

`

$$M_{\max} = M_{RHS} + \frac{1}{2}(D-2t)\left[\frac{D-2t}{2}\right]^2 f_{ck}$$

$$= 23186037.3 + \frac{1}{2}(114-2\times4.1)\left[\frac{114-2\times4.1}{2}\right]^2 24.8$$

= 26.857 kNm

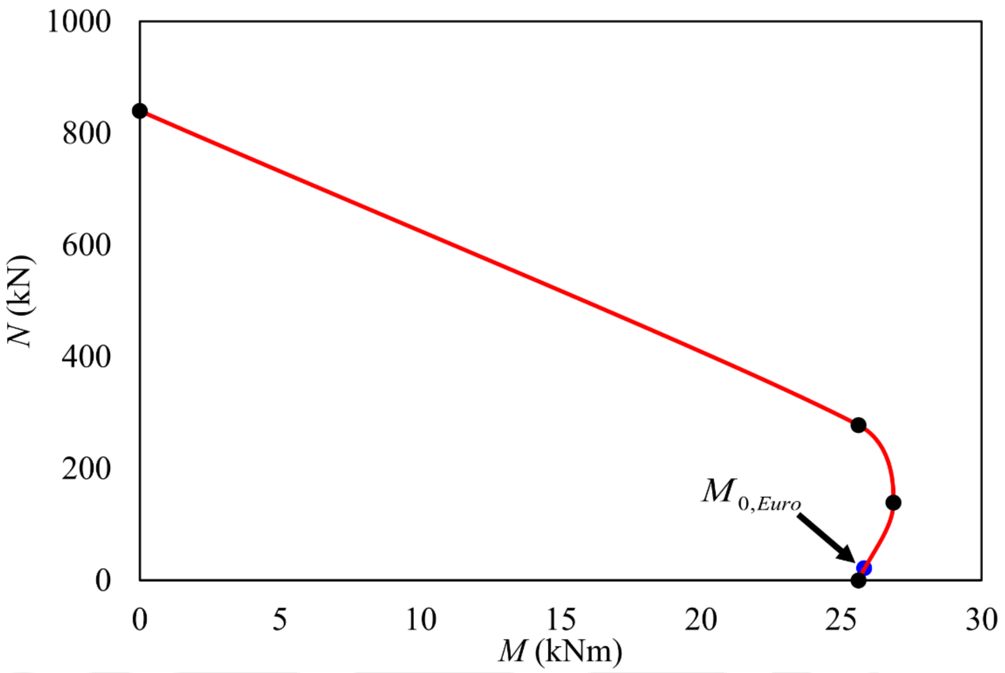

Figure A.1.2: *N*-*M* interaction curve

N_0=22 kN

$f_{ck}\times A_c$ = 277.60 kN

$0.5 \times f_{ck}\times A_c$ = 138.80 kN

Here,

$$N_0 \leq 0.5 A_c f_{ck}$$

Hence

$$M_{0,Euro} = M_p + \frac{N_0}{0.5 A_c f_{ck}}\left(M_{\max} - M_p\right)$$

`

= 25.813 kNm

And

$$P_{0,Euro} = \frac{M_{0,Euro}}{L} = \frac{25.813}{650}$$

=39.712 kN

Based on the data obtained from the experimental results, the following equations have been proposed to estimate the ultimate lateral strength of square partially confined concrete filled steel tubular columns:

$$\gamma = \frac{P_{u0,Exp}}{P_{u0,Euro}} = \frac{49}{39.714} = 1.23$$

$$\beta = \frac{M_{0,Euro}}{P_{0,Euro}\gamma} = \frac{25.813}{39.712 \times 1.23} = 528.459 \text{ mm}$$

$$\alpha = \frac{\beta}{\beta - 1.5D} - 0.0033D_i = \frac{528.459}{528.459 - 1.5 \times 114} - 0.0033 \times 60 = 1.28$$

$$P_{u,60} = \frac{M_{0,Euro}}{(\beta - 1.5D)\alpha} = \frac{25.813}{(528.459 - 1.5 \times 114D)1.28} = \mathbf{56.42\ kN}$$

Problem A.2: To estimate the ultimate lateral strength of circular partially confined concrete-filled steel tubular columns, diameter and height of inner steel tube is 60 mm and 1.5D respectively.

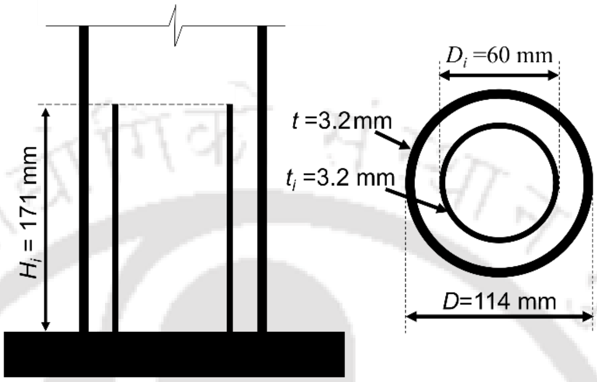

Figure A.2.1: Partially confined circular CFST columns

Mechanical and geometric properties:

N_0= 22 kN

N=0.03

D=114 mm

D_i = 60 mm (inner CHS diameter)

t= 3.2 mm

f_{cu}= 31 MPa

f_y= 312 MPa

L= 600 mm

Solution:

$f_{ck} = 0.8 \times f_{cu} = 24.8$ MPa

$$A_c = \frac{\pi}{4}(114-(2\times3.2))^2 = 9093.172 \text{ mm}^2$$

$$A_a = \frac{\pi}{4}(114^2 - 107.6^2) = 1113.8856 \text{ mm}^2$$

$$I_c = \frac{\pi}{64} 107.6^4 = 6582543.718 \text{ mm}^4$$

$$I_a = \frac{\pi}{64}(114^4 - 107.6^4) = 1711457.068 \text{ mm}^4$$

$$E_a = 165000 \text{MPa}$$

$$E_c = 22000\left(\frac{f_{ck}}{10}\right)^{0.3} = 22000\left(\frac{24.8}{10}\right)^{0.3} = 28891 \text{ MPa}$$

$$(EI)_{eff} = E_a I_a + 0.6 E_c I_c = (165000 \times 1711457.068) + (0.6 \times 28891 \times 6582543.718)$$

$$= 396495025326 \text{ N mm}^2$$

As per the Eurocode provisions (**Eurocode 4 1994**), following data has been obtained:

$$N_{cr} = \frac{\pi^2 (EI)_{eff}}{(k_e L)^2} = \frac{\pi^2 \times 396495025326}{600^2} = 10870 \text{ kN}$$

$$N_{pl,Rk} = A_a f_y + A_c f_{ck} = 1113.8856 \times 312 + 9093.172 \times 24.8 = 573 \text{ kN}$$

$$\bar{\lambda} = \sqrt{\frac{N_{pl,Rk}}{N_{cr}}} = \sqrt{\frac{573}{10870}} = 0.230 \quad < \mathbf{0.5 \ (Satisfied)}$$

$$\eta_c = 4.9 - 18.5\bar{\lambda} + 17\bar{\lambda}^2 = 4.9 - 18.5 \times 0.23 + 17 \times 0.23^2 = 1.549$$

$$\eta_a = 0.25(3 + 2\bar{\lambda}) = 0.25(3+2\times0.23) = 0.865$$

$$N_u = A_a \eta_a f_y + A_c f_{ck}\left[1 + \eta_c \frac{t}{D}\frac{f_y}{f_{ck}}\right]$$

$$= 1113.88 \times 0.865 \times 312 + 9093.172 \times 24.8\left[1 + 1.549 \times \frac{3.2}{114} \times \frac{312}{24.8}\right]$$

= 649.38 kN

$$r_m = \left(\frac{D-t}{2}\right) = \left(\frac{114-3.2}{2}\right) = 55.4$$

$$r_i = \left(\frac{D-2t}{2}\right) = \left(\frac{114-2\times3.2}{2}\right) = 53.8$$

$$F_{CHS} = \frac{\frac{1}{8}\frac{f_{ck}}{f_y}\frac{D}{t}}{1+\frac{1}{4}\frac{f_{ck}}{f_y}\frac{D}{t}} = \frac{\frac{1}{8}\times\frac{24.8}{312}\times\frac{114}{3.2}}{1+\frac{1}{4}\times\frac{24.8}{312}\times\frac{114}{3.2}} = 0.20724$$

$$\gamma_0 = \frac{\pi}{2}F_{CHS} = \frac{\pi}{2}\times 0.20724 = 0.32554$$

$$M_p = 4 f_y t r_m^2 \cos\gamma_0 + \frac{2}{3} f_{ck} r_i^3 \cos^3\gamma_0$$

$$= 4\times312\times3.2\times55.4^2\cos(0.32554) + \frac{2}{3}\times24.8\times53.8^3\cos^3(0.32554)$$

=13.8030 kNm

$$M_{\max} = 4 f_y t r_m^2 + \frac{2}{3} f_{ck} r_i^3 = 4\times312\times3.2\times55.4^2 + \frac{2}{3}\times24.8\times53.8^3$$

=14.831 kNm

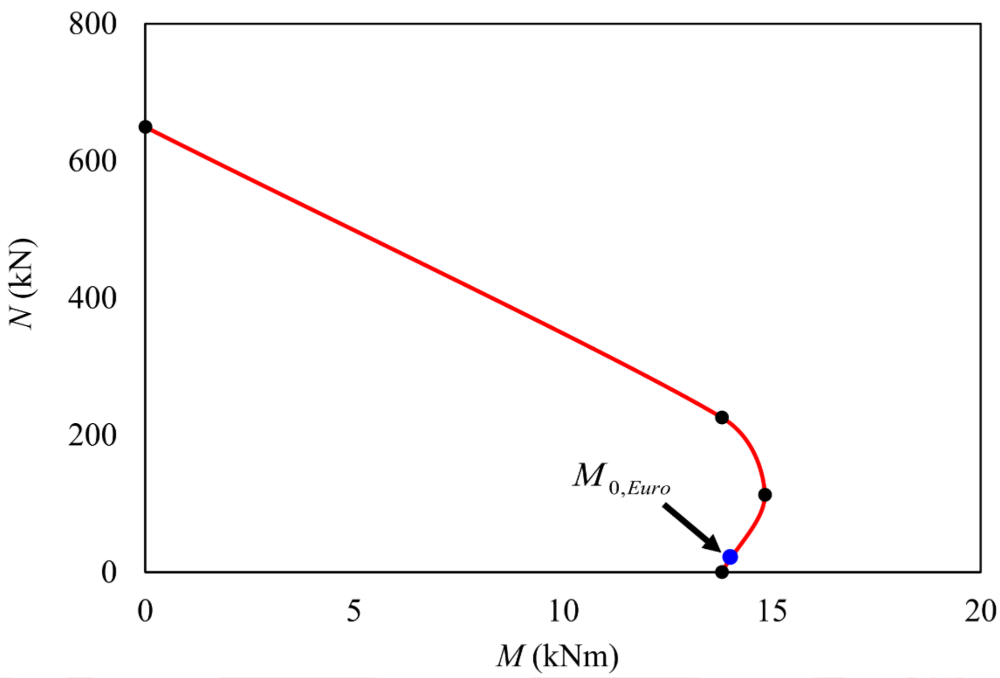

Figure A.2.2: *N*-*M* interaction curve

N_0=22 kN

$f_{ck}\times A_c$ = 225.51 kN

$0.5 \times f_{ck}\times A_c$ = 112.75 kN

Here,

$$N_0 \le 0.5 A_c f_{ck}$$

Hence

$$M_{0,Euro} = M_p + \frac{N_0}{0.5 A_c f_{ck}} \left(M_{\max} - M_p \right)$$

= 14 kNm

$$P_{0,Euro} = \frac{M_{0,Euro}}{L} = \frac{14}{0.6} = 23.34 \text{ kN}$$

Based on the data obtained from the experimental results, the following equations have been proposed to estimate the ultimate lateral strength of circular partially confined concrete filled steel tubular columns:

$$\gamma = \frac{P_{u0,Exp}}{P_{u0,Euro}} = \frac{27}{23.34} = 1.15$$

$$\beta = \frac{M_{0,Euro}}{P_{0,Euro}\gamma} = \frac{14}{23.34 \times 1.15} = 522 \text{ mm}$$

$$\alpha = \frac{\beta}{\beta - 1.5D} - 0.0036D_i = \frac{522}{522 - 1.5 \times 114} - 0.0036 \times 60 = 1.27$$

$$P_{u,60} = \frac{M_{0,Euro}}{(\beta - 1.5D)\alpha} = \frac{14}{(0.522 - 1.5 \times 0.114) \times 1.27} = \mathbf{31.38\ kN}$$

`

This page is intentionally left blank

Appendix B

CHARACTERISATION OF RAW MATERIALS TO PREPARE CONCRETE MIX DESIGN AND CHEMICALCOMPOSITIONS OF USED STEEL TUBES

Table B.1: Specific gravity of aggregates

Description	FA (sand) (in gm)	CA (10 mm) (in gm)	CA (20 mm) (in gm)
Weight of sample taken	500	500	2002
Weight of saturated and surface dry aggregate (C)	500	500	2002
Weight of pycnometer/bucket + sample + water (A)	1846	1840	2113
Weight of pycnometer/bucket +water (B)	1538	1530	872.87
Weight of oven dry sample (D)	497	497	1996
Specific gravity = ((D)/(C-(A-B))) × 100	2.59	2.63	2.62

Table B.2: Specific gravity of cement

Description	Weight
Cement sample	63 gm
Initial reading	0.5
Final reading	22.1
Specific gravity	2.92

B.1: Mix design of M25 grade of concrete used to cast the columns

$$f'_{ck} = f_{ck} + 1.65 \times s$$

$= 25 + 1.65 \times 4$ (S = 4, as per IS:10262 2009)

=31.6 MPa

Water-cement ratio assumed = 0.52

For 10 mm MSA (maximum size of aggregate), water content = 208 kg

Cement content $= \dfrac{208}{0.52}$ = 400 kg/m^3

As per Table 3 of IS:10262 2009,

For 10 mm MSA Coarse aggregate and Zone - II fine aggregate,

Volume of coarse aggregate= 0.46

Volume of fine aggregate =1-0.46= 0.54

a) Volume of concrete = 1 m^3

b) Volume of cement $= \dfrac{400}{2.92} \times \dfrac{1}{1000}$ = .137

c) Volume of water $= \dfrac{208}{1000}$ = 0.208

d) Volume of chemical admixture = Nil

e) Volume of all in aggregate $= a - (b + c + d)$ = 1-(0.137+0.208) = 0.655

f) Mass of coarse aggregate = e × volume of coarse aggregate × specific gravity of coarse aggregate × 1000 = 0.655 × 0.46 × 2.63 × 1000 = 792.4 kg

g) Mass of fine aggregate = e × volume of fine aggregate × specific gravity of fine aggregate × 1000 = 0.655 × 0.54 × 2.59 × 1000 = 916.1 kg

Mix proportion

Cement	= 400 kg/m^3
Water	= 208 kg/m^3
Fine aggregate	= 916.1 kg/m^3
Coarse aggregate	= 792.4 kg/m^3
Water –cement ratio	= 0.52

B.2: Mix design of M30 grade of concrete used to cast footing for the columns

$$f'_{ck} = f_{ck} + 1.65 \times s$$

$= 30 + 1.65 \times 5$ (*S* = 5, as per IS:10262 2009)

= 38.25 MPa

Water-cement ratio assumed =0.48

For 20 mm MSA (maximum size of aggregate), water content = 186 kg

Cement content = $= \dfrac{186}{0.48}$ = 387.5 kg/m^3

As per Table 3 of IS:10262 2009,

For 20 mm MSA Coarse aggregate and Zone - II fine aggregate,

Volume of coarse aggregate= 0.62

Volume of fine aggregate =1-0.62= 0.38

a) Volume of concrete = 1 m^3

b) Volume of cement $= \frac{387.5}{2.92} \times \frac{1}{1000}$ = .133

c) Volume of water $= \frac{186}{1000}$ = 0.186

d) Volume of chemical admixture = Nil

e) Volume of all in aggregate $= a - (b + c + d)$ = 1-(0.133+0.186) = 0.68

f) Mass of coarse aggregate = e × volume of coarse aggregate × specific gravity of coarse aggregate × 1000 = 0.68 × 0.62 × 2.62 × 1000 = 1104.592 kg

g) Mass of fine aggregate = e × volume of fine aggregate × specific gravity of fine aggregate × 1000 = 0.68 × 0.38 × 2.59 × 1000 = 669.256 kg

Mix proportion

Cement = 387.5 kg/m^3

Water = 186 kg/m^3

Fine aggregate = 669.256 kg/m^3

Coarse aggregate = 1104.592 kg/m^3

Water –cement ratio = 0.48

Table B.3: Cubic compressive strength of the design mix for M25 grade concrete

Cubes of M25 grade concrete	Peak load (kN)	f_{cu} (MPa)	Average f_{cu} (MPa)
150 ×150 ×150 mm	660	29.33	
150 ×150 ×150 mm	720	32.00	
150 ×150 ×150 mm	710	31.56	~ 31
150 ×150 ×150 mm	750	33.33	
150 ×150 ×150 mm	610	27.11	

Table B.4: Cubic compressive strength of the design mix for M30 grade concrete

Cubes of M30 grade concrete	Peak load (kN)	f_{cu} (MPa)	Average f_{cu} (MPa)
150 ×150 ×150 mm	895	39.78	~ 39
150 ×150 ×150 mm	900	40.00	
150 ×150 ×150 mm	840	37.33	
150 ×150 ×150 mm	920	40.89	
150 ×150 ×150 mm	840	37.33	

Table B.5: Optical Emission Spectrometer analysis results

Steel tubes	Summary of chemical composition (%)											
	C	Fe	Si	Mn	P	S	Cr	Ni	Mo	Cu	Nb	V
C114-3.2	0.055	99.464	0.044	0.387	0.024	0.008	0.005	0.007	-	0.003	-	0.002
C114-3.2 (1)	0.052	99.479	0.043	0.383	0.023	0.007	0.003	0.006	-	0.002	-	0.002
S114-4.06	0.077	99.487	0.095	0.281	0.033	0.010	0.004	0.007	-	0.003	-	0.002
S114-4.06 (1)	0.078	99.482	0.095	0.283	0.033	0.011	0.005	0.007	-	0.004	-	0.002
c50-3.2	0.031	99.536	0.065	0.200	0.010	0.004	0.028	0.020	0.010	0.002	0.095	-
c60-3.2	0.023	99.593	0.030	0.171	0.007	0.008	0.029	0.022	0.012	0.003	0.010	-